UNSTEADY AND STEADY HYPERSONIC INTERACTIONS WITH SURFACE MASS TRANSFER

By

NADUVATH KURUVILLA VARGHESE

DEPARTMENT OF AERONAUTICAL ENGINEERING

INDIAN INSTITUTE OF TECHNOLOGY KANPUR

OCTOBER, 1980

UNSTEADY AND STEADY HYPERSONIC INTERACTIONS WITH SURFACE MASS TRANSFER

A Thesis Submitted
in Partial Fulfilment of the Requirements
for the Degree of

DOCTOR OF PHILOSOPHY

By
NADUVATH KURUVILLA VARGHESE

to the

DEPARTMENT OF AERONAUTICAL ENGINEERING
INDIAN INSTITUTE OF TECHNOLOGY KANPUR
OCTOBER, 1980

CERTIFICATE

This is to certify that this thesis entitled, 'Unsteady and Steady Hypersonic Interactions with Surface Mass Transfer' , by Sri N.K. Varghese is a record of work carried out under my supervision and has not been submitted elsewhere for a degree.

(R.N. Gupta)
Professor
Dept. of Aeronautical Engineering
Indian Institute of Technology
Kanpur

October - 1980

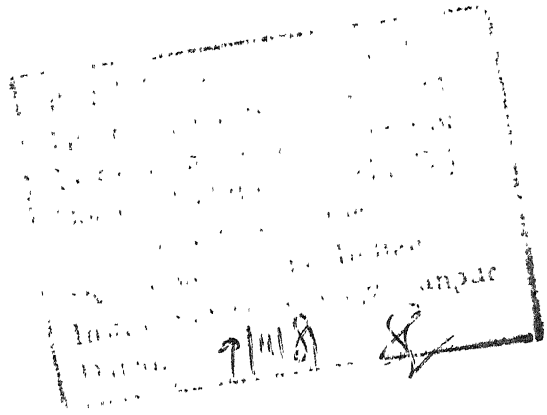

ACKNOWLEDGEMENTS

I hereby place on record my sincere and heartfelt thanks to Dr. R.N. Gupta who suggested this problem, guided the research and encouraged with constant interest throughout the course of this work.

My thanks are also due to Dr. A.C. Jain for his valuable comments and suggestions during the progress of this work.

I may take this opportunity to thank my wife Santha for her patience and forbearance.

Also my thanks are due to Mr. K. Joy David, Mr. P.M. Scaria and Mr. D.D. Satiaraj for proof reading.

I thank Mr. S.K. Tewari and Mr. G.L. Misra for their excellent typing and patience.

At last, but not the least, thanks to DEC 1090 SYSTEM of IIT/K for its fast and faithful co-operation during the course of computations.

TABLE OF CONTENTS

Page

LIST OF TABLES

LIST OF FIGURES

Figure | Page

Figure | Page

LIST OF SYMBOLS

All dimensional quantities are represented with an asterisk as superscript. The corresponding non-dimensional quantities are represented without the superscript. Symbols having only local significance are defined in the text where they appear.

a^*	velocity of sound
c_i	mass fraction of species (i=1,2)
c_p^*	specific heat at constant pressure
C_L	lift coefficient
C_D	drag coefficient
D_{12}^*	binary diffusion coefficient
f	transformed stream function, defined in (2.34)
f_0, f_1, f_2, f_3	function of η appearing in the expansion of f in (3.10)
F_S^*, F_N^*	tangential and normal force acting on either side of the wedge
h^*	enthalpy
H^*	total enthalpy
H	$= H^*/(\frac{1}{2} \times u_\infty^{*2})$
H_0, H_1, H_2, H_3	function of η appearing in the expansion of H in (3.11)

I_0, I_1, I_2, I_3	integrals defined in (3.35)
$\bar{I}$	integral defined in (3.48b)
k^*	thermal conductivity
K	function defined in (1.6)
k_x	ratio of consecutive stepsizes in x
k_t	ratio of consecutive stepsizes in t
L_e	Lewis number $\rho^* D_{12}^* c_p^*/k^*$
L^*	length of wedge
M	Mach number
p^*	pressure
p	$= p^*/p_\infty^*$
p_0, p_1, p_2, p_3	constants in the expansion of p in (3.8)
$\bar{p}$	$=p/p_0\bar{x}$
Pr	prandtl number = $\mu^* c_p^*/k^*$
q^*	local heat transfer rate per unit area
Q^*	heat transfer rate per unit width from either side of the wedge
R^*	gas constant
R_u^*	universal gas constant
Re_{∞,x^*}	local Reynolds number defined in (1.8)

Re_{∞,L^*}	Reynolds number evaluated at the end of the wedge
S_1, S_2, S_3, S_4	integrals defined in (6.11), (6.12), (6.15) and (6.19)
t^*	time
t	$= t^* u_\infty^*/L^*$
T^*	absolute temperature
T	$= T^*/T_\infty^*$
u^*	velocity component in the x^* direction
u	u^*/u_∞^*
v^*	velocity component in the y^* direction
v	$= v^*/u_\infty^*$
x^*	streamwise coordinate
x	$= x^*/L^*$
y^*	normal coordinate
y	$= y^*/L^*$
Z	variable defined in (5.43)
α	injection parameter defined in (3.12b)
$\bar{\alpha}$	angle of attach
α_1	exponent of eqn. (5.40)
β	$= \frac{\gamma-1}{\gamma}$; the pressure gradient parameter
γ	specific heat ratio for air
δ^*	boundary layer displacement thickness
δ	$= \delta^*/L^*$

δ_0, δ_1, δ_2, δ_3	constants in the expansion of δ^* in (3.9)
Δ^*	displacement thickness of the unsteady boundary layer, given by (2.43)
Δx	stepsize in x
Δt	step-size in t
$\Delta \xi$	step-size in ξ
$\Delta \eta$	step-size in η
ξ	normal coordinate of transformation given by (5.40)
η	transformed normal coordinate
θ_b	angle of inclination of either side of the wedge
μ^*	coefficient of viscosity
μ	μ^*/μ^*_∞
ρ^*	density
ρ	ρ^*/ρ^*_∞
τ^*	shear stress at the surface
$\bar{\chi}$	hypersonic interaction parameter, defined in (1.7)
ψ	stream function defined in (2.15)

Subscripts

∞	evaluated in the free stream
e	evaluation in the outer layer
b	evaluation on the surface of the wedge
i, f	indicates condition before and after the impulsive changes in the angle of attack

n	evaluation at the n-th η-station
A	main stream fluid (air)
T, B	refers to the top and bottom surface of the wedge

Superscript

(i)	evaluation at the i-th t-station
'	differentiation with respect to η

SYNOPSIS

UNSTEADY AND STEADY HYPERSONIC INTERACTIONS WITH SURFACE MASS TRANSFER

A Thesis Submitted

In Partial Fulfilment of the Requirements

For the Degree of

DOCTOR OF PHILOSOPHY

By

NADUVATH KURUVILLA VARGHESE

to the

Department of Aeronautical Engineering
Indian Institute of Technology, Kanpur
October, 1980

A tneoretical study of the time-dependent and steady hypersonic viscous interaction with surface mass transfer has been described in this work. The problems analysed here are pertinent to the two-dimensional hypersonic flow over a slender wedge-wing commonly employed as lifting surface in hypersonic vehicles. For the purpose of analysis, the transformed flow governing equations have been obtained for the general case of a time-dependent flow over a slender wedge involving the surface mass transfer.

First the steady problem with homogeneous (same gas) and heterogeneous (foreign gas) injections is analysed. The surface injection presents a possible means of alleviating the aerodynamic heating problem which assumes formidable dimensions at hypersonic speeds. The use of injection is also made for

controlling the boundary layer and inducing the control forces on aerodynamic vehicles. Most of the earlier works connected with the study of surface mass transfer are without the study of the corresponding viscous-inviscid interaction phenomenon. Some of the strong-interaction flows involving surface mass transfer have been treated under the restrictive category of similar solutions. The present study treats the non-similar problem in an exact way for the entire viscous-inviscid interaction regime (from 'strong' to 'weak' including the 'transition') by using the complete tangent-wedge approximation for the calculation of interaction-induced pressure in the layer contained between the shock wave and the boundary layer. A series solution has been developed to initiate the solutions at the beginning of the strong-interaction regime. The laminar boundary layer equations for a binary mixture of perfect gases have been numerically solved for surface injections of helium and argon with variable fluid properties and various values of the wall injection parameter. The solutions have also been obtained with the injection/suction of air at the surface. The computed results include the conventional boundary layer parameters of displacement thickness, wall shear function, enthalpy gradient at the wall and viscous-inviscid interaction induced pressure. The comparative effectiveness of the various coolants for the high speed problem from the point of view of controlling the induced pressures is pointed out. The analysis of this steady

problem has been carried out by the two commonly employed numerical schemes due to Clutter & Smith and Marvin & Sheaffer. The Clutter-Smith technique employing the shooting method is highly accurate but fails to converge for certain problems with surface injection where the skin-friction and heat transfer become small. The finite-difference method (using the Crank-Nicolson scheme)due to Marvin & Sheaffer, although somewhat less accurate, has the distinct advantage of employing the dependent variables rather than their slopes to obtain solutions. Therefore,this method could provide results for the cases where the Clutter-Smith technique did not converge. The comparative advantages and disadvantages of the two methods are discussed in detail for the problems involving viscous-inviscid interactions.

The results from the steady problem have been further utilised to obtain the lift and drag coefficients, the lift to drag ratio, the position of the aerodynamic centre,and the heat transfer rate per unit width of the wedge-wing.

Next the time-dependent problem with surface injection/ suction of air has been analysed. The problems of maneuverability and control of hypersonic vehicles require the study of unsteady flows such as the one over a slender wedge after an impulsive change in the angle of attack of the wedge-wing. In the present work, the time history of such a time-dependent flow, till the final steady state is reached, is analysed and

the time-dependent solutions of the flow governing equations with air injection/suction are used for determining the temporal variations in the pressure, wall shear and heat transfer rate numerically. Time-dependent problem with foreign gas injection has not been considered here due to the large computational time required for such problems.

The parameters employed for defining both the steady as well as unsteady problems are the free stream Mach number M_∞, Reynolds number $R_{e_{\infty,L^*}}$ based on the free stream conditions and the length of the wedge L^*, the semi-wedge angle θ_b and the surface injection/suction parameter, α. For the unsteady problem, in addition, the initial and final angles of attack $\bar{\alpha}_i$ and $\bar{\alpha}_f$ are also defined. For the problems considered here M_∞ and $R_{e_{\infty,L^*}} >> 1$ and the angles involved θ_b, $\bar{\alpha}_i$, $\bar{\alpha}_f << 1$. However, the relative magnitudes of these various parameters are such that the combination $M_\infty^3 \sqrt{C/(R_{e_{\infty,L^*}})^{1/2}}$ remains finite and the product $M_\infty|\theta| \approx O(1)$, where θ is the maximum deflection of the wedge surface. Finally, two types of thermal wedge conditions on the wedge surface are used for the steady case: insulated wedge surface and the wedge surface maintained at a constant temperature. For the unsteady problem, however, only the latter thermal condition is employed. A comparison with the available results, wherever possible, is included.

CHAPTER I

STATEMENT OF THE PROBLEM AND ASSOCIATED LITERATURE

1.1 Introduction

The two problems analysed here are the problems of steady and unsteady hypersonic flow over a slender wedge-wing commonly employed as lifting surface in hypersonic vehicles. The surface heating of these wedge-wings assumes formidable proportions at hypersonic speed and the means are to be provided to control this heating. Cooling by the homogeneous or heterogeneous surface injection in the boundary layer provides an effective way of doing it. The behaviour of wedge-wings in steady hypersonic flow situations without the surface-injection control has been studied in detail during the past three decades. Not much attention, however, seems to have been given to the problem involving the surface injection/suction. Further, the problems of maneuverability and control of hypersonic vehicles require the study of unsteady flow such as the one over a slender wedge after an impulsive change in the angle of attack of the wedge-wing. We are particularly interested in the transient behaviours of the pressure distribution, shear stress and heat transfer rate along the sides of the wedge, which will furnish informations about the lift, drag and other aerodynamic coefficients. Thus, the

significance of the problems analysed here lies in determining the control characteristics and devising the effective ways of controlling the surface heating of hypersonic vehicles using wedge-shaped aerofoils.

Before discussing the associated literature with the problems outlined here, some more insight is provided into the unsteady flow phenomenon and the surface mass transfer. Taking the unsteady problem first, Fig.1.1, schematically represents such a flow over a slender wedge-wing.

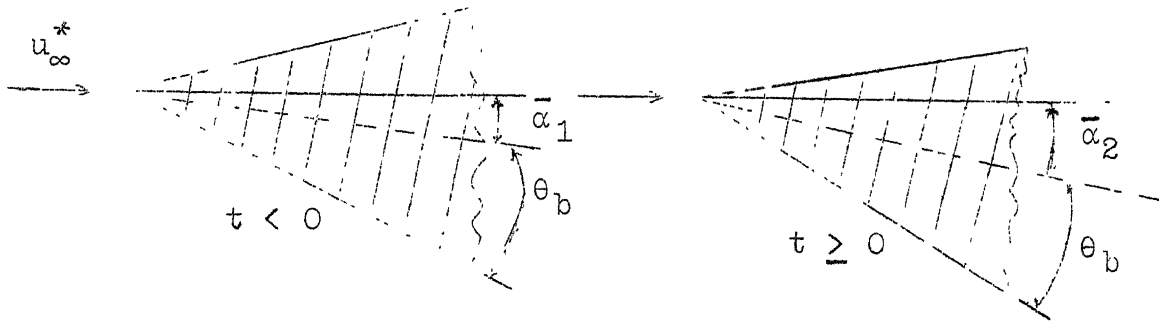

Fig. 1.1 Flow over a slender wedge-wing before and after the impulsive change in angle of attack.

The governing parameters are of the following order of magnitude:

$$M_\infty >> 1 \sim O(10)$$

$$Re_{\infty,L^*} = \frac{\rho_\infty^* u_\infty^* L^*}{\mu_\infty^*} \sim O(10^6)$$

and

$$\bar{\alpha}_1,\ \bar{\alpha}_2,\ \theta_b \sim O(5^\circ)$$

where ρ_∞^* , u_∞^* , μ_∞^* denote density, velocity and viscosity, respectively, in the free stream and L^* is the length of the wedge.

Since for a slender wedge with a sharp leading edge the shock is attached to the leading edge, the flow on one side of the wedge is independent of the flow on the other side and, therefore, we can consider them separately. The problem, therefore, reduces to determining the unsteady hypersonic viscous flow over an inclined surface following an impulsive change in the angle of inclination. The disturbances due to the presence of the wedge are confined within a thin curved shock beyond which the free stream conditions prevail. Similar model of an inclined surface (with the shock attached at the leading edge) replacing a wedge-wing may also be used for the steady problem. Thus, the flow-model shown in Figure 1.2 for the hypersonic flow over an inclined surface (or flat plate) may be used for analysing the problems under consideration.

In any unsteady viscous flow problem there are two separate time scales involved:

(i) $\bar{\tau}_{inv}$ - characteristic time given by L^*/u_∞^* , where L^* is a representative body dimension and u_∞^* is the free stream velocity.

(ii) $\bar{\tau}_v$ - characteristic time for the diffusion of heat and vorticity in the boundary layer.

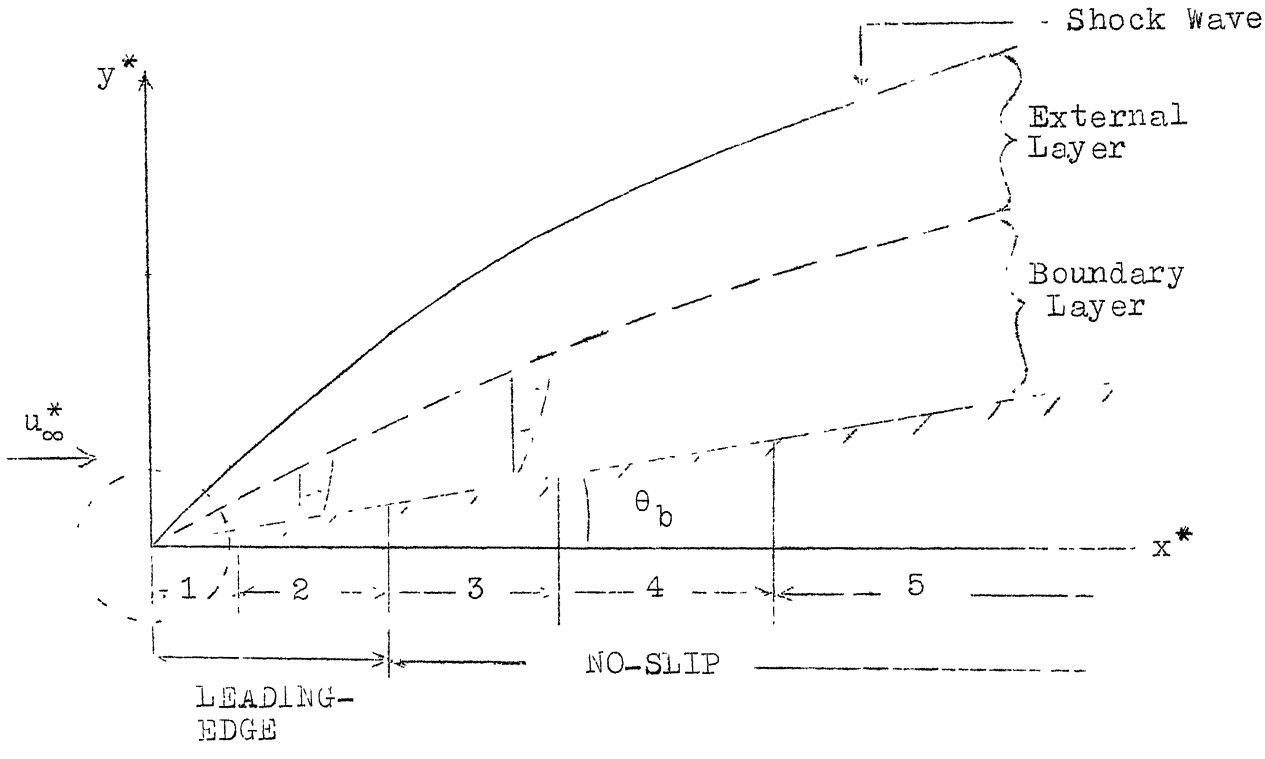

1. Free-molecular flow region
2. Continuum-flow region with slip-boundary condition
3. Strong-interaction region
4. Transition region
5. Weak-interaction region

Fig. 1.2 Flow Regions Over an Inclined Flat Plate in Hypersonic Flow (Schematic)

In hypersonic flow these two time scales are of the same order of magnitude i.e. $O(10^{-3})$. Let $\bar{\tau}$ be the time in which a change in the flow conditions or the geometry of the solid body occurs. A nonsteady problem is that in which $\bar{\tau}$ is of the same order of magnitude as $\bar{\tau}_v$ or $\bar{\tau}_{inv}$ or less. By impulsive change we mean a change occuring in a time $\bar{\tau}$ $<<$ $\bar{\tau}_{inv}$, $\bar{\tau}_v$. In the other extreme case i.e. $\bar{\tau} >> \bar{\tau}_{inv}$, $\bar{\tau}_v$ the flow may be considered as quasi-steady.

The unsteady as well as steady hypersonic viscous flow over a slender body is characterized by the presence of a high temperature, low-density boundary layer adjacent to the body. This boundary layer is much thicker than the corresponding boundary layers in subsonic or moderately supersonic flows. As a result of the curvature of this thick boundary layer, a sufficiently large outward streamline deflection is induced to bring about an important change in the "effective" geometric shape of the body, with the result that pressure variations are propagated into the external inviscid layer. This external pressure field in turn feeds back into the boundary layer and affects its rate of growth. Thus the boundary layer and surrounding inviscid flow are mutually interdependent. This phenomenon, referred to in the literature as hypersonic viscous interaction or shock-boundary layer interaction, therefore, requires the solutions for a steady or unsteady boundary layer subjected to an "external (streamwise) pressure

gradient'' which is not known a priori, but which depends on the rate of growth of the boundary layer itself through the hypersonic inviscid flow relations.

Coming to the problem of surface injection, this presents a possible means of alleviating the formidable aerodynamic heating problem as pointed out earlier. In addition, the use of injection is also made for controlling the boundary layer and inducing the control forces on aerodynamic vehicle. The injection of the same or different gas through the boundary layer materially influences the rate of heat transfer to the surface, skin-friction and the viscous-interaction induced pressure field. Under the hypersonic flow conditions, the pressures induced by the thick boundary layer are greatly increased with surface mass transfer. For cooling purposes, either the injection of the same gas or that of a foreign gas (e.g. helium) may be used. If the injected gas is at the surface temperature, it would act as an ''insulant'' by altering the velocity profiles so that the heat conducted to the surface is reduced and, accordingly, the surface temperature would be smaller. In addition, the diffusion of a foreign gas would also reduce the viscous dissipation.

A review of literature on the interaction problem in two-dimensional steady/unsteady hypersonic viscous flows with or without surface mass transfer is presented in the following section.

1.2 Review of Literature

The flow regions, shown in Fig. 1.2, on an inclined flat plate are according to the model introduced by Lees and Probstein and contained in [1,2]. In the basic flow model postulated by them, two main flow regions can be distinguished: I, a ''leading-edge'' region; II, a region of no-slip.

In the leading edge region I, two sub-regions exist. The relatively small domain ''1'' around the leading edge is of the order of 20 mean free paths in breadth, and the concepts of Maxwell and Smoluchowski cannot be applied. This is also known as the free-molecular flow region. Downstream of zone 1 the lateral extent of the viscous layer is sufficiently large compared with the mean free path so that the Maxwell-Smoluchowski concept of a small region of slip and temperature jump at the surface with a main body of continuum flow is probably valid. Here, the shock emerges from the viscous region, and a distinct, larger inviscid layer exists. Zone 2 may be defined as the slip-flow region.

In region II, slip and temperature jump at the surface are, generally, negligible, and all concepts of continuum flow apply throughout. The domain of no-slip is divided into three sub-regions: (3) ''strong'' interaction region; (4) transition region; (5) ''weak'' interaction region. As we proceed downstream along the wedge the induced effects decay, and

eventually if the Reynolds number, Re_{∞,x^*}, becomes sufficiently high these effects must be weak. In the weak-interaction region (zone 5) the effects produced by the self-induced pressure gradient are essentially perturbations on the classical high Reynolds number flow. In the transition region (zone 4), as the name suggests, the interaction is neither ''strong'' nor ''weak''.

In part of region I and completely in region II, the flow field between the shock and the body surface is divided into two distinct regions, the external inviscid layer and the viscous boundary layer. In the external layer, the flow is governed by the inviscid Euler equations, whereas in the other region, the flow is governed by the boundary layer equations [3] as long as $(\delta^*/x^*)^2 \ll 1$. Thus, the hypersonic viscous interaction problem, mentioned earlier and as applicable to region II, has the following three aspects:

(i) The flow in the external layer can be considered as the inviscid hypersonic flow over an ''effective body'' given by the boundary layer displacement thickness added to the original body.

(ii) The distributions of pressure, tangential velocity and total enthalpy at the edge of the ''effective body'' determine the flow in the boundary layer.

(iii) The displacement thickness used to obtain the external inviscid flow should be consistent with the

displacement thickness obtained from the solution of the boundary layer equations subjected to the external pressure gradient.

The steady-flow interaction problem appears to have been studied in detail. Various approaches used to analyse the interaction problem for the steady flow are reviewed in detail by Hays and Probstein [2], Dorrance [4], Stewartson [5] and Moore [6]. Since our interest in the steady-flow problem is mainly under the conditions of surface mass transfer, only the basic characteristics of these approaches are outlined here briefly.

The flow in the external layer, which is equivalent to the inviscid hypersonic flow over a sharp-edged body of specified shape can be obtained by the method of characteristics, the shock expansion theory and the tangent-wedge approximation. The last method is the easiest of the three, gives results of good accuracy and has been used extensively in the hypersonic interaction problems. In the tangent wedge approximation the pressure at any point on a slender body of thickness $y_e^*(x^*)$ is approximated by the pressure across an oblique shock that produces the local flow deflection dy_e^*/dx^*. For free stream Mach number $M_\infty >> 1$ and for a slender body with $dy_e^*/dx^* << 1$, with the finite product of $K(x^*) = M_\infty dy_e^*/dx^*$, the tangent-wedge approximation may be written as [2]:

$$\frac{p_e^*(x^*)}{p_\infty^*} = 1 + \gamma K \left[\frac{\gamma+1}{4} K + \left\{\left(\frac{\gamma+1}{4}K\right)^2+1\right\}^{1/2}\right] + O(M_\infty^{-2}) \quad (1.1)$$

$$\frac{u_e^*(x^*)}{u_\infty^*} = 1 + O(M_\infty^{-2}) \quad (1.2)$$

$$\frac{H_e^*(x^*)}{\frac{1}{2} u_\infty^{*2}} = 1 + O(M_\infty^{-2}) \quad (1.3)$$

For small and large values of K, equation (1.1) can be expanded as:

$$\frac{p_e^*(x^*)}{p_\infty^*} = 1 + \gamma K + \frac{(\gamma+1)}{4} K^2 + \frac{(\gamma+1)^2}{32} K^3 + O(K^5) \quad (1.4)$$

and

$$\frac{p_e^*(x^*)}{p_\infty^*} = \frac{\gamma(\gamma+1)}{2} K^2 + \frac{3\gamma+1}{\gamma+1} - \frac{8\gamma}{(\gamma+1)^3} K^{-2} + O(K^{-4}) \quad (1.5)$$

For the hypersonic interaction problem K in the equation (1.1), (1.4) or (1.5) has to be replaced by:

$$K(x^*) = M_\infty \left[\frac{dy_b^*}{dx^*} + \frac{d\delta^*(x^*)}{dx^*}\right] \quad (1.6)$$

where $y_b^*(x^*)$ defines the body surface and $\delta^*(x^*)$ is the boundary layer displacement thickness. Since the displacement thickness δ^* in (1.6) is not known <u>a priori</u>, the use of tangent wedge approximation still retains the basic iterative nature of the interaction problem. However, the advantage obtained is that the inviscid flow in the external layer need

not be calculated explicitly. A disadvantage of employing the tangent wedge approximation is that the vorticity in the external layer due to the shock curvature, which may affect the structure of the boundary layer, can not be accounted for. However, for a sharp-edged slender body, the effects of the vorticity interaction can be neglected [2] beyond a region very close to the leading edge.

The extent of the interaction between the boundary layer and the inviscid external flow is characterized by the hypersonic interaction parameter, $\bar{\chi}$, defined as:

$$\bar{\chi} = M_\infty^3 \left(\frac{C}{R_{e\infty,x^*}} \right)^{1/2} \tag{1.7}$$

with

$$Re_{\infty,x^*} = \frac{\rho_\infty^* u_\infty^* x^*}{\mu_\infty^*} \tag{1.8}$$

Here C is the coefficient of the linear viscosity-temperature relation.

For the strong-interaction flows, $\bar{\chi} >> 1$ and eq. (1.5) is the appropriate expansion of the tangent-wedge approximation. For the weak interaction flows, eq. (1.4) is to be used corresponding to $\bar{\chi} \leq O(1)$. For the general case, where a continuous solution is sought from strong to weak interaction region through the transition region, no simplifications to eq. (1.1) can be made.

The foregoing discussion gives some insight into the interaction problem in steady hypersonic flows without the surface mass transfer. With homogeneous (same) or heterogeneous (different) surface mass transfer, the interaction problem becomes little more complex. Most of the earlier works connected with the analysis of surface mass transfer are without the study of the corresponding interaction problem. We will briefly describe in the next few paragraphs some of these works pertinent to the surface mass transfer problem.

The basic features of surface mass transfer effects are found in the early studies of the low-speed boundary layer. Schlichting [7] and Emmons and Leigh [8] investigated the incompressible similarity boundary layer on a flat plate with air injection at the surface. Their results indicate marked reduction in wall shear. Compressibility effects were first included in studies of air injection by Lees [9], Eckert and Livingwood [10], Low [11], and others. Lees investigated the stability of the compressible laminar boundary layer with air injection, Eckert and Livingwood carried out simplified calculation to obtain the effects of air injection and comparisons of convection, transpiration, and film cooling; and Low completed the exact solution for compressible flow with $v_b \propto \bar{x}^{1/2}$ and constant Prandtl number. All investigators confirmed the benefits of air injection upon the reduction of heat transfer and equillibrium wall temperature.

In a recent work, Inger and Swean [12] have presented a comprehensive study of similarity solutions for vectored injection and suction of air in non-adiabatic laminar boundary layers with zero axial pressure gradient. However, in a hypersonic flow with surface mass transfer, it is necessary to consider the self induced pressure gradients resulting from the displacement of the external flow field due to the presence of a relatively thick boundary layer.

The effects of vectored air injection in the ''weak-to-moderate'' interaction region have been investigated by Inger and Swean [13]. They treated the interaction effect as a small, non-similar perturbation caused by the self-induced pressure gradient on a basic self-similar isobaric flow solution with heat transfer and vectored air injection. Considering both upstream and downstream vectored injection, their results show that the physical properties of the flow situation are significantly influenced by both the velocity and angle of injection. Zien [14] investigated the unsteady boundary layer on a flat plate with surface mass transfer. Results on skin-friction, heat transfer rate and weak interaction pressures were obtained under conditions of surface mass transfer that correspond to similarity solution in steady flow.

The foregoing discussion was on cases of homogeneous injection in which the external flow and the injected fluid are of the same medium. When the injected fluid is different,

a binary mixture boundary layer flow results with the diffusion phenomenon having an important influence.

In a detailed investigation, Baron [15] derived the complete equations for laminar flow of a binary mixture on the basis of the equations of change resulting from Enskog's solution of the Boltzmann equation. It was shown that although the mass and momentum conservation equation remained unchanged, additional terms appeared in the energy equation to account for the interaction between energy and mass fluxes. The descriptive system was augmented by a component mass-continuity relation. The equations were solved to yield similar solutions for a flat plate with zero axial pressure gradient, both Prandtl and Schmidt numbers being taken as unity. Helium and Carbon-di-oxide injections were considered. Greater reductions in skin-friction and heat transfer were reported for the injection of gases lighter than air as compared to heavier gas injection. Wuest [16] obtained similar solutions with variable fluid properties whose dependence on temperature and concentration was represented by semi-empirical formulae. Integral forms of the boundary layer equations were also derived. A more general analysis of the problem (not restricted to similar flows) was made by Moran and Scott [17]. The equations were solved in terms of Crocco variables using a finite-difference technique. The method requires starting profiles and is not apparently capable of handling large changes taking place in the streamwise

direction. Culick [18] presented an approximate analysis of the compressible turbulent boundary layer on a porous flat plate with distributed surface mass transfer, Li and Gross [19] obtained similar solutions for the hypersonic laminar boundary layer on a flat plate considering strong-interaction and normal surface injection of a foreign gas. A set of analytical expressions were derived relating the induced pressure at the wall, wall heat transfer, and skin-friction in terms of parameters describing the strong interaction flow. However, the mathematical restriction on body shape and injection velocity necessary for the existence of similar solutions disallow the treatment of problems of practical interest.

Jaffe, Lind and Smith [20] investigated the hypersonic laminar boundary layer on a cone with surface mass transfer; and described a general method for solving such a problem. Numerical results were obtained for injection of helium, argon and air, but the hypersonic interaction phenomenon was not considered. Jain and Li [21] investigated the binary boundary layer flow characterised by finite external stream Mach number and finite pressure gradient. A Gortler's type series solution was developed. They carried out detailed computations of the thermodynamic and transport properties of hydrogen-air and helium-air mixtures and presented a number of graphs to illustrate their behaviour.

Blottner [22] solved the boundary layer equations for a multicomponent flow with finite chemical reactions. He evolved a scheme for solving the governing equations for a flow problem involving a large number of chemical species and obtained results in the case of a cone and a hyperboloid subjected to a high Mach number flow. Marvin and Sheaffer [23] suggested a numerical method for solving non-similar and similar boundary layer equations, including binary gas injection for non-reacting gases. They got the starting profiles by solving the similarity equations obtained by putting $x=0$ in the non-similar case. This approach is not mathematically sound since it assumes the validity of the boundary layer equations at the leading edge. They did not analyse the associated interaction problem also.

Gupta and co-workers [24,25] very recently presented results for the case of homogeneous and heterogeneous vectored injection cooling at hypersonic speeds. They also obtained the first order correction to the displacement induced pressures for the problem of strong-interaction flows which may not be treated under the category of similar solutions. However, the complete interaction problem involving the recomputation of the flow field from the modified induced pressure field was not considered.

Now, coming to the unsteady flows, the interaction problem, in comparison with the steady state, is further

complicated because the lateral velocity of the unknown displacement surface also affects the external flow. Lighthill [26] presented an extension of the tangent wedge approximation to obtain the time-dependent pressure on a slender moving body of shape $y_e^*(x^*,t^*)$ placed in an inviscid hypersonic stream. This extension was based on the ''piston analogy'' of Hays [27] who observed the equivalence between the steady two-dimensional flow over an arbitrary body and the unsteady one-dimensional flow in front of a moving piston. The pressure in front of a piston moving with a velocity w^* in a stationary compressible medium is given by

$$p = \frac{p^*}{p_\infty^*} = 1 + \gamma \frac{w^*}{a_\infty^*} \left[\frac{\gamma+1}{4} \frac{w^*}{a_\infty^*} + \left\{ \left(\frac{\gamma+1}{4} \frac{w^*}{a_\infty^*} \right)^2 + 1 \right\}^{1/2} \right] \qquad (1.9)$$

where a_∞^* is the velocity of sound and the subscript ∞ refers to conditions in the undisturbed gas. Equation (1.9) is analogus to the corresponding tangent wedge approximation (1.1) if one identifies w^* with the normal velocity component induced because of the slope of the body and neglects quantities of $O(M_\infty^{-2})$. For a moving body an additional term $\partial y_e^*/\partial t^*$ is introduced in the normal velocity component. Thus the instantaneous pressure $p_e^*(x^*,t^*)$ on the body is given by eq. (1.9) with

$$\frac{w^*(x^*,t^*)}{a_\infty^*} = \frac{1}{a_\infty^*} \left(u_e^* \frac{\partial y_e^*}{\partial x^*} + \frac{\partial y_e^*}{\partial t^*} \right) = K(x^*,t^*) \qquad (1.10)$$

where u^* is the velocity component in the x^* direction.

Miles [28] has discussed the expressions (1.9) and (1.10) and its application to the unsteady pressure in inviscid hypersonic flow. For the small and large values of K, the expansions of expression (1.9) are similar to equations (1.4) and (1.5) with the meaning of K given by eq. (1.10). The first two terms of the small K expansion, equation (1.4), lead to the acoustic approximation formula, while the piston theory of Lighthill [26] corresponds to the first four terms.

For the unsteady interaction problem y_e^* in eq. (1.10) should be replaced by $(y_b^* + \Delta^*)$, where $\Delta^*(x^*,t^*)$ is the displacement thickness for the unsteady boundary layer, introduced by Moore and Ostrach [29].

Examples of unsteady interaction problems include the works of Reshotko, Rodkiewicz, Gupta & co-workers [30,31,32,33,73]. They considered the unsteady weak-interaction flow on a semi-infinite flat plate at zero-incidence after the free stream Mach number was impulsively increased/decreased by a small amount (of O(1%)). The pressure on the plate was assumed constant for calculating the unsteady boundary layer and a small unsteady perturbation was calculated from the boundary layer solutions. This approach is justified because of the small change involved in the problem. Gupta and Rodkiewicz [34,35,36] later considered the unsteady strong interaction flow for the stepwise-accelerated flat plate in the direction of its original motion.

The problem of impulsive motion of a flat plate involving the development of the flow from initial unsteady state described by Rayleigh to the ultimate steady state described by Blasius has been solved by Hall [37]. His results were limited to the case of an incompressible flow. Hall employed the natural coordinates, namely, the three independent variables in space and time. Stewartson [38,39] and Dennis and Walker [40,41] obtained solutions in terms of the two transformed independent variables. Their results are identical to those of Hall [37]. Ban and Kuerti [42] have also made important contributions in the area of unsteady flows with particular application to shock tube flow. Gupta [43] extended their work to the case of a non-linear problem. These works are now overtaken by those of Dennis and Stewartson.

Based on the work of Marvin and Sheaffer [23], Nath [44,45] and his co-workers treated the unsteady compressible boundary layer flow. Their results, however, do not include the viscous interaction effects.

The unsteady problem involving the binary-diffusion of perfect gases was analysed by Gupta and co-workers [46,47] with application to expansion tube flows. This analysis without the binary-diffusion, was also extended to the case of unsteady turbulent boundary layer flow [48,49].

The time-dependent interaction problems involving the lateral motion of the body are solely confined to cases of

harmonic oscillations. King [50] and Orlik-Rückemann [51] considered the interaction on an oscillating slender wedge. These are examples of quasi-steady analysis, that is the flow at any instant was assumed to be the steady flow corresponding to the conditions prevailing at that instant. Demetri and Gupta [52] have also analysed the compressible oscillating boundary layers but their results are limited to supersonic flow problems without incorporating the viscous interaction effects.

The interaction problems involving impulsive lateral motion of the body are very few in the literature [53]. The method of solution is based on 'quasilinearization' which essentially is an extension of the Newton-Raphson method of solving the algebraic and transcendental equations. The results of ref. [54] do not have a monotonically increasing variation with time. However, the wavy behavior of the induced pressure and the gradient of the enthalpy at the wall is not explained and there is no physical basis to justify this wave-like variation in time.

1.3 Description of the Present Work

The present work is concerned with the study of the steady and unsteady high speed viscous-interaction flows which may not be treated under the category of similar solutions. This analysis has been undertaken with the objective of evaluating the viscous interaction-induced pressures, displacement thickness,

shear-stress and wall heat-transfer functions etc. over a slender wedge-wing or equivalently an inclined flat plate moving at hypersonic speeds with surface injections of air, argon and nelium. For the steady flow case, variable fluid properties are used and the solutions are obtained for various values of the wall injection fluxes. The viscous interaction pressure is calculated by employing the tangent-wedge approximation and the variables employed are similar to those of refs. [53] and [54]. For the unsteady problem involving the small impulsive lateral motion of a slender wedge-wing, an extension of the tangent-wedge approximation is used. For this case, however, the constant fluid properties are used with the surface injection of air only.

In Chapter II of the present work, the details of the derivation of transformed governing equations are given. Chapter III deals with the steady flow over an inclined flat plate with air injection/suction at the surface. A four-term series solution needed to supply the starting profiles (and other details) for the strong-interaction region is developed here. This solution is used to specify the initial conditions in space to carry out the numerical integration from strong to the weak interaction regime. An elaborate (and more accurate) numerical integration scheme (sometimes known as "difference-differential" or Clutter-Smith technique) employing the shooting method is described in the latter parts of this chapter; and the results are discussed toward its end. Chapter IV deals

with the details of the numerical integration for the above method.

Chapter V is concerned with the heterogeneous injection (employing argon and helium) under the steady flow conditions. In the beginning portions of this chapter the shooting method for argon injection is presented; and in the letter part a finite-difference scheme after envisaging a new transformation is described. The main results are also discussed at the end of this chapter.

Chapter VI indicates the utilization of results, of the previous chapters, on the two sides of the wedge yielding the characteristics of the two-dimensional wing for steady flows with and without surface mass transfer. Similar results for the unsteady problem are not given due to the prohibitive computer time required for such calculations.

Last Chapter deals with the unsteady problem with air injection/suction on an inclined flat plate following an impulsive change in the angle of inclination. The required initial conditions in time are derived from the steady state solutions of Chapter III and the solution to the unsteady problem is sought by a finite-difference scheme similar to the one used in Chapter V. Here the finite-difference scheme is preferred over the "difference-differential" technique employing shooting method for the reasons explained in this chapter.

CHAPTER II

THE FLOW GOVERNING EQUATIONS

2.1 Time-Dependent Two-Dimensional Compressible Boundary Layer Equations for a Binary Gas-Mixture of Perfect Gases

The unsteady laminar boundary layer equations for a binary gas-mixture with no chemical reactions are considered for the analysis of two-dimensional high speed flow over an inclined surface. The governing equations in the Cartesian Co-ordinate system with origin fixed to the leading edge of the flat plate are [15] :

Continuity Equation :

$$\frac{\partial \rho^*}{\partial t^*} + \frac{\partial(\rho^* u^*)}{\partial x^*} + \frac{\partial(\rho^* v^*)}{\partial y^*} = 0 \qquad (2.1)$$

Momentum Equations :

$$\rho^* \left[\frac{\partial u^*}{\partial t^*} + u^* \frac{\partial u^*}{\partial x^*} + v^* \frac{\partial u^*}{\partial y^*} \right] = - \frac{\partial p^*}{\partial x^*} + \frac{\partial}{\partial y^*} \left(\mu^* \frac{\partial u^*}{\partial y^*} \right) \qquad (2.2)$$

$$0 = \frac{\partial p^*}{\partial y^*} \qquad (2.3)$$

Energy Equation :

$$\rho^* \left[\frac{\partial H^*}{\partial t^*} + u^* \frac{\partial H^*}{\partial x^*} + v^* \frac{\partial H^*}{\partial y^*} \right] = \frac{\partial p^*}{\partial t^*} + \frac{\partial}{\partial y^*} \left(\frac{\mu^*}{Pr} \frac{\partial H^*}{\partial y^*} \right) +$$

$$+ \frac{\partial}{\partial y^*} \left[\mu^* \left(1 - \frac{1}{Pr}\right) \frac{\partial}{\partial y^*} \left(\frac{u^{*2}}{2} \right) \right] + \frac{\partial}{\partial y^*} \left[\mu^* \frac{Le}{Pr} \left(1 - \frac{1}{Le}\right) \sum_i h_i^* \frac{\partial c_i}{\partial y^*} \right] \qquad (2.4)$$

Continuity of Species Equation :

$$\rho^* \left[\frac{\partial c_i}{\partial t^*} + u^* \frac{\partial c_i}{\partial x^*} + v^* \frac{\partial c_i}{\partial y^*} \right] = \frac{\partial}{\partial y^*} \left(\rho^* D_{12}^* \frac{\partial c_i}{\partial y^*} \right) \qquad (2.5)$$

Equation of State :

$$p^* = \bar{R}^* \rho^* T^* \qquad (2.6)$$

And the Viscosity-temperature-species Concentration Relation :

$$\mu^* = \mu^* (c_i, T^*) \qquad (2.7)$$

with $H^* = c_p^* T^* + \frac{1}{2} u^{*2}$

$$c_p^* = \sum_i c_i c_{pi}^*$$

$$\bar{R}^* = \sum_i c_i R_i^*$$

Now we write

$$x = \frac{x^*}{L^*}, \quad y = \frac{y^*}{L^*}, \quad t = \frac{t^* u_\infty^*}{L^*}, \quad u = \frac{u^*}{u_\infty^*}, \quad v = \frac{v^*}{u_\infty^*}, \quad p = \frac{p^*}{p_\infty^*},$$

$$\rho = \frac{\rho^*}{\rho_\infty^*}, \quad T = \frac{T^*}{T_\infty^*}, \quad \nu = \frac{\mu^*}{\mu_\infty^*}, \quad H = \frac{H^*}{\frac{1}{2} u_\infty^{*2}}, \quad h_i = \frac{h_i}{\frac{1}{2} u_\infty^{*2}}, \quad c_p = \frac{c_p^*}{c_{p\infty}^*}$$

and $k = \frac{k^*}{k_\infty^*}$.

Thus, the non-dimensional form of the equations (2.1) through (2.6) are :

$$\frac{\partial \rho}{\partial t} + \frac{\partial}{\partial x} (\rho u) + \frac{\partial}{\partial y} (\rho v) = 0 \qquad (2.8)$$

$$\frac{\partial u}{\partial t} + u \frac{\partial u}{\partial x} + v \frac{\partial u}{\partial y} = - \frac{\beta}{2} \frac{1}{p} \frac{\partial p}{\partial x} \left[H-u^2 \right] \left[\frac{1 + c_1(s - 1)}{1 + c_1(r - 1)} \right]$$

$$+ \frac{1}{Re_{\infty,L^*}} \frac{1}{\rho} \frac{\partial}{\partial y} \left(\mu \frac{\partial u}{\partial y} \right) \tag{2.9}$$

$$0 = \frac{\partial p}{\partial y} \tag{2.10}$$

$$\frac{\partial H}{\partial t} + u \frac{\partial H}{\partial x} + v \frac{\partial H}{\partial y} = \beta \frac{1}{p} \frac{\partial p}{\partial t} \left[H-u^2 \right] \left[\frac{1 + c_1(s - 1)}{1 + c_1(r - 1)} \right]$$

$$+ \frac{1}{Re_{\infty,L^*}} \frac{1}{\rho} \left[\frac{\partial}{\partial y} \left(\frac{\mu}{Pr} \frac{\partial H}{\partial y} \right) + \frac{\partial}{\partial y} \left\{ \mu \left(\frac{Pr-1}{Pr} \right) \frac{\partial u^2}{\partial y} \right\} + \frac{\partial}{\partial y} \left\{ \frac{\mu}{Pr} (Le-1) \right.\right.$$

$$\left.\left. \left(\frac{1}{c_1 + \frac{1}{r-1}} \right) (H-u^2) \right\} \right] \tag{2.11}$$

Where $\beta = \frac{\gamma-1}{\gamma}$

$$\frac{\partial c_i}{\partial t} + u \frac{\partial c_i}{\partial x} + v \frac{\partial c_i}{\partial y} = - \frac{1}{Re_{\infty,L^*}} \frac{1}{\rho} \frac{\partial}{\partial y} \left(\frac{Le}{Pr} \mu \frac{\partial c_i}{\partial y} \right) \tag{2.12}$$

and

$$p = \bar{m} \rho T \tag{2.13}$$

$$\mu = \mu(c_i, T) \tag{2.14}$$

where $\bar{m} = \Sigma . c_i \frac{m_A^*}{m_i^*}$

$s = m_A^*/m_1^*$

$\beta = \frac{\gamma-1}{\gamma}$

$$Re_{\infty,L^*} = \frac{u_\infty^* \rho_\infty^* L^*}{\mu_\infty^*}$$

$$Pr = \frac{\mu^* c_p^*}{k^*}$$

$$Le = \frac{\rho^* D_{12}^* c_p^*}{k^*}$$

The details of simplifications employed in obtaining equations (2.9) and (2.11) are given in Appendix A.

2.2 Transformations of the Governing Equations :

The governing equations are now transformed to bring them to a form suitable for numerical solution. First we introduce a stream function, ψ, defined by

$$\rho u = \frac{\partial \psi}{\partial y} \tag{2.15}$$

and the Dorodnitsyn-Howarth transformation

$$\bar{x} = x \tag{2.16a}$$

$$\bar{y} = \int_{y_b}^{y} \rho \, dy \tag{2.16b}$$

$$\bar{t} = t \tag{2.16c}$$

Now for any function $\zeta(x,y,t)$ we obtain the following relations:

$$\frac{\partial \zeta}{\partial x} = \frac{\partial \zeta}{\partial \bar{x}} + \frac{\partial \bar{y}}{\partial x} \frac{\partial \zeta}{\partial \bar{y}} \tag{2.17a}$$

$$\frac{\partial \zeta}{\partial y} = \rho \frac{\partial \zeta}{\partial \bar{y}} \tag{2.17b}$$

$$\frac{\partial \zeta}{\partial t} = \frac{\partial \bar{y}}{\partial t} \frac{\partial \zeta}{\partial \bar{y}} + \frac{\partial \zeta}{\partial \bar{t}} \tag{2.17c}$$

Then Equations (2.15) and (2.8) reduces to

$$u = \frac{\partial \psi}{\partial \bar{y}} \tag{2.18}$$

$$v = -\frac{1}{\rho} \left(\frac{\partial \psi}{\partial \bar{x}} + \frac{\partial \bar{y}}{\partial x} \frac{\partial \psi}{\partial \bar{y}} + \frac{\partial \bar{y}}{\partial \bar{t}}\right) \tag{2.19}$$

With the help of relations (2.16) through (2.19), equations (2.9), (2.11) and (2.12) can be written as :

$$\frac{\partial^2 \psi}{\partial \bar{y} \partial \bar{t}} + \frac{\partial \psi}{\partial \bar{y}} \frac{\partial^2 \psi}{\partial \bar{x} \partial \bar{y}} - \frac{\partial \psi}{\partial \bar{x}} \frac{\partial^2 \psi}{\partial \bar{y}^2} = -\frac{\beta}{2} \frac{1}{p} \frac{\partial p}{\partial \bar{x}} \left[H - \left(\frac{\partial \psi}{\partial \bar{y}}\right)^2\right] \left[\frac{1 + c_1(s-1)}{1 + c_1(r-1)}\right]$$

$$+ \frac{1}{Re_{\infty,L^*}} \frac{\partial}{\partial \bar{y}} \left(\lambda C p \frac{\partial^2 \psi}{\partial \bar{y}^2}\right) \tag{2.20}$$

$$\frac{\partial H}{\partial \bar{t}} + \frac{\partial \psi}{\partial \bar{y}} \frac{\partial H}{\partial \bar{x}} - \frac{\partial \psi}{\partial \bar{x}} \frac{\partial H}{\partial \bar{y}} = \beta \frac{1}{p} \frac{\partial p}{\partial \bar{t}} \left[H - \left(\frac{\partial \psi}{\partial \bar{y}}\right)^2\right] \left[\frac{1 + c_1(s-1)}{1 + c_1(r-1)}\right]$$

$$+ \frac{1}{Re_{\infty,L^*}} \left[\frac{\partial}{\partial \bar{y}} \left(\frac{\lambda C p}{Pr} \frac{\partial H}{\partial \bar{y}}\right) + 2 \frac{\partial}{\partial \bar{y}} \left\{\frac{\lambda C p}{Pr} (Pr-1) \frac{\partial \psi}{\partial \bar{y}} \frac{\partial^2 \psi}{\partial \bar{y}^2}\right\}\right.$$

$$\left. + \frac{\partial}{\partial \bar{y}} \left\{\frac{\lambda C p}{Pr} (Le-1) \left(\frac{r-1}{c_1(r-1)+1}\right) \left(H - \left(\frac{\partial}{\partial \bar{y}}\right)^2\right) \frac{\partial c_1}{\partial \bar{y}}\right\}\right] \tag{2.21}$$

$$\frac{\partial c_i}{\partial \bar{t}} + \frac{\partial \psi}{\partial \bar{y}} \frac{\partial c_i}{\partial \bar{x}} - \frac{\partial \psi}{\partial \bar{x}} \frac{\partial c_i}{\partial \bar{y}} = \frac{1}{Re_{\infty,L^*}} \frac{\partial}{\partial \bar{y}} \left(\frac{\lambda C p}{Pr} Le \frac{\partial c_i}{\partial \bar{y}}\right) \tag{2.22}$$

where $\bar{C} = \mu\rho$.

For homogeneous injection

$$\mu = C\ T \tag{2.23}$$

$$p = \rho T \tag{2.24}$$

and $$\mu\rho = C\ p \tag{2.25}$$

where C is the Chapman-Rubesin linear viscosity constant and is given by

$$C = T_b^{1/2} \left[\frac{1 + S^*/T_\infty^*}{T_b + S^*/T_\infty^*} \right] \tag{2.26}$$

The values of S^* in the above relation is taken as 110^oK.

With heterogeneous injection

$$\mu\rho = \lambda\ C\ p \tag{2.27}$$

where $\lambda = \frac{\bar{C}}{C\ p}$ and has a value of unity for air injection or no injection case. At this stage we introduce the normalised pressure function

$$\bar{p}(x,t) = \frac{p(x,t)}{p_o\ \bar{x}} \tag{2.28}$$

and change $\bar{x}$, $\bar{y}$, $\bar{t}$ to $\bar{\bar{x}}$, η, $\bar{\bar{t}}$ defined by

$$\bar{\bar{x}} = \bar{x} \tag{2.29a}$$

$$\eta = \frac{\bar{y}}{2(p_o\ \bar{x}\ \bar{\bar{x}})^{1/2}} \left(\frac{Re_{\infty,L^*}}{C}\right)^{1/2} \tag{2.29b}$$

and $$\bar{\bar{t}} = \bar{t} \tag{2.29c}$$

Noting that $\bar{x} = \bar{x}_{L*}\, x^{-1/2}$, where

$$\bar{x}_{L*} = M_\infty^3 \left(\frac{C}{Re_{\infty,L*}}\right)^{1/2} \tag{2.30}$$

is the interaction parameter evaluated at the edge of the wedge, we can write

$$\eta = A\, \bar{y}\, \bar{x}^{-\frac{1}{4}} \tag{2.31}$$

where

$$A = \frac{1}{2} \left(\frac{Re_{\infty,L*}}{C\, p_o\, \bar{x}_{L*}}\right)^{1/2} \tag{2.32}$$

is a constant. For any function $\zeta(\bar{x},\bar{y},\bar{t})$ we have

$$\frac{\partial \zeta}{\partial \bar{x}} = \frac{\partial \zeta}{\partial \bar{\bar{x}}} - \frac{\eta}{4\bar{\bar{x}}} \frac{\partial \zeta}{\partial \eta} \tag{2.33a}$$

$$\frac{\partial \zeta}{\partial \bar{y}} = A\, \bar{\bar{x}}^{-\frac{1}{4}} \frac{\partial \zeta}{\partial \eta} \tag{2.33b}$$

$$\frac{\partial \zeta}{\partial \bar{t}} = \frac{\partial \zeta}{\partial \bar{\bar{t}}} \tag{2.33c}$$

Further we define

$$f(\bar{\bar{x}}, \eta, \bar{\bar{t}}) = A\, \bar{\bar{x}}^{-\frac{1}{4}}\, \psi(\bar{x},\bar{y},\bar{t})$$

or,
$$\psi = \frac{1}{A\, \bar{\bar{x}}^{-1/4}}\, f \tag{2.34}$$

Now using expressions (2.33) and (2.34) in (2.20), (2.21) and (2.22) we get

$$4\bar{\bar{x}}\frac{\partial^2 f}{\partial \bar{\bar{t}}\partial\eta} + 4\bar{\bar{x}}\left(\frac{\partial f}{\partial\eta}\frac{\partial^2 f}{\partial\bar{\bar{x}}\partial\eta} - \frac{\partial f}{\partial\bar{\bar{x}}}\frac{\partial^2 f}{\partial\eta^2}\right) - f\frac{\partial^2 f}{\partial\eta^2} - \bar{p}\frac{\partial}{\partial\eta}\left(\lambda\frac{\partial^2 f}{\partial\eta^2}\right)$$

$$+ \beta\left(\frac{2\bar{\bar{x}}}{\bar{p}}\frac{\partial\bar{p}}{\partial\bar{\bar{x}}} - 1\right)\left[H - \left(\frac{\partial f}{\partial\eta}\right)^2\right]\left[\frac{1 + c_1(s-1)}{1 + c_1(r-1)}\right] = 0 \qquad (2.35)$$

$$4\bar{\bar{x}}\frac{\partial H}{\partial\bar{\bar{t}}} + 4\bar{\bar{x}}\left(\frac{\partial f}{\partial\eta}\frac{\partial H}{\partial\bar{\bar{x}}} - \frac{\partial H}{\partial\eta}\frac{\partial f}{\partial\bar{\bar{x}}}\right) - f\frac{\partial H}{\partial\eta} - 4\beta\frac{\bar{\bar{x}}}{\bar{p}}\frac{\partial\bar{p}}{\partial\bar{\bar{t}}}\left[H-\left(\frac{\partial f}{\partial\eta}\right)^2\right]$$

$$\left[\frac{1 + c_1(s-1)}{1 + c_1(r-1)}\right] - \bar{p}\left[\frac{\partial}{\partial\eta}\left(\frac{\lambda}{Pr}\frac{\partial H}{\partial\eta}\right) + 2\frac{\partial}{\partial\eta}\left\{\frac{\lambda}{Pr}(Pr-1)\right.\right.$$

$$\left.\left.\frac{\partial f}{\partial\eta}\frac{\partial^2 f}{\partial\eta^2}\right\}\right] - \bar{p}\frac{\partial}{\partial\eta}\left[\frac{\lambda}{Pr}(Le-1)\left\{\frac{r-1}{c_1(r-1)+1}\right\}\right.$$

$$\left.\left\{H - \left(\frac{\partial f}{\partial\eta}\right)^2\right\}\frac{\partial c_1}{\partial\eta}\right] = 0 \qquad (2.36)$$

$$4\bar{\bar{x}}\frac{\partial c_i}{\partial t} + 4\bar{\bar{x}}\left(\frac{\partial f}{\partial\eta}\frac{\partial c_i}{\partial\bar{\bar{x}}} - \frac{\partial f}{\partial\bar{\bar{x}}}\frac{\partial c_i}{\partial\eta}\right) - f\frac{\partial c_i}{\partial\eta} - \bar{p}\frac{\partial}{\partial\eta}\left(\frac{\lambda}{Pr}Le\frac{\partial c_i}{\partial\eta}\right) = 0$$

(2.37)

The co-ordinates x and t have not been distorted in the transformations. This facilitates the retrieval of physically significant results from the solutions of the transformed equations. The distortion of the co-ordinate normal to the surface provides a uniform computational domain as the boundary layer thickness varies from a very small value (close to the leading edge) to a fairly large value at the

weak-interaction region. Thus we can write equations (2.35) through (2.37) in the form :

$$4x \frac{\partial^2 f}{\partial t \partial \eta} + 4x \left(\frac{\partial f}{\partial \eta} \frac{\partial^2 f}{\partial x \partial \eta} - \frac{\partial^2 f}{\partial \eta^2} \frac{\partial f}{\partial x}\right) - f \frac{\partial^2 f}{\partial \eta^2} - \bar{p} \frac{\partial}{\partial \eta} \left(\lambda \frac{\partial^2 f}{\partial \eta^2}\right)$$

$$+ \beta \left(\frac{2x}{\bar{p}} \frac{\partial \bar{p}}{\partial x} - 1\right) \left[H - \left(\frac{\partial f}{\partial \eta}\right)^2\right] \left[\frac{1 + c_1(s-1)}{1 + c_1(r-1)}\right] = 0 \qquad (2.38)$$

$$4x \frac{\partial H}{\partial t} + 4x \left(\frac{\partial f}{\partial \eta} \frac{\partial H}{\partial x} - \frac{\partial H}{\partial \eta} \frac{\partial f}{\partial x}\right) - f \frac{\partial H}{\partial \eta} - 4\beta \frac{x}{\bar{p}} \frac{\partial \bar{p}}{\partial t} \left[H - \left(\frac{\partial f}{\partial \eta}\right)^2\right]$$

$$\left[\frac{1 + c_1(s-1)}{1 + c_1(r-1)}\right] - \bar{p} \frac{\partial}{\partial \eta} \left[\frac{\lambda}{Pr} \left[\frac{\partial H}{\partial \eta} + 2(Pr-1) \frac{\partial f}{\partial \eta} \frac{\partial^2 f}{\partial \eta^2}\right.\right.$$

$$\left.\left. + (Le-1) \left\{\frac{r-1}{c_1(r-1)+1}\right\} \left\{H - \left(\frac{\partial f}{\partial \eta}\right)^2\right\} \frac{\partial c_1}{\partial \eta}\right]\right] = 0 \qquad (2.39)$$

$$4x \frac{\partial c_i}{\partial t} + 4x \left(\frac{\partial f}{\partial \eta} \frac{\partial c_i}{\partial x} - \frac{\partial f}{\partial x} \frac{\partial c_i}{\partial \eta}\right) - f \frac{\partial c_i}{\partial \eta} - \bar{p} \frac{\partial}{\partial \eta} \left(\frac{\lambda}{Pr} Le \frac{\partial c_i}{\partial \eta}\right) = 0 \qquad (2.40)$$

where $\bar{p} = \bar{p}(x,t)$ is given by the expression (2.51) given in next section.

In the next section we discribe the equations required for interaction with the flow in the external layer.

2.3 The Interaction Equations :

For the unsteady flow over a flat plate inclined at a small angle θ_b to the main flow, the "effective body" shape is given by

$$y_e^*(x^*,t^*) = \theta_b\, x^* + \Delta^*(x^*,t^*) \tag{2.41}$$

The normal velocity component at the edge of this effective body is given by equation (1.10)

$$w^*(x^*,t^*) = u_e^* \left[\theta_b + \frac{\partial \Delta^*}{\partial x^*}\right] + \frac{\partial \Delta^*}{\partial t^*} \tag{2.42}$$

Here $\Delta^*(x^*,t^*)$ is the displacement thickness of the unsteady boundary layer, given by Moore and Ostrach [55]. At high speeds the displacement and boundary layer thickness are approximately same. With the present notation the differential equation for Δ^* becomes

$$\frac{\partial}{\partial x^*}\left[\rho_e^* u_e^* \Delta^* - \int_{y_b^*}^{y_e^*} (\rho_e^* u_e^* - \rho^* u^*)\, dy^*\right] + \frac{\partial}{\partial t^*}\left[\rho_e^* \Delta^* - \int_{y_b^*}^{y_e^*} (\rho_e^* - \rho^*)\, dy^*\right] = 0 \tag{2.43}$$

Using the continuity for the external flow

$$\frac{\partial \rho_e^*}{\partial t^*} + \frac{\partial}{\partial x^*}(\rho_e^* u_e^*) = 0 \tag{2.44}$$

equation (2.43) may be simplified to :

$$\rho_e^*\left[\frac{\partial \Delta^*}{\partial t^*} + u_e^* \frac{\partial \Delta^*}{\partial x^*}\right] = \frac{\partial}{\partial x^*}\left[\rho_e^* u_e^* \int_{y_b^*}^{y_e^*} \left(1 - \frac{\rho^* u^*}{\rho_e^* u_e^*}\right) dy^*\right] + \frac{\partial}{\partial t^*}\left[\rho_e^* \int_{y_b^*}^{y_e^*} \left(1 - \frac{\rho^*}{\rho_e^*}\right) dy^*\right] \tag{2.45}$$

Applying the transformations of the last section on the two integrals appearing equation (2.45) it is seen that

$$\int_{y_b^*}^{y_e^*} \left(1 - \frac{\rho^* u^*}{\rho_e^* u_e^*}\right) dy^* \approx \int_{y_b^*}^{y_e^*} \left(1 - \frac{\rho^*}{\rho_e^*}\right) dy^* \qquad (2.46)$$

$$\approx \frac{(\gamma-1)L^*(\bar{x}_{L^*})^{1/2}}{\sqrt{p_o}\, M_\infty} \frac{x^{3/4}}{\bar{p}} \int_o^\infty \left[\frac{1 + c_1(s-1)}{1 + c_1(r-1)}\right]\left[H - \left(\frac{\partial f}{\partial \eta}\right)^2\right] d\eta \qquad (2.47)$$

where terms of $O(\bar{M}_\infty^{-2})$ have been neglected from the integrand of the last integral. Writing δ^* for both the integrals in equation (2.45) and using (2.44) once again, we get

$$\frac{\partial \Delta^*}{\partial t^*} + u_e^* \frac{\partial \Delta^*}{\partial x^*} = \frac{\partial \delta^*}{\partial t^*} + u_e^* \frac{\partial \delta^*}{\partial x^*} \qquad (2.48)$$

A further simplification is obtained if u_e^* is replaced by u_∞^*. This is consistent with Stewartson [5] and Goldsworthy [56] that

$$u_e = \frac{u_e^*}{u_\infty^*} = 1 + O(\bar{M}_\infty^{-2})$$

Finally we get from (2.42) and (2.48), after non-dimensionalising,

$$K(x,t) = M_\infty(\theta_b + \frac{\partial \delta}{\partial x} + \frac{\partial \delta}{\partial t}) \qquad (2.49)$$

and

$$\delta(x,t) = \frac{\delta^*}{L^*} = \frac{\gamma-1}{\sqrt{p_o}} \frac{\sqrt{\bar{x}_{L^*}}}{M_\infty} \frac{x^{3/4}}{\bar{p}} \int_o^\infty \left[\frac{1+c_1(s-1)}{1+c_1(r-1)}\right]\left[H - \left(\frac{\partial f}{\partial \eta}\right)^2\right] d\eta \qquad (2.50)$$

where $\bar{p} = \dfrac{p}{p_o \bar{x}}$

$$= \frac{1}{p_o \bar{x}} \left[1 + \gamma K \left[\frac{\gamma+1}{4} K + \{ (\frac{\gamma+1}{4} K)^2 + 1 \}^{1/2} \right] \right] \quad (2.51)$$

For flows involving surface mass transfer, displacement thickness Δ^* or the boundary layer thickness δ^* should be replaced by their effective values [57] :

$$\Delta^*_{eff} = \Delta^* + \int_o^{x^*} \frac{\rho_b^* v_b^*}{\rho_e^* u_e^*} dx^* \quad (2.52)^*$$

$$\delta^*_{eff} = \delta^* + \int_o^{x^*} \frac{\rho_b^* v_b^*}{\rho_e^* u_e^*} dx^* \quad (2.53)^*$$

where Δ^* and δ^* are the values without surface mass transfer.

The last terms of the above equations are due to the injected mass flow at the surface. Now from the equation of state (2.6), for the quantities across the boundary layer we may write :

$$\frac{\rho_b^*}{\rho_e^*} = \frac{T_e^*}{T_b^*} \quad (2.54)$$

From the hypersonic assumption of equation (1.3) we also have

$$\frac{H_e^*}{\frac{1}{2} u_\infty^{*2}} \approx 1 \text{ implying that } T_e^* \approx 0. \text{ More appropriately,}$$

it is implied that $T_e^*/T_b^* << 1$. Therefore, the contribution from the surface mass transfer effect may be neglected in equations (2.52) and (2.53) at hypersonic speeds.

* added for completeness

2.4 Boundary and Initial Conditions

The boundary conditions in η are given by the conditions on the wedge surface and at the outer edge of the boundary layer. On the surface of the wedge the streamwise component of velocity is zero and the wedge is either insulated or held at a constant temperature. Thus,

at $y^* = y_b^*$

$$u^* = 0 \tag{2.55a}$$

$$v^* = v_b^*(x^*) \tag{2.55b}$$

$$c_1 = c_{1b}(x^*) \tag{2.55c}$$

$$\frac{\partial T^*}{\partial y^*} = 0 \quad \text{(for insulated wedge surface)} \tag{2.55d}$$

or

$$T^* = T_b^* = \text{constant (for constant temperature wedge surface)} \tag{2.55e}$$

For a given problem, $v_b^*(x^*)$ and $c_{1b}(x^*)$ are related to each other. Eckert has suggested that the convective and molecular transport terms for air must be balanced at the surface with foreign gas injection. Thus, for a zero net flux of the free-stream gas, namely, air at the surface, Eckert proposed the following relation between $v_b^*(x^*)$ and $c_{1b}(x^*)$ for a physically realistic solution from the aerodynamic point of view :

$$(\rho^* v^*)_b = - \left[\frac{\rho^* D_{12}^*}{1 - c_1} \frac{\partial c_1}{\partial y^*} \right]_b$$

In terms of the transformed variables we have

at $\eta = 0$

$$\frac{\partial f}{\partial \eta} = 0 \tag{2.56a}$$

$$f + 4x \frac{\partial f}{\partial x} = - \rho_b v_b(x) \frac{2 \sqrt{Re_{\infty,L^*}}}{\sqrt{C p_o}} \frac{\sqrt{x}}{\sqrt{\bar{x}}} \tag{2.56b}$$

$$\frac{\partial c_1}{\partial \eta} = \left(\frac{Pr}{\mu Le}\right) (1-c_1) \frac{C p_o}{\rho_b} \bar{x} \left(f + 4x \frac{\partial f}{\partial x}\right) \tag{2.56c}$$

$$\frac{\partial H}{\partial \eta} = 0 \tag{2.56d}$$

or

$$H_b(x) = \frac{c^*_{pb}(x) T^*_b}{\frac{1}{2} u^{*2}_\infty} = \left[r c_{1b} + (1-c_{1b}) \right] \frac{2T_b}{(\gamma-1) M^2_\infty} \tag{2.56e}$$

where T_b is the constant wall temperature and $r = c^*_{p_1}/c^*_{p_2}$.

At the edge of the boundary layer the tangential velocity and the total enthalpy should match with the corresponding quantities in the external layer and the injected species concentration vanishes. Thus

at $y^* = y^*_e$

$$u^* = u^*_e \tag{2.57a}$$

$$H^* = H^*_e \tag{2.57b}$$

$$c_1 = 0 \tag{2.57c}$$

In terms of the transformed variables we have

at $\eta \to \infty$

$$\frac{\partial f}{\partial \eta} = 1 \qquad (2.58a)$$

$$H = 1 \qquad (2.58b)$$

$$c_1 = 0 \qquad (2.58c)$$

where terms of order M_∞^{-2} have been neglected.

In addition to the above conditions, in the normal direction, the initial conditions in x and t are also required. These are discussed in chapters III, V and VII.

In boundary layer calculations it is customary to satisfy the conditions (2.58) at a finite value $\eta = \eta_e$. The value of η_e is chosen sufficiently large such that in the resulting computations $|f'(\eta_e) - 1| \leq 10^{-4}$ and $|H(\eta_e)-1| \leq 10^{-4}$. From experimental executions a value of $\eta_e = 5.5$ is found to be sufficient to suffice this condition.

CHAPTER III

THE STEADY FLOW ON AN INCLINED FLAT PLATE WITH HOMOGENEOUS INJECTION

3.1 Introduction

Equations (2.38) through (2.40) may be specialised for the steady hypersonic flow on a flat plate inclined at a small angle θ_b to the free stream and with air injection on the flat surface. With air injection the equation of state takes the form given by equation (2.24) and the viscosity law is given by equation (2.23). They are

$$p = \rho T$$

and $$\mu = c\ T$$

Thus the momentum equation (2.38) and energy equation (2.39) become

$$\bar{p}\ \frac{\partial^3 f}{\partial \eta^3} + f\ \frac{\partial^2 f}{\partial \eta^2} - 4x\left(f'\frac{\partial f'}{\partial x} - \frac{\partial f}{\partial x}\ \frac{\partial^2 f}{\partial \eta^2}\right) = \beta\left[\frac{2x}{\bar{p}}\ \frac{d\bar{p}}{dx} - 1\right]\left[H - \left(\frac{\partial f}{\partial \eta}\right)^2\right] \tag{3.1}$$

and

$$\frac{\bar{p}}{Pr}\ \frac{\partial^2 H}{\partial \eta^2} + f\ \frac{\partial H}{\partial \eta} - 4x\left(\frac{\partial f}{\partial \eta}\ \frac{\partial H}{\partial x} - \frac{\partial H}{\partial \eta}\ \frac{\partial f}{\partial x}\right)$$

$$= \frac{\bar{p}}{Pr}\ 2(1-Pr)\left[\left(\frac{\partial^2 f}{\partial \eta^2}\right)^2 + \frac{\partial f}{\partial \eta}\ \frac{\partial^3 f}{\partial \eta^3}\right] \tag{3.2}$$

For this case $\bar{p} = \bar{p}(x)$ is given by (2.51) with

$$K(x) = M_\infty(\theta_b + \frac{d\delta}{dx}) \qquad (3.3)$$

and $\delta = \delta(x)$ given by (2.50). Equations (3.1) and (3.2) are the same as those given in ref. [58] for the no-injection case.

3.2 Boundary and Initial Conditions

The boundary conditions for this problem may be obtained by taking $c_{1b}(x) = 0$ in equations (2.56) and (2.58). Then equation (2.56c) can be dropped and (2.56e) becomes:

$$H = H_b = \text{constant}$$

For obtaining the initial condition in x, a series expansion solution is given in the next section.

3.3 Series Expansion Solution

In this section a scheme for solving the steady strong interaction case by series expansion is described. Making use of proper expansions [2] for $\bar{p}, \delta, f$ and H in terms of the interaction parameter $\bar{\chi}$ and $k_b (= M_\infty \theta_b)$ the partial differential equations (3.1) and (3.2) are reduced to a sequence of ordinary differential equations. The unknown constants appearing in the expansion of p, δ, etc. are then determined from the solution of these ordinary differential equations in accordance with the tangent-wedge equation. In this section solutions for terms upto third order are carried out for arbitrary but a constant value of Pr.

For the steady problem $\bar{p} = \bar{p}(x)$ is given by the tangent-wedge approximation of equation (2.51) :

$$\bar{p} = \frac{1}{p_o \bar{\chi}} \left[1 + \gamma K \left[\frac{\gamma+1}{4} K + \left\{ \left(\frac{\gamma+1}{4} K \right)^2 + 1 \right\}^{1/2} \right] \right]$$

with $K(x) = M_\infty (\theta_b + \frac{d\delta}{dx})$

and $\delta = \delta(x)$ is given by (2.50). If we define a constant k_b

$$k_b = M_\infty \theta_b \tag{3.4}$$

then

$$K(x) = k_b + M_\infty \frac{d\delta}{dx} \tag{3.5}$$

For large values of $K(x)$ the above expression for $\bar{p}$ gives (see equation (1.5))

$$\bar{p} = \frac{1}{p_o \bar{\chi}} \left[\frac{\gamma(\gamma+1)}{2} K^2 + \frac{3\gamma+1}{\gamma+1} - \frac{8\gamma}{(\gamma+1)^3} K^{-2} + O(K^{-4}) \right]$$

For the strong interaction region ($\bar{\chi} >> 1$) an order of magnitude analysis [2] shows that

$$M_\infty \frac{\delta}{x} \propto \bar{\chi}^{1/2} \tag{3.6}$$

or

$$M_\infty \frac{d\delta}{dx} \propto \bar{\chi}^{1/2} \tag{3.7}$$

Writing $K(x) = k_b + \text{constant } \bar{\chi}^{1/2}$ and substituting in the expansion (1.5) for p for large value of K, we have for $\bar{\chi} >> 1$

$$\bar{p}(x) = p_o \bar{\chi} \left[1 + \frac{p_1 k_b}{\bar{\chi}^{1/2}} + \frac{p_2 + p_3 k_b^2}{\bar{\chi}} + O(\bar{\chi}^{-3/2}) \right] \tag{3.8}$$

where $p_i (i=0,1,2,3)$ are constants to be determined.

Consistent with (3.8) we have for δ

$$\frac{\delta(x)}{x} = \frac{\delta_o \bar{x}^{1/2}}{M_\infty} \left[1 + \frac{\delta_1 k_b}{\bar{x}^{1/2}} + \frac{\delta_2 + \delta_3 k_b^2}{\bar{x}} + O(\bar{x}^{-3/2}) \right] \qquad (3.9)$$

where $\delta_i (i=0,1,2,3)$ are constants.

In view of the expansions (3.8) and (3.9), Lees and Probstein [1] suggested the following expansions for f and H:

$$f(x,\eta) = f_o(\eta) + \frac{f_1(\eta) k_b}{\bar{x}^{1/2}} + \frac{f_2(\eta) + f_3(\eta) k_b^2}{\bar{x}} + O(\bar{x}^{-3/2}) \qquad (3.10)$$

and

$$H(x,\eta) = H_o(\eta) + \frac{H_1(\eta) k_b}{\bar{x}^{1/2}} + \frac{H_2(\eta) + H_3(\eta) k_b^2}{\bar{x}} + O(\bar{x}^{-3/2}) \qquad (3.11)$$

Using the expansion (3.10), we may also write

$$f + 4x \frac{\partial f}{\partial x} = f_o(\eta) + \frac{f_1(\eta) k_b}{\bar{x}^{1/2}} + \frac{f_2(\eta) + f_3(\eta) k_b^2}{\bar{x}} + \cdots$$

$$+ \frac{f_1(\eta) k_b}{\bar{x}^{1/2}} + 2 \left[\frac{f_2(\eta) + f_3(\eta) k_b^2}{\bar{x}} \right] + \cdots$$

Hence from (2.56b) for the steady problem we can obtain:

$$- \rho v \frac{Re_{\infty,L^*}^{1/2}}{\sqrt{C p_o}} \frac{x^{1/2}}{\bar{x}^{1/2}} = \frac{1}{2} \left[f_o(\eta) + 2 \frac{f_1(\eta) k_b}{\bar{x}^{1/2}} + 3 \frac{f_2(\eta) + f_3(\eta) k_b^2}{\bar{x}} + \cdots \right]$$

so that

$$- \rho_b v_b \frac{Re_{\infty,x^*}^{1/2}}{\sqrt{C p_o \bar{x}}} = \frac{1}{2} \left[f_o(0) + \frac{2 f_1(0) k_b}{\bar{x}^{1/2}} + 3 \frac{f_2(0) + f_3(0) k_b^2}{\bar{x}} + \cdots \right] \qquad (3.12a)$$

The equation (3.12a) gives the required form of the surface mass flux $\rho_b v_b$ so that for $\bar{x} \to \infty$ similarity structure of the solution is obtained. This, injection/suction is performed according to the relationship :

$$\frac{\rho_b v_b}{\sqrt{C\ \rho_o}} \frac{Re_{\infty,x^*}^{1/2}}{\bar{x}^{1/2}} = \alpha + \frac{\alpha_o}{\bar{x}^{1/2}} + \frac{\alpha_1}{\bar{x}} + \ldots \qquad (3.12b)$$

where α, α_o, α_1,... are all constants of order unity.

If we consider the special case $\alpha_n = 0$ for $n = 0,1,2,\ldots$, then

$$f_o(0) = -2\alpha \qquad (3.13a)$$

$$f_1(0) = f_2(0) = f_3(0) = 0 \qquad (3.13b)$$

We can also rewrite (3.12b) as

$$v_b = \frac{\sqrt{C\ p_o}}{\rho_o} \frac{\bar{x}^{1/2}}{\sqrt{Re_{\infty,x^*}}} \left[\alpha + \frac{\alpha_o}{\bar{x}^{1/2}} + \frac{\alpha_1}{\bar{x}} + \ldots \right] \qquad (3.12c)$$

$$v_b = \left[\frac{\sqrt{C\ p_o}}{\rho_b} \frac{\bar{x}^{1/2}}{\sqrt{Re_{\infty,x^*}}} \right] \alpha = (v_b)_o \text{ with } \alpha_n = 0 \qquad (3.12d)$$

Thus, in seeking the series solution, v_b should be of the form given by equations (3.12c) or (3.12d). However, a [illegible] form of v_b, used with the numerical solution of non-similar equations (3.1) and (3.2) can be of the type given below :

$$v_b = (v_b)_o + K_1 (\bar{x}_1 - \bar{x}) \qquad (3.12e)$$

With $Re_{\infty,x^*} \sim O(10^5)$ the normal velocity in equation (3.12c) or (3.12d) will be small relative to the tangential velocity as long as $\alpha \sim O(1)$. The value of $\bar{x}$ at the beginning of the strong interaction region is $\sim O(10^2)$. For this value of $\bar{x}$, it is noted that $(\delta/x)^2 \ll 1$. Thus, the boundary layer approximations are valid in the hypersonic flow as long as this condition is met [74].

where K_1 is a constant of $O(10^{-6})$. In terms of the dimensionless stream function eq. (3.12e) may be written as

$$\left(f + 4x \frac{\partial f}{\partial x}\right)_b = -2\alpha - \frac{2K_1}{\sqrt{C\, p_o}} \rho_b \sqrt{Re_{\infty,x^*}} \left[\frac{\bar{x}_1 - \bar{x}}{\sqrt{\bar{x}}}\right] \qquad (3.13a)$$

or, after replacing the density by pressure with the help of the equation of state,

$$\left(f + 4x \frac{\partial f}{\partial x}\right)_b = -2\alpha - \frac{4K_1}{(\gamma-1)} \frac{\sqrt{p_o}\, M_\infty\, \bar{p}}{H_b} \left[\frac{\bar{x}_1 - \bar{x}}{\sqrt{\bar{x}}}\right] \qquad (3.13b)$$

Next, the x-derivatives of δ can be obtained from (3.9). Then from (3.5) we can get $K(x)$. Using this $K(x)$ in (1.5) and then comparing with (3.8), we can obtain the following relations between the two sets of constants $\delta_i (i=0,1,2,3)$ and $p_i (i=0,1,2,3)$.

$$p_o = \frac{9}{32} (\gamma+1)\, \delta_o^2 \qquad (3.14a)$$

$$p_1 = \frac{8}{3} \left(\delta_1 + \frac{1}{\delta_o}\right) \qquad (3.14b)$$

$$p_2 = \frac{10}{3} \delta_2 + \frac{32}{9} \frac{3\gamma+1}{\gamma(\gamma+1)^2} \frac{1}{\delta_o^2} \qquad (3.14c)$$

$$p_3 = \frac{10}{3} \delta_3 + \frac{16}{9} \left(\delta_1 + \frac{1}{\delta_o}\right)^2 \qquad (3.14d)$$

On inserting the expansions (3.8), (3.10) and (3.11) in the equations (3.1) and (3.2) and equating the terms of the same order on the two sides we get the following sets of coupled ordinary differential equations for $f_i(\eta)$, $H_i(\eta)$ $(i=0,1,2,3)$:

$$f_o''' + f_o f_o'' + \beta(H_o - f_o'^2) = 0 \qquad (3.15a)$$

$$H_o'' + Prf_o H_o' - 2(1-Pr)\left[(f_o'')^2 + f_o' f_o'''\right] = 0 \qquad (3.15b)$$

$$f_1''' + f_o f_1'' - f_o' f_1' + 2f_o'' f_1 + \beta\,(H_1 - 2f_o' f_1')$$

$$= p_1\left[\tfrac{3}{2}\beta(H_o - f_o'^2) - f_o f_o''\right] \qquad (3.16a)$$

$$H_1'' + Prf_o H_1' - Prf_o' H_1 - 2(1-Pr)(f_o' f_1''' + 2f_o'' f_1'' + f_o''' f_1')$$

$$= -2PrH_o' f_1 + p_1 Prf_o H_o' \qquad (3.16b)$$

$$f_2''' + f_o f_2'' - 2f_o' f_2' + 3f_o'' f_2 + \beta(H_2 - 2f_o' f_2')$$

$$= p_2\left[2\beta(H_o - f_o'^2) + f_o f_o''\right] \qquad (3.17a)$$

$$H_2'' + Prf_o H_2' - 2Prf_o' H_2 - 2(1-Pr)\,(f_o' f_2''' + 2f_o'' f_2'' + f_o''' f_2')$$

$$= -3PrH_o' f_2 + p_2 Prf_o H_o' \qquad (3.17b)$$

$$f_3''' + f_o f_3'' - 2f_o' f_3' + 3f_o'' f_3 + \beta(H_3 - 2f_o' f_3')$$

$$= p_3\left[2\beta(H_o - f_o'^2) + f_o f_o''\right] - p_1^2\,\tfrac{\beta}{2}\,(H_o - f_o'^2)$$

$$+ p_1\left[\tfrac{\beta}{2}\,(H_1 - 2f_o' f_1') - f_1'''\right] - 2f_1 f_1'' + (1+\beta) f_1'^2 \qquad (3.18a)$$

$$H_3'' + Prf_o H_3' - 2Prf_o' H_3 + 3PrH_o' f_3$$

$$- 2(1-Pr)\,(f_o' f_3''' + 2f_o'' f_3'' + f_o''' f_3')$$

$$= p_3 Prf_o H_o' + p_1\left[2(1-Pr)(f_o' f_1''' + 2f_o'' f_1'' + f_o''' f_1') - H_1''\right]$$

$$+ 2(1-Pr)\left[f_1 f_1''' + (f_1'')^2\right] + Pr(f_1' H_1 - 2f_1 H_1') \qquad (3.18b)$$

Here primes denote differentiation with respect to η. In equations (3.16) through (3.18) the unknown constants $p_i (i = 1,2,3)$ occur in the inhomogeneous parts. To remove these unknowns we introduce a further change of variables following ref. [64]

$$\bar{f}_1 = \frac{f_1}{p_1}, \quad \bar{H}_1 = \frac{H_1}{p_1} \tag{3.19}$$

$$\bar{f}_2 = \frac{f_2}{p_2}, \quad \bar{H}_2 = \frac{H_2}{p_2} \tag{3.20}$$

$$\bar{f}_3 = (f_3 - p_3\bar{f}_2)/p_1^2, \quad \bar{H}_3 = (H_3 - p_3\bar{H}_2)/p_1^2 \tag{3.21}$$

From equations (3.16) through (3.18) one obtains the following differential equations for $\bar{f}_i(\eta)$ and $\bar{H}_i(\eta)$ $(i = 1,2,3)$:

$$L_i^{(1)}(\bar{f}_i) + \beta \bar{H}_i = F_i^{(1)}(\eta) \tag{3.22a}$$

$$L_i^{(2)}(\bar{H}_i) + L_i^{(3)}(\bar{f}_i) = F_i^{(2)}(\eta) \tag{3.22b}$$

The linear operators $L_i^{(j)}$ $(i,j=1,2,3)$ are given by

$$L_i^{(1)} = \frac{d^3}{d\eta^3} + f_o \frac{d^2}{d\eta^2} - (a_i+2\beta)f_o' \frac{d}{d\eta} + b_i f_o'' \tag{3.23}$$

$$L_i^{(2)} = \frac{d^2}{d\eta^2} + Prf_o \frac{d}{d\eta} - a_i Prf_o' \tag{3.24}$$

$$L_i^{(3)} = -2(1-Pr)\left(f_o' \frac{d^3}{d\eta^3} + 2f_o'' \frac{d^2}{d\eta^2} + f_o''' \frac{d}{d\eta}\right) + b_i PrH_o' \tag{3.25}$$

with $a_1 = 1$, $a_2 = a_3 = 2$, $b_1 = 2$, $b_2 = b_3 = 3$. The functions $F_i^{(1)}$, $F_i^{(2)}$ are given by

$$F_i^{(1)}(\eta) = d_i\beta(H_o - f_o'^2) + f_o''f_o \quad \text{for} \quad i=1,2 \tag{3.26}$$

$$F_i^{(1)}(\eta) = (\bar{f}_1'' - f_o'')(f_o - 2\bar{f}_1) - \bar{f}_1' \left[f_o' - (1+\beta)\bar{f}_1' \right]$$

$$+ \tfrac{3}{2}\beta(\bar{H}_1 - 2f_o'\bar{f}_1') - 2\beta(H_o - f_o'^2) \quad \text{for} \quad i=3 \tag{3.27}$$

$$F_i^{(2)}(\eta) = PrH_o'f_o \quad \text{for} \quad i=1,2 \tag{3.28}$$

$$F_i^{(2)}(\eta) = Pr(\bar{H}_1' - H_o')(f_o - 2\bar{f}_1) + Pr\bar{H}_1(\bar{f}_1' - f_o')$$

$$+ 2(1-Pr)\left[(\bar{f}_1'')^2 + \bar{f}_1\bar{f}_1''' \right] \quad \text{for} \quad i=3 \tag{3.29}$$

with $d_1 = 1.5$ and $d_2 = 2$.

The boundary conditions can be written as

$$f_o(0) = -2\alpha \tag{3.30a}$$

$$f_o'(0) = 0 \tag{3.30b}$$

$$H_o'(0) = 0 \text{ (for insulated surface)} \tag{3.30c}$$

or, $H_o(0) = H_b$ (for constant temperature surface) (3.30d)

$$f_o'(\eta_e) = 1 \tag{3.31a}$$

$$H_o(\eta_e) = 1 \tag{3.31b}$$

and for $\bar{f}_i$, $\bar{H}_i$ (i = 1,2,3)

$$\bar{f}_i(0) = 0 \tag{3.32a}$$

$$\bar{f}_i'(0) = 0 \tag{3.32b}$$

$$\bar{H}_i'(0) = 0 \text{ (for insulated surface)} \tag{3.32c}$$

or, $$\bar{H}_i(0) = 0 \text{ (for constant temperature surface)} \tag{3.32d}$$

$$\bar{f}_i(\eta_e) = 0 \tag{3.33a}$$

$$\bar{H}_i(\eta_e) = 0 \tag{3.33b}$$

In order to determine the unknown constants p_i, δ_i (i=0,1,2,3) we insert the expressions (3.8), (3.10) and (3.11) in (2.50) to obtain the following expressions for δ:

$$\frac{\delta(x)}{x} = \frac{\gamma-1}{(p_o)^{1/2}} \frac{\bar{x}^{1/2}}{M_\infty} \left[I_o + p_1(I_1-I_o) \frac{k_b}{\bar{x}^{1/2}} \right.$$

$$\left. + \{p_2(I_2-I_o) + [p_3(I_2-I_o) + p_1^2(I_3-I_1+I_o)] k_b^2\}/\bar{x} \right] \tag{3.34}$$

where $$I_o = \int_o^\infty (H_o - f_o'^2) d\eta \tag{3.35a}$$

$$I_1 = \int_o^\infty (\bar{H}_1 - 2f_o'\bar{f}_1') d\eta \tag{3.35b}$$

$$I_2 = \int_o^\infty (\bar{H}_2 - 2f_o'\bar{f}_2') d\eta \tag{3.35c}$$

$$I_3 = \int_0^\infty \left[\bar{H}_3 - 2f_0'\bar{f}_3' - (\bar{f}_1')^2\right] d\eta \qquad (3.35d)$$

On comparing (3.34) with (3.9) we get

$$\delta_0 = \frac{\gamma-1}{\sqrt{p_0}} I_0 \qquad (3.36a)$$

$$\delta_1 = p_1\left(\frac{I_1}{I_0} - 1\right) \qquad (3.36b)$$

$$\delta_2 = p_2\left(\frac{I_2}{I_0} - 1\right) \qquad (3.36c)$$

$$\delta_3 = p_3\left(\frac{I_2}{I_0} - 1\right) + p_1^2\left[\frac{(I_3 - I_1)}{I_0} + 1\right] \qquad (3.36d)$$

Using (3.36) and (3.14) the following expressions for p_i are obtained:

$$p_0 = \frac{3}{4}(\gamma-1)\left[\frac{\gamma(\gamma+1)}{2}\right]^{1/2} I_0 \qquad (3.37a)$$

$$p_1 = \frac{8\, p_0^{1/2}}{(\gamma-1)(11I_0 - 8I_1)} \qquad (3.37b)$$

$$p_2 = \frac{8(3\gamma+1)}{(\gamma^2-1)\left[2\gamma(\gamma+1)\right]^{1/2}(13I_0 - 10I_2)} \qquad (3.37c)$$

$$p_3 = \frac{p_1^2(40I_3 - 40I_1 + 43I_0)}{(52I_0 - 40I_2)} \qquad (3.37d)$$

The solution of ordinary differential equations (3.15a), (3.15b), (3.22a) and (3.22b) is obtained by the

shooting method of chapter IV. Except for the finite-difference approximations involved in the replacement of x-derivatives appearing in equations (3.1) and (3.2) whereby these partial differential equations are reduced to ordinary differential equations, the remaining procedure is similar to the one described there.

3.4 Solution of the Steady Problem

The series expansion solution discussed earlier has an error of order $\bar{\chi}^{3/2}$; and hence this solution is suitable only for high values of $\bar{\chi}$. Since $\bar{\chi}$ can be taken as small as unity, the solutions obtained from the series expansion method could be in error for such values of $\bar{\chi}$. In the present section a numerical method employing the complete tangent-wedge approximation of eq. (2.51) is presented. Since the complete tangent-wedge approximation is used, the obtained results are equally accurate for large and small values of $\bar{\chi}$.

For the method presented here it is required to specify the initial values of $f(x_1, \eta)$, $H(x_1, \eta)$ and $\bar{p}(x_1)$ on an initial line $x = x_1$. The values given by the series expansion solution on a line $x = x_1$ (with $x_1 = 1/1024$ corresponding to $\bar{\chi} \sim O(10^2)$) near the leading edge are used as the initial values. These initial values will be highly accurate due to the large value of $\bar{\chi}$ near the leading edge.

The initial conditions are, therefore

$$f(x_1,\eta) = f_o(\eta) + \frac{p_1\bar{f}_1(\eta)k_b}{\bar{x}_1^{1/2}} + \frac{p_2\bar{f}_2(\eta)+\left[p_3\bar{f}_2(\eta)+p_1^2\bar{f}_3(\eta)\right]k_b^2}{\bar{x}_1} \qquad (3.38a)$$

$$H(x_1,\eta) = H_o(\eta) + \frac{p_1\bar{H}_1(\eta)k_b}{\bar{x}_1^{1/2}} + \frac{p_2\bar{H}_2(\eta)+\left[p_3\bar{H}_2(\eta)+p_1^2\bar{H}_3(\eta)\right]k_b^2}{\bar{x}_1} \qquad (3.38b)$$

$$\bar{p}(x_1) = 1 + \frac{p_1k_b}{\bar{x}_1^{1/2}} + \frac{p_2+p_3k_b^2}{\bar{x}_1} \qquad (3.38c)$$

where $\bar{x}_1 = \bar{x}_L^*/\sqrt{x_1}$

The interaction between the boundary layer and the external layer is to be dealt with by an iterative procedure. Each iteration loop comprises of the two parts given below:

(i) First the governing equations (3.1) and (3.2) are solved for a given $\bar{p}(x)$ distribution, in the region $x_1 \leq x \leq 1$, $0 \leq \eta \leq \eta_e$ subject to the initial conditions (3.38a), (3.38b) and (3.38c) and the boundary conditions of section 3.2 and (3.13b).

(ii) Next a new $\bar{p}(x)$ distribution is obtained from the solutions $f(x,\eta)$, $H(x,\eta)$ of (i) making use of equations (2.50), (2.51), (3.5) and (3.38a), (3.38b) and (3.38c).

The steps (i) and (ii) are repeated until $\bar{p}(x)$ converges within a specified tolerance.

3.4a Solution of the Boundary Layer Equations

It can be observed from the series expansion solutions that the x-derivatives of different flow variables, f,H,$\bar{p}$, etc. are large for small values of x and the x-dependence decreases in the down stream direction. For the same degree of accuracy we can use larger step sizes toward the trailing edge. Here in this work the following arrangement of x-stations with step sizes increasing in a geometric progression is employed :

$$\Delta x_1 = x_1 \approx 0\ (10^{-3}) \tag{3.39a}$$

$$\Delta x_2 = 0\ (10^{-2}),\ x_2 = \Delta x_1 + \Delta x_2 \tag{3.39b}$$

$$\Delta x_j = x_j - x_{j-1} = k_x\ \Delta x_{j-1},\ j = 3,4,\ldots,J \tag{3.39c}$$

Here k_x is a constant greater than 1 and J is an integer such that $x_J = 1$.

In equations (3.1) and (3.2) the x-derivatives appear in the form $4x \frac{\partial \zeta}{\partial x}$. A finite difference formula for this term for the present arrangement of x-stations can be written as :

$$\left[4x \frac{\partial \zeta}{\partial x} \right]_j = D_j\ \zeta_j - (D_j + E_j)\ \zeta_{j-1} + E_j\ \zeta_{j-2},\quad j = 2,3,\ldots,J \tag{3.40}$$

where ζ_j represents $\zeta(x_j)$ and the coefficients D_j, E_j are given by :

$$D_j = 4x_j/\Delta x_j,\quad j = 2$$

$$= \frac{4(2k_x + 1)}{k_x+1} \frac{x_j}{\Delta x_j}, \quad j = 3,4,\ldots,J \qquad (3.41a)$$

$$E_j = 0, j = 2$$

$$= \frac{4k_x^2}{k_x+1} \frac{x_j}{\Delta x_j}, \quad j = 3,4,\ldots,J \qquad (3.41b)$$

Expressions (3.41a) and (3.41b) correspond to two-point backward difference formula for $j = 2$ and three-point backward difference formula for $j = 3,4,\ldots,J$.

Substituting (3.40) in (3.1) and (3.2), we get

$$\bar{p}_j f'''_j + f''_j \left[(1+D_j) f_j - (D_j+E_j) f_{j-1} + E_j f_{j-2} \right]$$

$$- f'_j \left[(D_j+Q_j) f'_j - (D_j+E_j) f'_{j-1} + E_j f'_{j-2} \right]$$

$$+ Q_j H_j = 0 \qquad (3.42)$$

and

$$\frac{\bar{p}_j}{Pr} H''_j + H'_j \left[(1+D_j) f_j - (D_j+E_j) f_{j-1} \right.$$

$$\left. + E_j f_{j-2} \right] - f'_j \left[D_j H_j - (D_j+E_j) H_{j-1} + E_j H_{j-2} \right]$$

$$+ 2 \bar{p}_j \frac{(Pr-1)}{Pr} \left[f''_j)^2 + f_j f'''_j \right] = 0 \qquad (3.43)$$

In equations (3.42) and (3.43) the prime represents differentiation with respect to η and the function $Q(x)$ is defined by

$$Q(x) = \beta \left[1 - \frac{2x}{\bar{p}} \frac{d\bar{p}}{dx} \right] \qquad (3.44)$$

At any station $x = x_j$, f_{j-1}, H_{j-1}, f_{j-2} and H_{j-2} are all known functions of η and $\bar{p}_j$, Q_j, D_j, E_j are known constants. Thus equations (3.42) and (3.43) form a set of coupled nonlinear ordinary differential equations for f_j and H_j of the form :

$$\beta_1 f''' + \beta_2 ff'' + \zeta_1(\eta)\, f'' + \beta_3 f'^2 + \zeta_2(\eta)\, f' + \beta_4 H = 0 \qquad (3.45)$$

$$\beta_5 H'' + \beta_6 fH' + \zeta_3(\eta)\, H' + \beta_7 f'H + \zeta_4(\eta)\, f' + \beta_8 \left[(f'')^2 + ff''' \right] = 0 \qquad (3.46)$$

where β's are known constants and the ζ's are known functions of η. The boundary conditions are :

$$f'_b = 0 \qquad (3.47a)$$

$$\left(f + 4x \frac{\partial f}{\partial x}\right)_b = -2\alpha - \frac{4K_1}{(\gamma-1)} \frac{\sqrt{p_o}\, M_\infty\, \bar{p}}{H_b} \left[\frac{\bar{x}_1 - \bar{x}}{\sqrt{\bar{x}}} \right] \qquad (3.47b)$$

$$H'_b = 0 \quad \text{or} \quad H_b = \text{constant} \qquad (3.47c)$$

$$f'(\eta_e) = H(\eta_e) = 1 \qquad (3.47d)$$

By solving the ordinary differential equation problem (3.45), (3.46), (3.47) at $x = x_2, x_3, \ldots, x_J$ we can generate a numerical solution of the partial differential equations (3.1) and (3.2) in the region $x_1 \leq x \leq x_J$, $0 < \eta < \eta_e$. The method outlined here was first suggested by Hartree and Womersley [59] and is known as the difference-differential or Clutter-Smith technique in the literature [60]. This has been used extensively by Smith and Co-workers [60,61,62] for the solution of boundary layer problems. Because

of the use of backward difference formulas for the x-derivatives, this implicit method is inherently stable [60].

Equations (3.45), (3.46) and (3.47) can be considered as a fifth order nonlinear boundary value problem with three conditions specified at $\eta = 0$ and the other two specified at $\eta = \eta_e$. Such a problem can only be solved iteratively. The most common method employed in the solution of such problems is the shooting method where the solution to the boundary value problem is obtained by solving a sequence of initial value problems. The detailed procedure for doing this is described in Chapter IV. It may be mentioned here that the shooting method is an integral part of the Clutter-Smith technique [60].

3.5 Solution of the Interaction Equation

After solving the boundary layer-equations the pressure distribution can be obtained using the equations (2.50) and (2.51) with $\delta = \delta(x)$ and $\bar{p} = \bar{p}(x)$. First we introduce the normalized quantities $\bar{\delta}(x)$ and $\bar{I}(x)$:

$$\bar{\delta}(x) = M_\infty \frac{\delta(x)}{\delta_o \bar{x}_L^{*1/2}} \bar{x}^{-\frac{3}{4}} \qquad (3.48a)$$

$$\bar{I}(x) = \int_0^\infty (H - f'^2)\, d\eta / I_o \qquad (3.48b)$$

where δ_o and I_o are defined in section 3.3. And from equation (2.50) $\bar{p}(x)$ can be taken as

$$\bar{p}(x) = \frac{\bar{I}(x)}{\bar{\delta}(x)} \tag{3.49}$$

From (2.51)

$$\bar{p}(x) = \frac{1}{p_o \bar{x}} \left[1 + \gamma K \{ \frac{\gamma+1}{4} K + \left[(\frac{\gamma+1}{4} K)^2 + 1 \right]^{\frac{1}{2}} \} \right]$$

which upon inversion gives

$$K(x) = \frac{(\bar{p}\, p_o\, \bar{x} - 1)}{\left[\gamma^2 + (p_o\, \bar{p}\, \bar{x} - 1) \frac{\gamma(\gamma+1)}{2} \right]^{1/2}} \tag{3.50}$$

or

$$S(x) = \frac{\xi_3\, \bar{I}/\bar{\delta} - x^{1/2}}{\left[\frac{\gamma(\gamma+1)}{2}\, \xi_3\, \bar{I}/\bar{\delta} + \frac{\gamma(\gamma-1)}{2}\, x^{1/2} \right]^{1/2}} \tag{3.51}$$

where

$$S(x) = x^{1/4}\, K(x) \tag{3.52}$$

and $\xi_3 = p_o\, \bar{x}_{L^*}$.

Now, from (3.5)

$$K(x) = k_b + M_\infty \frac{d\delta}{dx}$$

and using relations (3.48a) and (3.52) we get

$$S(x) = k_b\, x^{1/4} + \xi_4 \left(\frac{3}{4} \bar{\delta} + x \frac{d\bar{\delta}}{dx} \right) \tag{3.53}$$

where $\xi_4 = \delta_o\, \bar{x}_{L^*}^{1/2}$

or

$$\frac{d\bar{\delta}}{dx} = \frac{S(x)}{x\ \xi_4} - \frac{3\bar{\delta}}{4x} - \frac{k_b}{\xi_4\ x^{3/4}} \qquad (3.54)$$

when $S(x)$ is substituted from (3.51), equation (3.54) becomes a non-linear first-order ordinary differential equation in $\bar{\delta}$. This can be integrated as an initial value problem using fourth-order Runge-Kutta method. The initial value of $\bar{\delta}$ at $x = x_1$ is obtained from :

$$\bar{\delta} = \bar{\delta}(x_1) = \frac{\int_0^\infty \left[H(x_1, \eta) - f'^2(x_1, \eta) \right] d\eta}{I_o\ \bar{p}(x_1)} \qquad (3.55)$$

where $f(x_1,)$, $H(x_1,)$ and $\bar{p}(x_1)$ are those given by series expansion solution at the initial line $x = x_1$. Then having obtained $\bar{\delta}(x)$, relation (3.49) provides $\bar{p}(x)$ by using $\bar{I}(x)$ evaluated from the solutions of the governing equations (3.1) and (3.2).

3.6 Results of the Steady Flow with Air Injection

The results of the series expansion solution are presented in Tables 3.1 and 3.2 for $Pr = 0.72$ and $\gamma = 1.4$. In the first table the various results are tabulated for several values of the injection/suction parameter, α, and a fixed value of the wall enthalpy, $H_b = 0.5$. The second table contains results for a fixed value of $\alpha (= 0.3)$ and the wall enthalpy is given different constant values. For comparison purposes the zero-order problem was solved separately for

TABLE 3.1

RESULTS FROM THE SERIES SOLUTION WITH INJECTION/SUCTION

$Pr = .72,\ \gamma = 1.4,\ H_b = .5$

	$\alpha = .2$	$\alpha = .4$	$\alpha = .5$	$\alpha = -1.0$	$\alpha = -2.0$
$f_o''(0)$	.4060	.25188	.19849	2.1587	3.9971
$\bar{f}_1''(0)$	-.09375	-.07226	-0.16357	-1.9843	-3.9502
$\bar{f}_2''(0)$	-.17773	-.11328	-.09375	-1.9423	-3.898
$\bar{f}_3''(0)$	0.11914	0.03417	.32226	1.9328	3.9296
$H_o'(0)$	0.06927	0.016911	.002894	.7564	1.4208
$\bar{H}_1'(0)$	-.016301	0.04026	.03480	-.6708	-1.2811
$\bar{H}_2'(0)$	0.00835	0.03764	.036189	-.65002	-1.2635
$\bar{H}_3'(0)$	-.013256	-.009733	.007369	.4587	.65495
I_o	1.1754	1.3252	1.40498	.58447	.38539
I_1	.36908	0.3501	.08751	.47182	.33776
I_2	.41351	0.6034	-.2023	.3882	.34521
I_3	-.12489	-.16632	-.0782	-.11594	-.07040
δ_o	.6954	.73844	.76034	.4904	.39822
δ_1	-.92968	-.8970	-.93949	-.6922	-.6224
δ_2	-.97217	-.8133	-.94259	-1.510	-1.1186
δ_3	.2427	.25029	.124303	-.5452	-1.6030
p_o	.45706	.5153	.54632	.2272	.14985
p_1	1.3552	1.2191	1.001897	3.5916	5.0365
p_2	1.4997	1.4934	.82395	4.4985	10.729
p_3	1.2682	1.2058	.6653	1.4075	.99818

TABLE 3.2

RESULTS FROM THE SERIES SOLUTION WITH INJECTION

$Pr = .72,\ \gamma = 1.4,\ \alpha = 0.3$

	$H_b = 1.0$	$H_b = .75$	$H_b = .5$	$H_b = .25$	$H_b = 0.1$
$f_0''(0)$	.4426	.38023	.31614	.25025	.2096
$\bar{f}_1''(0)$	-.18359	-.12817	-.068359	-.0062866	.07031
$\bar{f}_2''(0)$	-.2739	-.20898	-.13281	-.022949	-.000488
$\bar{f}_3''(0)$	0.16601	.10937	.05224	.007049	-.019287
$H_0'(0)$	-.06113	-.007439	.03953	.078938	.09842
$\bar{H}_1'(0)$	.02173	.019153	.028287	.032797	.06308
$\bar{H}_2'(0)$	.02751	.022769	.031043	.03359	.03934
$\bar{H}_3'(0)$	-.017475	-.016695	-.018896	-.02361	-.039399
I_0	1.9224	1.62917	1.29879	.92756	.6783
I_1	.6750	.5474	.45865	.25123	.07672
I_2	.7224	.5925	.31923	.30157	.08096
I_3	-.22859	-.18767	-.168995	-.13361	-.18966
δ_0	.8894	.81875	.73104	.61779	.5283
δ_1	-.7125	-.7805	-.86591	-1.0684	-1.3303
δ_2	-.5872	-.69729	-.92079	-1.2475	-1.838
δ_3	.14636	.17255	.16736	.27521	.22132
p_0	.7475	.6335	.505029	.36067	.26377
p_1	1.0981	1.175535	1.3386	1.4672	1.4999
p_2	.9408	1.09587	1.22087	1.8486	2.0872
p_3	.7893	.92065	1.00586	1.4556	1.8002

TABLE 3.3

COMPARISON WITH THE SIMILAR SOLUTIONS OF COHEN AND RESHOTKO [63]

$\beta = .5$, $H_b = .6$, $Pr = 1.0$, $\alpha = 0.0$

Ref. [63]	Present work
$H_b' = 0.2090$	$H_b' = 0.20774$
$f_b'' = 0.7946$	$f_b'' = 0.7914$

$\beta = 0.5$, $H_b = 0.6$, $Pr = 1.0$, $\alpha = 0.0$ and the results are tabulated in Table 3.3 against the similar solutions of Cohen and Reshotko [63]. There is quite good agreement between the results computed here and those of [63]. Table 3.4 shows the non-injection results by different methods used here against the values given by ref. [64]. The variation between the results obtained in ref. [64] and those obtained here by Clutter-Smith technique is due to the starting procedure adopted. In the work of Chattopadhyay and Rodkiewicz [64] the solutions were started by fourth-order Runge-Kutta method and then switched over to the predictor-corrector technique for further integration across the boundary layer. The same step-size was used for starting as well as for further integration. Hence the accuracy of the results near the surface is questionable. In the present computations employing the shooting method a more accurate starting procedure

TABLE 3.4

COMPARISON WITH THE NO-INJECTION RESULTS OF REF. [64]

$Pr = .72$, $\gamma = 1.4$, $H_b = .5$

	Results From Ref. [64]	Present Results Obtained by	
		Clutter-Smith Technique [61]	*Method of Finite Differences [23]
$f_o''(0)$		.6185	.655514
$\bar{f}_1''(0)$		-.3164	-.33606
$\bar{f}_2''(0)$		-.3554	-.3597
$\bar{f}_3''(0)$		.25585	.26555
$H_o'(0)$		.1505	.14985
$\bar{H}_1'(0)$		-.06267	-.05278
$\bar{H}_2'(0)$		-.04572	-.04249
$\bar{H}_3'(0)$		.01615	0.019339
I_o	**.86725	1.0314	.86417
I_1	.39369	.50681	.39215
I_2	.37513	.4618	.37391
I_3	-.11225	-.15649	-.1117
δ_o	0.59719	.65146	.59631
δ_1	-.99449	-.8835	-.99432
δ_2	- 1.2628	-1.0501	-1.2652
δ_3	0.30868	.23246	.31536
p_o	0.33702	.4010	.33603
p_1	1.8134	1.737	1.8204
p_2	2.2196	1.9016	2.2302
p_3	1.8510	1.5292	1.87968

*Values obtained by Method described in Chapter V

as suggested by Clutter and Smith [61] incorporating the Taylor's series expansion near the wall has been adopted. Table 3.4 also contains the results obtained by a finite-difference method [23]. Even though these values compare favourably with those of ref. [64] the present results obtained by the shooting method appear to be more accurate. The finite-difference method, however, appears better suited [23] in comparison to the Clutter-Smith technique [61,65] for problems involving surface mass transfer where skin-friction and heat transfer become small.

In Fig. 3.1 and 3.2 the starting velocity and enthalpy profiles, $f'(x_1, \eta)$ and $H(x_1, \eta)$, obtained from the series expansion solution for $\bar{x}_{L^*} = 8$, $M_\infty = 20$, $H_b = 0.5$, $\gamma = 1.4$, $Pr = 0.72$, $\theta_b = 2^\circ$ and for different values of α are shown. These profiles are calculated at a distance of $x_1 = 1/1024$ from the leading edge which corresponds to the value of $\bar{x}_1$ equal to 256. With this value of $\bar{x}_1$, the profiles obtained from equations (3.38a) and (3.38b) would be highly accurate. From the starting station to the next one the step-size was taken to be approximately equal to 1/100 and the value of $k_x = 1.4$. This yields 14 stations from $x = 0.0$ to $x = 1.0$. The calculations in the η-direction were started with a step-size of 0.1/16 and this step-size was slowly increased to 0.1 for use with the predictor-corrector formula.

In Fig. 3.3 a comparison of the variations of p and δ along the plate obtained from the series expansion solution

and shooting method are given by $M_\infty = 20$, $\bar{x}_{L*} = 8$, $H_b = 0.5$, $Pr = 0.72$, $\gamma = 1.4$, $\theta_b = 2^o$ and for no-injection case. The agreement between the series solution and the shooting method of solution decreases along the length of the plate with the decreasing value of $\bar{x}$ because of the larger error terms in the series solution.

Figures 3.4 through 3.7 show the variations of p, δ, f_b'' and H_b' along the plate for a fixed value of the injection parameter ($\alpha = 0.3$) with different values of H_b(=0.1,0.25,0.5, 0.75,1.0), $M_\infty = 20$, $\bar{x}_{L*} = 8$, $\gamma = 1.4$, $Pr = 0.72$, $\theta_b = 2^o$ and $K_1 = 10^{-6}$. With the increase in the value of the wall enthalpy, the induced pressures are larger due to the greater displacement of the outer flow caused by the hotter fluid in the boundary layer as shown in Figures 3.4 and 3.5. Fig. 3.6 shows the distribution of the wall shear function for different values of H_b and the trend is similar to the one noted in Figures 3.4 and 3.5. The wall enthalpy-gradient, however, decreases with increase in H_b as shown in Fig. 3.7. This is due to the reason that the difference in enthalpy between the external layer and the plate surface exerts substantial influence on the wall enthalpy-gradient which is a measure of the heat conducted.

Figures 3.8 through 3.11 present the effect of varying the injection/suction parameter, α, on the distributions of p, δ, f_b'' and H_b' along the plate for $M_\infty = 20$, $\bar{x}_{L*} = 8$, $H_b = 0.75$,

Pr = 1.0, γ = 1.4, $\theta_b = 2^o$ and $K_1 = 10^{-6}$. With injection (i.e. for positive values of α) p and δ increase because of the presence of larger amount of fluid in the boundary layer. Because of the surface injection the velocity and enthalpy profiles are less fuller as compared to the no-injection case and accordingly their wall gradients will be smaller. When the fluid from the boundary layer is sucked out (i.e. for negative values of α) the boundary layer thins down giving smaller induced pressures due to the lesser displacement of the external flow as indicated by the lower values of δ. Because of the thinner boundary layer with suction, the velocity and enthalpy profiles are more fuller as compared to the no-injection case, resulting in very high values for their wall gradients. Hence whereas injection reduces the shear stress and heat transfer to the plate, these are increased by suction. However, the converse is true about their effect on the induced pressure.

Figures 3.12 through 3.15 show the variations of p, δ, f_b'' and H_b' with θ_b along the plate of $M_\infty = 20$, $\bar{x}_{L^*} = 8$, $\gamma = 1.4$, Pr = 0.72, $K_1 = 10^{-6}$, $H_b = 0.5$ and a fixed value of the injection parameter $\alpha(= 0.2)$. In Fig. 3.12 the increase in pressure with the increasing values of θ_b is due to greater inviscid compression with the larger wedge angles.

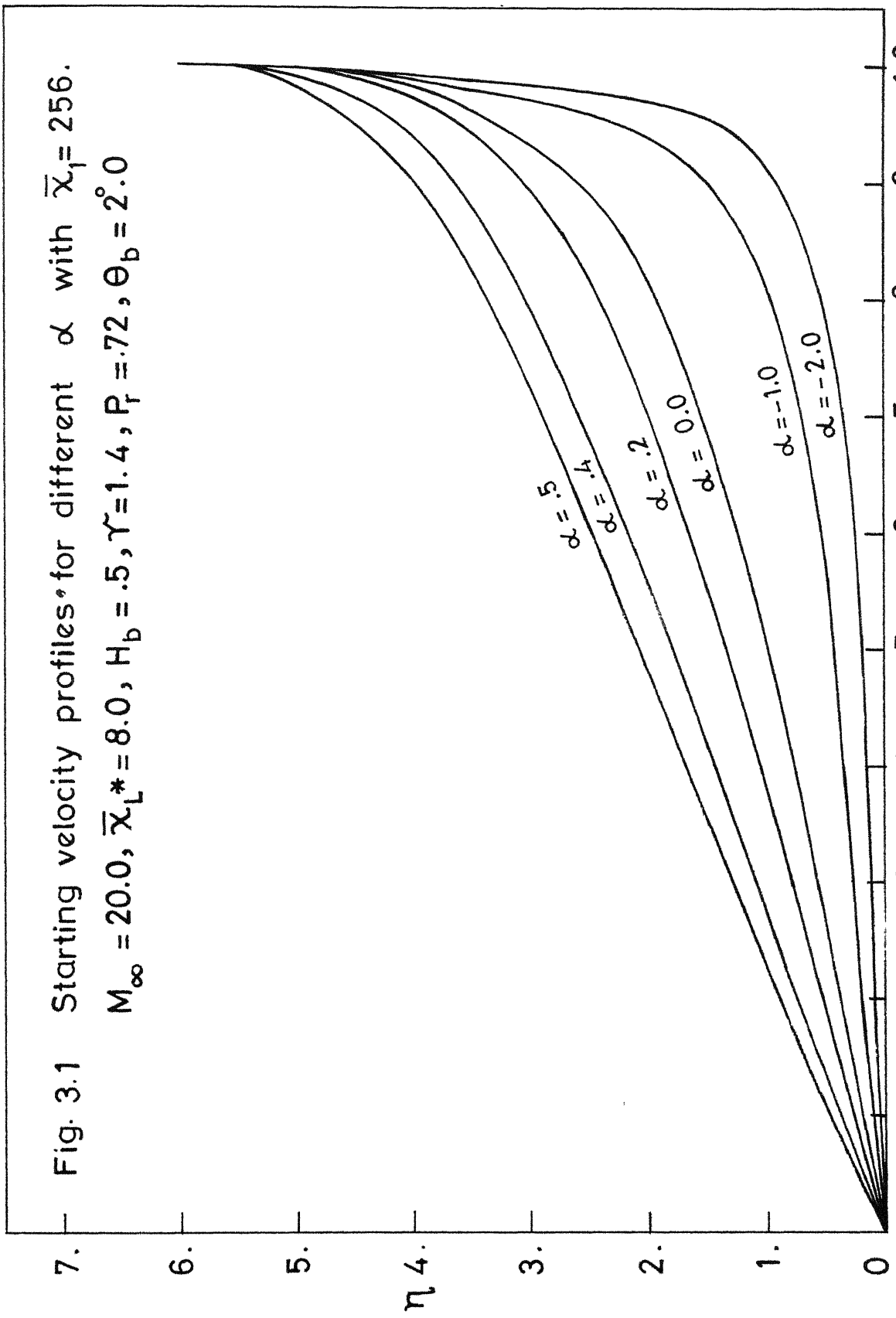
Fig. 3.1 Starting velocity profiles* for different α with $\overline{x}_1$= 256.
M_∞ = 20.0, $\overline{x}_L$* = 8.0, H_b = .5, γ=1.4, P_r = .72, θ_b = 2°.0
α = .5
α = .4
α = .2
α = 0.0
α = -1.0
α = -2.0
η
f'(x1, η)
0
1.
2.
3.
4.
5.
6.
7.
.1
.2
.3
.4
.5
.6
.7
.8
.9
1.0

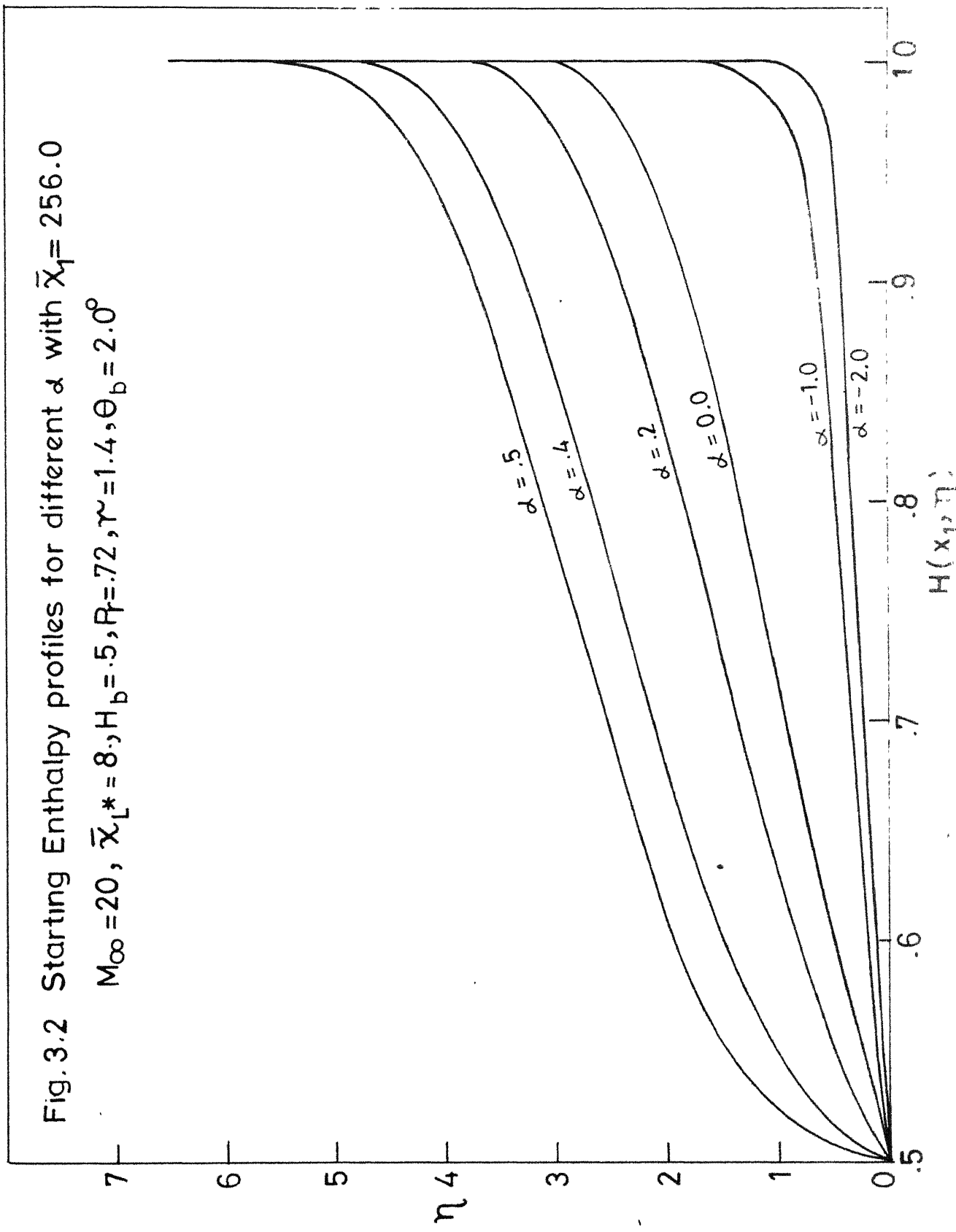
Fig. 3.2 Starting Enthalpy profiles for different α with $\bar{\chi}_1$= 256.0
M_∞=20, $\bar{\chi}_{L^*}$=8., H_b=.5, P_r=.72, γ=1.4, θ_b=2.0°
α=.5
α=.4
α=.2
α=0.0
α=-1.0
α=-2.0
η
$H(x_1,\eta)$
0
1
2
3
4
5
6
7
.5
.6
.7
.8
.9
1.0

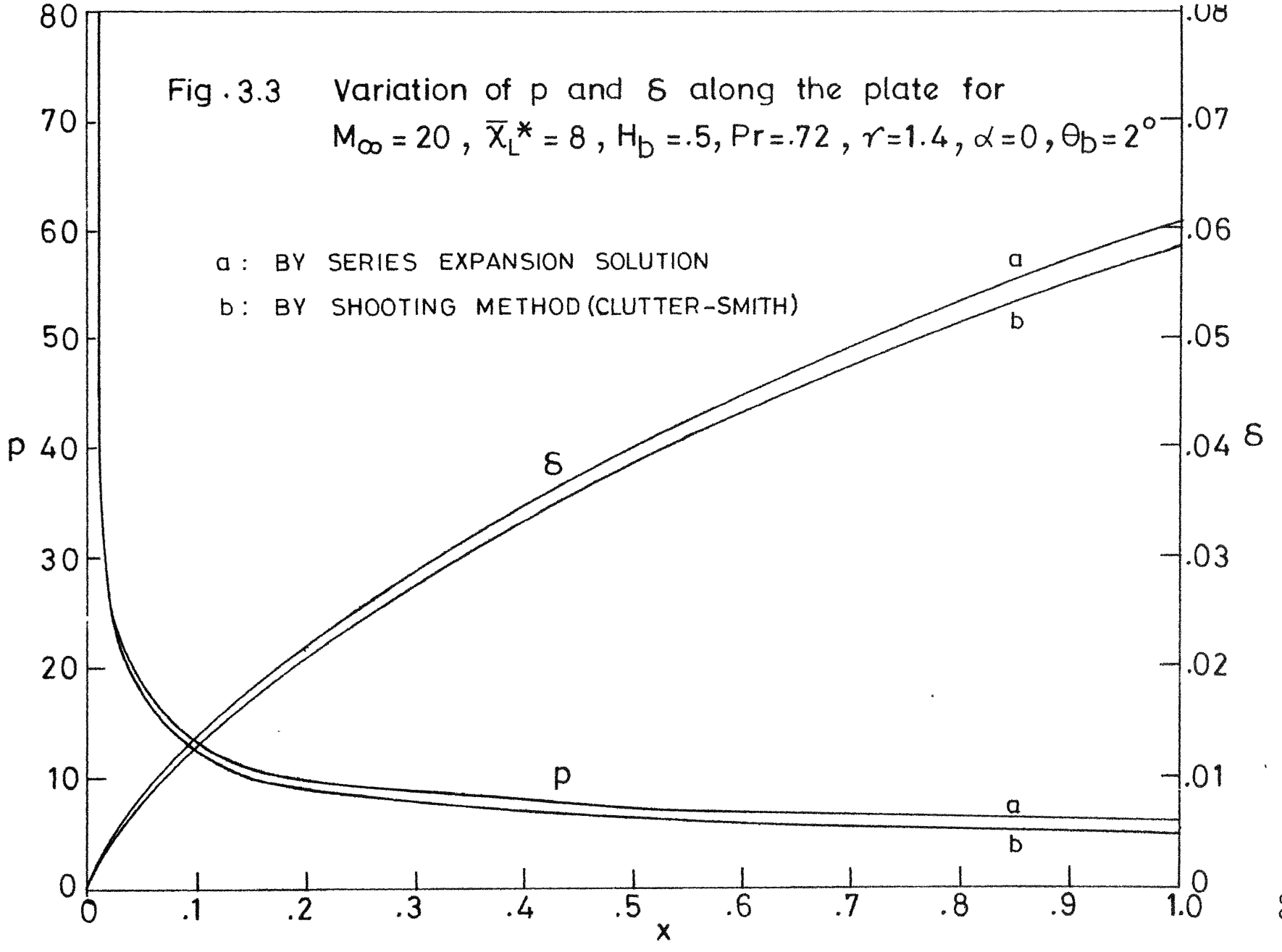
Fig . 3.3 Variation of p and δ along the plate for
$M_\infty = 20$, $\bar{X}_L^* = 8$, $H_b = .5$, $Pr = .72$, $\gamma = 1.4$, $\alpha = 0$, $\theta_b = 2^\circ$
a : BY SERIES EXPANSION SOLUTION
b : BY SHOOTING METHOD (CLUTTER-SMITH)
p
δ
a
b
x
0
.1
.2
.3
.4
.5
.6
.7
.8
.9
1.0
10
20
30
40
50
60
70
80
.01
.02
.03
.04
.05
.06
.07
.08

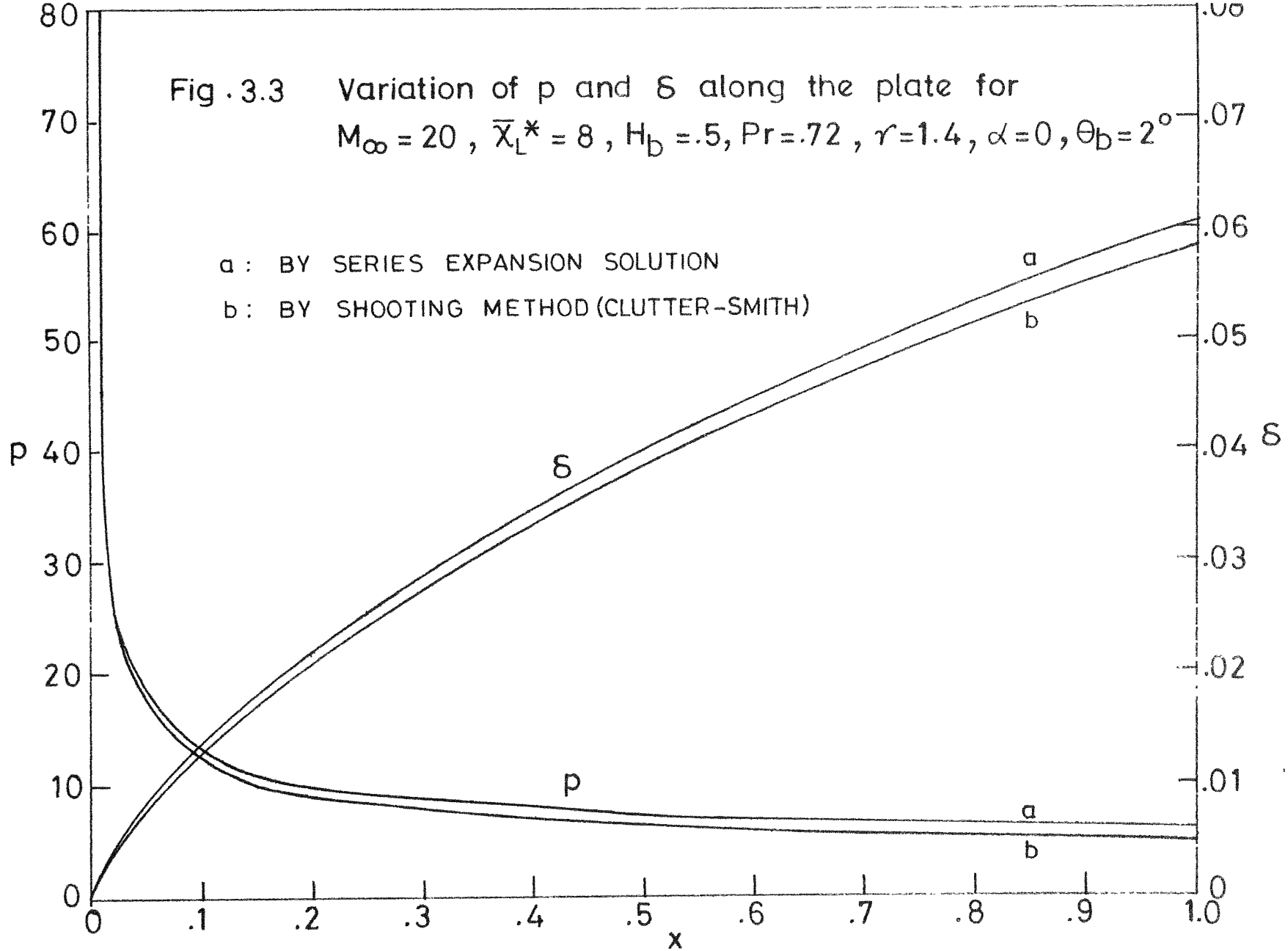
Fig . 3.3 Variation of p and δ along the plate for
$M_\infty = 20$, $\bar{\chi}_L^* = 8$, $H_b = .5$, $Pr = .72$, $\gamma = 1.4$, $\alpha = 0$, $\theta_b = 2^\circ$
a : BY SERIES EXPANSION SOLUTION
b : BY SHOOTING METHOD (CLUTTER-SMITH)
p
δ
a
b
x
0
.1
.2
.3
.4
.5
.6
.7
.8
.9
1.0
10
20
30
40
50
60
70
80
.01
.02
.03
.04
.05
.06
.07

Fig. 3.4 Variation of pressure along the p[illegible]

$M_\infty = 20, \bar{\chi}_L^* = 8, \alpha = 0.3, \gamma = 1.4, P_r = .72, \theta_b = 2^\circ, K_1 = 10^{-6}$

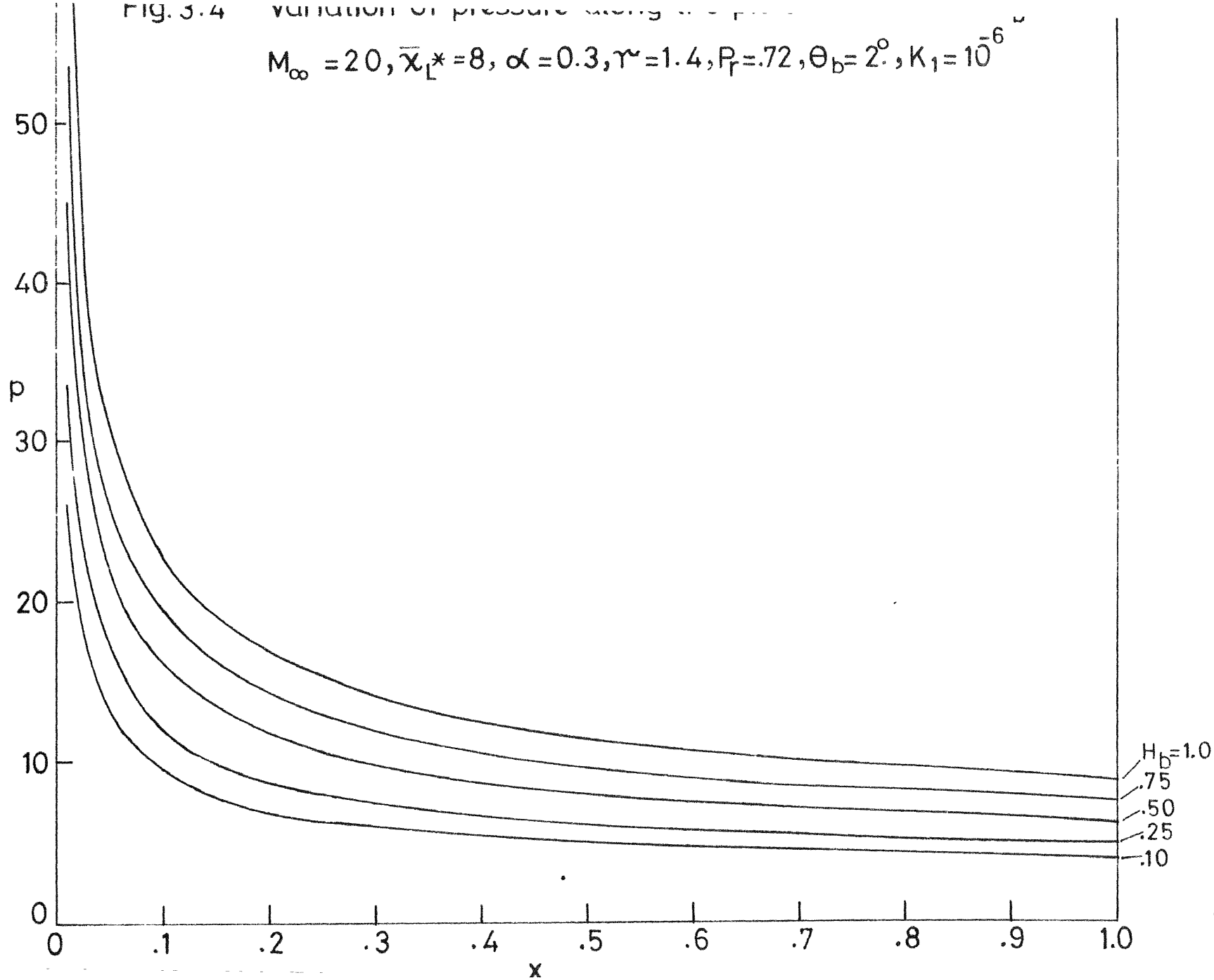

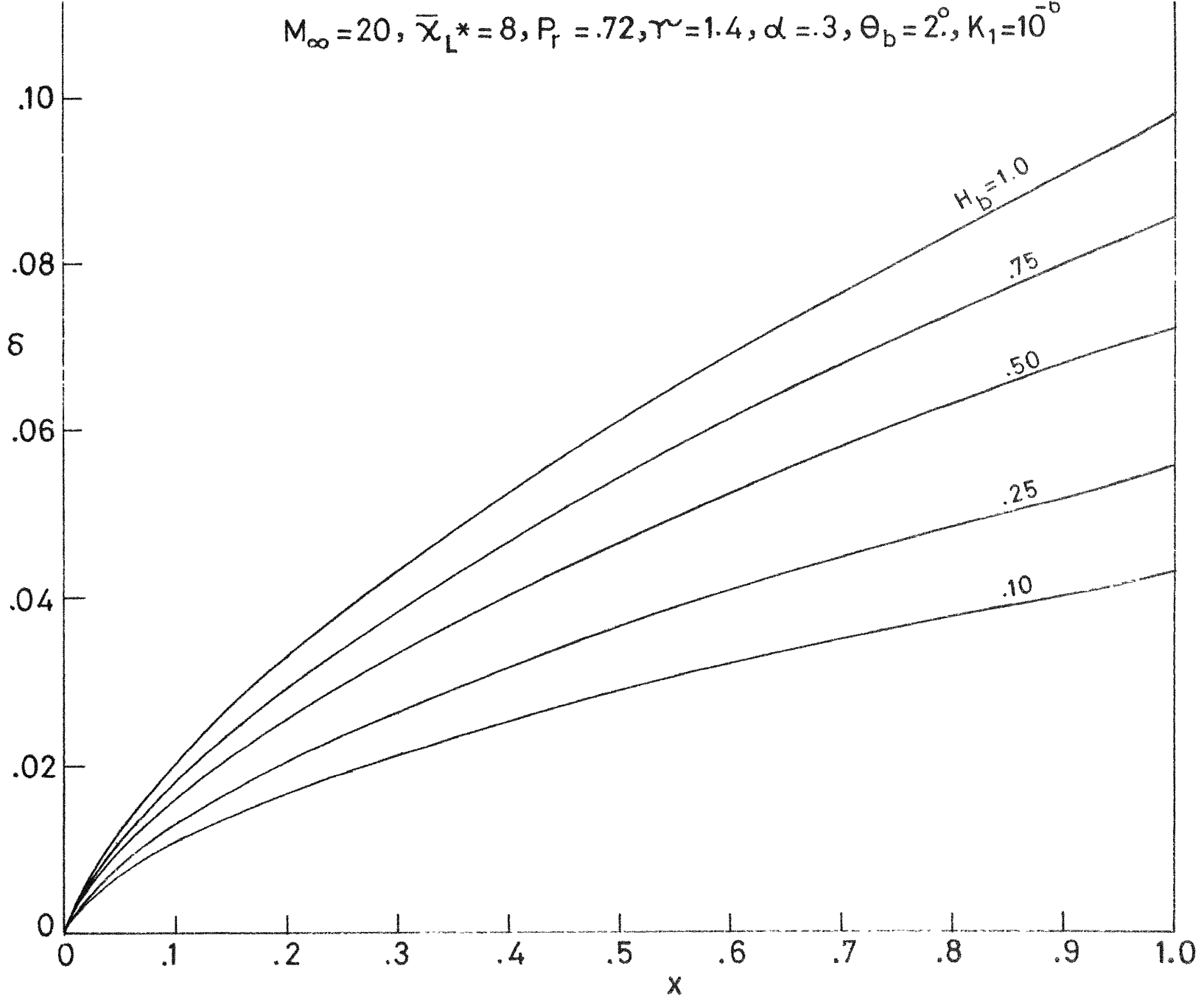
$M_\infty = 20$, $\bar{\chi}_L^* = 8$, $P_r = .72$, $\gamma = 1.4$, $\alpha = .3$, $\theta_b = 2°$, $K_1 = 10^{-5}$
$H_b = 1.0$
.75
.50
.25
.10
δ
0
.02
.04
.06
.08
.10
0
.1
.2
.3
.4
.5
.6
.7
.8
.9
1.0
x

Fig. 3.6 Variation of f_b'' along the plate for different H_b

$M_\infty = 20, \overline{\chi}_{L^*} = 8, P_r = .72, \gamma = 1.4, \alpha = .3, K_1 = 10^{-6}, \theta_b = 2^\circ$.

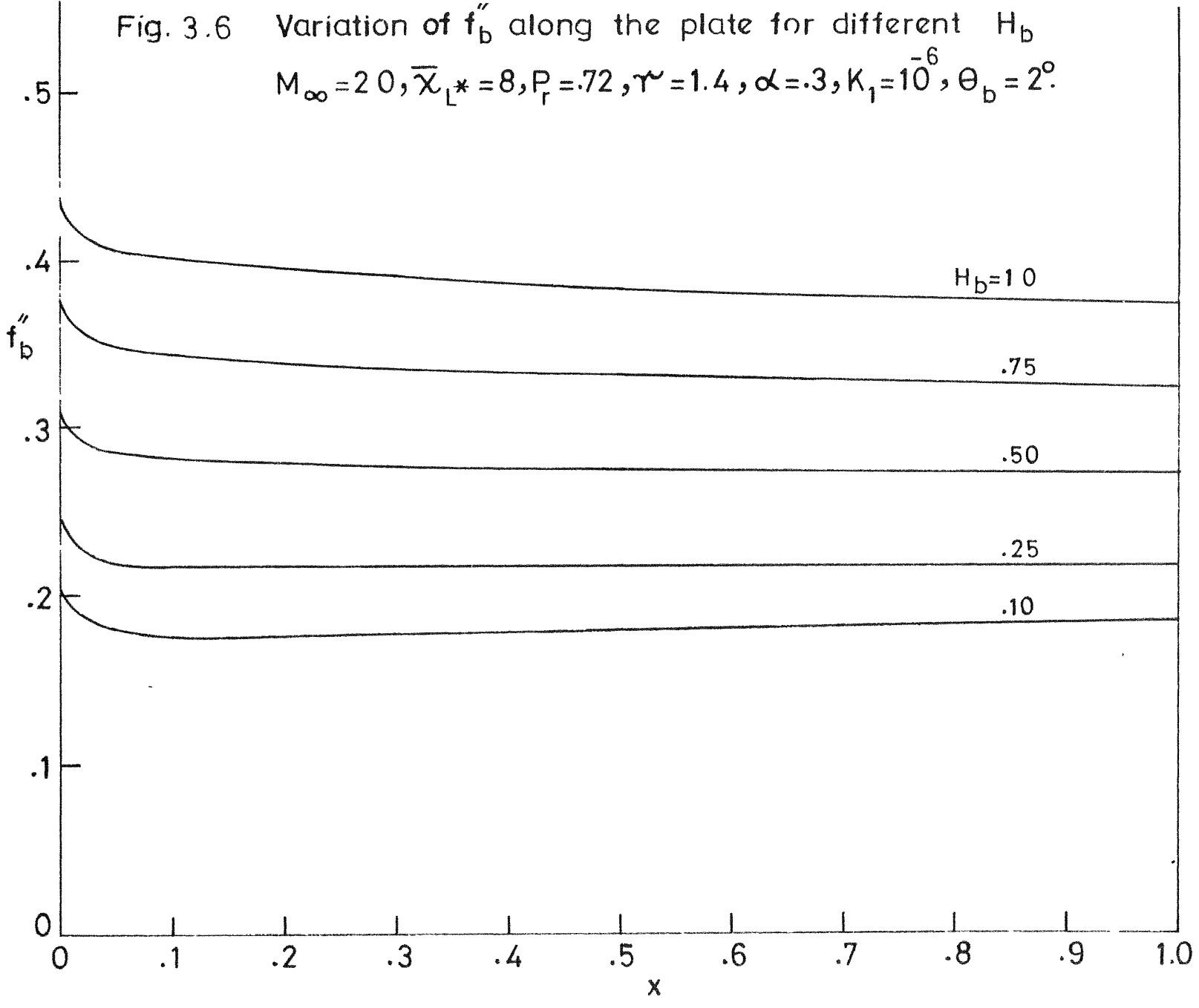

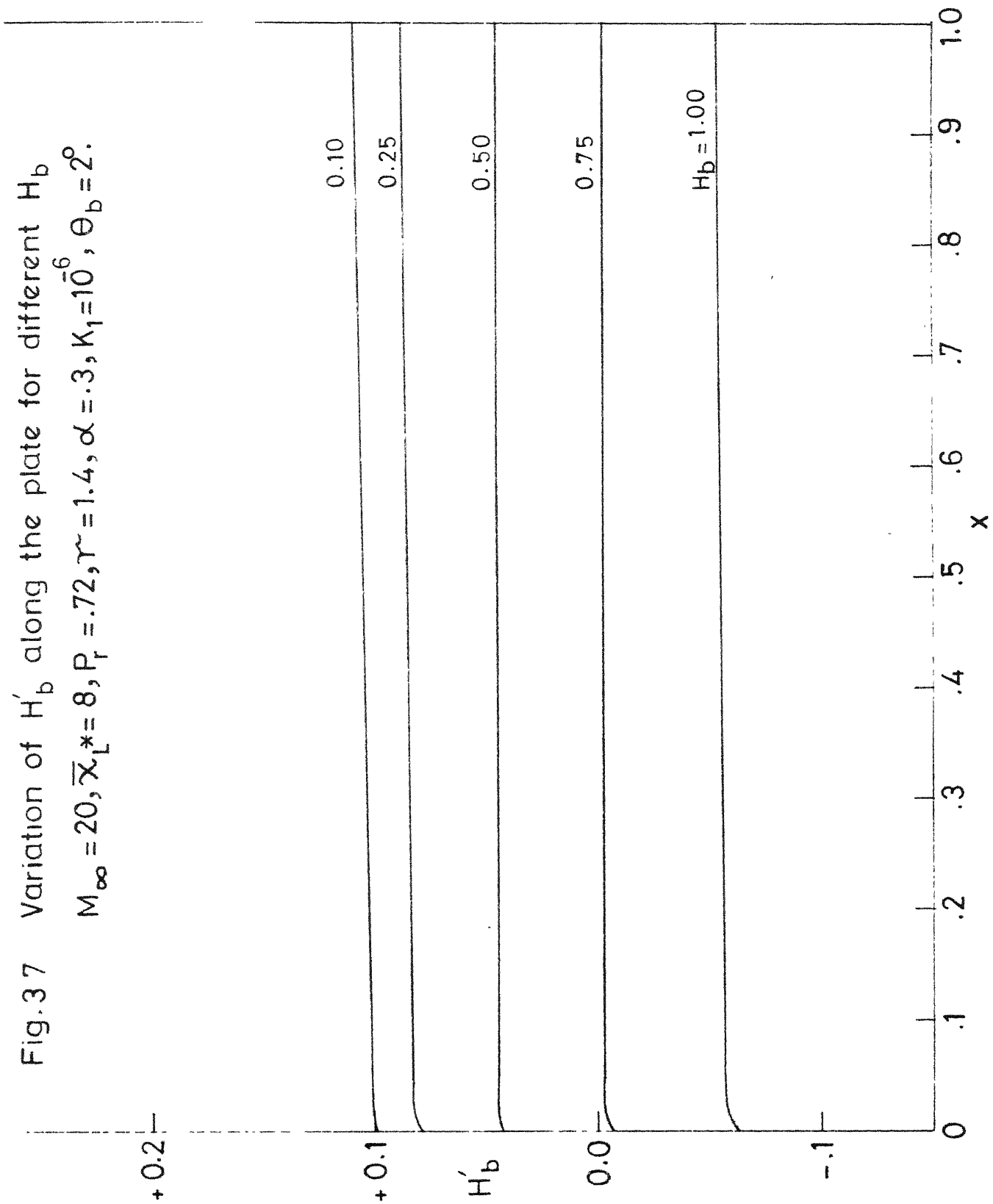

Fig.37 Variation of H'_b along the plate for different H_b

$M_\infty = 20, \overline{\chi}_L^* = 8, P_r = .72, \gamma = 1.4, \alpha = .3, K_1 = 10^{-6}, \theta_b = 2^\circ$.

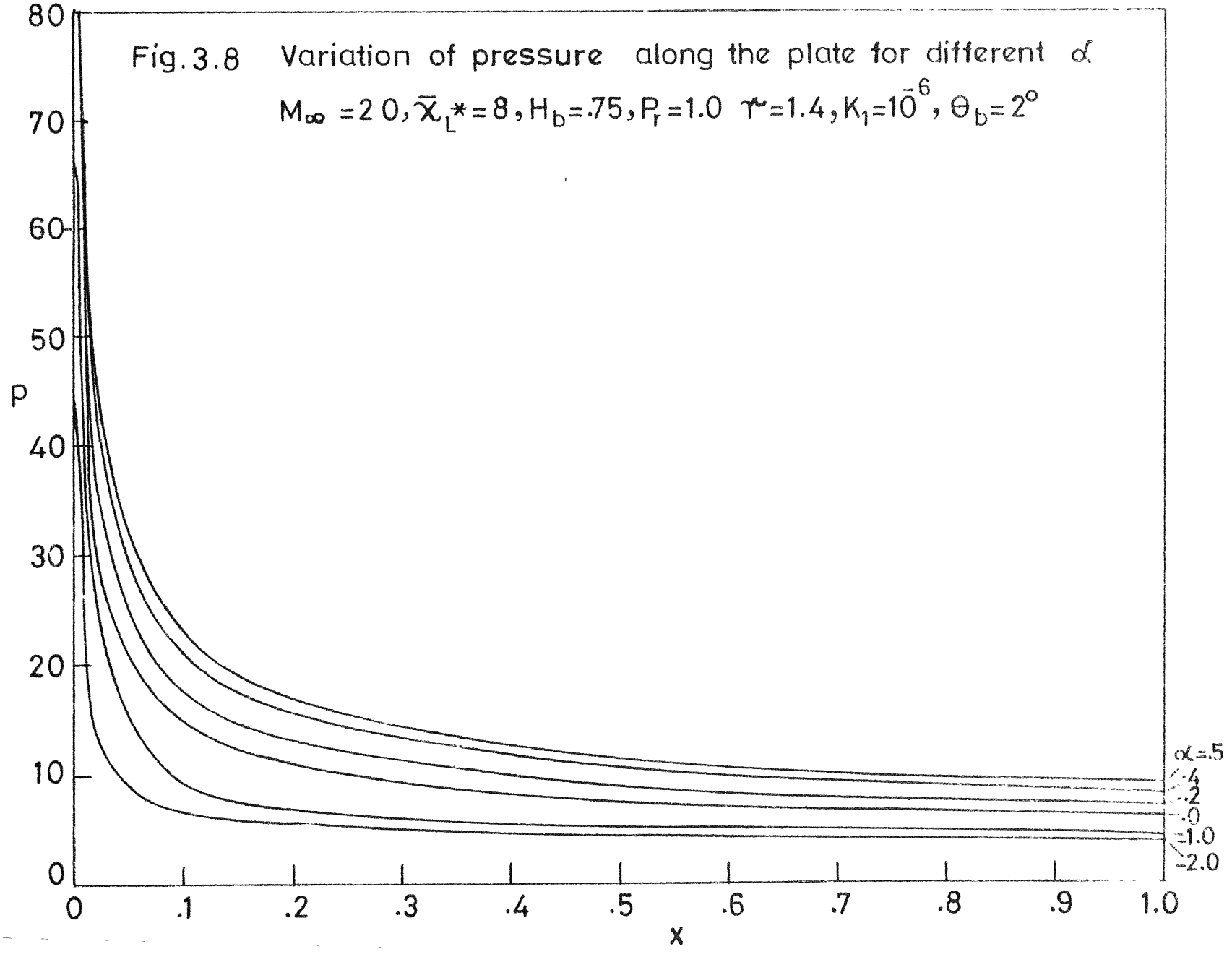
Fig. 3.8 Variation of pressure along the plate for different α
$M_\infty = 20, \bar{\chi}_L^* = 8, H_b = .75, P_r = 1.0\ \gamma = 1.4, K_1 = 10^{-6}, \theta_b = 2^\circ$
P
x
0
10
20
30
40
50
60
70
80
.1
.2
.3
.4
.5
.6
.7
.8
.9
1.0
α=.5
.4
.2
.0
-1.0
-2.0

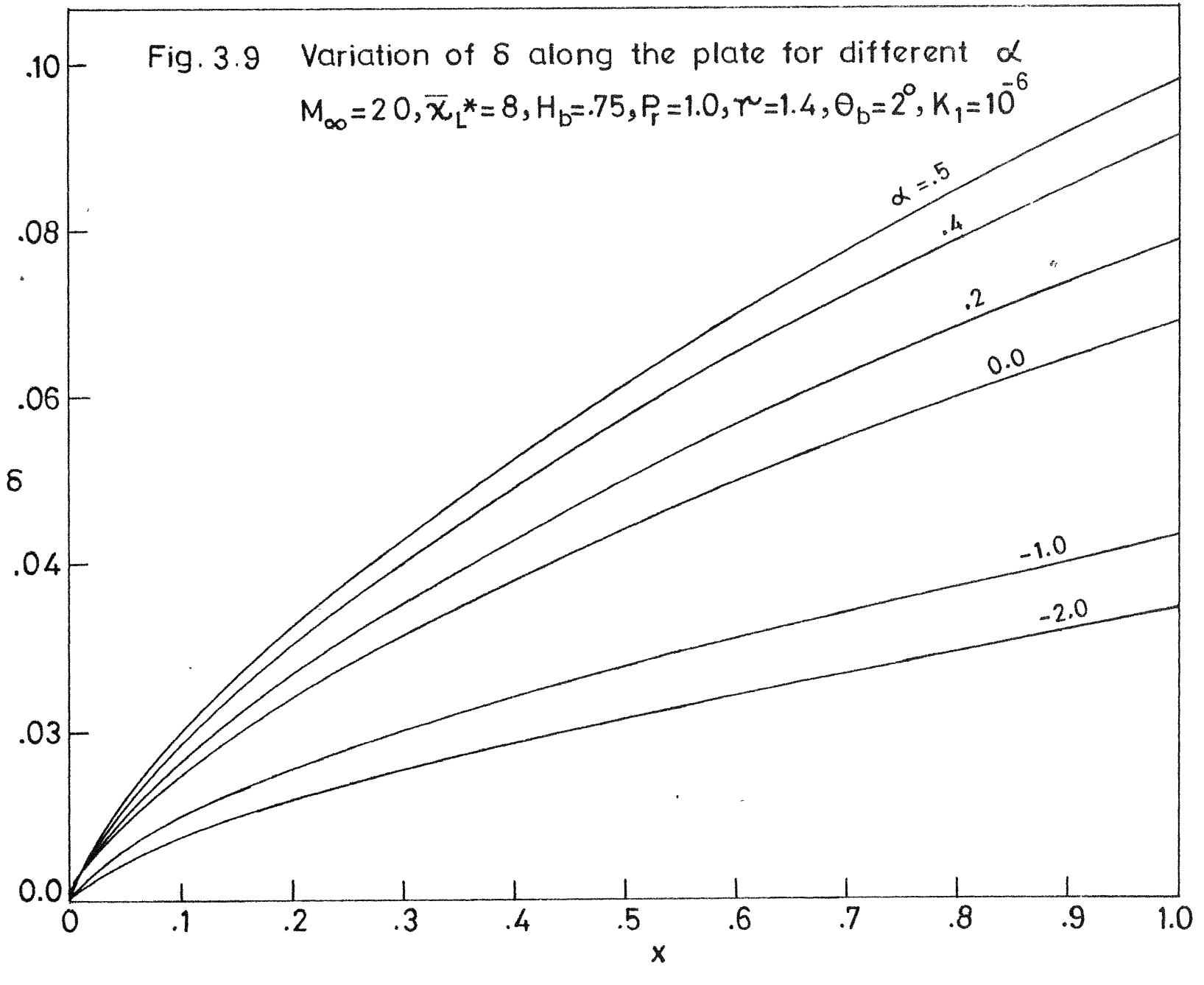
Fig. 3.9 Variation of δ along the plate for different α
$M_\infty = 20, \bar{x}_L^* = 8, H_b = .75, P_r = 1.0, \gamma = 1.4, \theta_b = 2^\circ, K_1 = 10^{-6}$
α = .5
.4
.2
0.0
-1.0
-2.0
δ
x
.10
.08
.06
.04
.03
0.0
0
.1
.2
.3
.4
.5
.6
.7
.8
.9
1.0

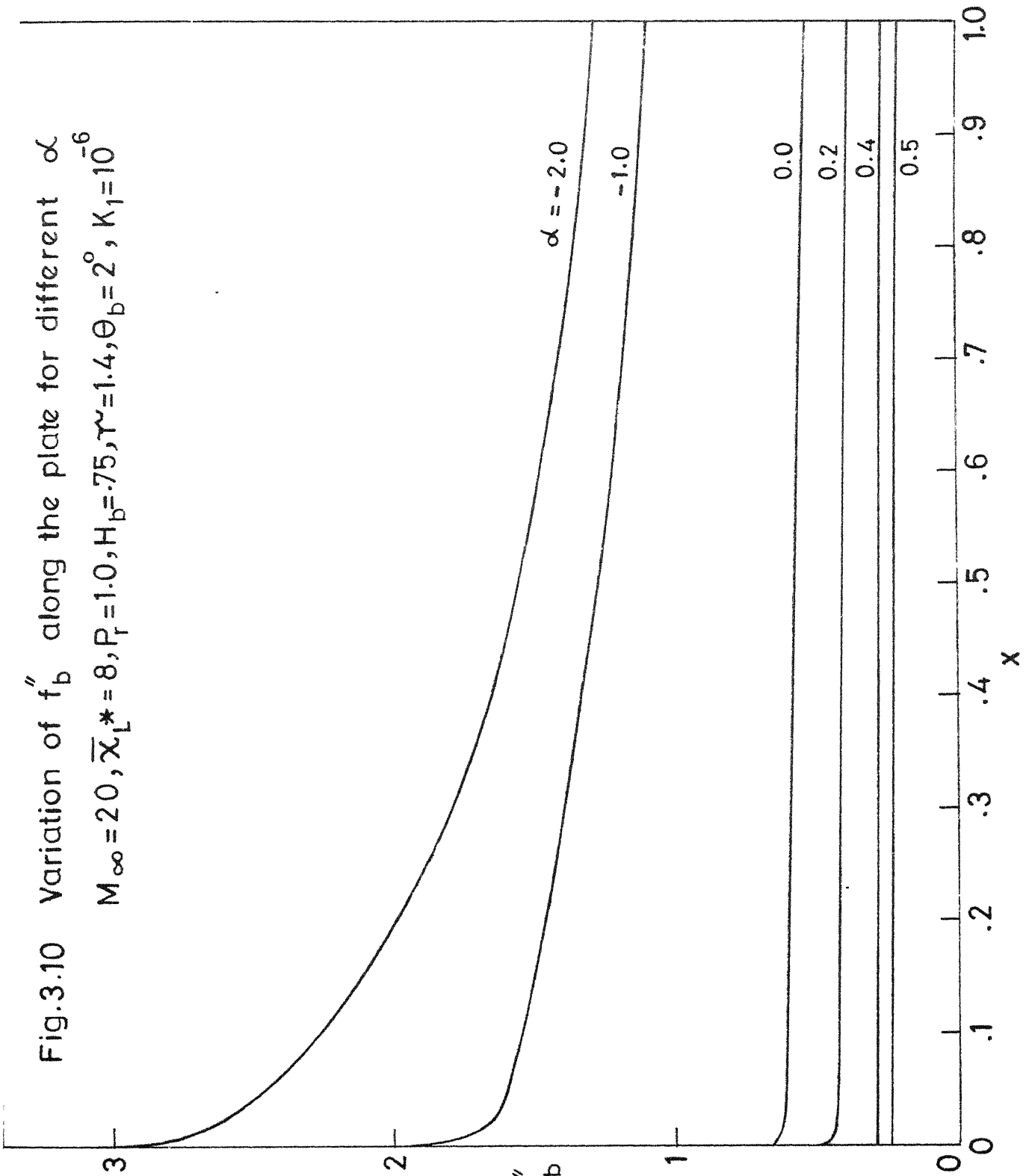

Fig.3.10 Variation of f_b'' along the plate for different α

$M_\infty = 2.0, \bar{\chi}_L^* = 8, P_r = 1.0, H_b = .75, \tau = 1.4, \theta_b = 2^\circ, K_1 = 10^{-6}$

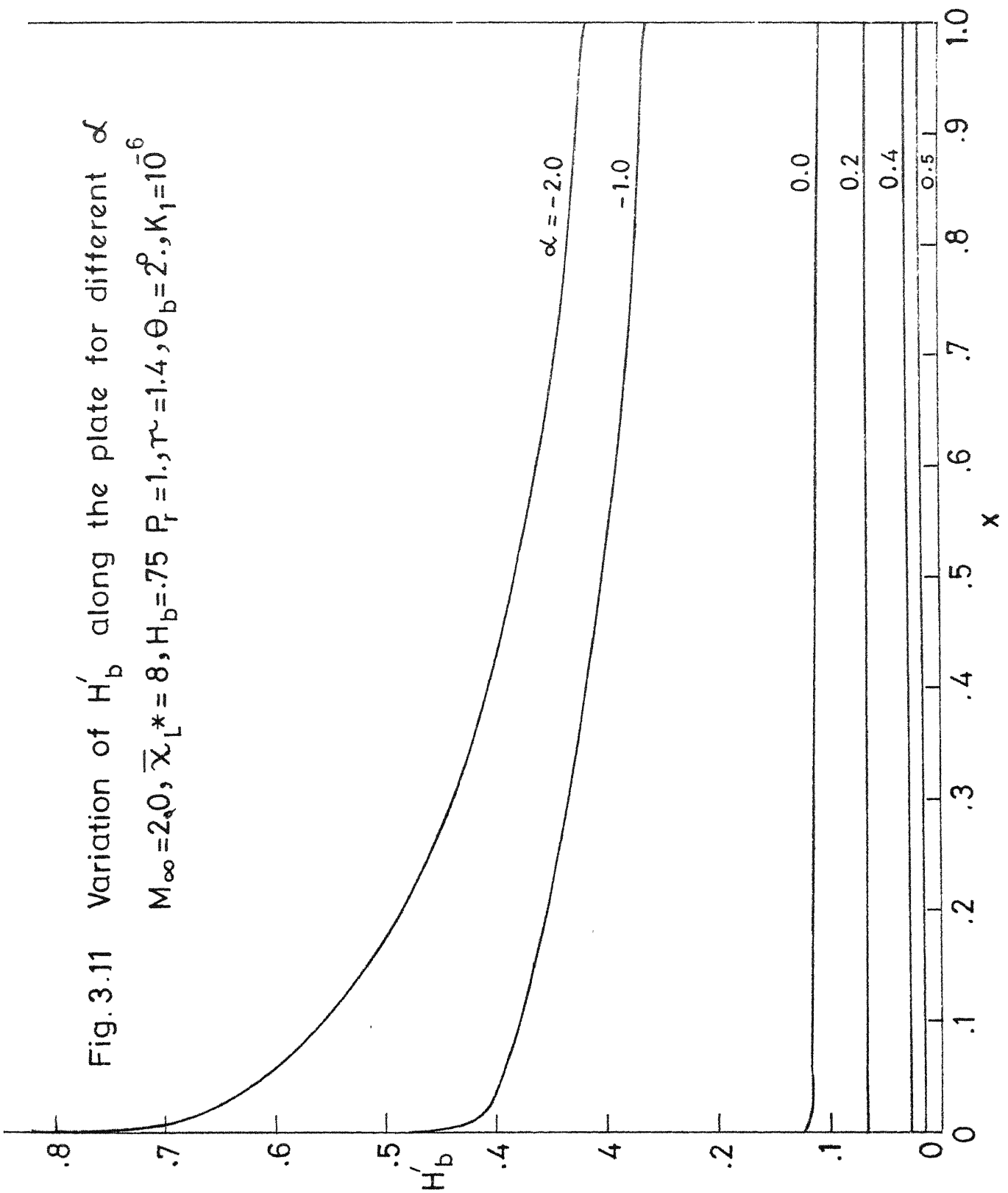
Fig. 3.11 Variation of H_b' along the plate for different α
$M_\infty = 2.0$, $\bar{\chi}_L^* = 8$, $H_b = .75$ $P_r = 1.$, $\tau = 1.4$, $\theta_b = 2^0$., $K_1 = 10^{-6}$
H_b'
x
$\alpha = -2.0$
-1.0
0.0
0.2
0.4
0.5
0
.1
.2
.3
.4
.5
.6
.7
.8
.9
1.0
.2
.4
.5
.6
.7
.8

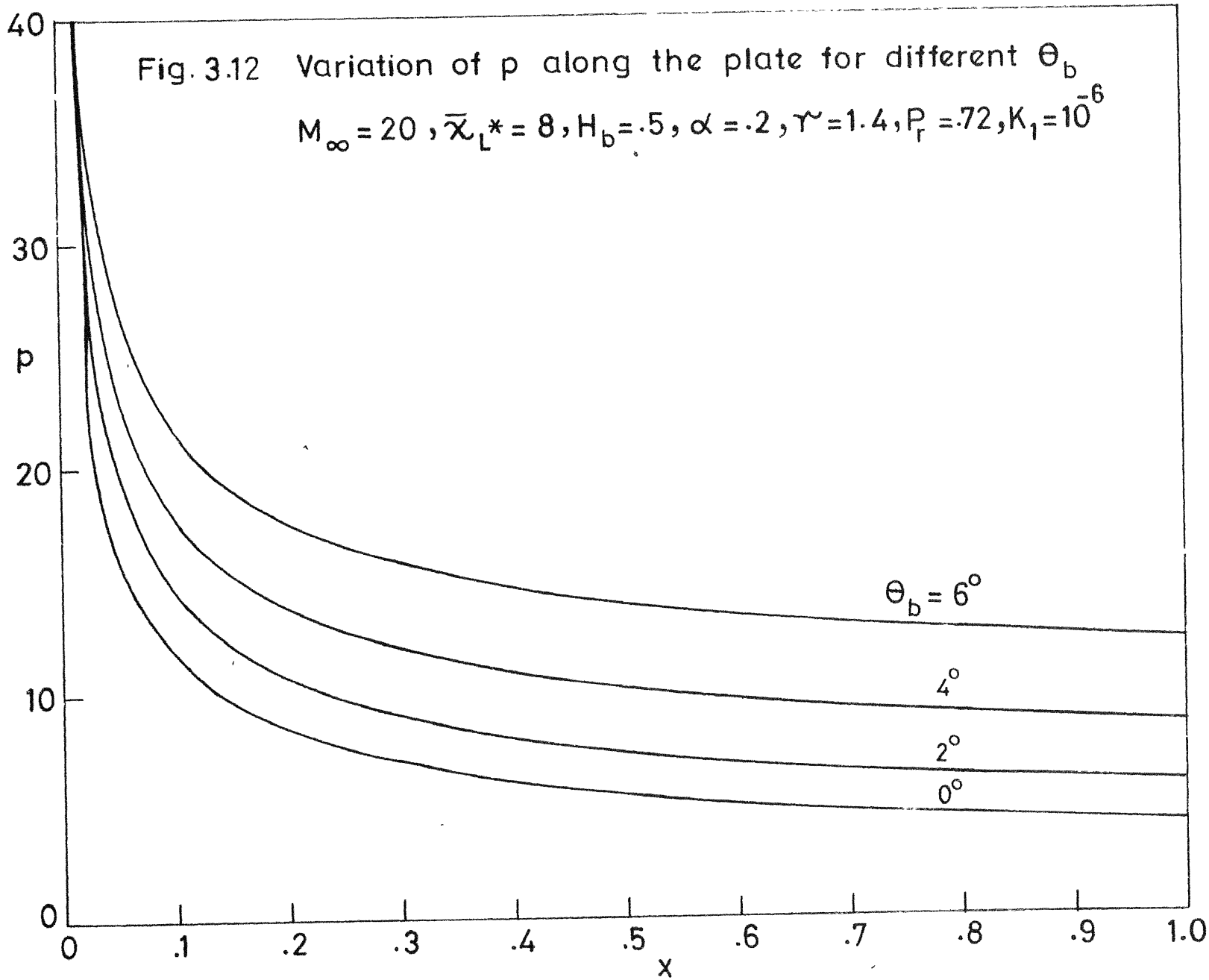
Fig. 3.12 Variation of p along the plate for different θ_b
$M_\infty = 20, \bar{\chi}_L^* = 8, H_b = .5, \alpha = .2, \gamma = 1.4, P_r = .72, K_1 = 10^{-6}$
40
30
20
10
0
p
$\theta_b = 6^\circ$
4°
2°
0°
0
.1
.2
.3
.4
.5
.6
.7
.8
.9
1.0
x

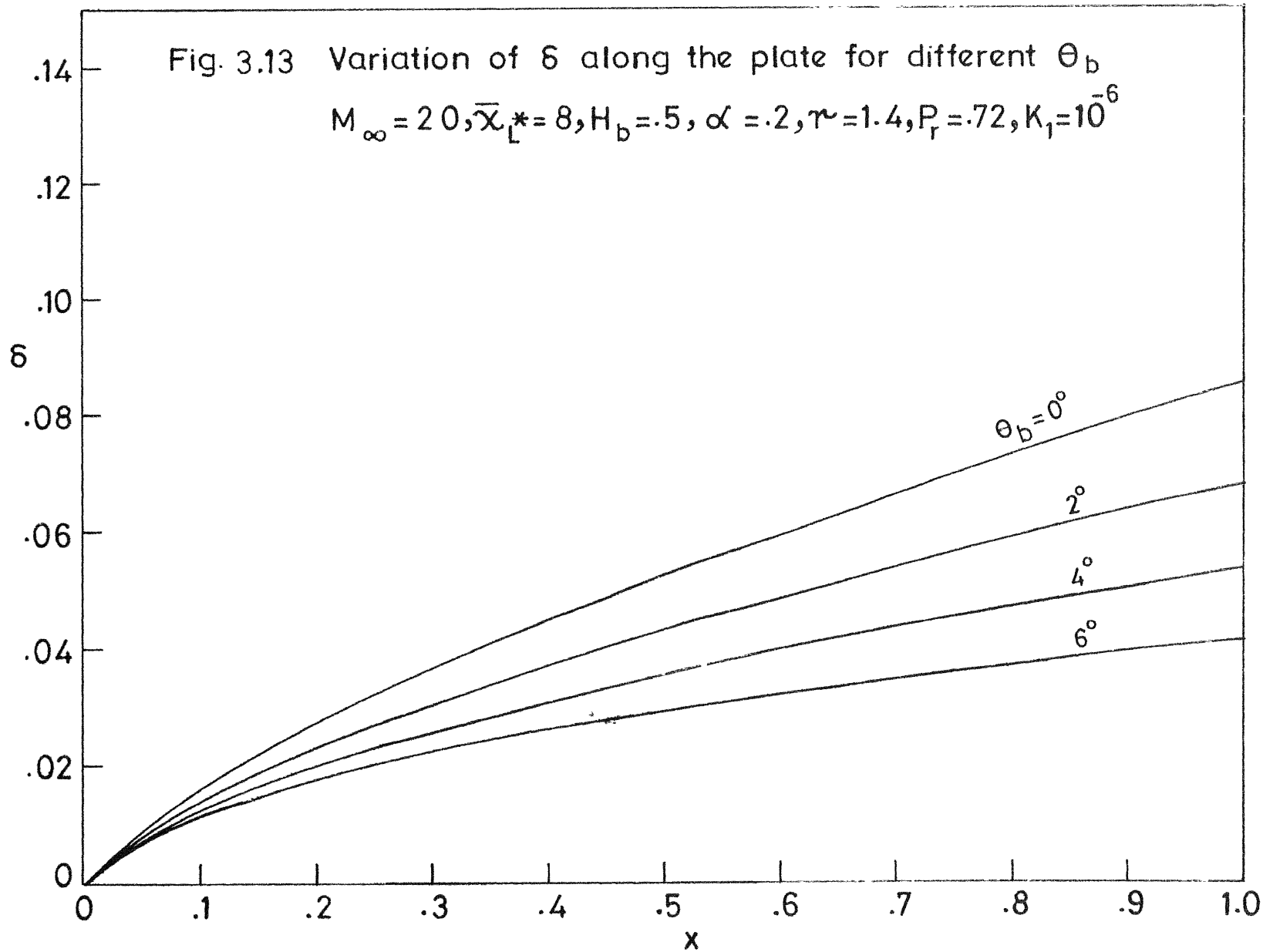
Fig. 3.13 Variation of δ along the plate for different Θ_b
$M_\infty = 20, \bar{\chi}_L^* = 8, H_b = .5, \alpha = .2, \gamma = 1.4, P_r = .72, K_1 = 10^{-6}$
δ
x
$\Theta_b = 0°$
2°
4°
6°
0
.02
.04
.06
.08
.10
.12
.14
.1
.2
.3
.4
.5
.6
.7
.8
.9
1.0

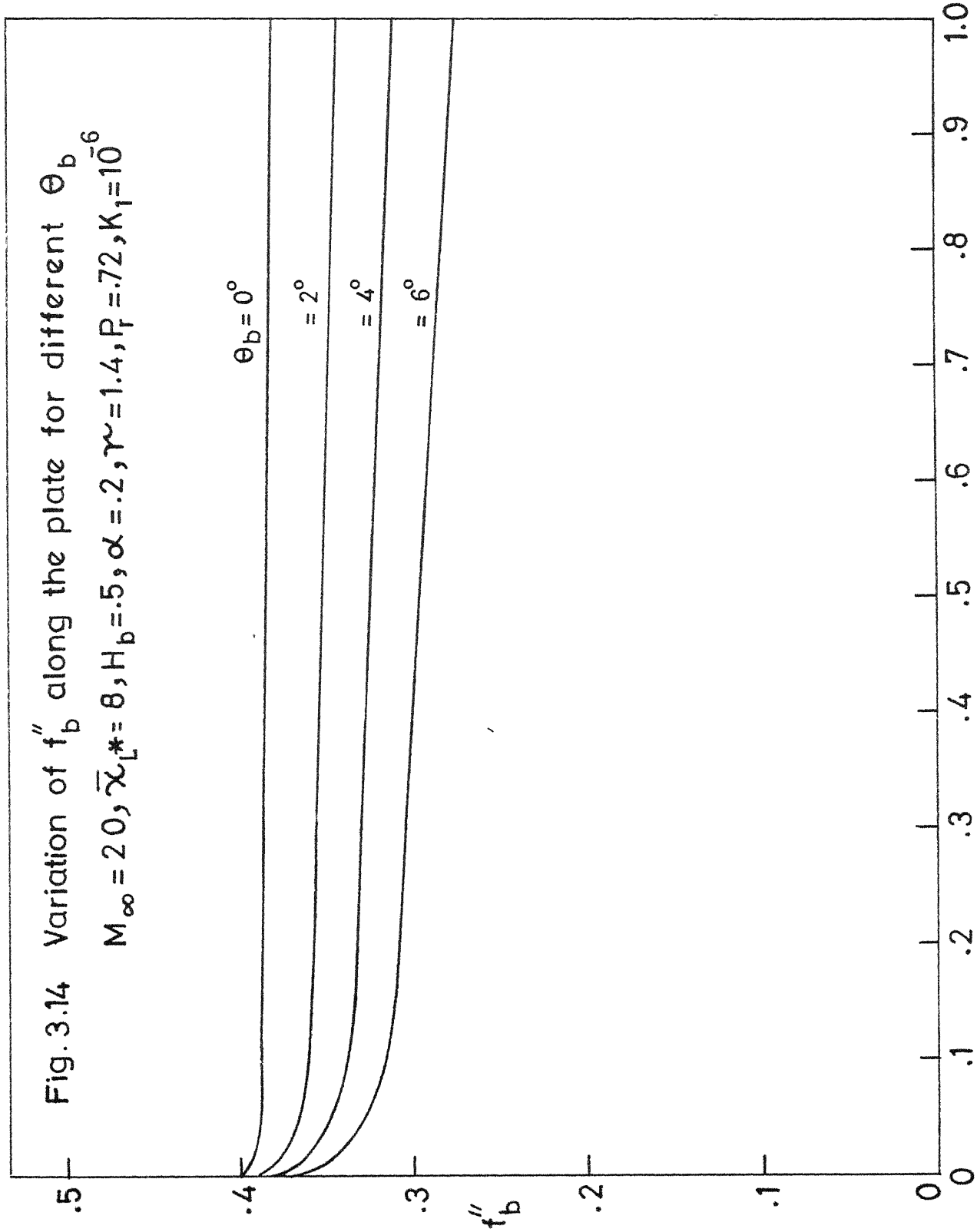
Fig. 3.14 Variation of f_b'' along the plate for different θ_b
$M_\infty = 2.0, \bar{\chi}_L^* = 8, H_b = .5, \alpha = .2, \gamma = 1.4, P_r = .72, K_1 = 10^{-6}$
$\theta_b = 0°$
$= 2°$
$= 4°$
$= 6°$
f_b''
x
0
.1
.2
.3
.4
.5
.6
.7
.8
.9
1.0
.5
.4
.3
.2
.1

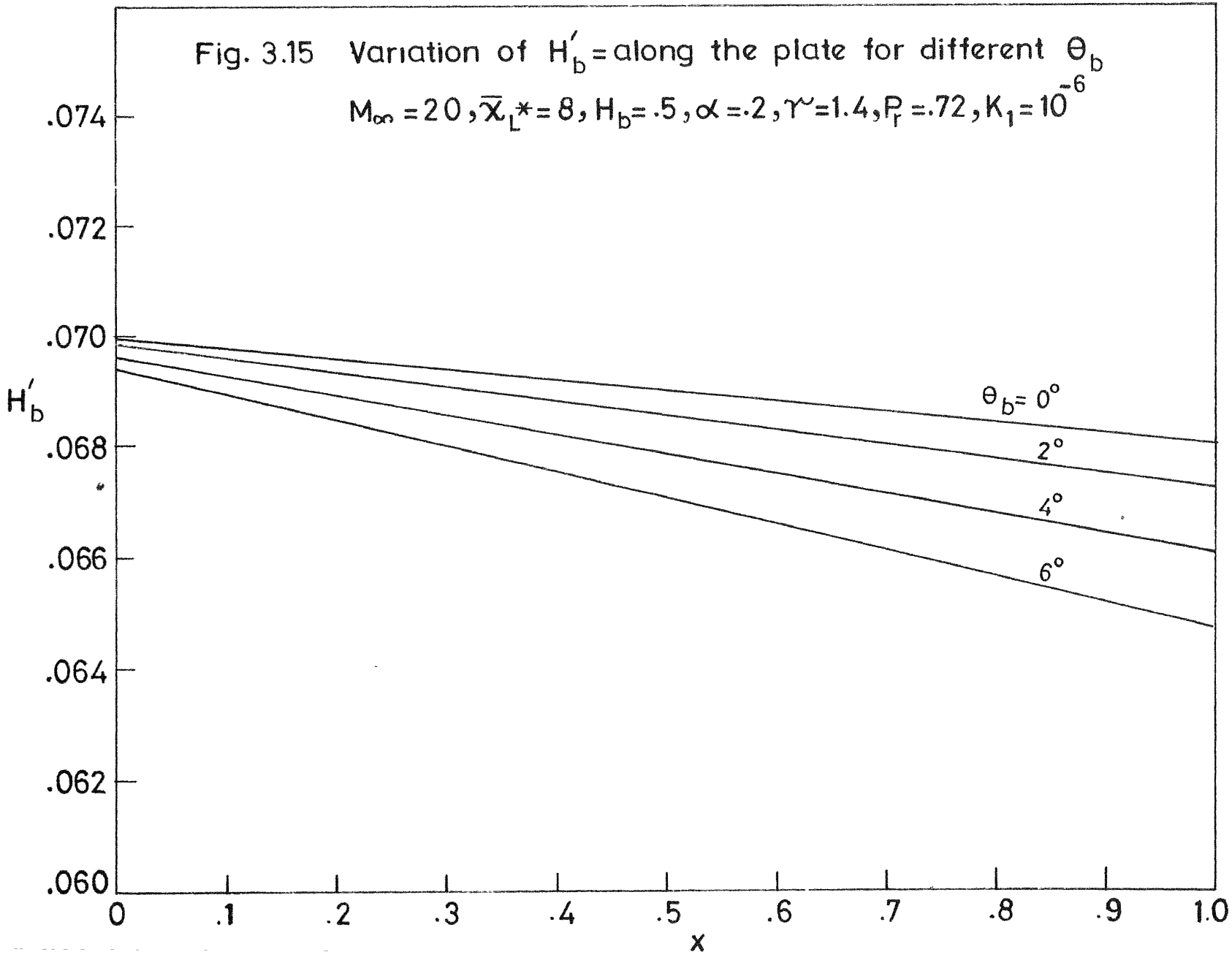
Fig. 3.15 Variation of H_b' = along the plate for different θ_b
$M_\infty = 20, \bar{\chi}_L^* = 8, H_b = .5, \alpha = .2, \gamma = 1.4, P_r = .72, K_1 = 10^{-6}$
H_b'
.074
.072
.070
.068
.066
.064
.062
.060
$\theta_b = 0°$
2°
4°
6°
0
.1
.2
.3
.4
.5
.6
.7
.8
.9
1.0
x

CHAPTER IV

DETAILS OF THE CLUTTER-SMITH METHOD OF NUMERICAL SOLUTION

4.1 Method of Solution

The method of solution is similar to the one described in ref. [61]. The x-derivatives in the momentum and energy equations are replaced by backward finite differences, so that the partial differential equations are approximated by ordinary differential equations. Then the problem of solution is essentially to find the unknown boundary conditions at the wall that satisfy the known boundary conditions. This is done with the help of shooting method with a cut-and-try approach. This procedure is described in the subsequent sections. The momentum equation (3.1) and the energy equation (3.2) are interdependent (or coupled) and must be solved simultaneously.

Of the several procedures possible for solving these equations simultaneously, the one used here is described below for a specified x-station.

Initially an enthalpy distribution is assumed at the given x-station and then a solution to the momentum equation is obtained using the cut-and-try procedure. Values of the stream function f and the velocity function f' from the first solution of the momentum equation are now used to obtain

a solution of the energy equation. This new enthalpy distribution is used to solve the momentum equation again. This iteration is continued until convergence of the solutions to the momentum equation is obtained to a specified accuracy. This procedure is depicted schematically in Fig. 4.1.

The details of the method of solution of the momentum and energy equations at a particular x-station are given in sections 4.1 and 4.2 and the formulas required for performing the integrations are given in section 4.4. The method of integration is a predictor-corrector multi-step method that uses the Falkner multiple-integration extrapolation formulas and the Adams-type multiple-integration interpolation formulas.

4.2 Solution of the Momentum Equation

At any x-station on the plate the momentum equation (3.1) is first rewritten with the following substitutions:

$$\begin{aligned} f &= \Phi + \eta \\ f' &= \Phi' + 1 \\ f'' &= \Phi'' \\ f''' &= \Phi''' \end{aligned} \tag{4.1}$$

Then the boundary conditions become

at $\eta = 0$

$$\Phi_b = f_b \tag{4.2a}$$

$$\Phi'_b = -1 \tag{4.2b}$$

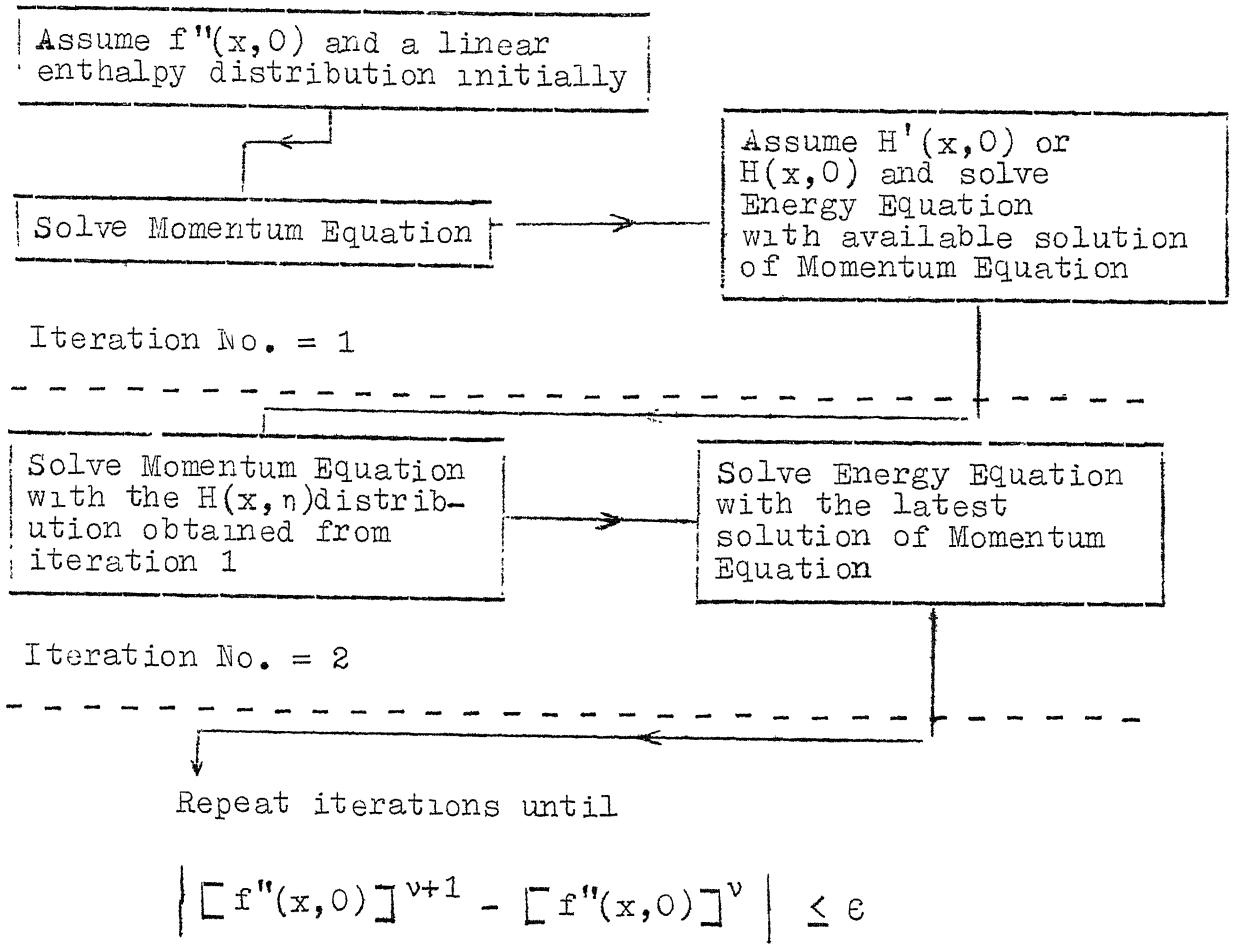

where ϵ is an accuracy input of $O(10^{-5})$ and ν stands for the iteration number.

Fig. 4.1 Flow diagram for solving the Boundary Layer Equations at an x-station.

at $\eta \rightarrow \eta_e$

$$\Phi' = 0 \qquad (4.3$$

The substitution given by eq. (4.1) is made to reduce the round-off errors in the computer program. With the replacement of the x-derivatives by finite-difference schemes as explained in section 3.4a of chapter III, the momentum eq. (3.1) becomes a third-order non-linear ordinary differential equation. The boundary conditions for the equation at the surface and boundary layer edge are given by (4.2) and (4.3) respectively.

Then the procedure is to solve (3.1) as an initial value problem with trial values of Φ_b'' as a third boundary condition. Now the search for the correct value of Φ_b'' is made by trying several values of Φ_b'' until the solutions for Φ' are bounded in a specified region. Specifically, three solutions of the momentum equation are sought with trial values of Φ_b'' such that Φ' at $\eta_{max} = \eta_e$ is between the bounds of $-K_2 \leq \Phi'(\eta_e) \leq K_2$. Both η_e and K_2 are inputs to the computer program. Atleast one of the three solutions must be high $(\Phi'(\eta_e) > 0)$ and one low $(\Phi'(\eta_e) < 0)$. The Lagrangian three point interpolation utilizing these three solutions is then used to determine the correct solution that satisfies the outer boundary condition $(\Phi'(\eta_e) = 0)$. The solution can be made as accurate as

desired by restricting the values of the bounds K_2. Typically K_2 would have a value 1 for five place accuracy.

In considering the solution of (3.1) as an initial value problem, Φ'' is first determined from:

$$\Phi'' = \int_0^\eta \Phi''' \, d\eta + \Phi_b'' \tag{4.4}$$

Here the value of Φ''' is given by (3.1) and Φ_b'' is the trial value. The integration in (4.4) is carried out by using the predictor-corrector technique at locations away from the wall. The Taylor's series expansion with a shorter step-size is used to start the solution near the wall. The details of the integration procedure are given in ref. [61]. Other quantities needed in the solution of (3.1) are obtained from:

$$\Phi' = \int_0^\eta \Phi'' \, d\eta + \Phi_b' \tag{4.5}$$

$$\Phi = \int_0^\eta \Phi' \, d\eta + \Phi_b \tag{4.6}$$

4.3 Solution of the Energy Equation

Similar to the case of momentum equation, here also we make the following substitution in the energy equation (3.2).

$$\begin{aligned} H &= G + 1 \\ H' &= G' \\ H'' &= G'' \end{aligned} \tag{4.7}$$

with this substitution the boundary conditions become:

at $\eta = 0$

$$G_b = H_b - 1 \qquad (4.8a)$$

at $\eta = \eta_e$

$$G = 0 \qquad (4.8b)$$

With the values of the stream function and its derivatives known, the energy equation (3.2) is a linear second-order equation. The associated boundary conditions are given by (4.8a) and (4.8b). After replacing the x-derivatives by the finite-difference approximation, eq. (3.2) is converted into an initial value problem by the specification of a trial value of G_b'. Two trial values are used and the resulting solutions are linearly combined to give the particular solution satisfying the outer boundary condition.

The integration formulas similar to those used for the solution of the momentum equation are employed to perform the necessary integrations. These formulas are used to obtain two solutions G_1 and G_2 of the equation (3.2). To avoid errors, one high and one low solutions are obtained such that $G_1(\eta_e) > 0$ and $G_2(\eta_e) < 0$. For better accuracies these solutions may again be bounded by:

$$0 < G_1(\eta_e) < K_3 \qquad (4.9a)$$

$$0 > G_2(\eta_e) > -K_3 \qquad (4.9b)$$

where K_3 is an input to the program. Its typical value may be of order 100.

The two solutions G_1 and G_2 are now combined go give the correct particular solution G:

$$G = AG_1 + (1-A)\, G_2 \tag{4.10}$$

where

$$A = \frac{G_2(\eta_e)}{G_2(\eta_e) - G_1(\eta_e)} \tag{4.11}$$

4.4 Method of Integration

This section is intended to give the details of the integration formulas employed in seeking the solutions to the governing equations. A special procedure involving the Taylor's series expansion is required to start the integration near the wall. The details of this are provided in Ref. [61]. Here we consider the general situation (away from the wall) where the equations have been integrated up to η_n and we are interested to obtain values of Φ and G and their derivatives at $\eta_{n+1}(=\eta_n + \Delta\eta)$. The extrapolation and interpolation formulas are used to approximate the integration indicated in (4.4), (4.5) and (4.6). The two-step procedure used in the integration is:

(i) the extrapolation formulas are used first, with the known values of Φ''' and Φ'' at the stations n, n-1, n-2 and n-3, to obtain the values of Φ, Φ', Φ'', and Φ''' at station n+1. The formulas employed are

$$\Phi''_{n+1)_E} = \Phi''_n + \frac{\Delta\eta}{24}\left[55\Phi'''_n - 59\Phi'''_{n-1} + 37\Phi'''_{n-2} - 9\Phi'''_{n-3}\right] \quad (4.12)$$

$$\Phi'_{n+1)_E} = \Phi'_n + \frac{\Delta\eta}{24}\left[55\Phi''_n - 59\Phi''_{n-1} + 37\Phi''_{n-2} - 9\Phi''_{n-3}\right] \quad (4.13)$$

$$\Phi_{n+1)_E} = \Phi_n + \Phi'_n + \frac{(\Delta\eta)^2}{360}\left[323\Phi''_n - 264\Phi''_{n-1} + 159\Phi''_{n-2} - 38\Phi''_{n-3}\right] \quad (4.14)$$

where the subscript E denotes ''extrapolated''. The errors in these formulas are proportional to $(\Delta\eta)^5$ or $(\Delta\eta)^6$. Further details of these formulas are given in ref. [61]. The value of Φ''' at n+1 can now be determined using the momentum equation and the extrapolated values of Φ'', Φ' and Φ.

(ii) The interpolation formulas can now be used to determine more exact values of Φ'', Φ', and Φ''' at the (n+1)th station. These formulas are

$$\Phi''_{n+1} = \Phi''_n + \frac{\Delta\eta}{24}\left[9\Phi'''_{n+1)_E} + 19\Phi'''_n - 5\Phi'''_{n-1} + \Phi'''_{n-2}\right] \quad (4.15)$$

$$\Phi'_{n+1} = \Phi'_n + \frac{\Delta\eta}{24}\left[9\Phi''_{n+1} + 19\Phi''_n - 5\Phi''_{n-1} + \Phi''_{n-2}\right] \quad (4.16)$$

$$\Phi_{n+1} = \Phi_n + \Delta\eta\,\Phi'_n + \frac{(\Delta\eta)^2}{360}\left[38\Phi''_{n+1} + 171\Phi''_n - 36\Phi''_{n-1} + 7\Phi''_{n-2}\right] \quad (4.17)$$

Finally the values of Φ'''_{n+1} is obtained by again using the momentum equation and the interpolated values above. The errors in the interpolation formulas are much smaller in their

magnitude as compared to those in the extrapolation formulas. Also, they are opposite in sign.

The formulas required for the integration of the energy equation are similar to those given above. For details reference may be made to the work of Clutter and Smith [61].

CHAPTER V

STEADY FLOW ON AN INCLINED FLAT PLATE WITH HETEROGENEOUS INJECTION

5.1 Introduction

Equations (2.38) through (2.40) for the steady hypersonic flow on a flat plate inclined at a small angle θ_b to the free stream and with injection of a foreign gas may be written as

$$\bar{p}\,\frac{\partial}{\partial\eta}\left(\lambda\,\frac{\partial^2 f}{\partial\eta^2}\right)+f\,\frac{\partial^2 f}{\partial\eta^2}-4x\left[\frac{\partial f}{\partial\eta}\,\frac{\partial^2 f}{\partial x\partial\eta}-\frac{\partial f}{\partial\eta}\,\frac{\partial^2 f}{\partial\eta^2}\right]$$
$$=\beta\left(2\,\frac{x}{\bar{p}}\,\frac{\partial\bar{p}}{\partial x}-1\right)\left[H-\left(\frac{\partial f}{\partial\eta}\right)^2\right]\left[\frac{1+c_1(s-1)}{1+c_1(r-1)}\right] \qquad (5.1)$$

$$\bar{p}\,\frac{\partial}{\partial\eta}\left[\frac{\lambda}{Pr}\,\frac{\partial H}{\partial\eta}+2(Pr-1)\,\frac{\partial f}{\partial\eta}\,\frac{\partial^2 f}{\partial\eta^2}+(Le-1)\left[\frac{r-1}{c_1(r-1)+1}\right]\right.$$
$$\left.\left[H-\left(\frac{\partial f}{\partial\eta}\right)^2\right]\frac{\partial c_1}{\partial\eta}\right]+f\,\frac{\partial H}{\partial\eta}-4x\left(\frac{\partial f}{\partial\eta}\,\frac{\partial H}{\partial x}-\frac{\partial H}{\partial\eta}\,\frac{\partial f}{\partial x}\right)=0 \qquad (5.2)$$

$$\bar{p}\,\frac{\partial}{\partial\eta}\left(\frac{\lambda}{Pr}\,Le\,\frac{\partial c_i}{\partial\eta}\right)+f\,\frac{\partial c_i}{\partial\eta}-4x\left(\frac{\partial f}{\partial\eta}\,\frac{\partial c_i}{\partial x}-\frac{\partial f}{\partial x}\,\frac{\partial c_i}{\partial\eta}\right)=0 \qquad (5.3)$$

Further for a binary mixture (i=1,2):

$$c_2=1-c_1 \qquad (5.4)$$

Thus we need to retain the species concentration equation for one of the species only.

The equations (5.1) through (5.3) are solved by an extension of the Clutter-Smith technique [65]. The variations in the Clutter-Smith method for the case of heterogeneous injection are described in the next section. Other details are the same as those given in chapter IV. Before going to the method of solution we will consider some of the fluid properties required for the computations of the binary mixture of perfect gases in the boundary layer. The suffixes 1 and 2 used for the fluid properties refer to the injectant (argonor helium) and the free steam fluid (air) respectively.

The fluid properties required are c^*_p, $c^*_{p_1}$, $c^*_{p_2}$, k^*, k^*_1, k^*_2, μ^*, μ^*_1, μ^*_2 and D^*_{12} and some combinations of these that give the parameters Le and Pr.

For ρ^* and c^*_p of the mixture the following expressions are used:

$$\rho^* = \frac{p^*}{R^*_u T^*} \left[\frac{M_1 M_2}{c_2(M_1 - M_2) + M_2} \right] \tag{5.5}$$

where R^*_u is the universal gas constant having a value of

$8.3196 \times 10^3 \quad \frac{m^2}{sec^2\text{-}K}$

$$c^*_p = (1-c_2)\, c^*_{p_1} + c_2\, c^*_{p_2} \tag{5.6}$$

For monatomic gases like argon and helium c_{p_1} are :

$$c^*_{p_{Ar}} = 5.2032 \times 10^2 \quad \frac{m^2}{sec^2\text{-}K} \tag{5.7}$$

$$c^*_{p_{He}} = 5.1988 \times 10^3 \quad \frac{m^2}{sec^2\text{-}K} \tag{5.8}$$

The variation of c^*_p for air is small over the temperature range under consideration and constant mean value of $c^*_{p_{Air}}$ is adopted to agree with the assumption of calorically perfect gas made earlier:

$$c^*_{p_{Air}} = 1.0383 \times 10^3 \quad \frac{m^2}{sec^2\text{-}K} \tag{5.9}$$

The viscosity of the binary gas mixture is obtained from the following expression derived from Wilke's formula [66]:

$$\mu^* = \frac{\mu_1^*}{1+G_{12}\frac{X_2}{X_1}} + \frac{\mu_2^*}{1+G_{21}\frac{X_1}{X_2}} \tag{5.10}$$

where

$$X_1 = \frac{(1-c_2)/M_1}{c_2/M_2+(1-c_2)/M_1} \tag{5.11a}$$

$$X_2 = \frac{c_2/M_2}{c_2/M_2+(1-c_2)/M_1} \tag{5.11b}$$

$$G_{12} = \frac{1}{\sqrt{8}}\left(1+\frac{M_1}{M_2}\right)^{-1/2}\left\{1+\left(\frac{\mu_1^*}{\mu_2^*}\right)^{1/2}\left(\frac{M_2}{M_1}\right)^{1/4}\right\}^2 \tag{5.11c}$$

Here μ_1^* and μ_2^* are the viscosities of the individual species.

$$M_2 = M_{Air} = 29$$

$$M_{He} = 4$$

$$M_{Ar} = 40$$

The viscosities of the individual species are obtained from polynomials that fit values obtained from the kinetic theory. These polynomials [20] have the form

$$\mu_j^* = A+BT^*+CT^{*2}+DT^{*3}+ET^{*4}+FT^{*5} \qquad (5.12)$$

The coefficients appearing in expression (5.12) are shown in table 5.1.

The thermal conductivities of the individual species are obtained from the Eucken relation [67]:

$$k_j^* = \frac{1}{4}\left(9\,\frac{c_{pj}^*}{c_{vj}^*}-5\right) c_{vj}^*\,\mu_j^* \qquad (5.13)$$

where c_{vj}^* is calculated by

$$c_{pj}^* = c_{vj}^* + R_u^*/M_j \qquad (5.14)$$

The thermal conductivities of the mixture are obtained by using the relation (5.16) and replacing the individual species viscosities by conductivities. The binary diffusion coefficients D_{12}^* are obtained from polynomials that fit values of $p^*D_{12}^*$ obtained from the kinetic theory. These polynomials [20] have the form:

$$p^*D_{12}^* = A+BT^*+CT^{*2}+DT^{*3}+ET^{*4}+FT^{*5} \qquad (5.15)$$

The various coefficients of the expression (5.15) are provided in table 5.2.

Table 5.1

Coefficients Appearing in the Polynomials for Viscosities of Individual Species, μ_j^* ($50K \leq T^* \leq 4000$ K) (Taken from Ref. [68])

Coefficients	Gas		
	He	Ar	Air
A	$2.6346879\ 10^{-6}$	$-2.6511108\ 10^{-7}$	$-9.25840\ 10^{-8}$
B	$6.849132\ 10^{-8}$	$9.262746\ 10^{-8}$	$7.698378\ 10^{-8}$
C	$-3.440510\ 10^{-11}$	$-6.88502\ 10^{-11}$	$-6.078874\ 10^{-11}$
D	$1.129453\ 10^{-14}$	$3.898027\ 10^{-14}$	$3.274786\ 10^{-14}$
E	$-9.0793378\ 10^{-19}$	$-1.038786\ 10^{-17}$	$-8.290185\ 10^{-18}$
F	$-9.149432\ 10^{-23}$	$1.036036\ 10^{-21}$	$7.917685\ 10^{-22}$

Table 5.2

Coefficients Appearing in the Polynomials for Binary Diffusion Coefficient, in $p^*D_{12}^*$ ($50\ K \leq T^* \leq 4000\ K$) (Taken from ref. [68])

Coefficients	Gas	
	He	Ar
A	$-4.341105\ 10^{-1}$	$-1.445589\ 10^{-1}$
B	$1.152878\ 10^{-2}$	$3.912013\ 10^{-3}$
C	$5.751873\ 10^{-5}$	$1.686750\ 10^{-5}$
D	$-1.051026\ 10^{-8}$	$-3.399687\ 10^{-19}$
E	$2.1970975\ 10^{-12}$	$6.880437\ 10^{-13}$
F	$-1.983057\ 10^{-16}$	$-5.965776\ 10^{-17}$

5.2 Method of Solution

At any given x-station (denoted as m in the finite-difference scheme) along the plate, the fluid properties, c_1 and G profiles computed from the previous (m-1) station are used to obtain a first solution of the momentum equation. The calculated stream function and its derivatives may be denoted by Φ_{NM}, Φ'_{NM}, Φ''_{NM}, where the subscript NM represents the iteration number. Using the same fluid properties and the newly calculated functions Φ_1, Φ'_1, Φ''_1 the species and energy equations are solved. Since the fluid properties are known these equations are linear and their solution is comparatively simple. The computed profiles may be denoted by $c_{1_{NSE}}$, $c'_{1_{NSE}}$, G_{NSE}, G'_{NSE}, where the subscript NSE signifies the iteration number. These solutions of the species and energy equations of NSE = 1 are used to recalculate the fluid properties still using the stream functions and its derivatives calculated for NM = 1 earlier. The species and energy equations are solved again using these new fluid properties. These solutions, denoted by NSE = 2 are used to compute fluid properties once again. This process is continued until the solutions to the energy and species equations converge to the desired accuracy:

$$|G'_{NSE} - G'_{NSE-1}| < \epsilon_2 \text{ and } |c'_{1_{NSE}} - c'_{1_{NSE-1}}| < \epsilon_3 \qquad (5.16)$$

where ϵ_2 and ϵ_3 are accuracy inputs. Satisfaction of the

convergence condition (5.16) implies convergence of the fluid properties as well. The same stream function denoted by subscript NM = 1 is used throughout this iteration loop. Upon satisfaction of the convergence condition (5.16), the momentum equation is solved a second time using the latest converged fluid properties and G and c_1 profiles. The computed stream function is denoted by NM = 2. This value of the stream function is now used again to solve the species and energy equations for obtaining the converged fluid properties as described above. This cycle of double iteration is continued until convergence of solutions of the momentum equation is obtained i.e., until

$$|\Phi''_{NM} - \Phi''_{NM-1}| < \epsilon_1 \qquad (5.17)$$

To start the solution at the first station profiles of ϕ and G are obtained from the series expansion solutions with air injection described in chapter III and the initial fluid properties for the iterative cycle are computed from these. During the course of computations of the heterogeneous injection case, it was found that four iterations of the species and energy equations satisfied conditions (5.16) if ϵ_2 and ϵ_3 ranged from 10^{-3} to 10^{-4}. Consequently, this iteration loop was carried four cycles each time and the condition (5.16) was not built into the program. For the momentum equation the accuracy input ϵ_1 was given a value 10^{-4}.

The flow diagram for solving the mutually coupled momentum, energy and the species concentration equation is given in Fig. 5.1.

In general, convergence was substantially slower if the injected gas differed considerably (e.g. helium) in physical properties from the external fluid (air) as compared to the case when the injected gas did not differ much (e.g. argon) from the external fluid. Thus, whereas the Clutter-Smith method gave results with a fast rate of convergence for the case of argon injection, it failed to give the trial solutions within the bounds at the last station along the plate with helium injection. Hence an alternative numerical method was sought for in the case with helium injection which is described in section 5.5. Section 5.3 and 5.4 give outlines of the Clutter-Smith technique used for the case of argon injection.

5.3 Solution of Momentum Equation

With the replacement of the x-derivatives by finite difference schemes as explained in section 3.4a of chapter III, the momentum equation (5.1) becomes a third order non-linear ordinary differential equation. Boundary conditions for the equation are specified at the surface and at the boundary layer edge by eqs. (2.56) and (2.58) respectively. The procedure to solve (5.1) as an initial value problem is the same as the one described in chapter IV.

In considering the solution of (5.1) as an initial value problem, Φ'' is first determined from:

$$\lambda\Phi'' = \int_0^{\eta} \frac{\partial}{\partial} (\lambda\Phi'')d\eta + \lambda_b \Phi_b'' \qquad (5.18)$$

Here λ_b is known and Φ_b'' is the trial value. The value of $\frac{\partial}{\partial \eta} (\lambda\Phi'')$ is given by (5.1). Similar to the procedure explained in chapter IV, the integration of eq. (5.18) is carried out using the predictor-corrector technique at locations away from the wall. The Taylor's series expansion with shorter step-size is used to initiate the solution near the wall. Other quantities needed in the solution of (5.1) are given by

$$\Phi'' = \frac{(\lambda\Phi'')}{\lambda} \qquad (5.19)$$

$$\Phi' = \int_0^{\eta} \Phi'' \, d\eta + \Phi_b' \qquad (5.20)$$

$$\Phi = \int_0^{\eta} \Phi' d\eta + \Phi_b \qquad (5.21)$$

If may be noted that this particular formulation avoids the necessity of computing normal derivatives of λ and thus eliminates a potential source of error.

5.4 Solution of the Energy and Species Equations

With the known values of stream function and fluid properties both energy and species equations (5.2) and (5.3) become second-order linear equation. Their solutions are

converted into initial value problems by the specification of $(\partial G/\partial \eta)_b$ for the energy equation and c_{1b} (and hence $(\partial c_1/\partial \eta)_b$) for the species equation. Two trial values are used in both cases and the resulting solutions are linearly combined to give the particular solution satisfying the outer boundary condition.

For any x-station the equation (5.2) and (5.3) are rewritten to give:

$$\frac{\partial \pi}{\partial \eta} = \left[-(\Phi+\eta)G'+4x\left\{(\Phi'+1)\frac{\partial G}{\partial x} - G'\frac{\partial \Phi}{\partial x}\right\}\right]/\bar{\rho} \qquad (5.22)$$

and

$$\frac{\partial \pi_1}{\partial \eta} = \left[-(\Phi+\eta)c_1'+4x\left\{(\Phi'+1)\frac{\partial c_1}{\partial x} - c_1'\frac{\partial \Phi}{\partial x}\right\}\right]/\bar{\rho} \qquad (5.23)$$

where

$$\pi = \frac{\lambda}{Pr}\left[G'+2(Pr-1)(\Phi'+1)\,\Phi''+(Le-1)\left\{\frac{r-1}{(r-1)c_1+1}\right\}\right.$$
$$\left.\left\{(G+1) - (\Phi'+1)^2\right\}\frac{\partial c_1}{\partial \eta}\right] \qquad (5.24)$$

$$\pi_1 = \frac{\lambda}{Pr}\,Le\,\frac{\partial c_1}{\partial \eta} \qquad (5.25)$$

$$\Phi = f-\eta \qquad (5.26)$$

$$G = H-1 \qquad (5.27)$$

With the substitutions given by equations (4.1) and (4.7) the boundary conditions (2.56) and (2.58) for the present case become

at $\eta \to \infty$

$$\Phi' = 0 \tag{5.28a}$$

$$G = 0 \tag{5.28b}$$

$$c_1 = 0 \tag{5.28c}$$

at $\eta = 0$

$$\Phi' = -1 \tag{5.29a}$$

$$\Phi + 4x \frac{\partial \Phi}{\partial x} = - \rho_b \, v_b(x) \frac{2\sqrt{Re_{\infty,L^*}}}{\sqrt{C \; p_o}} \sqrt{\frac{x}{\bar{x}}} \tag{5.29b}$$

$$\frac{\partial c_1}{\partial \eta} = \left(\frac{Pr}{\mu \, Le}\right)(1-c_{1b}) \frac{C \; \rho_o}{\rho_b} \bar{x} \left(\Phi + 4x \frac{\partial \Phi}{\partial x}\right) \tag{5.29c}$$

$$G_b = \left[c_{1b} \, (r - 1) + 1 \right] \frac{2T_b}{(\gamma-1) \, M_\infty^2} - 1 \tag{5.29d}$$

In eq. (5.29b) the right hand side, in general, is a function of x. However, in order to have the results comparable with those obtained for the case of air (homogeneous) injection, eq. (5.29b) is used in the form :

$$\Phi + 4x \frac{\partial \Phi}{\partial x} = -2\alpha \tag{5.29e}$$

In the computer program, the equations (5.22) and (5.23) are solved by programming a dummy equation of the form :

$$\bar{Z}' = \left[-(\Phi + \eta) \, \bar{Q}' + 4x \left\{ (\Phi'+1) \frac{\partial Q}{\partial x} - Q' \frac{\partial \Phi}{\partial x} \right\} \right] / \bar{p} \tag{5.30}$$

where $\bar{Z} = \bar{Z}(Q', Q)$.

The associated boundary conditions are :

at $\eta = \eta_e$

$$\bar{Q} = \bar{Q}_e \tag{5.31a}$$

at $\eta = 0$

$$\bar{Q} = \bar{Q}_b \tag{5.31b}$$

$$\bar{Q}' = \bar{Q}'_b \text{ (to be found)} \tag{5.31c}$$

Solutions of the energy and species equations are then obtained by solving equation (5.30) with the conditions (5.31) where for the energy equation

$$\bar{Z} = \pi \left(\frac{\partial G}{\partial \eta}, G\right) \tag{5.32}$$

$$\bar{Q} = G \tag{5.33}$$

$$\bar{Q}_e = 0 \tag{5.34}$$

$$\bar{Q}_b = G_b \tag{5.35}$$

and for the species equation

$$\bar{Z} = \pi_1 \left(\frac{\partial c_1}{\partial \eta}\right) \tag{5.36}$$

$$\bar{Q} = c_1 \tag{5.37}$$

$$\bar{Q}_e = 0 \tag{5.38}$$

$$\left(\frac{\partial \bar{Q}}{\partial \eta}\right)_b = \left(\frac{Pr}{\lambda\, Le}\right)_b (1-\bar{Q}_b) \frac{C\, p_o}{\rho_b}\, \bar{x} \left\{\Phi_b + 4x \left(\frac{\partial \Phi}{\partial x}\right)_b\right\} \tag{5.39}$$

It is to be noted that the specification of the wall concentration by relation (5.39) necessitates the recalculation

of G_b after each solution of the species equation. Hence G_b varies with $c^*_{p_b}$ for a constant surface temperature, T^*_b. $c^*_{p_b}$, in turn, is dependent on the surface concentration, c_{1b}, obtained from the solution of the species equation.

The method of solution of (5.39) is the similar to the one described in sec. 4.3 of Chapter IV.

In the Clutter-Smith procedure employed here and described in Chapters III and IV the x-derivatives are replaced by backward difference formulas and the partial differential equations thus become converted into ordinary differential equations. Because of the use of backward difference formulas for the x-derivatives, this implicit method is inherently stable. This method eventhough easy to apply and more efficient, has certain limitations especially, for the flow problems where skin-friction and heat transfer become small, as in the case of boundary layer injection. For such cases the derivative boundary conditions as $\eta \to \infty$ may not be satisfied and accordingly the solution may not converge. With argon injection, however, the convergence was easily obtained. But when a very light gas like helium was injected, convergence was difficult even at the beginning stations along the plate and it did not converge at the last station. The trial solutions for the momentum equation could not be obtained within the bounds. The reason for this was observed to be due to the fact that when, at the last station, the value of $\Phi''(0)$ was perturbed by an amount of $O(10^{-5})$ the value of Φ' at the

At the start of a station, assume fluid properties from the previous station.

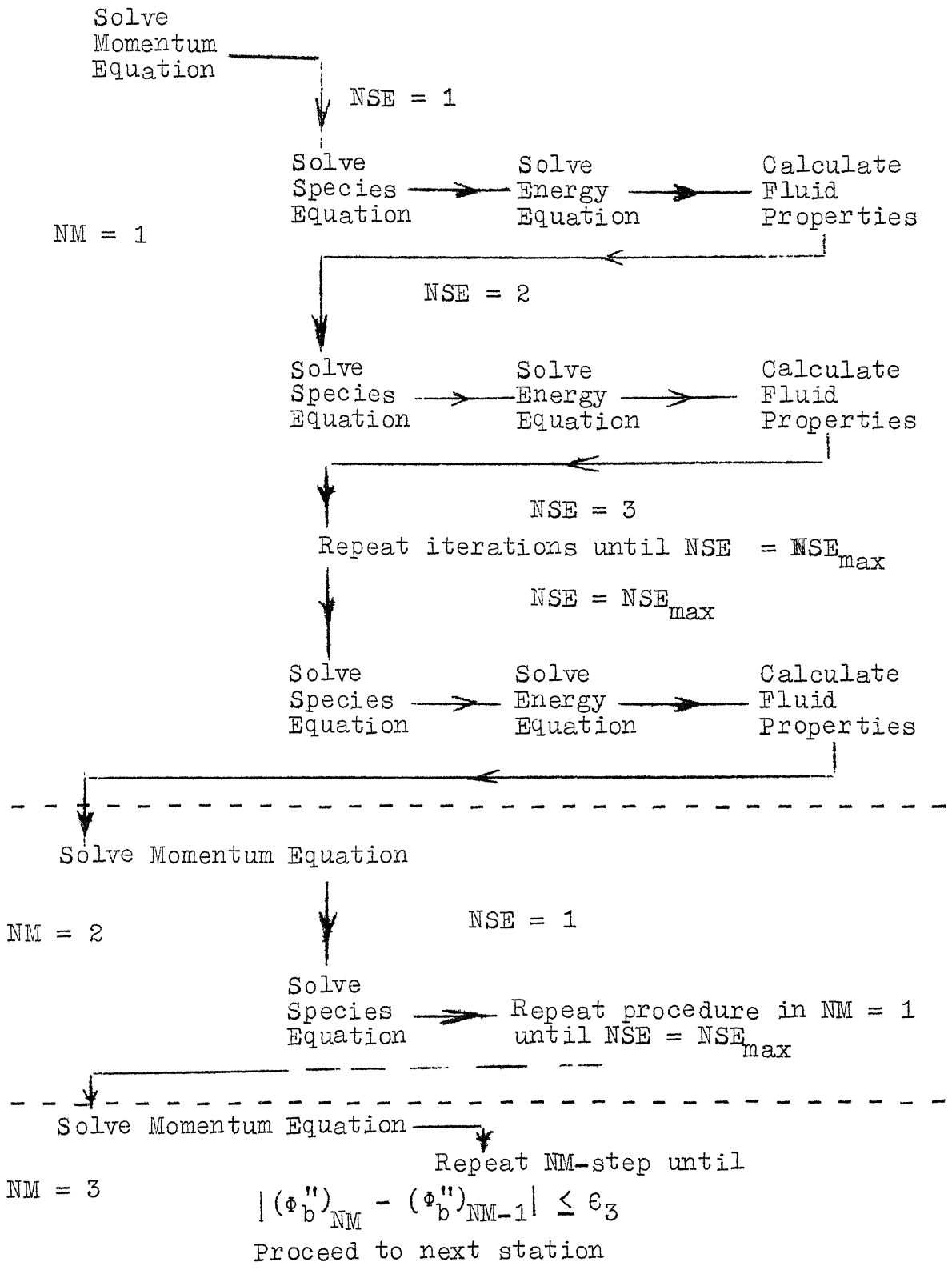

Fig. 5.1 Flow diagram for solving Boundary Layer Equations for a binary mixture at an x-station.

outer edge of the boundary layer was seen to change by an amount greater than 10^3. Hence for the case of helium injection a finite-difference method based on Crank-Nicolson implicit scheme was adopted. This is described in the next section.

5.5 Finite-difference Method for Heterogeneous Injection

To circumvent the difficulties which arose during the solution of the boundary-layer equation with helium injection a finite-differences method described in [23] is briefly presented here. In this method, the governing partial differential equations are transformed into new coordinates with finite ranges by means of a transformation which maps an infinite interval into a finite one. The resulting equations are solved by converting them into a matrix equation through the application of implicit finite-difference formulas. The matrix equations have a tridiagonal character and can be solved on a computer by making use of a suitable algorithm [69,23,70]. Only those details which are pertinent to the present problem are given here. For further details a reference may be made to the original paper [23]. The distinct advantage of the present method over the Clutter-Smith technique is that values of the dependent variables, rather than their slopes, are employed to obtain solutions. The associated disadvantage with this method is that there might be slight oscillations present in the quantities like $\partial^2 f/\partial \eta^2$ and $\partial H/\partial \eta$ etc. due to their computations from the finite-difference approximations.

First of all, the equations (5.1) to (5.3) are transformed from the (x-η)-coordinates system to the (x-ξ) system thereby replacing the infinite interval in the η-direction into a finite interval. The transformation employed is :

$$\xi = 1 - e^{\alpha_1 \eta} \tag{5.40}$$

For a system of finite-difference equations with a fixed number of ξ nodal points and a fixed interval $\Delta\xi$, α_1 is used as a scaling factor to provide an optimum distribution of nodal points across the boundary layer. A certain computer experimentation is done to achieve the optimum results. The following transformation equations are obtained from equation (5.40)

$$\frac{\partial \zeta}{\partial \eta} = \frac{\partial \zeta}{\partial \xi}\frac{\partial \xi}{\partial \eta} = \alpha_1(1-\xi)\frac{\partial \zeta}{\partial \xi} = Z\frac{\partial \zeta}{\partial \xi} \tag{5.41}$$

and

$$\frac{\partial^2 \zeta}{\partial \eta^2} = Z^2\frac{\partial^2 \zeta}{\partial \xi^2} - \alpha_1 Z\frac{\partial \zeta}{\partial \xi} \tag{5.42}$$

where $$Z = \alpha_1(1-\xi) \tag{5.43}$$

Using these transformation equations and using $F = f'$, equation (5.1) through (5.3) become

$$\bar{p}\,Z^2\frac{\partial \lambda}{\partial \xi}\frac{\partial F}{\partial \xi} + \bar{p}\,\lambda Z\left(Z\frac{\partial^2 F}{\partial \xi^2} - \alpha_1\frac{\partial F}{\partial \xi}\right) = -f Z\frac{\partial F}{\partial \xi}$$

$$- 4x\left(Z\frac{\partial f}{\partial x}\frac{\partial F}{\partial \xi} - F\frac{\partial F}{\partial x}\right) + \beta\left(\frac{2x}{\bar{p}}\frac{d\bar{p}}{dx} - 1\right)(H-F^2)\left[\frac{1+c_1(s-1)}{1+c_1(r-1)}\right] \tag{5.44}$$

$$\bar{\rho}\, Z^2 \left[\frac{\partial}{\partial \xi}\left(\frac{\lambda}{Pr}\right)\right]\left[\frac{\partial H}{\partial \xi} + 2(Pr-1)F\,\frac{\partial F}{\partial \xi} + (Le-1)\left\{\frac{r-1}{(r-1)c_1+1}\right\}\right.$$

$$\left.(H-F^2)\,\frac{\partial c_1}{\partial \xi}\right] + \bar{\rho}\left(\frac{\lambda}{Pr}\right)\left[Z^2\,\frac{\partial^2 H}{\partial \xi^2} - \alpha_1\, Z\,\frac{\partial H}{\partial \xi}\right.$$

$$+ 2Z^2\, F\,\frac{\partial Pr}{\partial \xi}\,\frac{\partial F}{\partial \xi} + 2(Pr-1)\left\{Z^2\left(\frac{\partial F}{\partial \xi}\right)^2 +\right.$$

$$\left.\left(Z^2\,\frac{\partial^2 F}{\partial \xi^2} - \alpha_1\, Z\,\frac{\partial F}{\partial \xi}\right) F\right\} + Z^2\,\frac{\partial Le}{\partial \xi}\left\{\frac{r-1}{c_1(r-1)+1}\right\}$$

$$(H-F^2)\,\frac{\partial c_1}{\partial \xi} + (Le-1)\left\{\frac{r-1}{c_1(r-1)+1}\right\}(H-F^2)\left(Z^2\,\frac{\partial^2 c_1}{\partial \xi^2}\right.$$

$$\left. - \alpha_1\, Z\,\frac{\partial c_1}{\partial \xi}\right) + (Le-1)\left\{\frac{r-1}{c_1(r-1)+1}\right\} Z^2\,\frac{\partial c_1}{\partial \xi}\left(\frac{\partial H}{\partial \xi} - 2F\,\frac{\partial F}{\partial \xi}\right)$$

$$\left. + (Le-1)(H-F^2)Z^2\left\{\frac{-(r-1)^2}{((r-1)c_1+1)^2}\right\}\left(\frac{\partial c_1}{\partial \xi}\right)^2\right]$$

$$= -f\, Z\,\frac{\partial H}{\partial \xi} + 4x\left(F\,\frac{\partial H}{\partial x} - Z\,\frac{\partial H}{\partial \xi}\,\frac{\partial f}{\partial x}\right) \qquad (5.45)$$

$$\bar{\rho}\, Z^2\,\frac{\partial}{\partial \xi}\left(\frac{\lambda Le}{Pr}\right)\frac{\partial c_1}{\partial \xi} + \bar{\rho}\,\frac{\lambda Le}{Pr}\left(Z^2\,\frac{\partial^2 c_1}{\partial \xi^2} - \alpha_1 Z\,\frac{\partial c_1}{\partial \xi}\right)$$

$$= -Z\, f\,\frac{\partial c_1}{\partial \xi} + 4x\left(F\,\frac{\partial c_1}{\partial x} - Z\,\frac{\partial f}{\partial x}\,\frac{\partial c_1}{\partial \xi}\right) \qquad (5.46)$$

where

$$f(x,\xi) = \int_0^{\xi} \frac{F}{Z}\, d\xi + f(x,0) \qquad (5.47)$$

The boundary conditions become

at $\xi = 0$

$$F = 0 \tag{5.48a}$$

$$H_b(x) = \left[r\, c_{1b} + (1-c_{1b}) \right] \frac{2T_b}{(\gamma-1)\, M_\infty^2} \tag{5.48b}$$

$$f + 4x \frac{\partial f}{\partial x} = -2\alpha \tag{5.48c}$$

$$\frac{\partial c_1}{\partial \xi} = \frac{(1-c_{1b})}{\alpha_1} \left(\frac{Pr}{\mu Le}\right)_b \frac{C\, p_o\, \bar{x}}{\rho_b} \left(f + 4x \frac{\partial f}{\partial x}\right) \tag{5.48d}$$

and at $\xi = 1$

$$F = 1 \tag{5.49a}$$

$$H = 1 \tag{5.49b}$$

$$c_1 = 0 \tag{5.49c}$$

5.6 Finite-difference Equations For the Non-Similar Problem

The mesh-point diagram for the Crank-Nicholson scheme is given in Fig. 5.2. With the N nodal points in the ξ-direction, we have

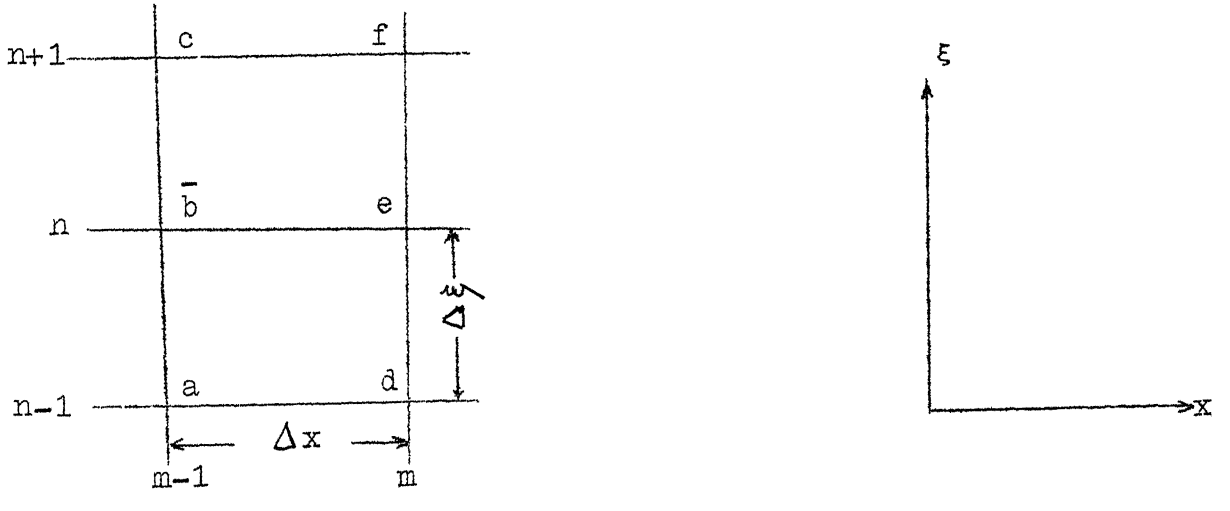

Fig. 5.2 Mesh-point diagram for Crank-Nicolson scheme.

$$(N - 1)\,\Delta\xi = 1 \tag{5.50}$$

The following finite-difference equations are used to reduce the non-similar boundary layer equations to a system of linear algebraic equations

$$G = G_e \tag{5.50a}$$

$$G_x = \frac{G_e - G_{\bar{b}}}{\Delta x} \tag{5.50b}$$

$$G_\xi = \frac{1}{4\Delta\xi}\,(G_e - G_a + G_f - G_d) \tag{5.50c}$$

$$G_{\xi\xi} = \frac{1}{2(\Delta\xi)^2}\,(G_e - 2G_{\bar{b}} + G_a + G_f - 2G_e + G_d) \tag{5.50d}$$

$$GM_x = G_{\bar{b}}\,\frac{M_e - M_{\bar{b}}}{\Delta x} \tag{5.50e}$$

$$G_\xi\,M_\xi = \frac{1}{8(\Delta\xi)^2}\left[(G_e - G_a)(M_f - M_d) + (G_f - G_d)(M_e - M_a)\right] \tag{5.50f}$$

$$G_\xi^2 = \frac{1}{4(\Delta\xi)^2}\left[(G_e - G_a)\,(G_f - G_d)\right] \tag{5.50g}$$

$$G^2 = G_{\bar{b}} \times G_e \tag{5.50h}$$

$$R_\xi = \frac{R_c - R_a}{2(\Delta\xi)} \tag{5.50c}$$

$$R_{\xi\xi} = \frac{R_c - 2R_{\bar{b}} + R_a}{(\Delta\xi)^2} \tag{5.50j}$$

Equations (5.50b - d) are used to approximate the unknowns and their derivatives. These are the Crank-Nicholson formulas.

The equations (5.50e - h) are used to make the unknowns to appear linearly. The central-difference equations (5.50i - j) are for the derivatives of fluid properties.

5.7 Method of Solution

To obtain a numerical solution, equations (5.44) through (5.46) are approximated by the finite-difference equations described in the previous section. The resulting equations are :

$$F_d \left[-\frac{\bar{p}\, Z^2\, \lambda_\xi}{4(\Delta\xi)} + \frac{\bar{p}\, \lambda\, Z^2}{2(\Delta\xi)^2} + \frac{\bar{p}\, \lambda\, \alpha_1\, Z}{4(\Delta\xi)} - \frac{Zf}{4\,\Delta\xi} - \frac{xZ}{(\Delta\xi)} f_x \right] +$$

$$F_e \left[-\frac{\bar{p}\, \lambda\, Z^2}{(\Delta\xi)^2} - \frac{4x}{\Delta x} F_{\bar{b}} + \beta\left(\frac{2x}{\bar{p}} \frac{d\bar{p}}{dx} - 1\right) \left\{ \frac{1+c_{1\bar{b}}(s-1)}{1+c_{1\bar{b}}(r-1)} \right\} F_{\bar{b}} \right] +$$

$$F_f \left[\frac{\bar{p}\, Z^2\, \lambda_\xi}{4\,\Delta\xi} + \frac{\bar{p}\, \lambda Z^2}{2(\Delta\xi)^2} - \frac{\bar{p}\, \lambda\, \alpha_1\, Z}{4\,\Delta\xi} + \frac{Zf}{4\,\Delta\xi} + \frac{x\, Z\, f_x}{\Delta\xi} \right]$$

$$= -\frac{\bar{p}\, Z^2\, \lambda_\xi}{4\,\Delta\xi} (F_c - F_a) - \frac{\bar{p}\, \lambda\, Z^2}{2(\Delta\xi)^2} (F_c - 2F_{\bar{b}} + F_a)$$

$$+ \frac{\bar{p}\, \lambda\, \alpha_1\, Z}{4\,\Delta\xi} (F_c - F_a) - \frac{Zf}{4\,\Delta\xi} (F_c - F_a) - \frac{x\, Z\, f_x}{\Delta\xi} (F_c - F_a)$$

$$- \frac{4x}{\Delta x} F_{\bar{b}}^2 + \beta\left(\frac{2x}{\bar{p}} \frac{d\bar{p}}{dx} - 1\right) H_{\bar{b}} \left\{ \frac{1 + c_{1\bar{b}}\,(s-1)}{1 + c_{1\bar{b}}\,(r-1)} \right\} \quad (5.51)$$

$$H_d \left[-\bar{p}\, Z^2 \left(\frac{\lambda}{Pr}\right)_\xi \frac{1}{4\,\Delta\xi} + \bar{p}\, \frac{\lambda}{Pr} \frac{Z^2}{2(\Delta\xi)^2} + \frac{\alpha_1\, Z\, \bar{p}\, (\lambda/Pr)}{4\,\Delta\xi} \right.$$

$$\left. - \frac{\bar{p}(\lambda/Pr)\, Z^2 (Le-1)\,(r-1)}{8(\Delta\xi)^2\,((r-1)\,c_{1\bar{b}} + 1)} (c_{1c} - c_{1a}) - \frac{fZ}{4(\Delta\xi)} - \frac{x\, Z\, f_x}{\Delta\xi} \right] +$$

$$H_e \left[\bar{p} z^2 \left(\frac{\lambda}{Pr}\right)_\xi (Le-1) \left\{\frac{r-1}{(r-1)c_{1_{\bar{b}}}+1}\right\} \left(c_{1_{\bar{b}}}\right) - \bar{p} \left(\frac{\lambda}{Pr}\right) \frac{Z^2}{(\Delta\xi)^2}\right.$$

$$+ \bar{p}\left(\frac{\lambda}{Pr}\right) Z^2 \, Le_\xi \left\{\frac{r-1}{(r-1)c_{1_{\bar{b}}}+1}\right\} \left(c_{1_{\bar{b}}}\right) + \bar{p} \frac{\lambda}{Pr} (Le-1)$$

$$\left\{\frac{r-1}{(r-1)c_{1_{\bar{b}}}+1}\right\} \left(Z^2 c_{1_{\bar{b}}\xi\xi} - \alpha_1 z \, c_{1_{\bar{b}}\xi}\right) + \bar{p} \frac{\lambda}{Pr} (Le-1) Z^2$$

$$\left.\left\{\frac{-(r-1)^2}{((r-1)c_{1_{\bar{b}}}+1)^2}\right\} \left(c_{1_{\bar{b}}\xi}\right)^2 - \frac{4x \, F_{\bar{b}}}{\Delta x}\right] +$$

$$H_f \left[\bar{p} Z^2 \left(\frac{\lambda}{Pr}\right)_\xi \frac{1}{4(\Delta\xi)} + \bar{p} \frac{\lambda}{Pr} \frac{Z^2}{2(\Delta\xi)^2} - \bar{p} \frac{\lambda}{Pr} \frac{\alpha_1 Z}{4(\Delta\xi)} + \bar{p} \frac{\lambda}{Pr}\right.$$

$$(Le-1) \left\{\frac{(r-1)Z^2}{(r-1)c_{1_{\bar{b}}}+1)}\right\} \frac{c_{1_{\bar{b}}} - c_{1a}}{8(\Delta\xi)^2} + \frac{fZ}{4(\Delta\xi)} + \left.\frac{xZfx}{\Delta\xi}\right] +$$

$$F_d \left[-\bar{p} Z^2 \left(\frac{\lambda}{Pr}\right)_\xi 2(Pr-1) \frac{F_{\bar{b}}}{4(\Delta\xi)} - \bar{p}\left(\frac{\lambda}{Pr}\right) \frac{Z^2 F_{\bar{b}} \, Pr_\xi}{2(\Delta\xi)}\right.$$

$$- \bar{p} \left(\frac{\lambda}{Pr}\right) \frac{(Pr-1)Z^2(Fc-Fa)}{2(\Delta\xi)^2} + \bar{p}\left(\frac{\lambda}{Pr}\right) \frac{(Pr-1)Z^2 F_{\bar{b}}}{(\Delta\xi)^2} +$$

$$+ \bar{p}\left(\frac{\lambda}{Pr}\right) \frac{\alpha_1 (Pr-1) Z \, F_{\bar{b}}}{2(\Delta\xi)} + \bar{p}\left(\frac{\lambda}{Pr}\right) (Le-1) \left\{\frac{r-1}{(r-1)c_{1_{\bar{b}}}+1}\right\}$$

$$\left.\left\{\frac{Z^2 \, F_{\bar{b}} (c_{1c} - c_{1a})}{4(\Delta\xi)^2}\right\}\right] +$$

$$F_e \left[-\bar{p} Z^2 \left(\frac{\lambda}{Pr}\right)_\xi (Le-1) \left\{\frac{r-1}{(r-1)c_{1_{\bar{b}}}+1}\right\} F_{\bar{b}} \, c_{1_{\bar{b}}\xi} - \bar{p} \left(\frac{\lambda}{Pr}\right) 2(Pr-1)\right.$$

$$\frac{Z^2 F_{\bar{b}}}{(\Delta\xi)^2} - \bar{p}\left(\frac{\lambda}{Pr}\right)Z^2\, Le_\xi \left\{\frac{r-1}{(r-1)c_{1_{\bar{b}}}+1}\right\} F_{\bar{b}}\, c_{1_{\bar{b}_\xi}} - \bar{p}\left(\frac{\lambda}{Pr}\right)(Le-1)$$

$$\left\{\frac{r-1}{(r-1)c_{1_{\bar{b}}}+1}\right\} F_{\bar{b}} Z\,(Z\, c_{1_{\bar{b}_{\xi\xi}}} - \alpha_1 c_{1_{\bar{b}_\xi}}) + \bar{p}\left(\frac{\lambda}{Pr}\right)(Le-1)$$

$$F_{\bar{b}}\, Z^2 \left\{\frac{(r-1)^2}{((r-1)c_{1_{\bar{b}}}+1)^2}\right\}(c_{1_{\bar{b}_\xi}})^2 +$$

$$F_f\left[\bar{p}\, Z^2\left(\frac{\lambda}{Pr}\right)_\xi \frac{(Pr-1)}{2(\Delta\xi)} F_{\bar{b}} + \bar{p}\left(\frac{\lambda}{Pr}\right)\frac{Z^2 F_{\bar{b}} Pr_\xi}{2(\Delta\xi)} + \bar{p}\left(\frac{\lambda}{Pr}\right)\right.$$

$$\left\{\frac{(Pr-1)Z^2(F_c-F_a)}{2(\Delta\xi)^2}\right\} + \bar{p}\left(\frac{\lambda}{Pr}\right)(Pr-1)\frac{Z^2 F_{\bar{b}}}{(\Delta\xi)^2} - \bar{p}\left(\frac{\lambda}{Pr}\right)$$

$$\left\{\frac{\alpha_1 Z F_{\bar{b}}(Pr-1)}{2(\Delta\xi)}\right\} - (Le-1)\left\{\frac{r-1}{(r-1)c_{1_{\bar{b}}}+1}\right\} Z^2\, \bar{p}\left(\frac{\lambda}{Pr}\right)\frac{F_{\bar{b}}}{4(\Delta\xi)^2}$$

$$\left.(c_{1c}-c_{1a})\right] +$$

$$c_{1d}\left[-\bar{p}\left(\frac{\lambda}{Pr}\right)\frac{(Le-1)Z^2}{8(\Delta\xi)^2}\left\{\frac{r-1}{(r-1)c_{1_{\bar{b}}}+1}\right\}\{(H_c-H_a) - 2F_{\bar{b}}\,(F_c-F_a)\}\right] +$$

$$c_{1f}\left[\bar{p}\left(\frac{\lambda}{Pr}\right)\frac{(Le-1)Z^2}{8(\Delta\xi)^2}\left\{\frac{r-1}{(r-1)c_{1_{\bar{b}}}+1}\right\}\{(H_c-H_a) - 2F_{\bar{b}}\,(F_c-F_a)\}\right]$$

$$= -\bar{p}\, Z^2\left(\frac{\lambda}{Pr}\right)_\xi \left[\frac{H_c-H_a}{4(\Delta\xi)} + 2(Pr-1)\frac{F_{\bar{b}}}{4(\Delta\xi)}(F_c-F_a)\right]$$

$$-\bar{p}\left(\frac{\lambda}{Pr}\right)\left[\frac{Z^2}{2(\Delta\xi)}(H_c - 2H_{\bar{b}} + H_a) - \frac{\alpha_1 Z}{4\Delta\xi}(H_c-H_a)\right.$$

$$+ \frac{Z^2 F_{\bar{b}} Pr_{\xi}}{2(\Delta\xi)} (F_c - F_a) + (Pr-1) \frac{Z^2 F_{\bar{b}}}{(\Delta\xi)^2} (Fe - 2F_{\bar{b}} + F_a)$$

$$- \frac{(Pr-1)\, \alpha_1 Z\, F_{\bar{b}} (F_c - F_a)}{2(\Delta\xi)} \Big] - \frac{fZ}{4(\Delta\xi)} (H_c - H_a)$$

$$- \frac{4x\, F_{\bar{b}}\, H_{\bar{b}}}{(\Delta x)} - \frac{Zx\, f_x (H_c - H_a)}{(\Delta\xi)} \qquad (5.52)$$

$$c_{1d} \Big[- \frac{p\, Z^2}{4(\Delta\xi)} \left(\frac{\lambda Le}{Pr}\right)_{\xi} + \left(\frac{\lambda Le}{Pr}\right) \frac{\bar{p}\, Z^2}{2(\Delta\xi)^2} + \left(\frac{\lambda Le}{Pr}\right) \frac{\alpha_1 \bar{p}\, Z}{4(\Delta\xi)}$$

$$- \frac{Zf}{4(\Delta\xi)} - \frac{xZf_x}{(\Delta\xi)} \Big] +$$

$$c_{1e} \Big[-\bar{p} \left(\frac{\lambda Le}{Pr}\right) \frac{Z^2}{(\Delta\xi)^2} - \frac{4xF_e}{(\Delta x)} \Big] +$$

$$c_{1f} \Big[\bar{p} \left(\frac{\lambda Le}{Pr}\right)_{\xi} \frac{Z^2}{4(\Delta\xi)} + \bar{p} \left(\frac{\lambda Le}{Pr}\right) \frac{Z^2}{2(\Delta\xi)^2} - \bar{p} \left(\frac{\lambda Le}{Pr}\right) \frac{\alpha_1 Z}{4(\Delta\xi)}$$

$$+ \frac{Zf}{4(\Delta\xi)} + \frac{xZf_x}{(\Delta\xi)} \Big]$$

$$= -\bar{p} \left(\frac{\lambda Le}{Pr}\right)_{\xi} \frac{Z^2}{4(\Delta\xi)} (c_{1c} - c_{1a}) - \bar{p} \left(\frac{\lambda Le}{Pr}\right) \Big[\frac{Z^2}{2(\Delta\xi)^2}$$

$$(c_{1c} - 2c_{1_{\bar{b}}} + c_{1a}) - \frac{\alpha_1 Z}{4(\Delta\xi)} (c_{1c} - c_{1a}) \Big] - \frac{Zf}{4(\Delta\xi)} (c_{1c} - c_{1a})$$

$$- \frac{4xF_e c_{1_{\bar{b}}}}{(\Delta x)} - \frac{xZf_x}{(\Delta\xi)} (c_{1c} - c_{1a}) \qquad (5.53)$$

In equations (5.51-53) following the first iteration quantities not subscripted with '$\bar{b}$' are evaluated at $(n\ ,\ m+1/2)$ by averaging quantities at (n,m) with those at $(n,m+1)$.

Now for the species equation both $c_1(0)$ and $c_1'(0)$ are unknowns at the wall. A special formulation is required to express $c_1(0)$ at the wall. The procedure is to express $c_1(0)$ in terms of $c_1(\Delta\xi)$ as outlined below:

From the boundary condition equation (5.48b) we may write:

$$\left[c_1(0)\right]_\xi = -\frac{2\alpha}{\alpha_1}\left[1-c_1(0)\right]\left(\frac{Pr}{Le}\right)_b \frac{C\,p_o\,\bar{x}}{(\mu\rho)_b} \qquad (5.54)$$

The species equation (5.46) specialised at the wall gives

$$\bar{p}\,\alpha_1^2\left[\left(\frac{\lambda Le}{Pr}\right)_\xi\right]_b\left[c_1(0)\right]_\xi + \bar{p}\left(\frac{\lambda Le}{Pr}\right)_b \alpha_1^2\left[\{c_1(0)\}_{\xi\xi} - \{c_1(0)\}_\xi\right]$$

$$= -\alpha_1 f_b\left[c_1(0)\right]_\xi - 4x\alpha_1\left[f(0)\right]_x\left[c_1(0)\right]_\xi \qquad (5.55)$$

Now, from the Taylor's series expansion we have

$$c_1(\Delta\xi) = c_1(0) + \Delta\xi\left[c_1(0)\right]_\xi + \frac{(\Delta\xi)^2}{2}\left[c_1(0)\right]_{\xi\xi} + \cdots \qquad (5.56)$$

Substituting for $\left[c_1(0)\right]_\xi$ from eq. (5.54) and for $\left[c_1(0)\right]_{\xi\xi}$ from eq. (5.55) in the above equation, we obtain

$$c_1(0) = \frac{c_1(\Delta\xi)}{1+A_s+B_s} + \frac{A_s+B_s}{1+A_s+B_s} \qquad (5.57)$$

where

$$A_s = \frac{(\Delta\xi)2\alpha}{\alpha_1} \left(\frac{Pr}{Le}\right)_b \frac{C\, p_o\, \bar{x}}{(\mu\rho)_b} \qquad (5.58a)$$

and

$$B_s = \left[(\Delta\xi)^2 \frac{\alpha}{\alpha_1} \left(\frac{Pr}{Le}\right)_b \frac{C\, p_o\, \bar{x}}{(\mu\rho)_b}\right]\left[-\alpha_1 f(0) - 4x\alpha_1 (f_x)_b\right.$$

$$\left. -\bar{p}\alpha_1^2 \{(\frac{\lambda Le}{Pr})_\xi\}_b + \bar{p}(\frac{\lambda Le}{Pr})_b\, \alpha_1^2\right] / \bar{p}(\frac{\lambda Le}{Pr})_b\, \alpha_1^2 \qquad (5.58b)$$

5.8 Starting Profiles

The solution at the first station on the plate is started by using the series expansion solution developed for air injection in chapter III. To use these solutions, only the **air injection** is used at the first two stations in the x-direction i.e. upto x=0.02. Beyond this value, the foreign gas injection is employed. It may again be mentioned here that initiating the solutions at x=0 as done in ref. [23] and other works is not correct, especially, for a high speed problem as pointed out in section 1.2 of chapter I. An alternate method could have been to develop a series solution for the binary gas-mixture. With the variable fluid properties for this case, this is somewhat more complex task.

In this section we recast the equations of the series expansion method for air injection in terms of the variables x and ξ. The resulting solution is then utilized for

specifying the initial conditions in x for obtaining the finite difference solution described in the previous section.

Through the use of transformation equation (5.41) and (5.42) we get the following equations for (3.15) and (3.22).

$$Z^2 \frac{\partial^2 F_o}{\partial \xi^2} - \alpha_1 Z \frac{\partial F_o}{\partial \xi} + f_o Z \frac{\partial F_o}{\partial \xi} + \beta \left[H_o - F_o^2 \right] = 0 \qquad (5.59a)$$

$$Z^2 \frac{\partial^2 H_o}{\partial \xi^2} - \alpha_1 Z \frac{\partial H_o}{\partial \xi} + Pr\, f_o Z \frac{\partial H_o}{\partial \xi} = 2(1-Pr)$$

$$\left[F_o \left(Z^2 \frac{\partial^2 F_o}{\partial \xi^2} - \alpha_1 Z \frac{\partial F_o}{\partial \xi} \right) + \left(Z \frac{\partial F_o}{\partial \xi} \right)^2 \right] \qquad (5.59b)$$

$$Z^2 \frac{\partial^2 \bar{F}_1}{\partial \xi^2} - \alpha_1 Z \frac{\partial \bar{F}_1}{\partial \xi} + f_o Z \frac{\partial \bar{F}_1}{\partial \xi} = (2\beta+1) F_o \bar{F}_1 - 2Z \frac{\partial F_o}{\partial \xi} \bar{f}_1 - \beta \bar{H}_1$$

$$+ 1.5\beta (H_o - F_o^2) + f_o Z \frac{\partial F_o}{\partial \xi} \qquad (5.60a)$$

$$Z^2 \frac{\partial^2 \bar{H}_1}{\partial \xi^2} - \alpha_1 Z \frac{\partial \bar{H}_1}{\partial \xi} = Pr \left[f_o Z \frac{\partial H_o}{\partial \xi} + F_o \bar{F}_1 - f_o Z \frac{\partial \bar{H}_1}{\partial \xi} \right]$$

$$+ 2(1-Pr) \left[F_o \left(Z^2 \frac{\partial^2 \bar{F}_1}{\partial \xi^2} - \alpha_1 Z \frac{\partial \bar{F}_1}{\partial \xi} \right) + 2Z^2 \frac{\partial F_o}{\partial \xi} \frac{\partial \bar{F}_1}{\partial \xi} \right.$$

$$\left. + \bar{F}_1 \left(Z^2 \frac{\partial^2 F_o}{\partial \xi^2} - \alpha_1 Z \frac{\partial F_o}{\partial \xi} \right) \right] - 2Pr\, Z \frac{\partial H_o}{\partial \xi} \bar{f}_1 \qquad (5.60b)$$

$$Z^2 \frac{\partial^2 \bar{F}_2}{\partial \xi^2} - \alpha_1 Z \frac{\partial \bar{F}_2}{\partial \xi} + Z f_o \frac{\partial \bar{F}_2}{\partial \xi} = 2F_o \bar{F}_2 (1+\beta) - 3Z \frac{\partial F_o}{\partial \xi} \bar{f}_2$$

$$+ 2\beta (H_o - F_o^2) + f_o Z \frac{\partial F_o}{\partial \xi} - \beta \bar{H}_2 \qquad (5.61a)$$

$$Z^2 \frac{\partial^2 \bar{H}_2}{\partial \xi^2} - \alpha_1 Z \frac{\partial \bar{H}_2}{\partial \xi} + Prf_o Z \frac{\partial \bar{H}_2}{\partial \xi} = 2PrF_o \bar{H}_2 + 2(1-Pr)$$

$$\left[F_o\left(Z^2 \frac{\partial^2 \bar{F}_2}{\partial \xi^2} - \alpha_1 Z \frac{\partial \bar{F}_2}{\partial \xi}\right) + 2Z^2 \frac{\partial F_o}{\partial \xi} \frac{\partial \bar{F}_2}{\partial \xi}\right.$$

$$\left. + \left(Z^2 \frac{\partial^2 F_o}{\partial \xi^2} - \alpha_1 Z \frac{\partial F_o}{\partial \xi}\right) \bar{F}_2\right] - 3Pr\bar{f}_2 Z \frac{\partial H_o}{\partial \xi} + Prf_o Z \frac{\partial H_o}{\partial \xi}$$

(61b)

$$Z^2 \frac{\partial^2 \bar{F}_3}{\partial \xi^2} - \alpha_1 Z \frac{\partial \bar{F}_3}{\partial \xi} + f_o Z \frac{\partial \bar{F}_3}{\partial \xi} = (2+2\beta) F_o \bar{F}_3$$

$$-3\bar{f}_3 Z \frac{\partial F_o}{\partial \xi} - \beta \bar{H}_3 + Z\left(\frac{\partial \bar{F}_1}{\partial \xi} - \frac{\partial F_o}{\partial \xi}\right)(f_o - Z\bar{f}_1)$$

$$-\bar{F}_1(F_o - (1+\beta)\bar{F}_1) + 1.5\beta(\bar{H}_1 - 2F_o\bar{F}_1) - 2\beta(H_o - F_o^2) \qquad (62a)$$

$$Z^2 \frac{\partial^2 \bar{H}_3}{\partial \xi^2} - \alpha_1 Z \frac{\partial \bar{H}_3}{\partial \xi} + Prf_o Z \frac{\partial \bar{H}_3}{\partial \xi} = 2PrF_o \bar{H}_3 + 2(1-Pr)$$

$$\left[F_o\left(Z^2 \frac{\partial^2 \bar{F}_3}{\partial \xi^2} - \alpha_1 Z \frac{\partial \bar{F}_3}{\partial \xi}\right) + 2Z^2 \frac{\partial F_o}{\partial \xi} \frac{\partial \bar{F}_3}{\partial \xi}\right.$$

$$\left. + \bar{F}_3\left(Z^2 \frac{\partial^2 F_o}{\partial \xi^2} - \alpha_1 Z \frac{\partial F_o}{\partial \xi}\right)\right] - 3Pr\bar{f}_3 Z \frac{\partial H_o}{\partial \xi}$$

$$+PrZ\left(\frac{\partial \bar{H}_1}{\partial \xi} - \frac{\partial H_o}{\partial \xi}\right)(f_o - 2\bar{f}_1) + Pr\bar{H}_1(\bar{F}_1 - F_o) + 2(1-Pr)$$

$$\left[Z^2\left(\frac{\partial \bar{F}_1}{\partial \xi}\right)^2 + \bar{f}_1\left(Z^2 \frac{\partial^2 \bar{F}_1}{\partial \xi^2} - \alpha_1 Z \frac{\partial \bar{F}_1}{\partial \xi}\right)\right] \qquad (5.62b)$$

In equations (5.59-62) the following substitutions are also made:

$F_o = f_o'$, $\bar{F}_1 = \bar{f}_1'$, $\bar{F}_2 = \bar{f}_2'$ and $\bar{F}_3 = \bar{f}_3'$, where primes denote differentiation with respect to η. The equations (5.59-62) correspond to similar form and a special scheme for finite differencing is to be adopted as given below.

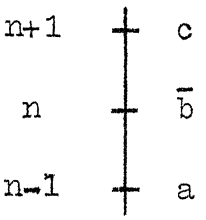

Fig. 5.3. Mesh-point diagram for similar solutions

$$M_\xi = \frac{1}{2(\Delta\xi)}(M_c - M_a)$$

$$M = \frac{1}{(\Delta\xi)^2}(M_c - 2M_{\bar{b}} + M_a)$$

$$M^2 = M_{\bar{b}}^{\nu+1} \; M_{\bar{b}}^{\nu} \qquad (5.63)$$

$$M_\xi G_\xi = \frac{1}{8(\Delta\xi)^2}\left[(M_c-M_a)^{\nu+1}(G_c-G_a)^{\nu} + (G_c-G_a)^{\nu+1}(M_c-M_a)^{\nu}\right]$$

$$(G_\xi)^2 = \frac{(G_c-G_a)^{\nu+1}\,(G_c-G_a)^{\nu}}{4(\Delta\xi)^2}$$

where superscript ν is the iteration number.

Substituting (5.63) into equations (5.59-62), we obtain

$$F_{oa}\left[\frac{Z^2}{(\Delta\xi)^2} + \frac{\alpha_1 Z}{2(\Delta\xi)} - \frac{Zf_o}{2(\Delta\xi)}\right] +$$

$$F_{oc}\left[\frac{Z^2}{(\Delta\xi)^2}-\frac{\alpha_1 Z}{2\Delta\xi}+\frac{Zf_o}{2\Delta\xi}\right]$$

$$F_{o\bar{b}}\left[\frac{-2Z^2}{(\Delta\xi)^2}-\beta F^{\nu}_{o\bar{b}}\right]=-\beta H_{o\bar{b}} \qquad (5.64a)$$

$$H_{oa}\left[\frac{Z^2}{(\Delta\xi)^2}+\frac{\alpha_1 Z}{2\Delta\xi}-\frac{Prf_o Z}{2\Delta\xi}\right]+$$

$$H_{oc}\left[\frac{Z^2}{(\Delta\xi)^2}-\frac{\alpha_1 Z}{2\Delta\xi}+\frac{Prf_o Z}{2\Delta\xi}\right]+H_{o\bar{b}}\left[\frac{-2Z^2}{(\Delta\xi)^2}\right]$$

$$=2(1-Pr)\left[\frac{F_{o\bar{b}}Z^2}{(\Delta\xi)^2}(F_{oc}-2F_{o\bar{b}}+F_{oa})-\frac{\alpha_1 ZF_{o\bar{b}}}{2(\Delta\xi)}\right.$$

$$\left.(F_{oc}-F_{oa})+Z^2\left\{\frac{F_{oc}-F_{oa}}{2(\Delta\xi)}\right\}^2\right] \qquad (5.64b)$$

$$\bar{F}_{1a}\left[\frac{Z^2}{(\Delta\xi)^2}+\frac{\alpha_1 Z}{2(\Delta\xi)}-\frac{f_o Z}{2(\Delta\xi)}\right]+$$

$$\bar{F}_{1c}\left[\frac{Z^2}{(\Delta\xi)^2}-\frac{\alpha_1 Z}{2(\Delta\xi)}+\frac{f_o Z}{2(\Delta\xi)}\right]+$$

$$\bar{F}_{1\bar{b}}\left[\frac{-2Z^2}{(\Delta\xi)^2}-(2\beta+1)F_{o\bar{b}}\right]=\frac{Z\bar{f}_1}{(\Delta\xi)}(F_{oc}-F_{oa})$$

$$-\beta\bar{H}_{1\bar{b}}+1.5\beta(H^2_{o\bar{b}}-F^2_{o\bar{b}})+\frac{f_o Z}{2(\Delta\xi)}(F_{oc}-F_{oa}) \qquad (5.65a)$$

$$\bar{H}_{1a}\left[\frac{Z^2}{(\Delta\xi)^2}-\frac{Prf_o Z}{2(\Delta\xi)}+\frac{\alpha_1 Z}{2(\Delta\xi)}\right]+$$

$$\bar{H}_{1c}\left[\frac{Z^2}{(\Delta\xi)^2}+\frac{Prf_o Z}{2(\Delta\xi)}-\frac{\alpha_1 Z}{2(\Delta\xi)}\right]+$$

$$\bar{H}_{1_{\bar{b}}}\left[\frac{-2Z^2}{(\Delta\xi)^2}-PrF_{o_{\bar{b}}}\right]=\frac{Prf_oZ}{2(\Delta\xi)}(H_{oc}-H_{oa})$$

$$+2(1-Pr)\left[\frac{F_{o_{\bar{b}}}Z^2}{(\Delta\xi)^2}(\bar{F}_{1c}-2\bar{F}_{1_{\bar{b}}}+\bar{F}_{1a})-\frac{F_{o_{\bar{b}}}\alpha_1 Z}{2(\Delta\xi)}(\bar{F}_{1c}-\bar{F}_{1a})\right.$$

$$+\frac{Z^2}{2(\Delta\xi)^2}(F_{oc}-F_{oa})(\bar{F}_{1c}-\bar{F}_{1a})+\frac{\bar{F}_{1_{\bar{b}}}Z^2}{(\Delta\xi)^2}(F_{oc}-2F_{o_{\bar{b}}}+F_{oa})$$

$$\left.-\frac{\bar{F}_{1_{\bar{b}}}\alpha_1 Z}{2(\Delta\xi)}(F_{oc}-F_{oa})\right]-\frac{Pr\bar{Z}f_1}{(\Delta\xi)}(H_{oc}-H_{oa}) \qquad (5.65b)$$

$$\bar{F}_{2a}\left[\frac{Z^2}{(\Delta\xi)^2}+\frac{\alpha_1 Z}{2(\Delta\xi)}-\frac{Zf_o}{2(\Delta\xi)}\right]+$$

$$\bar{F}_{2c}\left[\frac{Z^2}{(\Delta\xi)^2}-\frac{\alpha_1 Z}{2(\Delta\xi)}+\frac{Zf_o}{2(\Delta\xi)}\right]+$$

$$\bar{F}_{2_{\bar{b}}}\left[\frac{-2Z^2}{(\Delta\xi)^2}-2F_{o_{\bar{b}}}(1+\beta)\right]=-\frac{3Z\bar{f}_2}{2(\Delta\xi)}(F_{oc}-F_{oa})$$

$$+2\beta(H_{o_{\bar{b}}}-F^2_{o_{\bar{b}}})+\frac{f_oZ}{2(\Delta\xi)}(F_{oc}-F_{oa})-\beta\bar{H}_{2_{\bar{b}}} \qquad (5.66a)$$

$$\bar{H}_{2a}\left[\frac{Z^2}{(\Delta\xi)^2}-\frac{Prf_oZ}{2(\Delta\xi)}+\frac{\alpha_1 Z}{2(\Delta\xi)}\right]+$$

$$\bar{H}_{2c}\left[\frac{Z^2}{(\Delta\xi)^2}+\frac{Prf_oZ}{2(\Delta\xi)}-\frac{\alpha_1 Z}{2(\Delta\xi)}\right]+$$

$$\bar{H}_{2_{\bar{b}}}\left[\frac{-2Z^2}{(\Delta\xi)^2}-2PrF_{o_{\bar{b}}}\right]=2(1-Pr)\left[\frac{F_oZ^2}{(\Delta\xi)^2}(\bar{F}_{2c}-2\bar{F}_{2_{\bar{b}}}+\bar{F}_{2a})-\right.$$

$$\frac{F_o\alpha_1 Z}{2(\Delta\xi)}(\bar{F}_{2c}-\bar{F}_{2a})+\frac{2Z^2}{4(\Delta\xi)^2}(F_{oc}-F_{oa})(\bar{F}_{2c}-\bar{F}_{2a})+$$

$$\frac{\bar{F}_2 Z^2}{(\Delta\xi)^2}(F_{oc}-2F_{o\bar{b}}+F_{oa})-\frac{\alpha_1 Z\,\bar{F}_2}{2(\Delta\xi)}(F_{oc}-F_{oa})\Big]-$$

$$\frac{3Pr\,\bar{f}_2 Z}{2(\Delta\xi)}(H_{oc}-H_{oa})+\frac{Prf_o Z}{2(\Delta\xi)}(H_{oc}-H_{oa}) \qquad (5.66b)$$

$$\bar{F}_{3a}\left[\frac{Z^2}{(\Delta\xi)^2}+\frac{\alpha_1 Z}{2(\Delta\xi)}-\frac{f_o Z}{2(\Delta\xi)}\right]$$

$$\bar{F}_{3c}\left[\frac{Z^2}{(\Delta\xi)^2}-\frac{\alpha_1 Z}{2(\Delta\xi)}+\frac{f_o Z}{2(\Delta\xi)}\right]$$

$$\bar{F}_{3\bar{b}}\left[\frac{-2Z^2}{(\Delta\xi)^2}-(2+2\beta)F_{o\bar{b}}\right]=\frac{3\bar{f}_3 Z}{2(\Delta\xi)}(F_{oc}-F_{oc})-\beta\bar{H}_{3\bar{b}}+$$

$$\frac{Z}{2(\Delta\xi)}\left[(\bar{F}_{1c}-\bar{F}_{1a})-(F_{oc}-F_{oa})\right](f_o-2\bar{f}_1)-\bar{F}_{1\bar{b}}(F_{o\bar{b}}-(1+\beta)\bar{F}_{1\bar{b}})+$$

$$1.5\beta\,(\bar{H}_{1\bar{b}}-2F_{o\bar{b}}\bar{F}_{1\bar{b}})-2\beta\,(H_{o\bar{b}}-F^2_{o\bar{b}}) \qquad (5.67a)$$

$$\bar{H}_{3a}\left[\frac{Z^2}{(\Delta\xi)^2}+\frac{\alpha_1 Z}{2(\Delta\xi)}-\frac{Prf_o Z}{2(\Delta\xi)}\right]+$$

$$\bar{H}_{3c}\left[\frac{Z^2}{(\Delta\xi)^2}-\frac{\alpha_1 Z}{2(\Delta\xi)}+\frac{Prf_o Z}{2(\Delta\xi)}\right]+$$

$$\bar{H}_{3\bar{b}}\left[\frac{-2Z^2}{(\Delta\xi)^2}-2PrF_{o\bar{b}}\right]=2(1-Pr)\left[\frac{F_{o\bar{b}}Z^2}{(\Delta\xi)^2}(\bar{F}_{3c}-2\bar{F}_{3\bar{b}}+\bar{F}_{3a})-\right.$$

$$\frac{\alpha_1 Z F_{o\bar{b}}}{2(\Delta\xi)}(\bar{F}_{3c}-\bar{F}_{3a}) + \frac{2Z^2}{4(\Delta\xi)^2}(F_{oc}-F_{oa})(\bar{F}_{3c}-\bar{F}_{3a}) +$$

$$\frac{\bar{F}_{3\bar{b}} Z^2}{(\Delta\xi)^2}(F_{oc}-2F_{o\bar{b}}+F_{oa}) - \frac{\alpha_1 Z \bar{F}_{3\bar{b}}}{2(\Delta\xi)}(F_{oc}-F_{oa})\Big] -$$

$$\frac{3Pr\bar{f}_3 Z}{2(\Delta\xi)}(H_{oc}-H_{oa}) + \frac{PrZ}{2(\Delta\xi)}\Big[(\bar{H}_{1_c}-\bar{H}_{1_a})-(H_{oc}-H_{oa})\Big]$$

$$(f_o-2\bar{f}_1) + Pr\bar{H}_{1\bar{b}}(\bar{F}_{1\bar{b}}-F_{o\bar{b}}) + 2(1-Pr)\Big[\frac{Z^2}{4(\Delta\xi)^2}(\bar{F}_{1c}-\bar{F}_{1a})^2 +$$

$$\frac{\bar{f}_1 Z^2}{(\Delta\xi)^2}(\bar{F}_{1c}-2\bar{F}_{1\bar{b}}+\bar{F}_{1a}) - \frac{\bar{f}_1\alpha_1 Z}{2(\Delta\xi)}(\bar{F}_{1c}-\bar{F}_{1a})\Big] \qquad (5.67b)$$

In equations (5.64) through (5.67) the quantities not subscripted with '$\bar{b}$' are taken from the previous iteration. And after each iteration the functions f_o and $\bar{f}_i$ (i=1,2,3) are updated using integral relations similar to that of eq. (5.47).

5.9 Similarity Form

The similarity forms of the equations (5.38) through (5.40) are solved for comparison with the existing results [15]. These equations are obtained by taking the value of β as zero and $\bar{p}$ as unity:

$$Z^2 \frac{\partial\lambda}{\partial\xi}\frac{\partial F}{\partial\xi} + \lambda Z^2 \frac{\partial^2 F}{\partial\xi^2} - \lambda\alpha_1 Z \frac{\partial F}{\partial\xi} + fZ\frac{\partial F}{\partial\xi} = 0 \qquad (5.68)$$

$$Z^2\left[\frac{\partial}{\partial\xi}\left(\frac{\lambda}{Pr}\right)\right]\left[\frac{\partial H}{\partial\xi}+2(Pr-1)\,F\,\frac{\partial F}{\partial\xi}+(Le-1)\left\{\frac{r-1}{(r-1)c_1+1}\right\}\right.$$

$$\left.(H-F^2)\,\frac{\partial c_1}{\partial\xi}\right]+\frac{\lambda}{Pr}\left[Z^2\,\frac{\partial^2 H}{\partial\xi^2}-\alpha_1 Z\,\frac{\partial H}{\partial\xi}+2Z^2F\,\frac{\partial Pr}{\partial\xi}\,\frac{\partial F}{\partial\xi}+\right.$$

$$2(Pr-1)\left\{Z^2\left(\frac{\partial F}{\partial\xi}\right)^2+F\left(Z^2\,\frac{\partial^2 F}{\partial\xi^2}-\alpha_1 Z\,\frac{\partial F}{\partial\xi}\right)\right\}+Z^2\,\frac{\partial Le}{\partial\xi}$$

$$\left\{\frac{r-1}{(r-1)c_1+1}\right\}(H-F^2)\,\frac{\partial c_1}{\partial\xi}+(Le-1)\left\{\frac{r-1}{(r-1)c_1+1}\right\}(H-F^2)$$

$$\left(Z^2\,\frac{\partial^2 c_1}{\partial\xi^2}-\alpha_1 Z\,\frac{\partial c_1}{\partial\xi}\right)+(Le-1)\left\{\frac{r-1}{c_1(r-1)+1}\right\}Z^2\,\frac{\partial c_1}{\partial\xi}$$

$$\left(\frac{\partial H}{\partial\xi}-2F\,\frac{\partial F}{\partial\xi}\right)+(le-1)(H-F^2)Z^2\left\{\frac{-(r-1)^2}{((r-1)c_1+1)^2}\right\}$$

$$\left.\left(\frac{c_1}{\partial\xi}\right)^2\right]+fZ\,\frac{\partial H}{\partial\xi}=0 \qquad (5.69)$$

$$Z^2\left(\frac{\lambda Le}{Pr}\right)_\xi\,\frac{\partial c_1}{\partial\xi}+\left(\frac{\lambda Le}{Pr}\right)Z^2\,\frac{\partial^2 c_1}{\partial\xi^2}-\left(\frac{\lambda Le}{Pr}\right)\alpha_1 Z\,\frac{\partial c_1}{\partial\xi}+$$

$$fZ\,\frac{\partial c_1}{\partial\xi}=0 \qquad (6.70)$$

Substituting from the finite difference equations (5.63) into the above equations we obtain:

$$F_a\left[-\frac{-Z^2\lambda_\xi}{2(\Delta\xi)}+\frac{\lambda Z^2}{(\Delta\xi)^2}+\frac{\lambda\alpha_1 Z}{2(\Delta\xi)}-\frac{fZ}{2(\Delta\xi)}\right]+$$

$$F_c\left[\frac{Z^2\lambda_\xi}{2(\Delta\xi)}+\frac{\lambda Z^2}{(\Delta\xi)^2}-\frac{\lambda\alpha_1 Z}{2(\Delta\xi)}+\frac{fZ}{2(\Delta\xi)}\right]+$$

$$F_b\left[\frac{-2\lambda Z^2}{(\Delta\xi)^2}\right]=0 \qquad (5.71)$$

$$H_a \left[\frac{-Z^2}{2(\Delta\xi} \left(\frac{\lambda}{Pr}\right)_\xi + \left(\frac{\lambda}{Pr}\right) \frac{Z^2}{(\Delta\xi)^2} + \frac{\alpha_1 Z(\lambda/Pr)}{2(\Delta\xi)} - \right.$$

$$\left. \frac{(\lambda/Pr)Z^2(Le-1)}{4(\Delta\xi)^2} \left\{ \frac{(r-1)}{(r-1)(c_{1_{\bar{b}}}+1)} \right\} (c_{1c} - c_{1a}) - \frac{fZ}{2(\Delta\xi)} \right] +$$

$$H_c \left[\frac{Z^2}{2(\Delta\xi)} \left(\frac{\lambda}{Pr}\right)_\xi + \left(\frac{\lambda}{Pr}\right) \frac{Z^2}{(\Delta\xi)^2} - \frac{\alpha_1 Z(\lambda/Pr)}{2(\Delta\xi)} + \left(\frac{\lambda}{Pr}\right)(Le-1) \right.$$

$$\left. \left\{ \frac{r-1}{(r-1)c_{1_{\bar{b}}}+1} \right\} \frac{Z^2}{4(\Delta\xi)^2} (c_{1c}-c_{1a}) + \frac{fZ}{2(\Delta\xi)} \right] +$$

$$H_b \left[Z^2 \left(\frac{\lambda}{Pr}\right) (Le-1) \left\{ \frac{r-1}{(r-1)c_{1_{\bar{b}}}+1} \right\} c_{1_{\bar{b}_\xi}} - \frac{(\lambda/Pr)Z^2 2}{(\Delta\xi)^2} + \right.$$

$$\frac{\lambda}{Pr} Z^2 Le_\xi \left\{ \frac{r-1}{(r-1)c_{1_{\bar{b}}}+1} \right\} c_{1_{\bar{b}_\xi}} - \left(\frac{\lambda}{Pr}\right)(Le-1) \left\{ \frac{(r-1)Z}{(r-1)c_{1_{\bar{b}}}+1} \right\} (c_{1_{\bar{b}_\xi}})^2$$

$$\left. + \frac{\lambda}{Pr} (Le-1) \left\{ \frac{r-1}{(r-1)\, c_{1\bar{b}} + 1} \right\} \{ Z^2 \, c_{1\bar{b}_{\xi\xi}} - \alpha_1 \, Z \, c_{1\bar{b}_\xi} \} \right]$$

$$= -F_a \left[-\left(\frac{\lambda}{Pr}\right) \frac{(Pr-1)Z^2(F_c-F_a)^\nu}{2(\Delta\xi)^2} + \left(\frac{\lambda}{Pr}\right) \frac{2Z^2(Pr-1)F_{\bar{b}}^\nu}{(\Delta\xi)^2} + \right.$$

$$\left(\frac{\lambda}{Pr}\right) \frac{(Pr-1)\alpha_1 Z F_b^\nu}{(\Delta\xi)} + \left(\frac{\lambda}{Pr}\right)(Le-1) \left\{ \frac{r-1}{(r-1)c_{1_{\bar{b}}}+1} \right\}$$

$$\frac{Z^2(c_{1c}-c_{1a})\, F_b^\nu}{2(\Delta\xi)^2} - Z^2 \left(\frac{\lambda}{Pr}\right)_\xi \frac{(Pr-1)}{(\Delta\xi)} F_{\bar{b}}^\nu -$$

$$\left. \left(\frac{\lambda}{Pr}\right) \frac{Z^2 F_{\bar{b}}^\nu (Pr)_\xi}{(\Delta\xi)} \right] - F_c \left[\left(\frac{Z^2(F_c-F_a)^\nu}{2(\Delta\xi)^2} \right) \left(\frac{\lambda}{Pr}\right)(Pr-1) \right.$$

$$+ Z^2 \left(\frac{\lambda}{Pr}\right)_\xi \frac{(Pr-1)}{(\Delta\xi)} F_{\bar{b}}^\nu + \frac{\lambda}{Pr} \frac{Z^2 F_{\bar{b}}^\nu (Pr)_\xi}{(\Delta\xi)} + \frac{\lambda}{Pr} (Pr-1)$$

$$Z^2 \frac{\partial^2 F}{\partial \xi^2} - \alpha_1 Z \frac{\partial F}{\partial \xi} + fZ \frac{\partial F}{\partial \xi} = 0 \qquad (5.72)$$

$$\frac{Z}{Pr}\left(Z \frac{\partial^2 H}{\partial \xi^2} - \alpha_1 \frac{\partial H}{\partial \xi}\right) = \frac{2}{Pr}(1-Pr)\left[Z^2\left(\frac{\partial F}{\partial \xi}\right)^2 + FZ\left(Z \frac{\partial^2 F}{\partial \xi^2} - \alpha_1 \frac{\partial F}{\partial \xi}\right)\right] - f Z \frac{\partial H}{\partial \xi} \qquad (5.73)$$

The finite-difference form of the above equations may be obtained by using the expressions (5.59):

$$F_a\left[\frac{Z^2}{(\Delta\xi)^2} + \frac{\alpha_1 Z}{2(\Delta\xi)} - \frac{fZ}{2(\Delta\xi)}\right] + F_{\bar{b}}\left[\frac{-2Z^2}{(\Delta\xi)^2}\right] + F_c\left[\frac{2Z^2}{(\Delta\xi)^2} - \frac{\alpha_1 Z}{2(\Delta\xi)} + \frac{fZ}{2(\Delta\xi)}\right] = 0 \qquad (5.74)$$

$$H_a\left[\frac{Z^2}{Pr(\Delta\xi)^2} + \frac{\alpha_1 Z}{2Pr(\Delta\xi)} - \frac{fZ}{2(\Delta\xi)}\right] + H_{\bar{b}}\left[-\frac{2Z^2}{Pr(\Delta\xi)^2}\right] + H_c\left[\frac{Z^2}{Pr(\Delta\xi)^2} - \frac{\alpha_1 Z}{2Pr(\Delta\xi)} + \frac{fZ}{2(\Delta\xi)}\right] = \frac{2}{Pr}(1-Pr)$$

$$\left[\frac{Z^2}{4(\Delta\xi)^2}(F_c - F_a)^2 + \frac{Z^2}{(\Delta\xi)^2} F_{\bar{b}}\,(F_c - 2F_{\bar{b}} + F_a) - \frac{\alpha_1 Z F_{\bar{b}}}{2(\Delta\xi)}(F_c - F_a)\right] \qquad (5.75)$$

5.10 Results of the Steady Heterogeneous Injection Problem

Computations were carried out for a sharp wedge of semi-apex angle $\theta_b = 2^o$ at a freestream Mach number of 15. The value of H_b used was based on a constant surface temperature, T_b^*, of 1948.5K. Corresponding to an altitude of 30480m and standard atmospheric conditions, the following values of the various free stream variables have been used in the numerical computations:

$$T_\infty^* = 216.5 \text{ K}$$

$$a_\infty^* = 295.0 \text{ m/s}$$

$$u_\infty^* = 4440 \text{ m/s}$$

In figure 5.4 the variations of p and δ along the plate for a constant injection value of $\alpha=0.1$ for air and argon is given with $M_\infty=15$, $\bar{x}_{L^*} = 8$, $\gamma = 1.4$, $\theta_b = 2^o$, and $T_b = 9$. Since air is lighter than argon, the induced pressure and displacement thickness for argon will be lower than those for air injection with the same value of the injection parameter α as shown in this figure.

Figures 5.5 through 5.8. show the variations of p, δ, f_b'' and H_b' for different values of α (for argon injection) against the corresponding no-injection curves for $M_\infty = 15$, $\bar{x}_{L^*} = 8$, $T_b = 9$, $\gamma = 1.4$, and $\theta_b = 2$. Similar to the case for air injection, the induced pressures and the displacement thickness are larger whereas the wall shear function and the

enthalpy gradient are smaller with injection.

Fig. 5.9 shows the variation of wall enthalpy with argon injection against a non-injection case. The wall enthalpy decreases as α increases because the value of c_p^* for argon is less than that of air. Fig. 5.10 gives the variation of argon concentration through the boundary layer at $x = 0.5$ for different values of $\alpha(=0.1, 0.15)$ with $M_\infty=15$, $\bar{\chi}_L* = 8$, $T_b = 9$, $\theta_b = 2^\circ$, $\gamma = 1.4$. Figure 5.11 gives the wall concentration of the injectant for different values of injection ($\alpha = 0.1$ and 0.15) along the plate for $M_\infty = 15$, $\bar{\chi}_L* = 8$, $T_b = 9$, $\gamma = 1.4$ and $\theta_b = 2^\circ$. In obtaining the results of Figures 5.4 through 5.11 the Clutter-Smith technique employing the shooting method was adopted.

Figures 5.12 and 5.13 contain the distributions of p, δ, f_b'', and H_b' along the plate for argon injection by two different methods: (a) Clutter-Smith (shooting) method (b) finite-differences method with $M_\infty = 15$, $\bar{\chi}_L* = 8$, $T_b = 9$, $\theta_b = 2^\circ$, $\gamma = 1.4$ and $\alpha = 0.1$. As pointed out earlier, the Clutter-Smith technique did not work for the case involving the injection of a light gas like helium. The finite-difference method employed here to overcome this difficulty does give quite accurate results for both heavier and lighter than air injectants. This is evident from the comparison of this method with the Clutter-Smith technique for the case of argon injection as contained in Figs. 5.12 and 5.13. The accuracy of the finite-

difference method for the cases with air and helium injections is shown in Figures 5.14 through 5.16. These figures contain comparisons with the existing results [11,15]. As can be easily noticed, there is very good agreement between the present results and those of refs. [11] and [15] in all these figures. The results with carbon-di-oxide injection in Fig. 5.12 have been included for comparison against the argon injection as both gases have comparable molecular weights. It may be noticed in this figure that due to the difference in variables employed here and in ref. [15], proper scaling has been done for the purpose of comparison.

In Figures 5.17 through 5.20 are given the distributions of p, δ, f_b'' and H_b' for different injectants by the finite-differences method with $M_\infty = 15$, $\bar{x}_L{}^* = 8$, $\theta_b = 2^o$, $\gamma = 1.4$, $T_b = 9$ and $\alpha = 0.15$. The pressure and displacement thickness increase according to the decrease in molecular weight of the injectants as shown in Figs. 5.17 and 5.18. This is in accordance with the observations of Figure 5.4. The f_b'' curve for helium in Figure 5.19 shows a different behaviour. For the value of the injection parameter, α, considered here, there is an increase in the shear function as compared to the air and argon injection cases. This behaviour, however, can be explained if a reference is made to Fig. 5.15 described earlier. It may be noticed from this figure that at first there is an increase in the value of wall shear function with the

increase in injection parameter, α, up to a value of $\alpha = 0.1625$. Beyond this the shear function decreases and eventually its value becomes lower than the case with air and argon injections for $\alpha > 0.21$. The results for the enthalpy gradient at the wall are contained in Fig. 5.20. The trend of the results is similar to the one shown in Fig. 5.19.

The present analysis uses values of α in the range $-2 \leq \alpha \leq 0.5$ with negative values of α indicating suction. This is approximately the range covered by Zien [14]. However, the detailed results have been obtained for a value of $\alpha = 0.15$. This corresponds to a value of $f_b = -0.3$ shown in Fig. 5.15 where a comparison with the Baron's results [15] has been made. The present analysis loses its validity in the vicinity of separation point where f_b'' approaches zero. Figure 5.15 shows the range of α for different gases before the separation occurs. The present analysis was limited to the values of α well before the separation point is reached.

Finally, Figs. 5.19 and 5.20 are not the correct indicators of wall shear and heat transfer as is the case in absence of surface injection. Defining the skin-friction coefficient as

$$c_f = \tau_b^* / \tfrac{1}{2} \rho_\infty^* u_\infty^{*2} \qquad (5.76)$$

one may write, in terms of the transformations of Chapter II

$$c_f = \frac{\sqrt{p_o}}{M_\infty^3} (\bar{x}_L^*)^{3/2} \bar{p} \, x^{-3/4} (f'' \lambda)_{\eta=0} \qquad (5.77)$$

Or,
$$c_f \sim x^{-3/4}\, \bar{p}(f'' \lambda)_b \tag{5.78}$$

Therefore,
$$\frac{c_f - c_{f_o}}{c_{f_o}} = \frac{\bar{p}\, f_b'' \lambda_b}{(\bar{p}\, f_b'')_o} - 1 \tag{5.79}$$

where the subscript denotes the values without injection.

Similarly, by defining the dimensionless heat transfer rate as
$$-q_w = \frac{-q_w^*}{\frac{1}{2}\, \rho_\infty^*\, u_\infty^{*3}} \tag{5.80}$$

we may write for the Stanton number as
$$St = \frac{-q_w^*}{\frac{1}{2}\, \rho_\infty^*\, u_\infty^{*3}(1 - T_w^*/T_o^*)} \tag{5.81}$$

or, in terms of the transformed variables of Chapter II,
$$\frac{S_t - S_{t_o}}{S_{t_o}} = \frac{\bar{p}\left(\frac{\lambda}{Pr}\right)_b \left\{\left[\frac{\partial H}{\partial \eta} - \left(\frac{(r-1)\, H}{(r-1)c_1 + 1}\right)\frac{\partial c_1}{\partial \eta}\right]_b - \frac{2(c_{p_f}^* - c_{p_i}^*)}{u_\infty^{*2}}\, T_b^* \left(Le\, \frac{\partial c_1}{\partial \eta}\right)_b\right\}}{\left[\bar{p}\left(\frac{1}{Pr}\frac{\partial H}{\partial \eta}\right)_b\right]_o} - 1 \tag{5.82}$$

Figures 5.21 through 5.24 give the percentage changes in induced pressure, skin-friction coefficient, Stanton number, and boundary layer thickness with injection of various gases. These figures suggest that the lighter gases are more efficient coolants. However, they induce larger pressures.

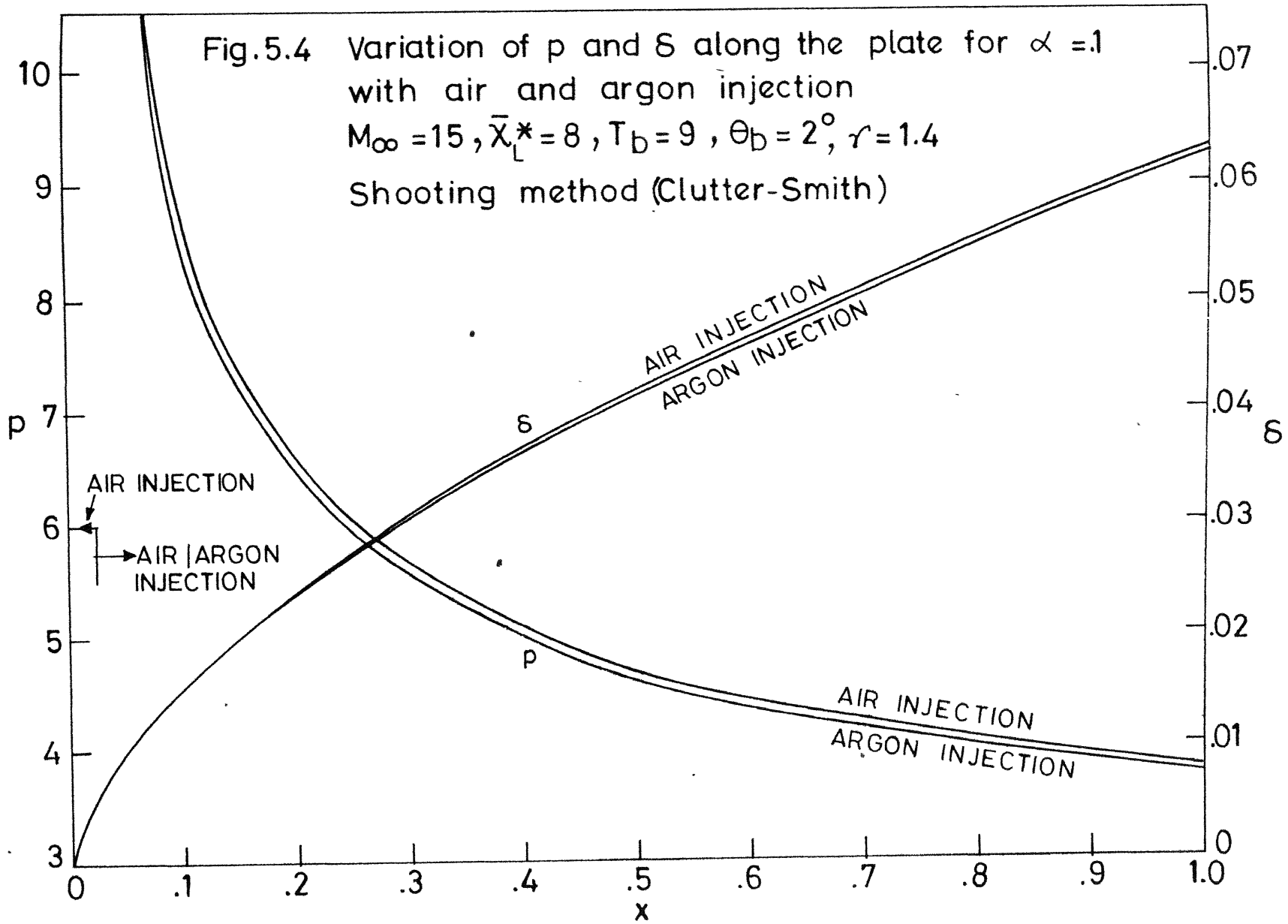
Fig. 5.4 Variation of p and δ along the plate for α = .1 with air and argon injection
$M_\infty = 15$, $\bar{\chi}_L^* = 8$, $T_b = 9$, $\theta_b = 2^\circ$, $\gamma = 1.4$
Shooting method (Clutter-Smith)
AIR INJECTION
ARGON INJECTION
δ
AIR INJECTION
AIR | ARGON INJECTION
p
AIR INJECTION
ARGON INJECTION
p
δ
x
10
9
8
7
6
5
4
3
.07
.06
.05
.04
.03
.02
.01
0
0
.1
.2
.3
.4
.5
.6
.7
.8
.9
1.0

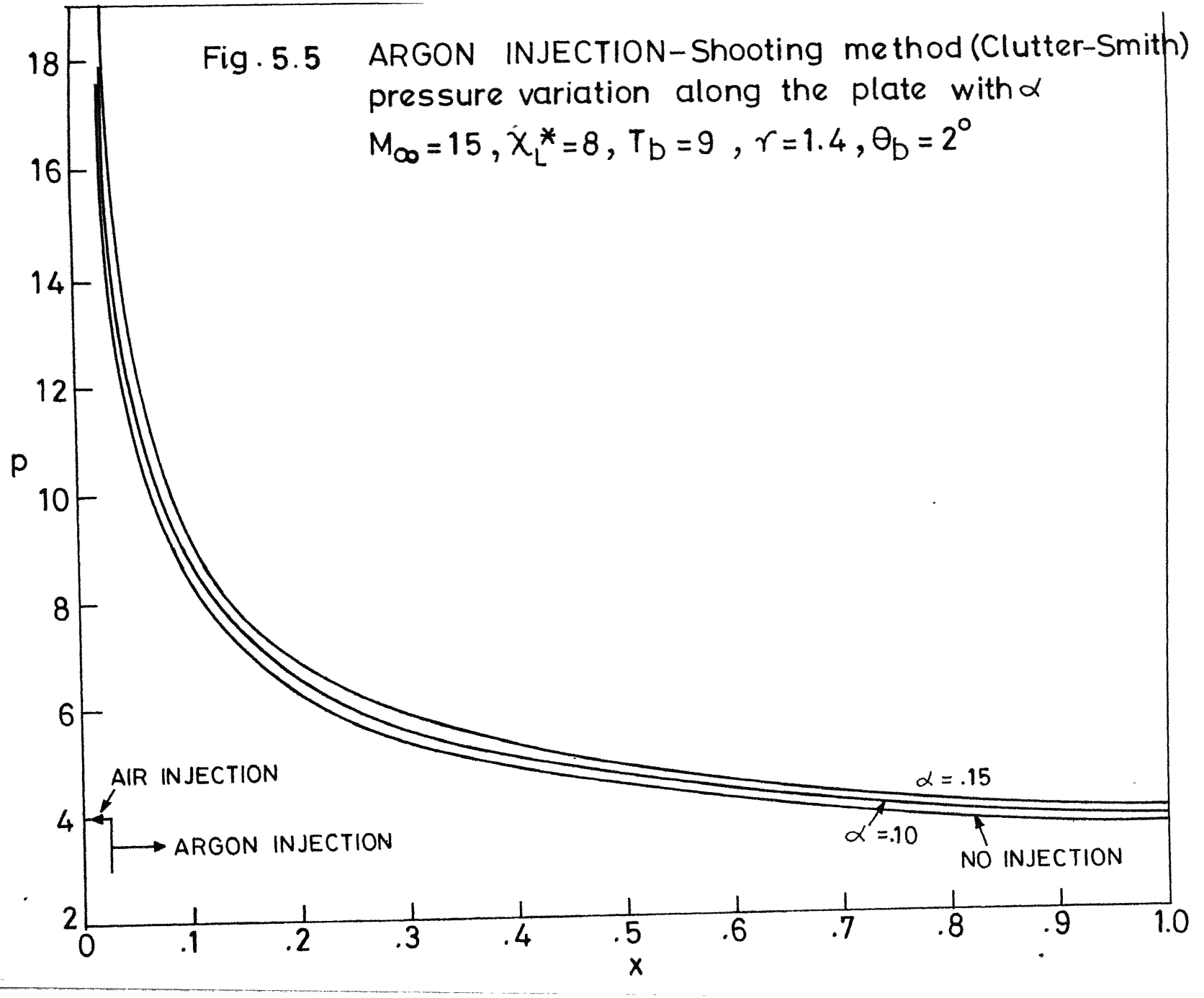
Fig. 5.5 ARGON INJECTION–Shooting method (Clutter-Smith)
pressure variation along the plate with α
$M_\infty = 15$, $\bar{\chi}_L^* = 8$, $T_b = 9$, $\gamma = 1.4$, $\theta_b = 2^\circ$
p
x
AIR INJECTION
ARGON INJECTION
α = .15
α =.10
NO INJECTION
18
16
14
12
10
8
6
4
2
0
.1
.2
.3
.4
.5
.6
.7
.8
.9
1.0

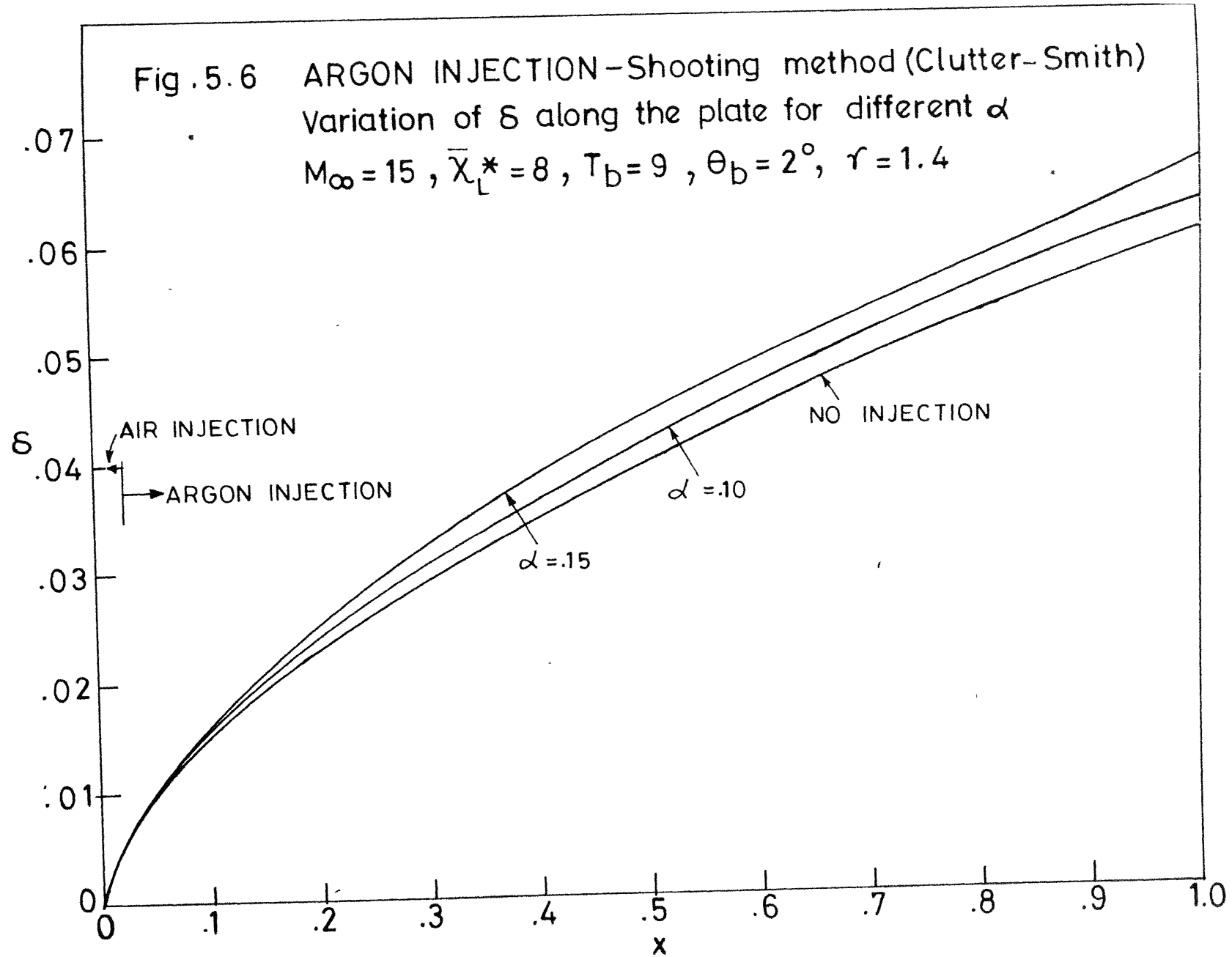
Fig . 5.6 ARGON INJECTION – Shooting method (Clutter – Smith)
Variation of δ along the plate for different α
$M_\infty = 15$, $\bar{\chi}_L^* = 8$, $T_b = 9$, $\theta_b = 2°$, $\gamma = 1.4$
.07
.06
.05
.04
.03
.02
.01
0
δ
AIR INJECTION
ARGON INJECTION
NO INJECTION
α =.10
α =.15
0
.1
.2
.3
.4
.5
.6
.7
.8
.9
1.0
x

Fig. 5·7 ARGON INJECTION – Shooting method (Clutter-Smith)
Variation of f_b'' along the plate for different α
$M_\infty = 15$, $\chi_L^* = 8$, $T_b = 9$, $\theta_b = 2°$, $\gamma = 1.4$

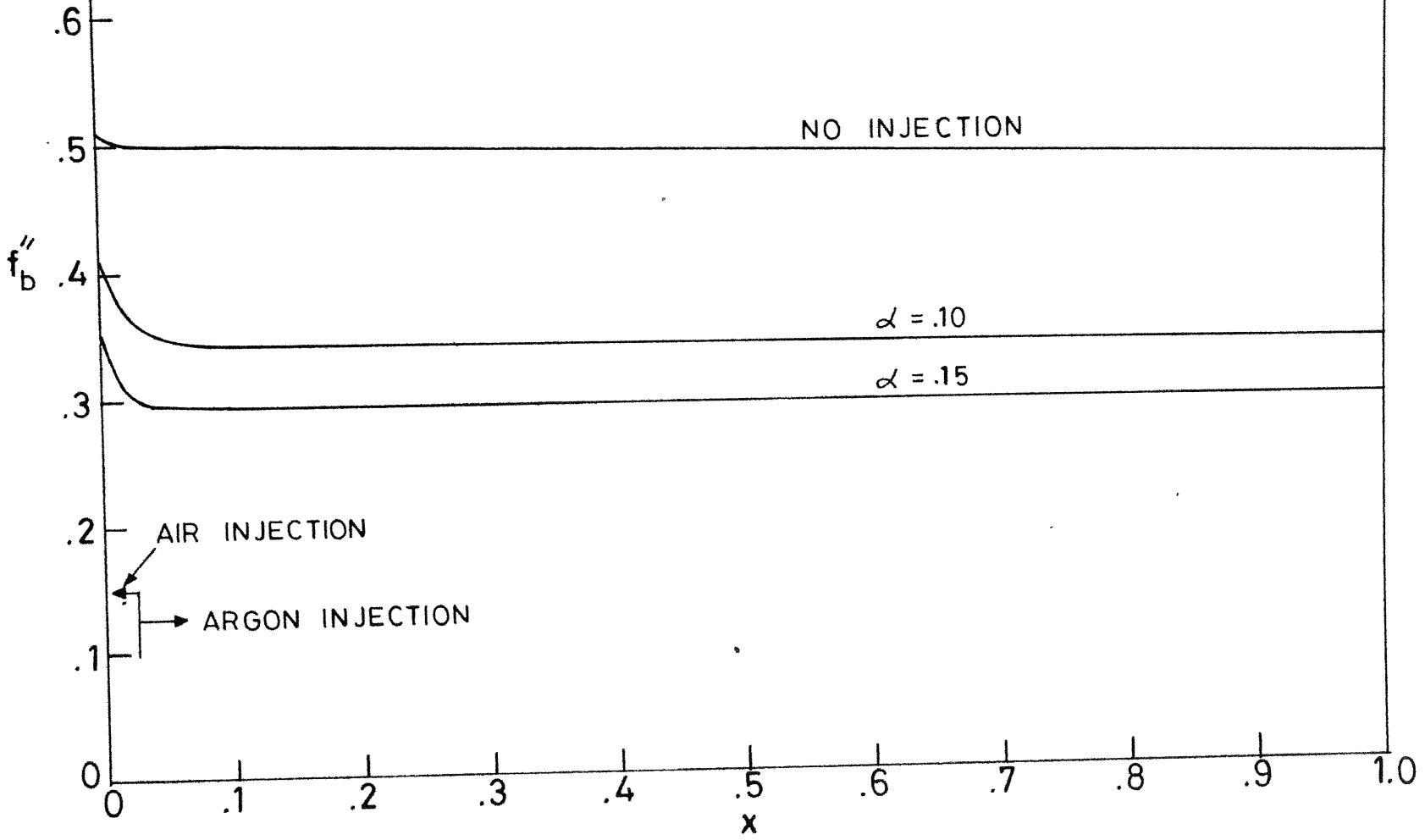

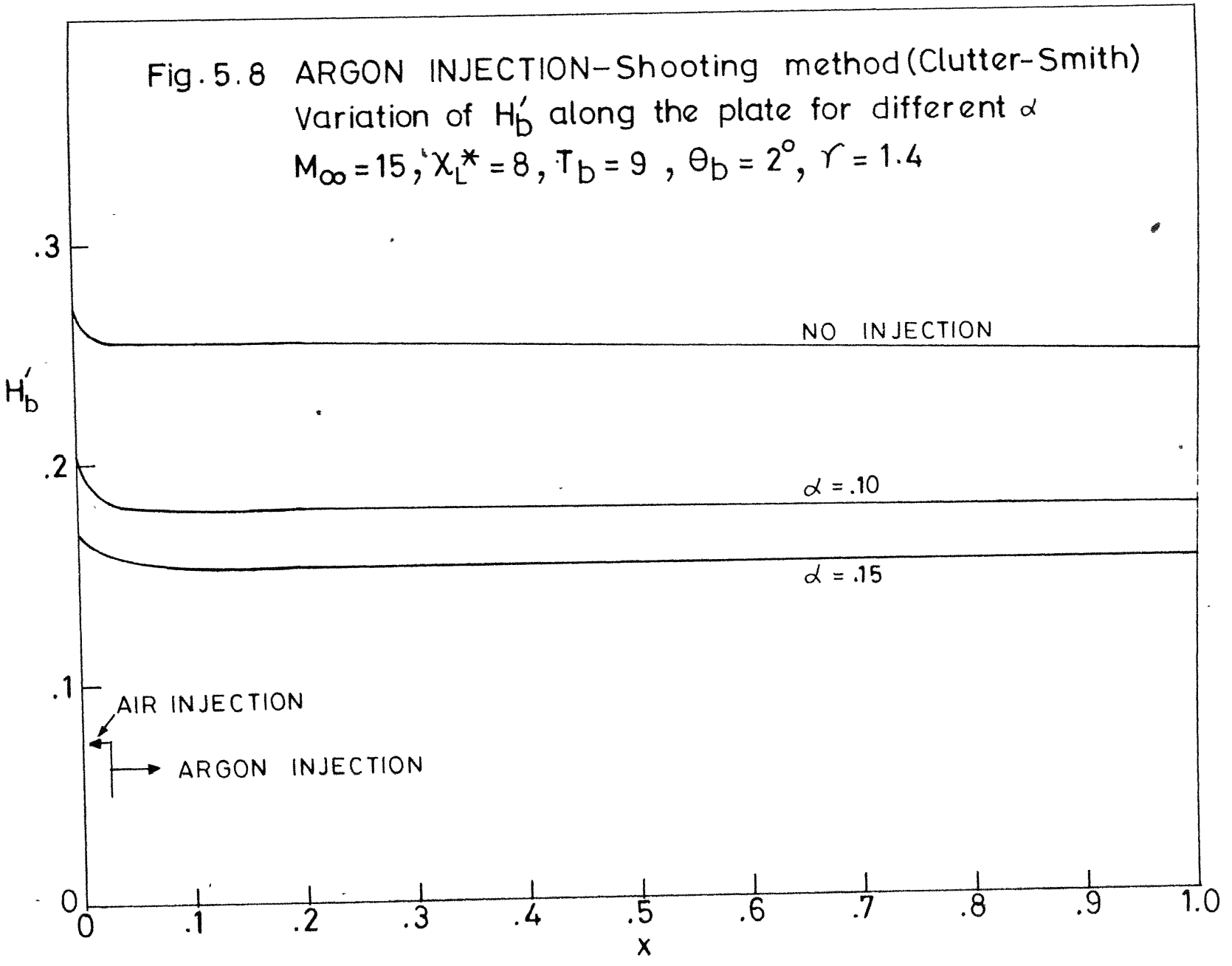
Fig. 5.8 ARGON INJECTION–Shooting method (Clutter-Smith)
Variation of H_b' along the plate for different α
$M_\infty = 15, \chi_L^* = 8, T_b = 9, \theta_b = 2^\circ, \gamma = 1.4$
H_b'
.3
.2
.1
0
NO INJECTION
α = .10
α = .15
AIR INJECTION
ARGON INJECTION
0
.1
.2
.3
.4
.5
.6
.7
.8
.9
1.0
x

Fig. 5.9 ARGON INJECTION – Shooting method (Clutter-Smith)
Variation of wall enthalpy along the plate with α
$M_\infty = 15, \bar{X}_L^* = 8, T_b = 9, \theta_b = 2^\circ, \gamma = 1.4$

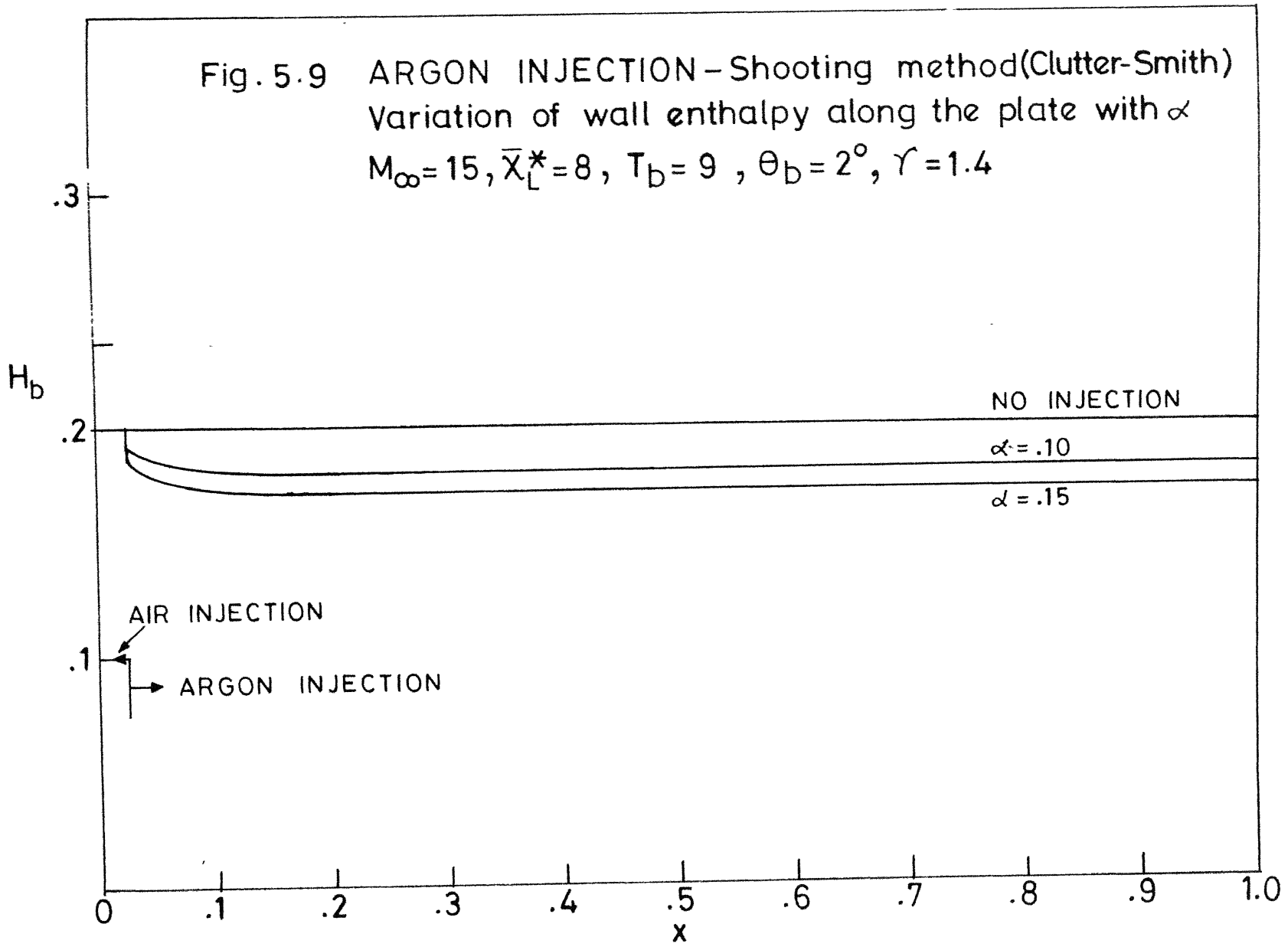

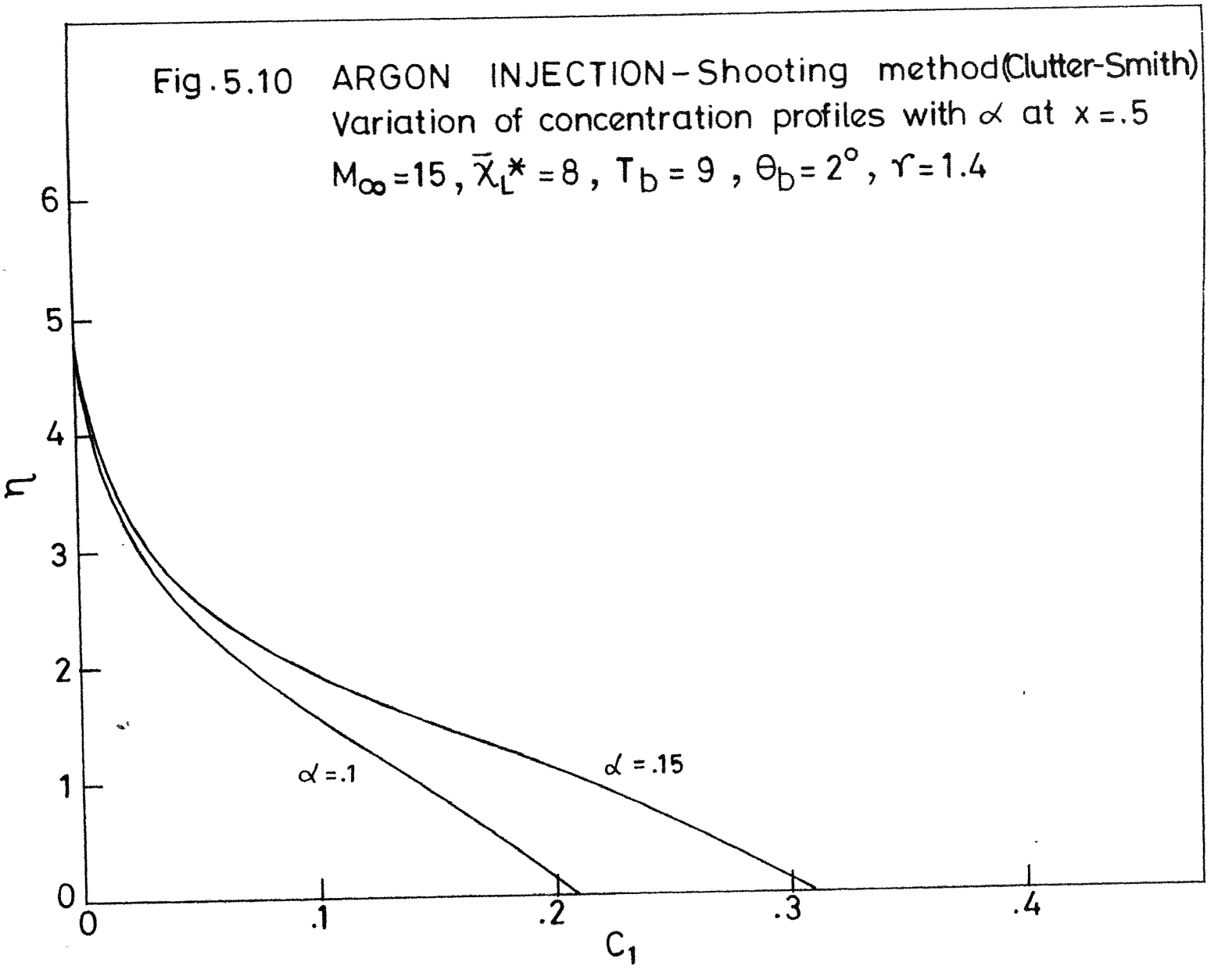
Fig.5.10 ARGON INJECTION-Shooting method(Clutter-Smith)
Variation of concentration profiles with α at x=.5
M∞=15, χ̄L*=8, Tb=9, θb=2°, γ=1.4
η
C1
α=.1
α=.15
0
1
2
3
4
5
6
.1
.2
.3
.4

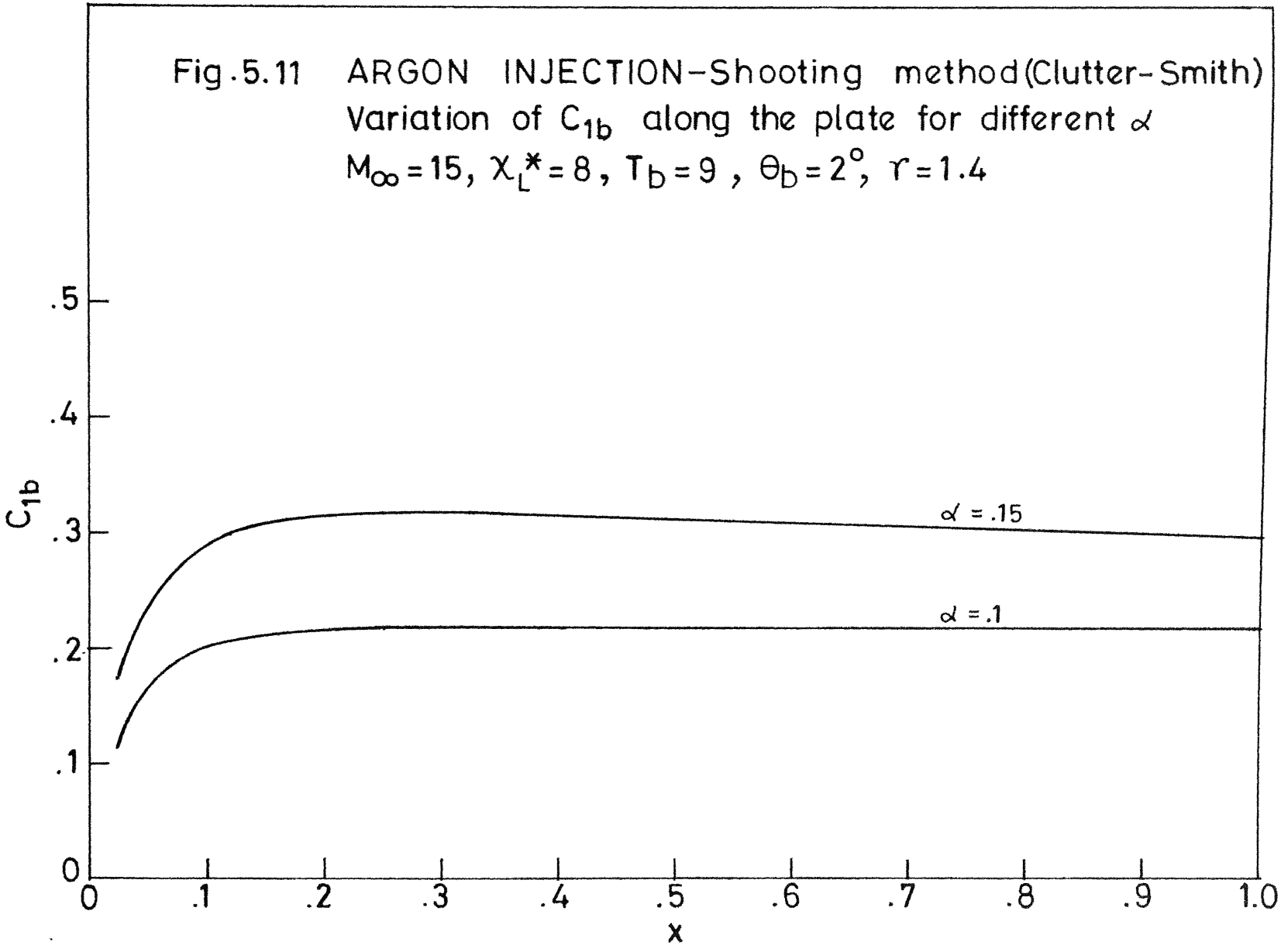
Fig.5.11 ARGON INJECTION-Shooting method(Clutter-Smith)
Variation of C_{1b} along the plate for different α
$M_\infty = 15$, $\chi_L^* = 8$, $T_b = 9$, $\theta_b = 2^\circ$, $\gamma = 1.4$
C_{1b}
.5
.4
.3
.2
.1
0
α = .15
α = .1
0
.1
.2
.3
.4
.5
.6
.7
.8
.9
1.0
x

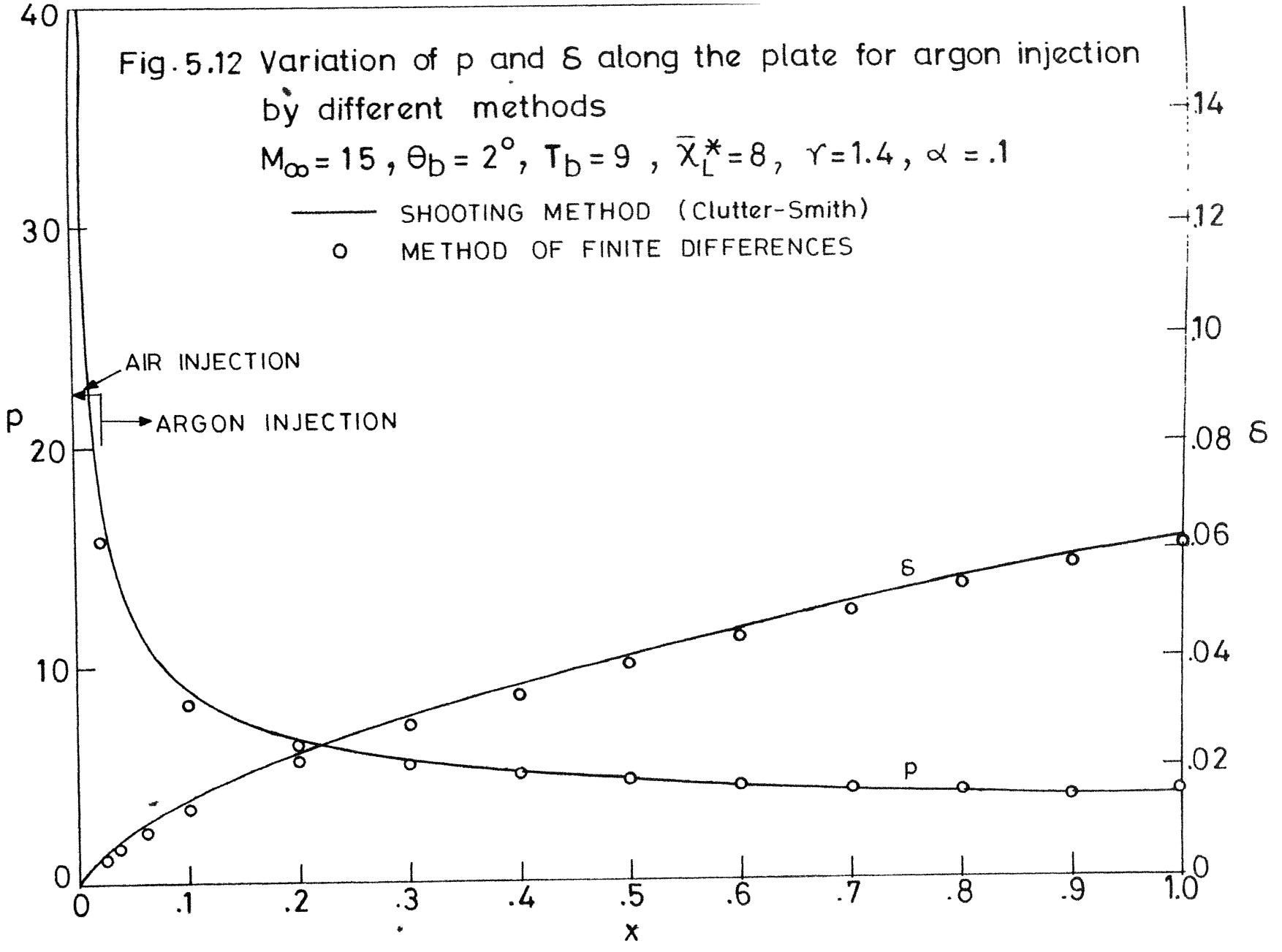
Fig. 5.12 Variation of p and δ along the plate for argon injection by different methods
$M_\infty = 15$, $\theta_b = 2^\circ$, $T_b = 9$, $\bar{\chi}_L^* = 8$, $\gamma = 1.4$, $\alpha = .1$
SHOOTING METHOD (Clutter-Smith)
METHOD OF FINITE DIFFERENCES
AIR INJECTION
ARGON INJECTION
p
δ
x
40
30
20
10
0
.14
.12
.10
.08
.06
.04
.02
0
.1
.2
.3
.4
.5
.6
.7
.8
.9
1.0

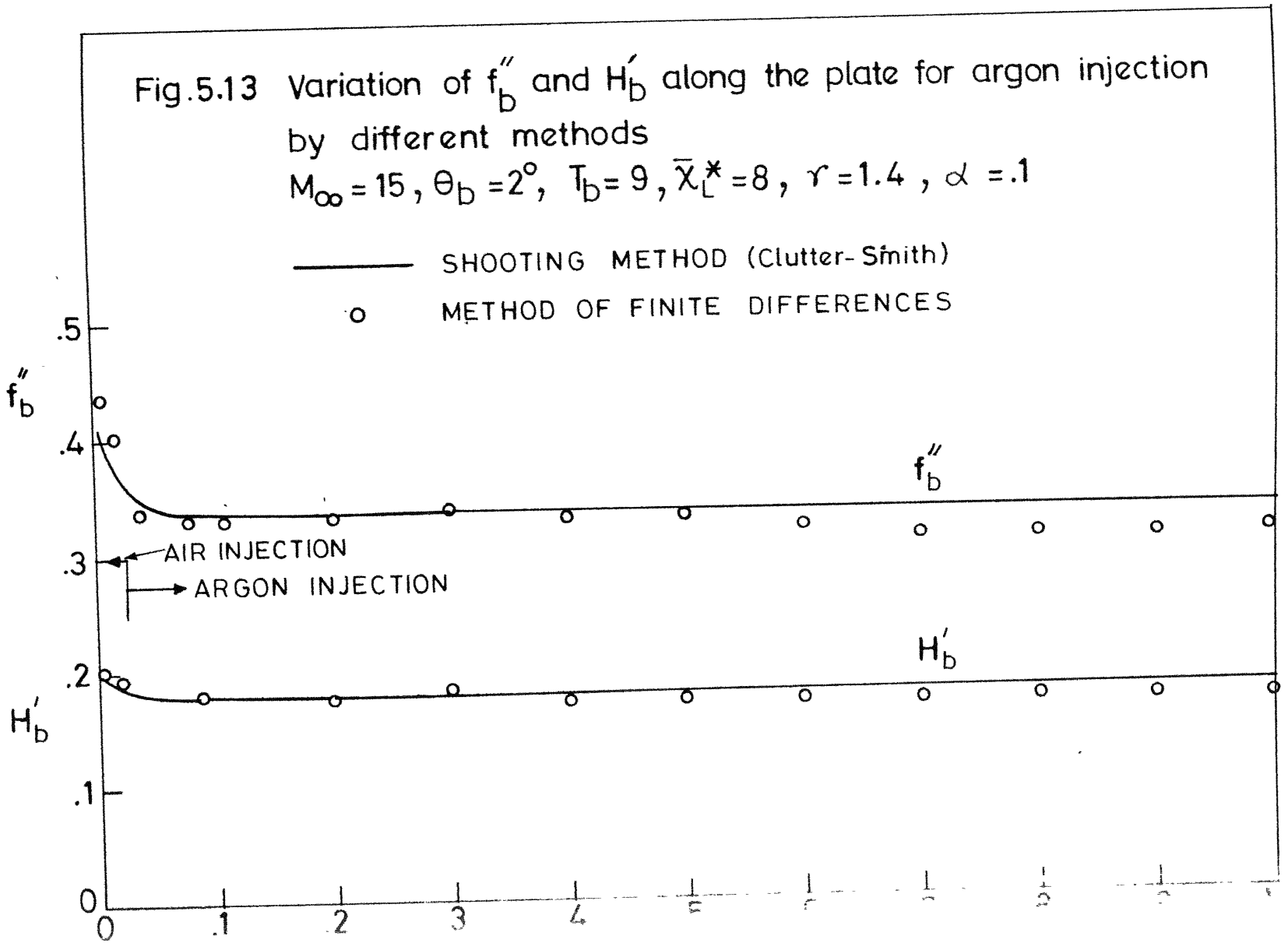
Fig.5.13 Variation of f_b'' and H_b' along the plate for argon injection by different methods
$M_\infty = 15$, $\theta_b = 2°$, $T_b = 9$, $\bar{\chi}_L^* = 8$, $\gamma = 1.4$, $\alpha = .1$
SHOOTING METHOD (Clutter-Smith)
METHOD OF FINITE DIFFERENCES
f_b''
H_b'
AIR INJECTION
ARGON INJECTION
.5
.4
.3
.2
.1
0
0
.1
.2
.3
.4

Fig. 5.14 Variation of profiles of velocity and temperature for air injection in similar solution

$\beta = 0$, $f(o) = -.5196$, $u_e^* = 2904$ ft/sec

$T_o^* = 1092°R$, $T_b^* = 493°R$, $T_e^* = 390°R$, $\alpha_1 = .5$

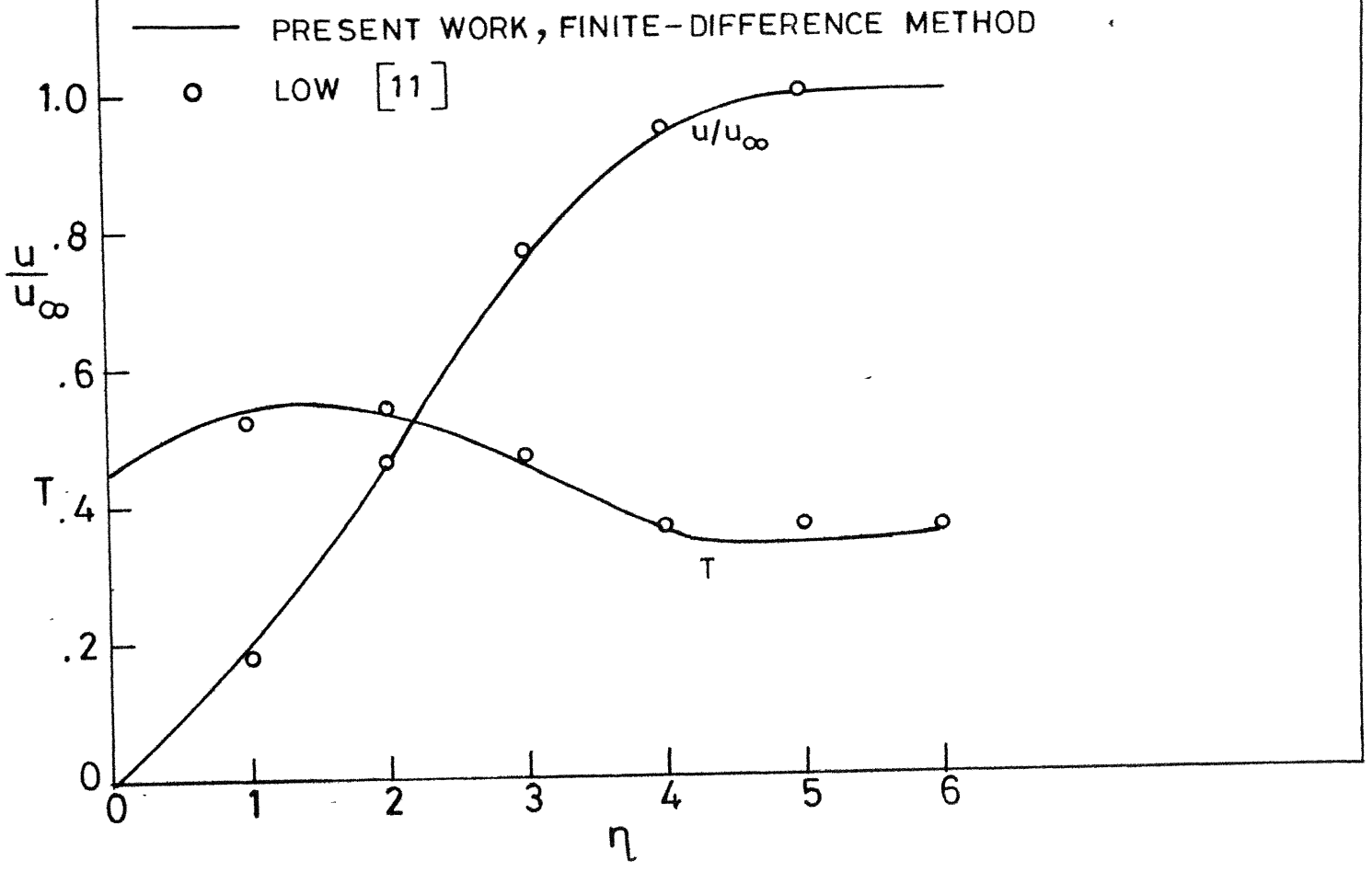

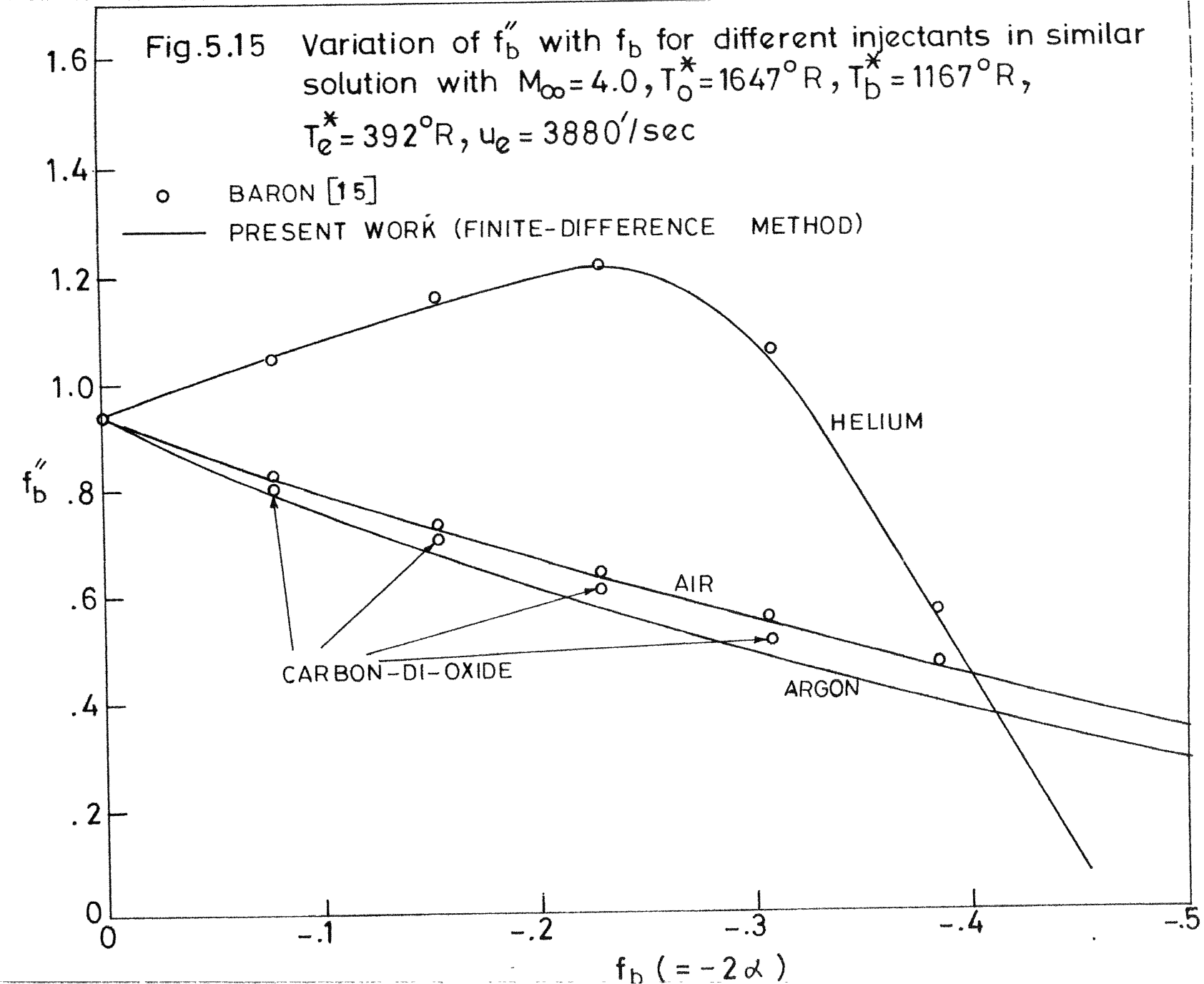
Fig.5.15 Variation of f_b'' with f_b for different injectants in similar solution with $M_\infty = 4.0$, $T_o^* = 1647°R$, $T_b^* = 1167°R$, $T_e^* = 392°R$, $u_e = 3880'/sec$
o BARON [15]
PRESENT WORK (FINITE-DIFFERENCE METHOD)
HELIUM
AIR
CARBON-DI-OXIDE
ARGON
f_b''
f_b ($= -2\alpha$)
1.6
1.4
1.2
1.0
.8
.6
.4
.2
0
-.1
-.2
-.3
-.4
-.5

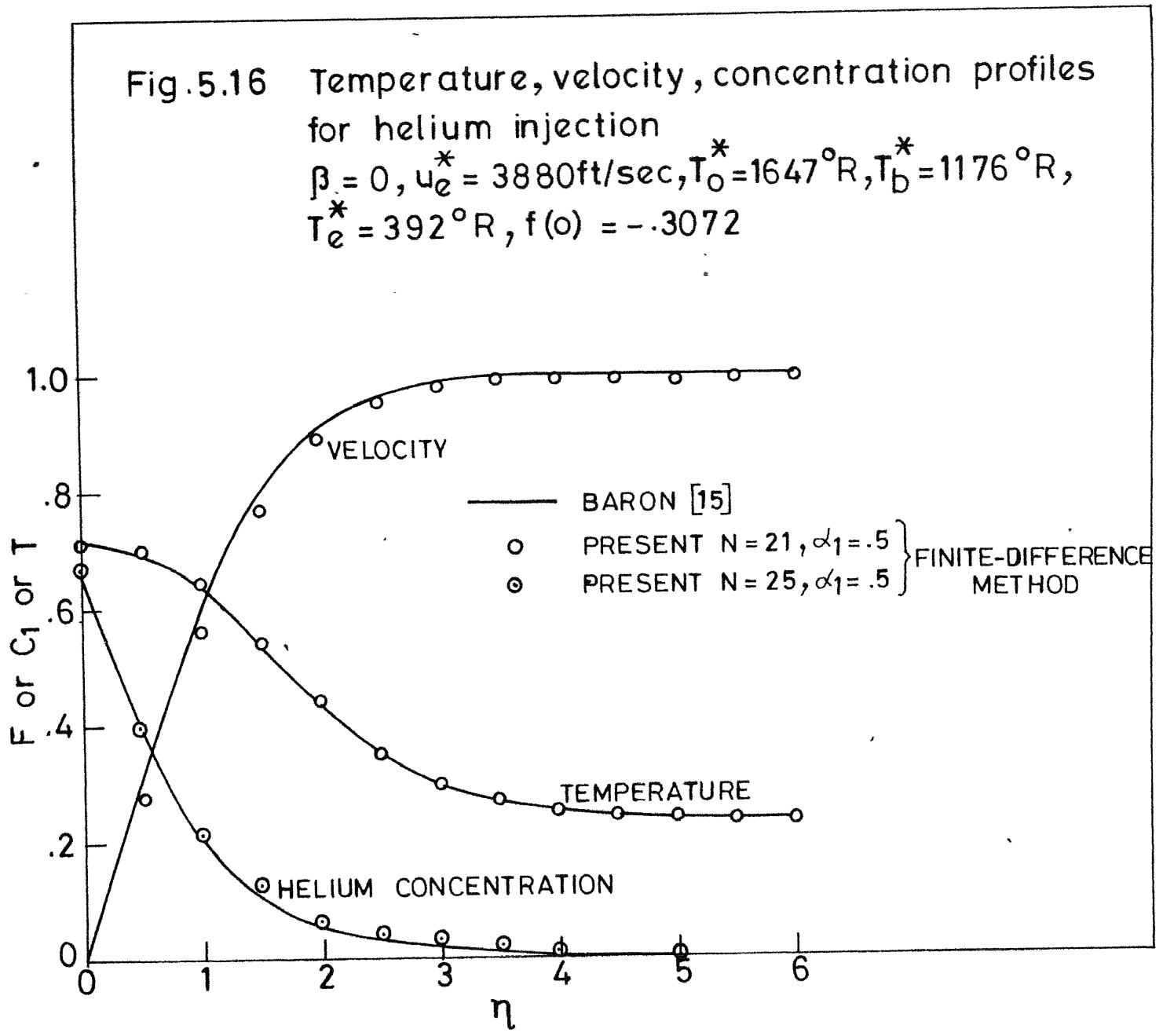
Fig. 5.16 Temperature, velocity, concentration profiles for helium injection
$\beta = 0$, $u_e^* = 3880$ ft/sec, $T_o^* = 1647°R$, $T_b^* = 1176°R$, $T_e^* = 392°R$, $f(o) = -.3072$
1.0
.8
.6
.4
.2
0
F or C_1 or T
VELOCITY
BARON [15]
PRESENT N = 21, $\alpha_1 = .5$
PRESENT N = 25, $\alpha_1 = .5$
FINITE-DIFFERENCE METHOD
TEMPERATURE
HELIUM CONCENTRATION
0
1
2
3
4
5
6
η

Fig.5.17 Pressure variation along the plate for different injectants
$M_\infty = 15$, $\bar{\chi}_L^* = 8$, $\theta_b = 2^\circ$, $\gamma = 1.4$, $T_b = 9$, $\alpha = .15$
Finite-differences method

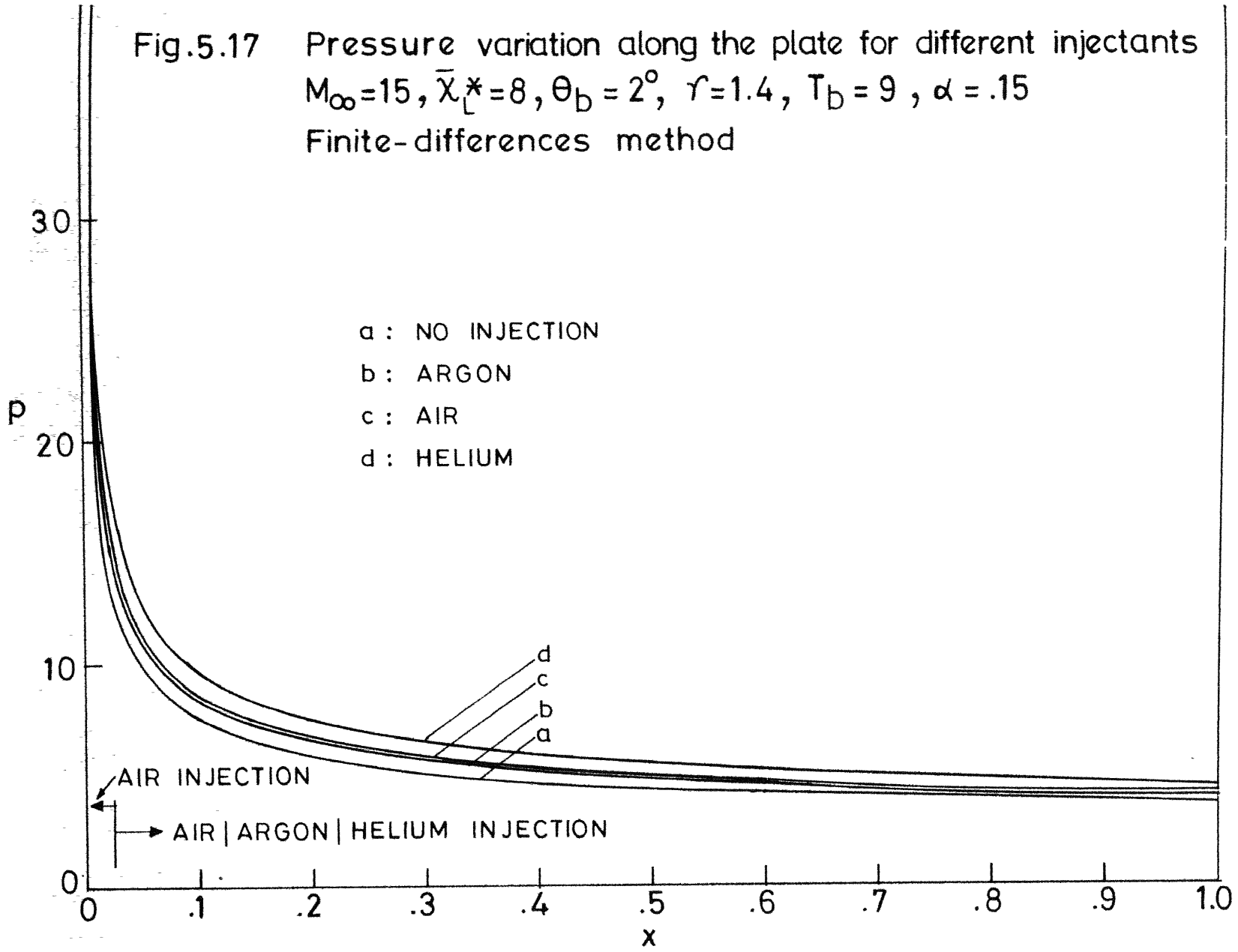

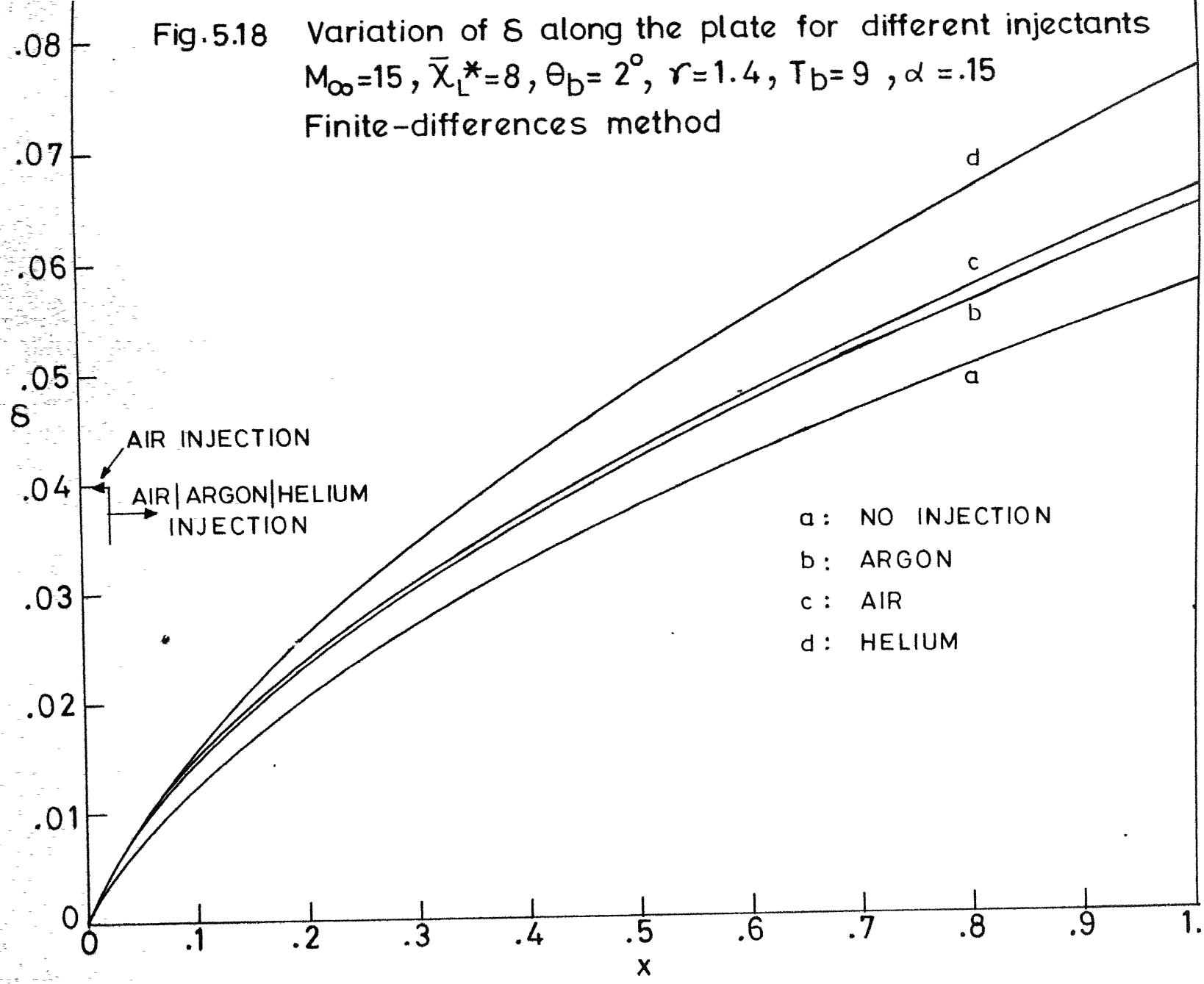
Fig.5.18 Variation of δ along the plate for different injectants
M_∞=15, $\bar{\chi}_L^*$=8, θ_b= 2°, γ=1.4, T_b= 9 , α =.15
Finite-differences method
δ
.08
.07
.06
.05
.04
.03
.02
.01
0
0
.1
.2
.3
.4
.5
.6
.7
.8
.9
1.0
x
d
c
b
a
AIR INJECTION
AIR | ARGON | HELIUM INJECTION
a: NO INJECTION
b: ARGON
c: AIR
d: HELIUM

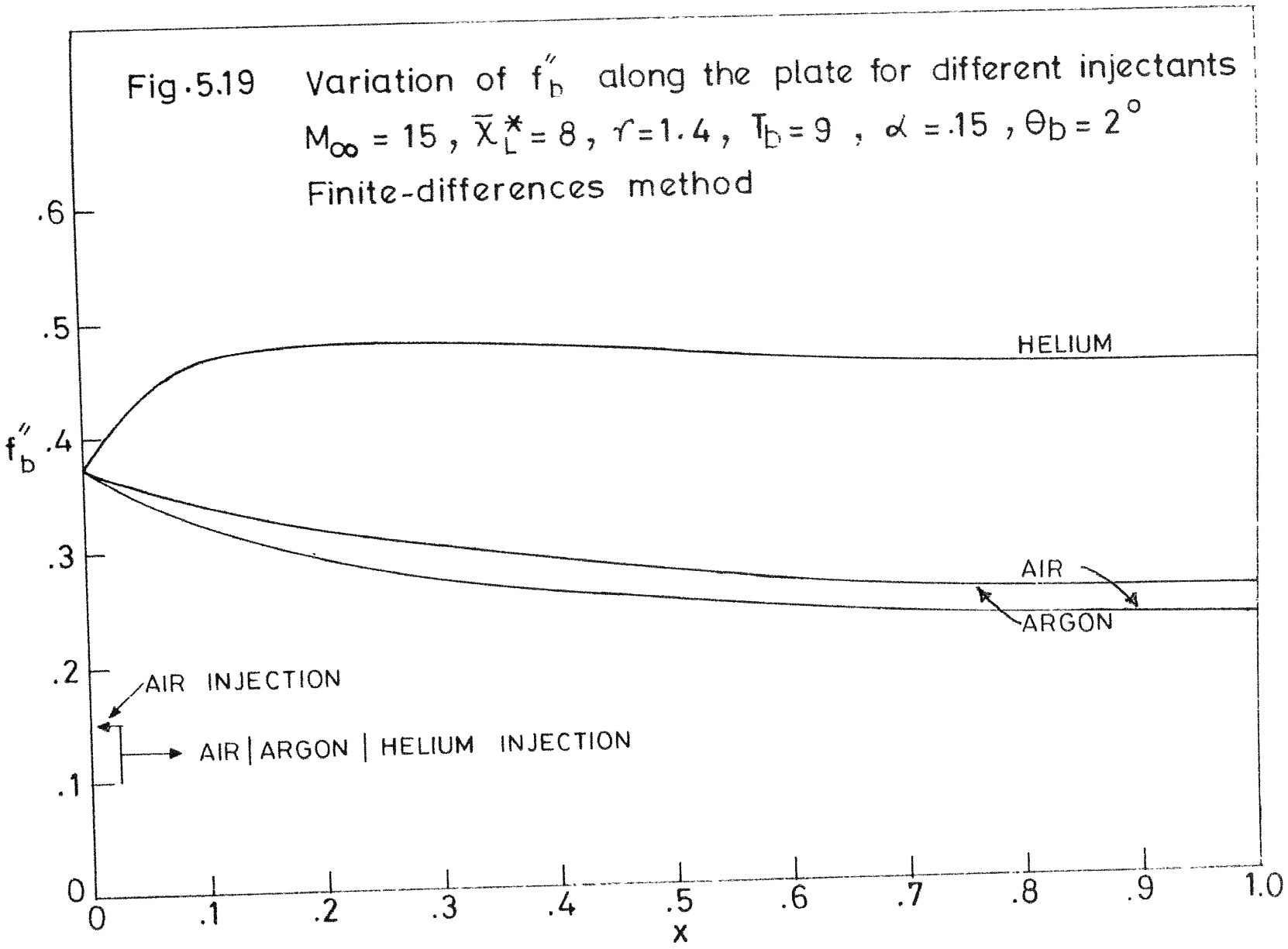
Fig.5.19 Variation of f''_b along the plate for different injectants
$M_\infty = 15$, $\bar{X}^*_L = 8$, $\gamma = 1.4$, $T_b = 9$, $\alpha = .15$, $\theta_b = 2^\circ$
Finite-differences method
f''_b
.6
.5
.4
.3
.2
.1
0
HELIUM
AIR
ARGON
AIR INJECTION
AIR | ARGON | HELIUM INJECTION
0
.1
.2
.3
.4
.5
.6
.7
.8
.9
1.0
x

Fig.5.20 Variation of H_b' along the plate for different injectants

$M_\infty = 15$, $\bar{X}_L^* = 8$, $\gamma = 1.4$, $\theta_b = 2^\circ$, $\alpha = .15$, $T_b = 9$

Finite-differences method

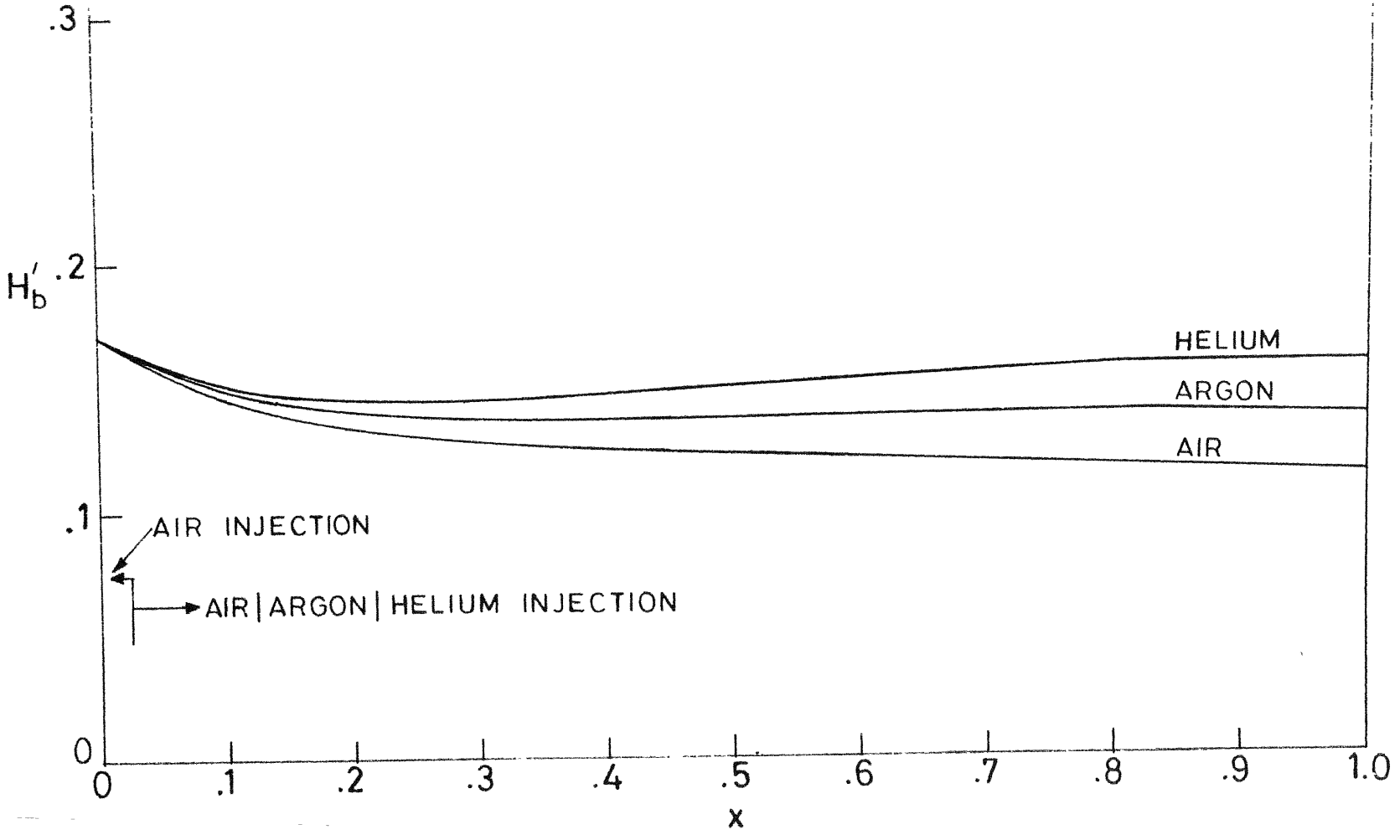

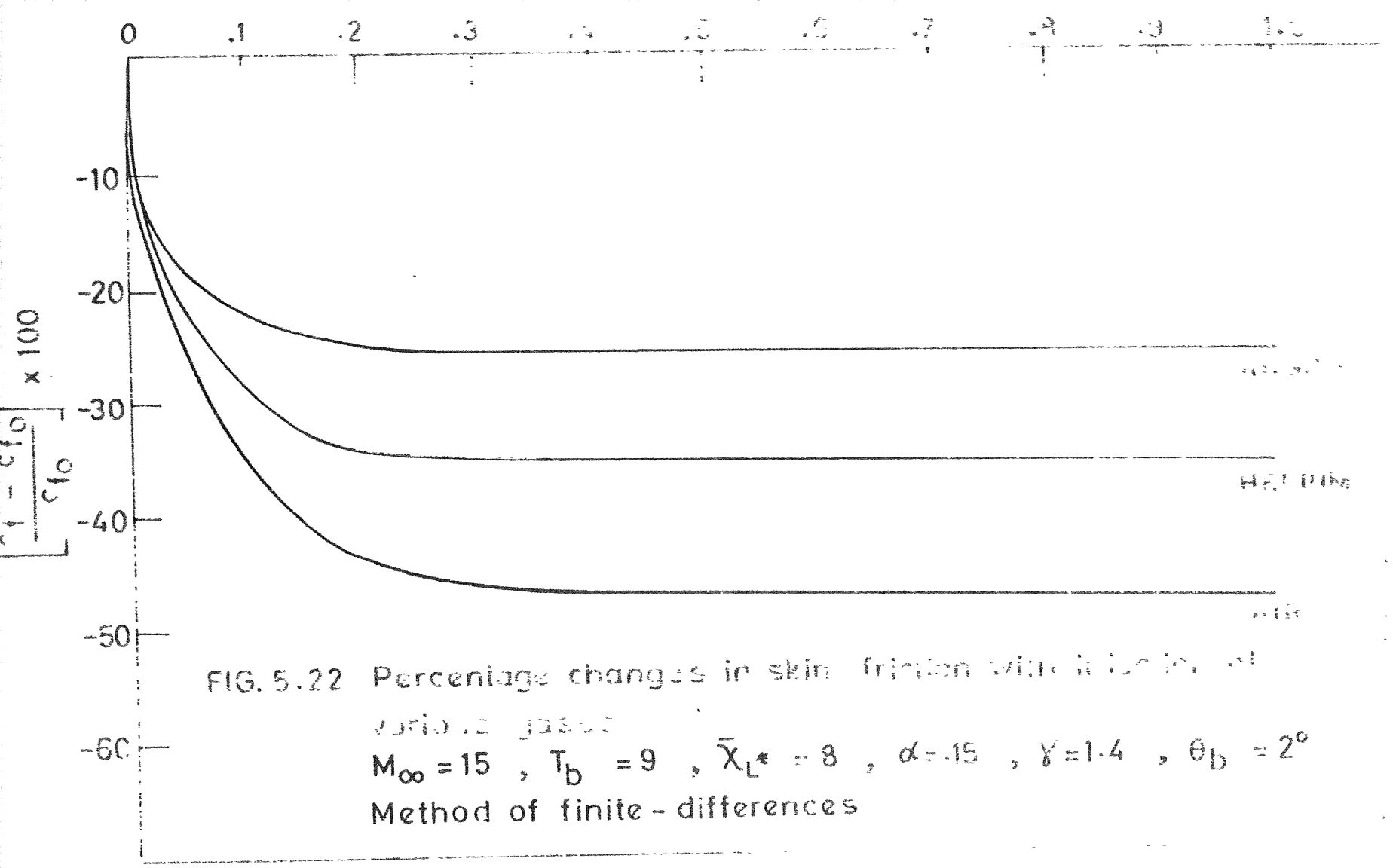

FIG. 5.22 Percentage changes in skin friction with [illegible]

[illegible] gases

$M_\infty = 15$, $T_b = 9$, $\bar{X}_L^* = 8$, $\alpha = 15$, $\gamma = 1.4$, $\theta_b = 2°$

Method of finite-differences

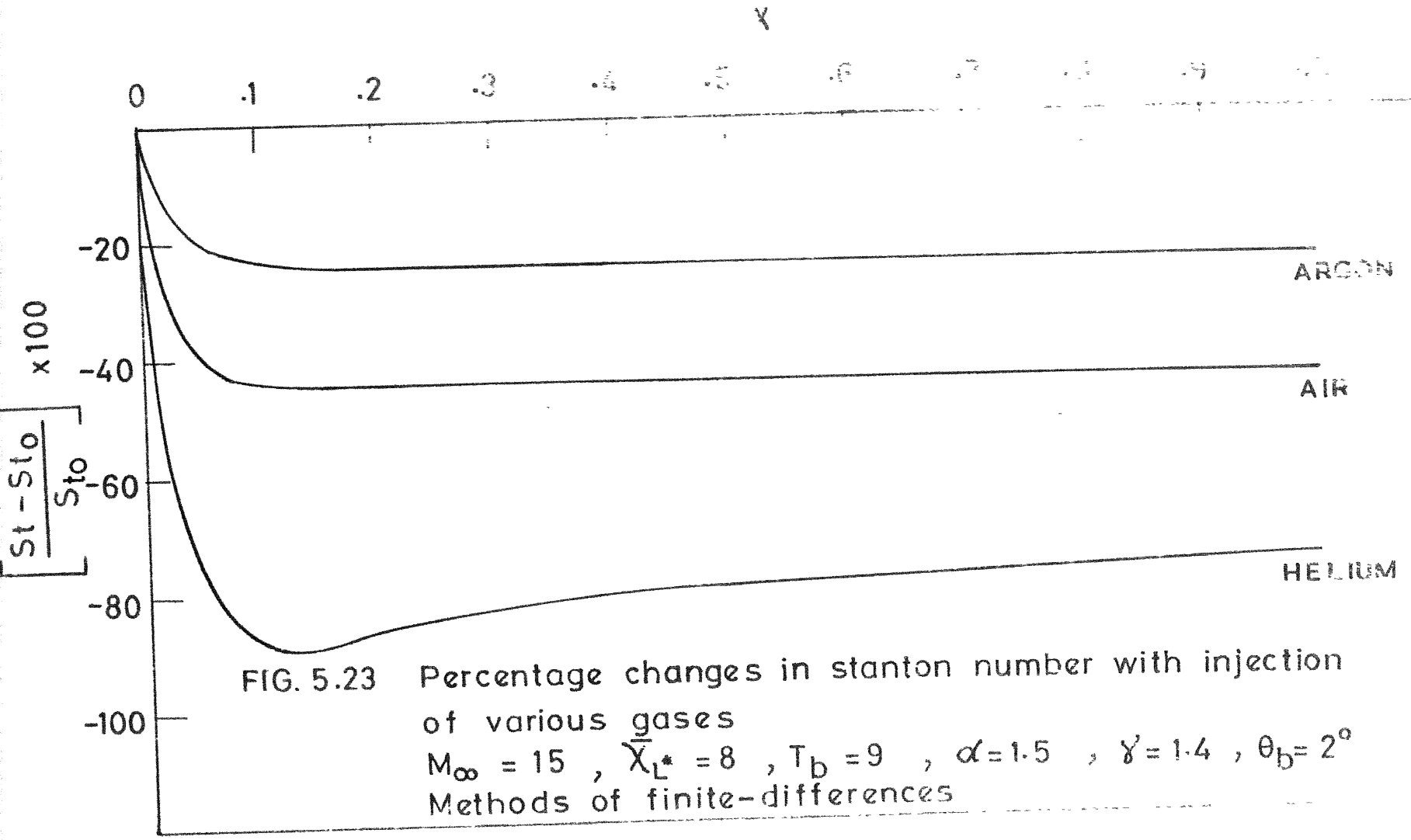

FIG. 5.23 Percentage changes in stanton number with injection of various gases

$M_\infty = 15$, $\bar{X}_{L^*} = 8$, $T_b = 9$, $\alpha = 1.5$, $\gamma = 1.4$, $\theta_b = 2^\circ$

Methods of finite-differences

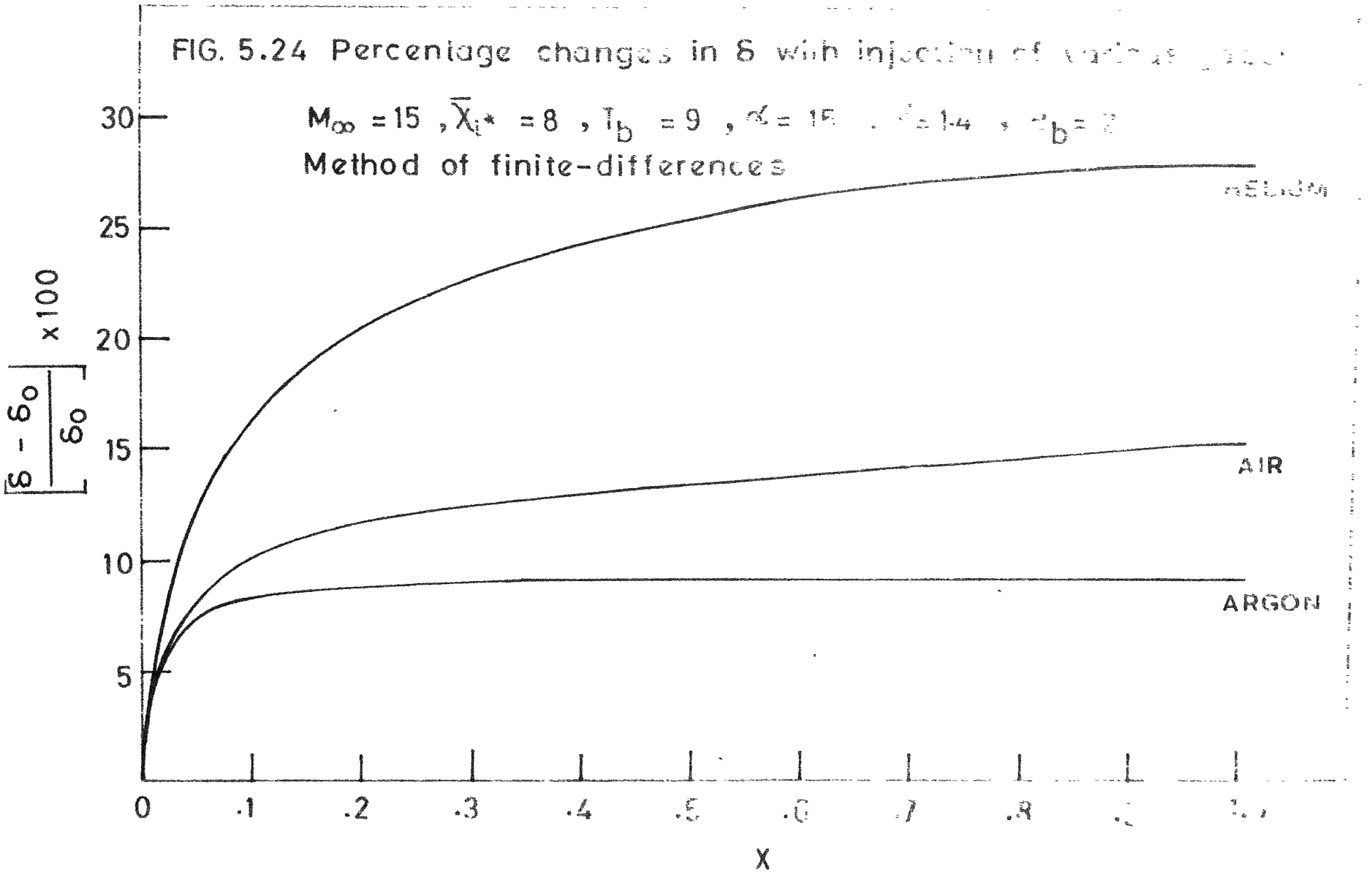
FIG. 5.24 Percentage changes in δ with injection of
$M_\infty = 15$, $\bar{\chi}_i^* = 8$, $T_b = 9$,
Method of finite-difference
HELIUM
AIR
ARGON
$\frac{\delta - \delta_0}{\delta_0} \times 100$
30
25
20
15
10
5
0
.1
.2
.3
.4
.5
.6
.7
.8
X

CHAPTER VI

UTILIZATION OF RESULTS OBTAINED WITH SURFACE MASS TRANSFER

6.1 Calculation of Important Parameters

In Fig. 6.1 the various forces acting on a slender wedge-wing of semi-apex angle θ_b at an angle of attach $\bar{\alpha}$ is shown. The subscripts T and B represent the top and bottom surfaces respectively.

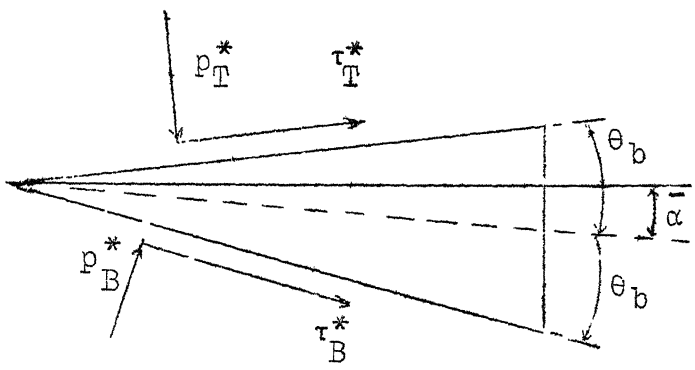

Fig. 6.1. Aerodynamic Forces Acting on a Wedge-Wing

The total normal force permit width acting on the two sides are

$$(F_N^*)_{T,B} = \int_o^{L^*} (p_{T,B}^*)\, dx^* \tag{6.1}$$

or

$$\frac{(F_N^*)_{T,B}}{\frac{1}{2}\rho_\infty^* u_\infty^{*2} L^*} = \frac{2p_o \bar{x}_L^*}{M_\infty^2} \int_o^1 x^{-1/2} (\bar{p})_{T,B}\, dx \tag{6.2}$$

The tangential force per unit width on the two sides are given by

$$(F_S^*)_{T,B} = \int_0^{L^*} (\tau^*)_{T,B}\, dx^* \tag{6.3}$$

where τ^* is the shear stress on the surface given by

$$\tau^* = \left(\mu^* \frac{\partial u^*}{\partial y^*}\right)_{y^*=y_b^*} \tag{6.4}$$

Using the variables of chapter II, we may write:

$$\tau^* = \frac{1}{2}\, \rho_\infty^*\, u_\infty^{*2}\, \frac{\sqrt{p_o}}{M_\infty^3}\, (\bar{x}_{L^*})^{3/2}\, \bar{p}\, x^{-3/4}\, f''\lambda|_{\eta=0} \tag{6.5}$$

Hence,

$$\frac{(F_S^*)_{T,B}}{\frac{1}{2}\, \rho_\infty^*\, u_\infty^{*2}} = \frac{\sqrt{p_o}}{M_\infty^3}\, \bar{L}^{*3/2} \int_0^1 x^{-3/4} (\bar{p}(f''\lambda)|_{\eta=0})_{T,B}\, dx \tag{6.6}$$

Now, the lift and drag coefficients can be obtained from

$$C_L = \frac{(F_N^*)_B - (F_N^*)_T - (F_S^*)_B\, \theta_B + (F_S^*)_T\, \theta_T}{\frac{1}{2}\, \rho_\infty^*\, u_\infty^{*2}\, L^*} \tag{6.7}$$

$$C_D = \frac{(F_S^*)_B + (F_S^*)_T + (F_N^*)_B\, \theta_B + (F_N^*)_T\, \theta_T}{\frac{1}{2}\, \rho_\infty^*\, u_\infty^{*2}\, L^*} \tag{6.8}$$

where $\theta_B = \theta_b + \bar{\alpha}$

and $\theta_T = \theta_b - \bar{\alpha}$

Using the expressions (6.2) and (6.6) in eqs. (6.7) and (6.8) we obtain:

$$C_L = \frac{2p_o\ \bar{x}_{L^*}}{\gamma M_\infty^2}\,(S_{1,B}-S_{1,T}) - \frac{\sqrt{p_o}\ \bar{x}_{L^*}^{3/2}}{M_\infty^3}\,(S_{2,B}\theta_B - S_{2,T}\theta_T) \tag{6.9}$$

$$C_D = \frac{\sqrt{p_o}\ \bar{x}_{L^*}^{3/2}}{M_\infty^3}\,(S_{2,B}+S_{2,T}) + \frac{2p_o\ \bar{x}_{L^*}}{\gamma M_\infty^2}\,(S_{1,B}\theta_B + S_{1,T}\theta_T) \tag{6.10}$$

where S_1 and S_2 represent the integrals

$$S_1 = \int_o^1 x^{-1/2}\ \bar{p}\ dx \tag{6.11}$$

$$S_2 = \int_o^1 \left[x^{-3/4}\ \bar{p}(f''\lambda)_{\eta=0} \right] dx \tag{6.12}$$

The aerodynamic centre is located by

$$x_{ac}^* = \frac{\int_o^{L^*} x^* p_B^* dx^* - \int_o^{L^*} x^* p_T^* dx^*}{\frac{1}{2}\ \rho_\infty^*\ u_\infty^{*2}\ L^*\ C_L} \tag{6.13}$$

In the non-dimensional form

$$x_{ac} = \frac{x_{ac}^*}{L^*} = \frac{S_{3,B} - S_{3,T}}{(S_{1,B}-S_{1,T}) - \frac{\gamma}{2}\frac{\sqrt{\bar{x}_{L^*}}}{\sqrt{p_o}M_\infty}\,(S_{2,B}\theta_B - S_{2,T}\theta_T)} \tag{6.14}$$

where

$$S_3 = \int_o^1 x^{1/2}\ \bar{p}\ dx \tag{6.15}$$

The heat transfer rate to the wedge per unit area at any point of the surface is given by

$$q^* = \left[k^* \frac{\partial T^*}{\partial y^*} + (c_{p1}^* - c_{p2}^*)T^*\ \rho^*\ D_{12}^* \frac{\partial c_1}{\partial y^*} \right]_{y=y_b^*} \tag{6.16}$$

Using the transformation of chapter II, we obtain:

$$q^* = \frac{1}{4} \frac{\sqrt{p_o}}{M_\infty^3} \rho_\infty^* u_\infty^{*3} \bar{x}_{L^*}^{3/2} \left(\frac{\bar{p}\, x^{-3/4}}{Pr}\right)_b \left[\frac{\partial H}{\partial \eta} + \frac{(r-1)H}{(r-1)c_1+1} (Le-1) \frac{\partial c_1}{\partial \eta}\right]_b \qquad (6.17)$$

If Q^* denote the total heat transfer rate per unit width to any one side of the wedge

$$\frac{(Q^*)_{T,B}}{\frac{1}{2} p_\infty^* u_\infty^{*3} L^*} = \frac{\sqrt{p_o}}{2 M_\infty^3} \bar{x}_{L^*}^{3/2} (S_4)_{T,B} \qquad (6.18)$$

where

$$S_4 = \int_0^1 \left[\frac{\bar{p}\, x^{-3/4} \lambda}{Pr} \left(\frac{\partial H}{\partial \eta} + \frac{(r-1)(Le-1)}{(r-1)c_1+1} H \frac{\partial c_1}{\partial \eta}\right)\right]_b dx \qquad (6.19)$$

In the case of air injection the integrals S_2 and S_4 become

$$(S_2)_{air} = \int_0^1 \left[x^{-3/4} \bar{p}\, f''\right]_b dx \qquad (6.20)$$

$$(S_4)_{air} = \frac{1}{Pr} \int_0^1 \left(\bar{p}\, x^{-3/4} \frac{\partial H}{\partial \eta}\right)_b dx \qquad (6.21)$$

The integrals $S_i (i=1,2,3,4)$ appearing in equations (6.11), (6.12), (6.15) and (6.19) have been evaluated by the Simpson's rule for unequal intervals as described in appendix B.

For the evaluation of C_L, C_D etc. the flow governing equations are solved twice for each value of the angle of attack: once for the top surface and second time for the bottom surface of the wedge. Obtaining of these results from the numerical integration of the governing equations, therefore, requires substantial computer time. The series expansion solution can also be used [71] to obtain these results without needing much computational time. The utility of these results, however, is limited to large values of the interaction parameter $\bar{\chi}$. Appendix C contains the expressions for various aerodynamic coefficients obtained by utilizing the series expansion solutions for the case with and without air injection.

6.2 Results of the Aerodynamic Characteristics with Surface Injection

Fig. 6.2 shows the comparison of the values of C_L, C_D and L/D obtained by the Clutter-Smith method and by using the series expansion solutions for various values of the angle of attack for the case of air injection with $M_\infty = 20$, $\bar{\chi}_L* = 8$, $H_b = 0.5$, $Pr = .72$, $\gamma = 1.4$, $\theta_b = 2^\circ$ and $\alpha = 0.5$. The agreement between the results obtained from these two methods appears to be good at small values of the angle of attach, $\bar{\alpha}$.

Table 6.1 gives the values of the integrals $S_i (i=1,2,3,4)$ and C_L, C_D, L/D, x_{ac} and Q (Q is the total heat transfer rate to the wedge per unit width obtained by adding the values for top and bottom surfaces of the wedge given by eq. (6.18))

for an angle of attack of 1° for both homogeneous (air) and heterogeneous (helium and argon) injection cases with $M_{\infty} = 15$, $\theta_b = 3^{\circ}$, $T_b = 9$, $\gamma = 1.4$, $\alpha = 0.15$. The calculations of the values of C_L, C_D and L/D for various values of the angle of attack was not performed due to the prohibitive computer time.

Table 6.1

Values of the Parameters for the Calculation of the Aerodynamic Characteristics of a wedge-wing with Surface Mass Transfer ($M_{\infty}=15$, $\bar{x}_L* = 8$, $T_b = 9$, $\gamma=1.4$, $\alpha=.15$, $\theta_b=3^{\circ}$, $\theta_T= 2^{\circ}$, $\theta_B=4^{\circ}$ and Pr = .72)

Angle of attack, $\bar{\alpha}=1^{\circ}$

Parameter	Injectant		
	Ar	He	Air
S_{1T}	3.18698	3.67411	3.23367
S_{2T}	2.20448	2.01544	1.76914
S_{3T}	1.21723	1.42376	1.24557
S_{1B}	4.02433	4.46287	4.22231
S_{2B}	2.30056	2.11976	2.00430
S_{3B}	1.61833	1.80220	1.72011
S_{4B}	1.42956	1.20748	0.97002
C_L	0.01004875	0.009469498	0.01193238
C_D	0.01971726	0.01908277	0.01749107
L/D	0.5096424	0.4962328	0.6821985
x_{ac}	0.4921834	0.4927840	0.4903794
Q	0.00450726	0.0020360	0.004127421

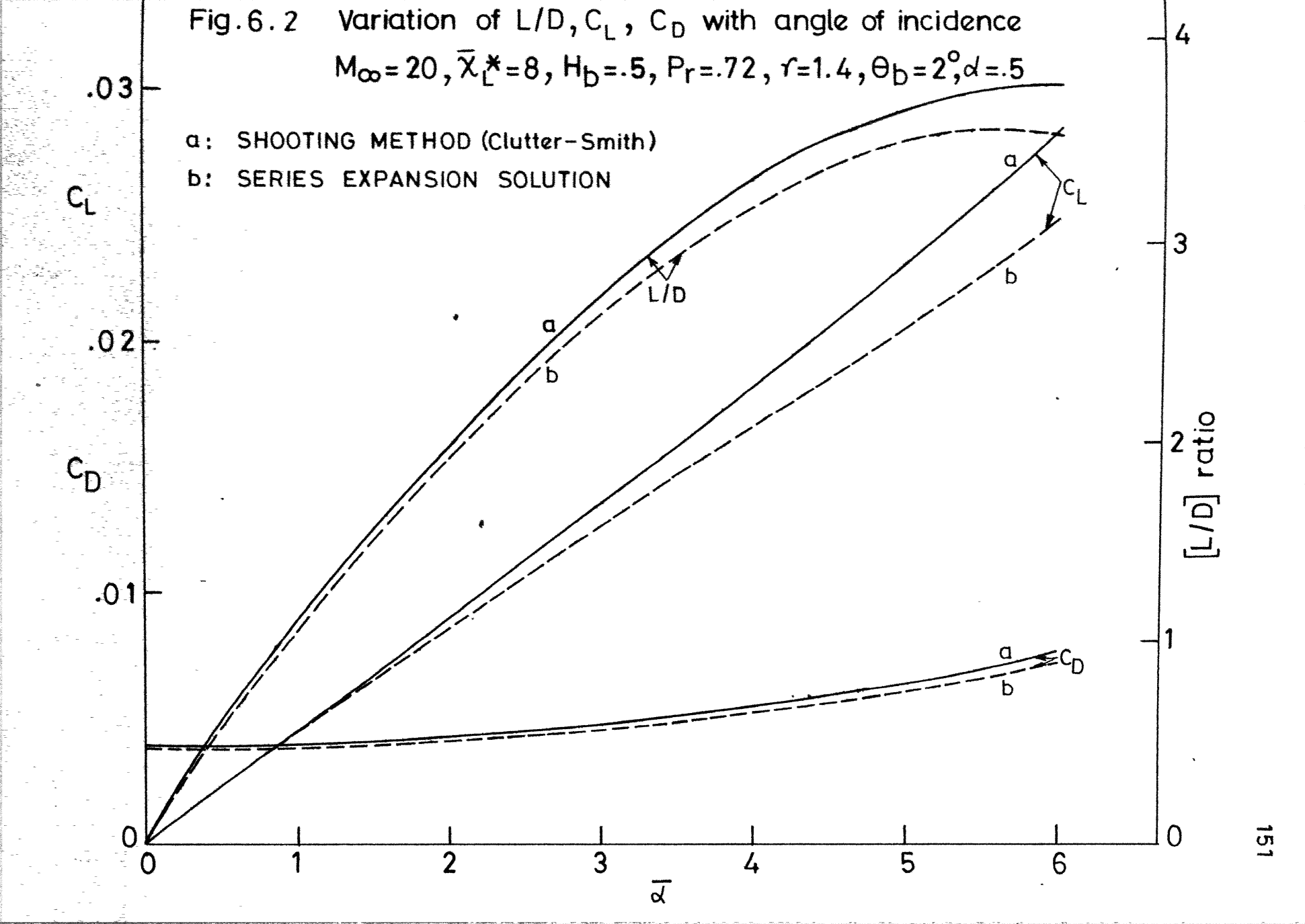
Fig. 6.2 Variation of L/D, C_L, C_D with angle of incidence
$M_\infty = 20, \bar{\chi}_L^* = 8, H_b = .5, P_r = .72, \gamma = 1.4, \theta_b = 2^\circ, \alpha = .5$
a: SHOOTING METHOD (Clutter-Smith)
b: SERIES EXPANSION SOLUTION
C_L
C_D
L/D
[L/D] ratio
$\bar{\alpha}$
a
b
.03
.02
.01
0
1
2
3
4
5
6

CHAPTER VII

UNSTEADY CASE OF HOMOGENEOUS INJECTION

In this chapter we propose to consider the problem of adjustment of the boundary layer when the inclination of the wall to the flow is impulsively changed from the value $\theta_{b,i}$ to $\theta_{b,f}$.

The procedure followed is described here under.

Step 1.

Calculate the boundary layer characteristics —f(x,) and H(x,) and the surface pressure distribution p(x) separately corresponding to the inclination $\theta_{b,i}$ and $\theta_{b,f}$. Let them be designated as f_i, H_i, p_i, f_f, H_f and p_f. Also calculate the surface pressure distribution with K of equation (3.5) calculated with k_b corresponding to $\theta_{b,f}$ and o corresponding to $\theta_{b,i}$. Call it p_{i-f}.

Step 2.

Write the unsteady governing equations and use the initial conditions

$$f(x,\eta)_{t=0} = f_i$$

$$H(x,\eta)_{t=0} = H_i$$

$$p(x)_{t=0} = p_{i-f}$$

Step 3.

Solve the unsteady governing equations and calculate the time required for f, H and p to attain the values f_f, H_f and p_f.

In other words, it is proposed to calculate the time required for the boundary layer to change from the steady state corresponding to plate inclination $\theta_{b,i}$ to that corresponding to the plate inclination $\theta_{b,f}$ if the pressure distribution on the plate is impulsively changed from the one corresponding to $\theta_{b,i}$ to that corresponding to $\theta_{b,f}$ (with β corresponding to $\theta_{b,i}$).

7.1 Flow Governing Equations and the Initial Conditions

The governing equations for this case may be obtained from eqns. (2.38) and (2.39) of Chapter II by putting $c_1 = 0$ in these equations :

$$\bar{p}\, f''' + f'' = -4x\left(\frac{\partial f}{\partial x} f'' - f' \frac{\partial f'}{\partial x}\right) + \beta\left(\frac{2x}{\bar{p}} \frac{d\bar{p}}{dx} - 1\right)(H - f'^2) + 4x \frac{\partial f'}{\partial t} \qquad (7.1)$$

$$\frac{\bar{J}}{Pr} H'' + f H' - 4x\left(f' \frac{\partial H}{\partial x} - H' \frac{\partial f}{\partial x}\right) = \frac{2\bar{p}}{Pr}(1 - Pr)(f''^2 + f'f''') + 4x \frac{\partial H}{\partial t} - 4\beta \frac{x}{\bar{p}} \frac{\partial \bar{p}}{\partial t}(H - f'^2) \qquad (7.2)$$

where $\bar{p}(x,t)$ is given by expression (2.51).

The steady state solution of Chapter III, corresponding to $\theta_b = \theta_{b,i}$, describe the flow on the plate prevailing at $t < 0$. At the instant of the impulsive change ($t=0$), the spatial distribution of the temperature and velocity field with respect to the plate is supplied by this steady state solution. But, the change in the inclination of the body changes the effective shape of the body which in turn changes the pressure distribution.

The initial conditions in x are specified at $x = x_1$ for $t \geq 0$. As in the steady problem, the series expansion solution for $\theta_b = \theta_{b,f}$ is assumed to give the solution at $x = x_1$ for $t \geq 0$. This assumes that the final steady state at $x = x_1$, is reached instantaneously. Because of the close proximity to the leading edge, the flow at $x = x_1$ is extremely insensitive to the inclination and the initial and final steady state solutions differ by less than 1 percent. Thus the initial conditions in x are given by

(i) For $x = x_1$ at $t > 0$

$$f(x_1,\eta,t) = f_o(\eta) + \frac{\bar{f}_1(\eta)\, p_1\, k_{b,f}}{\bar{x}_1^{1/2}} + \frac{p_2\, \bar{f}_2(\eta) + \left[p_3\, \bar{f}_2(\eta) + p_1^2\, \bar{f}_3(\eta)\right] k_{b,f}^2}{\bar{x}_1} \tag{7.3}$$

$$H(x_1,\eta,t) = H_o(\eta) + \frac{\bar{H}_1(\eta)\, p_1\, k_{b,f}}{\bar{x}_1^{1/2}} + \frac{p_2\, \bar{H}_2(\eta) + \left[p_3\, \bar{H}_2(\eta) + p_1^2\, \bar{H}_3(\eta)\right] k_{b,f}^2}{\bar{1}} \tag{7.4}$$

$$\bar{p}(x_1,t) = 1 + \frac{p_1\, k_{b,f}}{\bar{x}_1^{1/2}} + \frac{p_2 + p_3\, k_{b,f}^2}{\bar{x}_1} \tag{7.5}$$

where $\bar{x}_1 = \bar{x}_{L^*} \sqrt{\bar{x}_1}$ and $k_{b,f} = M_\infty\, \theta_{b,f}$

(ii) For $x > x_1$ at $t = 0$

$$f(x,\eta,0) = f^{(0)}(x,\eta) \tag{7.6}$$

$$H(x,\eta,0) = H^{(0)}(x,\eta) \qquad (7.7)$$

where $f^{(0)}$ and $H^{(0)}$ are the steady state solution corresponding to $v_b = v_{b,i}$ obtained by finite-difference solution of the steady case of the air injection problem. The initial pressure distribution $\bar{p}(x,0) = \bar{p}^{(0)}(x)$ is calculated by the same procedure as employed for the calculation of $f^{(0)}$ and $H^{(0)}$ but k_b will be replaced by $k_{b,f}$. Fig. 7.1 shows the various boundary and space conditions for the problem analysed here mathematically. The solution may be obtained by the numerical methods described in Chapters III, IV and V for the steady state problems after the time-dependent term is replaced by the backward finite difference approximation.

The Clutter-Smith method described in Chapters III and IV was tried first and it failed to converge for the reasons similar to those given in Chapter V. Therefore, the finite-difference method of Chapter V was used with the details provided in the next section.

7.3 Finite Difference Method for the Unsteady Homogeneous Injection Problem

The unsteady equations are solved at discrete time-steps t_i, $i = 1,2,3,\ldots$ with step-sizes progressively increasing in the positive t-direction :

$$t_1 = t_1 \qquad (7.8a)$$

$$t_i - t_{i-1} = \Delta t_i = k_t \, \Delta t_{i-1}, \quad i = 2,3, \ldots \qquad (7.8b)$$

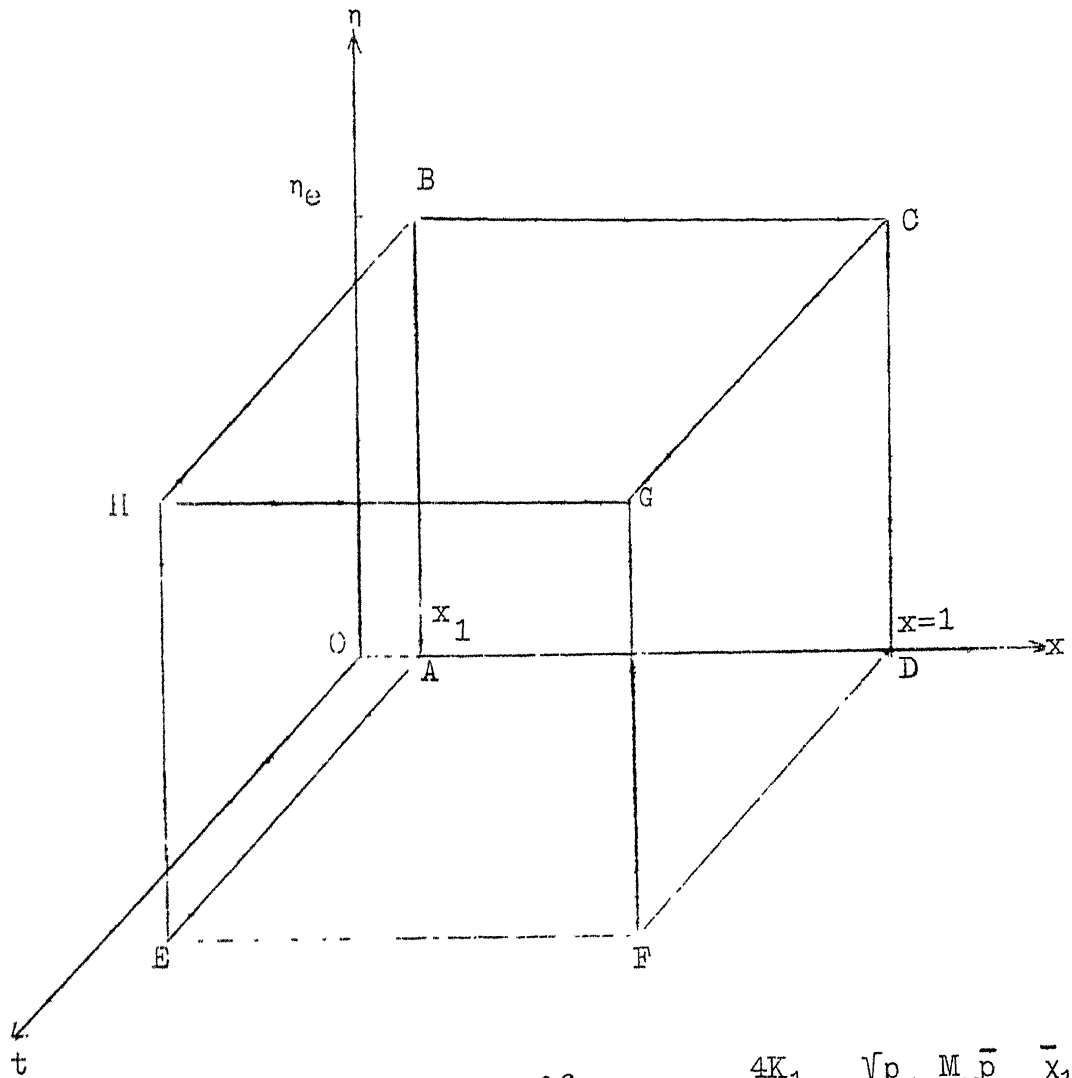

on ADFE : $f+4x\frac{\partial f}{\partial x} = -2\alpha - \frac{4K_1}{(\gamma-1)}\frac{\sqrt{p_o}\,M_\infty\bar{p}}{H_b}\left(\frac{\bar{x}_1-\bar{x}}{\sqrt{\bar{x}}}\right)$

$f'=0,\ H=H_b$ or $H'=0$

on GCBH : $f'=1,\ H=1$

on ADCB : $f=f^{(o)},\ H=H^{(o)},\ p=p^{(o)}$

on ABHE : $f=f_1,\ H=H_1,\ p=p_1$

Fig. 7.1. Diagramatic arrangement of the boundary and initial conditions

Here the first time step Δt_1 is taken of $O(10^{-3})$ and $k_t > 1$. The arrangement of t and x stations is shown below.

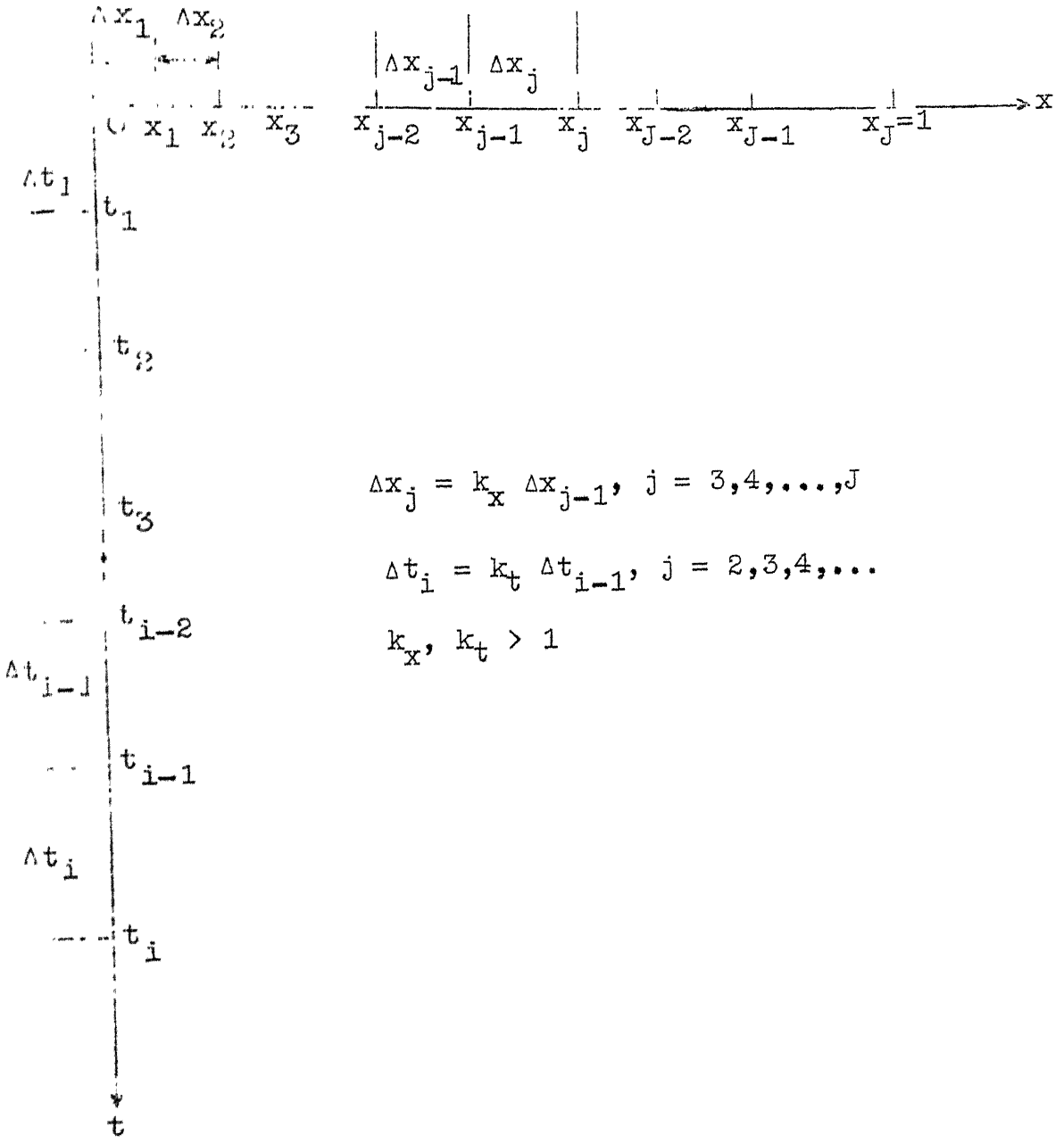

Figure 7.2 : Schematic Arrangement of x and t Stations

For any function $\omega(x,t)$ the first derivative in the backward difference form can be written as

$$\left(\frac{\partial \omega}{\partial t}\right)^{(i)} = u_i\ \omega^{(i)} - (u_i + v_i)\ \omega^{(i-1)} + v_i\ \omega^{(i-2)} \qquad (7.9a)$$

$$\left(\frac{\partial \omega}{\partial x}\right)^{(j)} = \ell_j\ \omega^{(j)} - (\ell_j + q_j)\ \omega^{(j-1)} + q_j\ \omega^{(j-2)} \qquad (7.9b)$$

where

$$\left.\begin{aligned} u_i &= \frac{1}{\Delta t_i} \\ \ell_j &= \frac{1}{\Delta x_j} \\ v_i &= 0 \\ q_j &= 0 \end{aligned}\right\} \quad \text{for } i = 1,\ j = 1,2 \qquad (7.10a)$$

$$\left.\begin{aligned} u_i &= \frac{1}{\Delta t_i}\left(\frac{2k_t+1}{k_t}\right) \\ \ell_j &= \frac{1}{\Delta x_j}\left(\frac{2k_x+1}{k_x}\right) \\ v_i &= \frac{1}{\Delta t_i}\left(\frac{k_t^2}{k_t+1}\right) \\ q_j &= \frac{1}{\Delta x_j}\left(\frac{k_x^2}{k_x+1}\right) \end{aligned}\right\} \quad \text{for } i \geq 2,\ j \geq 3 \qquad (7.10b)$$

With the help of finite-difference equations (5.44) and (7.9) equations (7.1) and (7.2), give (with $F = f'$) :

$$F_d\left[\frac{\bar{p}}{2(\Delta\eta)^2} - \frac{f}{4(\Delta\eta)} - \frac{x\ f_x}{(\Delta\eta)}\right] + F_f\left[\frac{\bar{p}}{2(\Delta\eta)^2} + \frac{f}{4(\Delta\eta)} + \frac{x\ f_x}{(\Delta\eta)}\right] +$$

$$F_c\left[\frac{-\bar{p}}{(\Delta\eta)^2} - 4x\ F_{\bar{b}}\ \ell_j + \beta\left(\frac{2x}{\bar{p}}\frac{d\bar{p}}{dx} - 1\right) F_{\bar{b}} - 4x\ u_i\right]$$

$$= \frac{-\bar{p}}{2(\Delta\eta)^2}(F_c - 2F_{\bar{b}} + F_a) - \frac{f}{4(\Delta\eta)}(F_c - F_a) - \frac{x\, f_x}{(\Delta\eta)}(F_c - F_a)$$

$$+ \beta\left(\frac{2x}{\bar{p}}\frac{d\bar{p}}{dx} - 1\right) H_e - 4x\, F_{\bar{b}}\, F_{\bar{b}1}(\ell_j + q_j) + 4x\, F_{\bar{b}}\, F_{\bar{b}1}\, q_j$$

$$+ 4x\left[-(u_i + v_i) F_e^{(i-1)} + v_i F_e^{i-2}\right] \qquad (7.11)$$

$$H_i\left[\frac{\bar{p}}{Pr}\frac{1}{(\Delta\eta)^2} - \frac{f}{4(\Delta\eta)} - \frac{x\, f_x}{(\Delta\eta)}\right] + H_f\left[\frac{\bar{p}}{Pr}\frac{1}{2(\Delta\eta)^2} + \frac{f}{4(\Delta\eta)}\right.$$

$$\left. + \frac{x\, f_x}{(\Delta\eta)}\right] + H_e\left[\frac{-\bar{p}}{Pr(\Delta\eta)^2} - 4x\, F_e\, \ell_j - 4x\, u_i + 4\beta\frac{x}{\bar{p}}\right.$$

$$\left. u_i\,\bar{p} - (u_i + v_i)\,\bar{p}^{i-1} + v_i\,\bar{p}^{i-2}\right]$$

$$= \frac{-\bar{p}}{2Pr(\Delta\eta)^2}(H_e - 2H_{\bar{b}} + H_a) - \frac{f}{4(\Delta\eta)}(H_e - H_a)$$

$$- 4x\, F_e\, H_{\bar{b}}(\ell_j + q_j) + 4x\, F_e\, H_e^{i-2}\, q_j - \frac{x\, f_x}{(\Delta\eta)}(H_e - H_a)$$

$$+ \frac{2\bar{p}}{Pr}(1 - Pr)\left[\frac{F_e}{2(\Delta\eta)^2}(F_c - 2F_{\bar{b}} + F_a + F_f - 2F_e + F_d)\right.$$

$$\left. + \frac{1}{4(\Delta\eta)^2}(F_f - F_d)(F_c - F_a)\right] + 4x\left[-(u_i + v_i) H_e^{i-1}\right.$$

$$\left. + v_i H_e^{i-2}\right] + 4\beta\frac{x}{\bar{p}}\left[u_i\,\bar{p} - (u_i + v_i)\,\bar{p}^{i-1} + v_i\,\bar{p}^{i-2}\right]F_e^2$$

(7.12)

In equations (7.11) and (7.12) the variables without the superscript refer to their values on the ith time-step and variables with subscript '$\bar{b}1$' stand for their values at the (j-2)th station. Subscripts '$\bar{b}$' and 'e' refer to the (j-1)th and (j)th stations respectively along the plate. If we put $u_i = v_i = 0$ in eqns. (7.11) and (7.12), the steady case equations are retrieved.

Since we are using backward difference formulas for the time-derivatives, they result in an implicit scheme which is inherently stable. At each time step $t = t_i$, $i = 2,3,4...$, we approximate $\bar{p}^{(i)}$ by extrapolation of values at the previous time-steps as explained later. Then the system of algebraic equations resulting from (7.11) and (7.12) is solved in the region $x_1 \leq x \leq x_j$, $0 \leq \eta \leq \eta_e$ using the initial condition (7.3 - b) and the boundary conditions (7.6 - 7). From the solution we then obtain $\bar{p}^{(i)}$ in accordance with the interaction equations (2.50) and (2.51) with $c_1 \equiv 0$. The solution then proceeds to the next time-step $t = t_i + 1$. It is continued until $|\frac{\partial \bar{p}}{\partial t}| < 10^{-4}$ and is then compared with the steady state solution corronding to $\theta = \theta_{b,f}$.

The extrapolation formula required for $\bar{p}^{(i)}$ is as follows :

$$\bar{p}^{(i)}_{(x)} = (1 + k_t)\, \bar{p}^{(i-1)}_{(x)} - k_t\, \bar{p}^{(i-2)}_{(x)} \qquad (7.13)$$

For the first time-step (i=1) $\bar{p}^{(i)}$ is taken to be $\bar{p}^{(0)}$, the value for t = 0. Now $d\bar{p}^{(i)}/dx$ can be obtained from $\bar{p}^{(i)}$ or can be extrapolated from the previous time-steps using a formula similar to (7.13).

The time-dependent term in eq. (7.16) be finite-differenced as:

$$\frac{\partial \bar{\delta}}{\partial t}^{(i)} = u_i \bar{\delta}^{(i)} - (u_i+v_i)\,\bar{\delta}^{(i-1)} + v_i \bar{\delta}^{(i-2)} \qquad (7.18)$$

When eqs. (7.18) and (7.17) are substituted into equation (7.16), we get an ordinary non-linear first order differential-equation with the initial value of $\bar{\delta} = \bar{\delta}(x_1,t)$ specified at all time-steps. This can be integrated by the fourth-order Runge-Kutta method to obtain $\bar{\delta}$ and then $\bar{p}$ can be computed from:

$$\bar{p}(x,t) = \bar{I}(x,t)/\bar{\delta}(x,t) \qquad (7.19)$$

with

$$\bar{I}(x,t) = \int_0^\infty \left[H(x,\eta,t) - f'^2(x,\eta,t) \right] d\eta / I_0 \qquad (7.20)$$

where I_0 is defined in section 3.3 of chapter III.

It may be mentioned here that equation (7.19) is another form of eq. (2.50) with $c_1 \equiv 0$.

7.4 Results of the Unsteady Problem with and without Air Injection

Fig. 7.3 through 7.5 present the distribution of $\bar{p}(x,0,t)$, $f''(x,0,t)$ and $H'(x,0,t)$ with time for no-injection case i.e. $\alpha = 0.0$ with $Pr = .72$, $\gamma = 1.4$, $H_b = 0.5$, $\bar{x}_L^* = 8$, $M_\infty = 20$ and the change in angle of attack from 2° to 6°. The initial and final states are also indicated in these figures. The figures also contain the location of the condition

$t^*u_\infty^*/x^* = 1$ which correspond to the discontinuity quoted in the literature [5,30]. The discontinuity appears to have been avoided by suitable formulation of the variables, and in particular by avoiding the variable of the type $t^*u_\infty^*/x^*$.

Fig. 7.6 through 7.8 show the variation of $\bar{p}(x,t)$, $f''(x,0,t)$ and $H'(x,0,t)$ with time for the case of air injection (α=0.15) with $P = .72$, $\gamma = 1.4$, $H_b = .5$, $\bar{x}_L* = 8$, $M_\infty = 20$ and the change in angle of attack from 2^o to 6^o. The initial and final steady states are also indicated. Here even though the value of $\bar{p}(x,t)$ is smaller compared with the no-injection case, the value of p would be higher because of the somewhat larger value of p_o in the relation: $p = (p_o \bar{x})\,\bar{p}$. Fig. 7.9 contains the variation of δ along the plate for different times for air injection (α=.15) with $Pr = .72$, $\gamma = 1.4$, $H_b = .5$, $\bar{x}_L* = 8$, $M_\infty = 20$ and the change in angle of attach from 2^o to 6^o.

In Fig. 7.10 through 7.12 are given the distribution of $\bar{p}(x,t)$, $f''(x,0,t)$ and $H'(x,0,t)$ with time for the case with suction at the wall ($\alpha = -0.5$) with $Pr = .72$, $\gamma = 1.4$, $H_b = 0.5$, $\bar{x}_L* = 8$, $M_\infty = 20$, and the change in angle of attach from 2^o to 6^o. The initial and final steady states are also shown in these figures. The value of p calculated from $\bar{p}$ for this case would be lower as compared to the no-injection case due to the smaller value of p_o in the relation: $p = (p_o \bar{x})\,\bar{p}$.

Finally, Fig. 7.13 gives the variation of δ along the plate for different times for the suction case ($\alpha = -.5$) with $Pr = .72$, $\gamma = 1.4$, $H_b = .5$, $\bar{x}_{L^*} = 8$, $M_\infty = 20$ and the change in angle of attack from 2° to 6°.

Figures 7.3 through 7.13 indicate that the induced pressure, the wall shear and heat transfer functions and the boundary layer thickness approach the final steady state values at $t \approx 10$. Closer to the leading edge, the steady state is reached earlier.

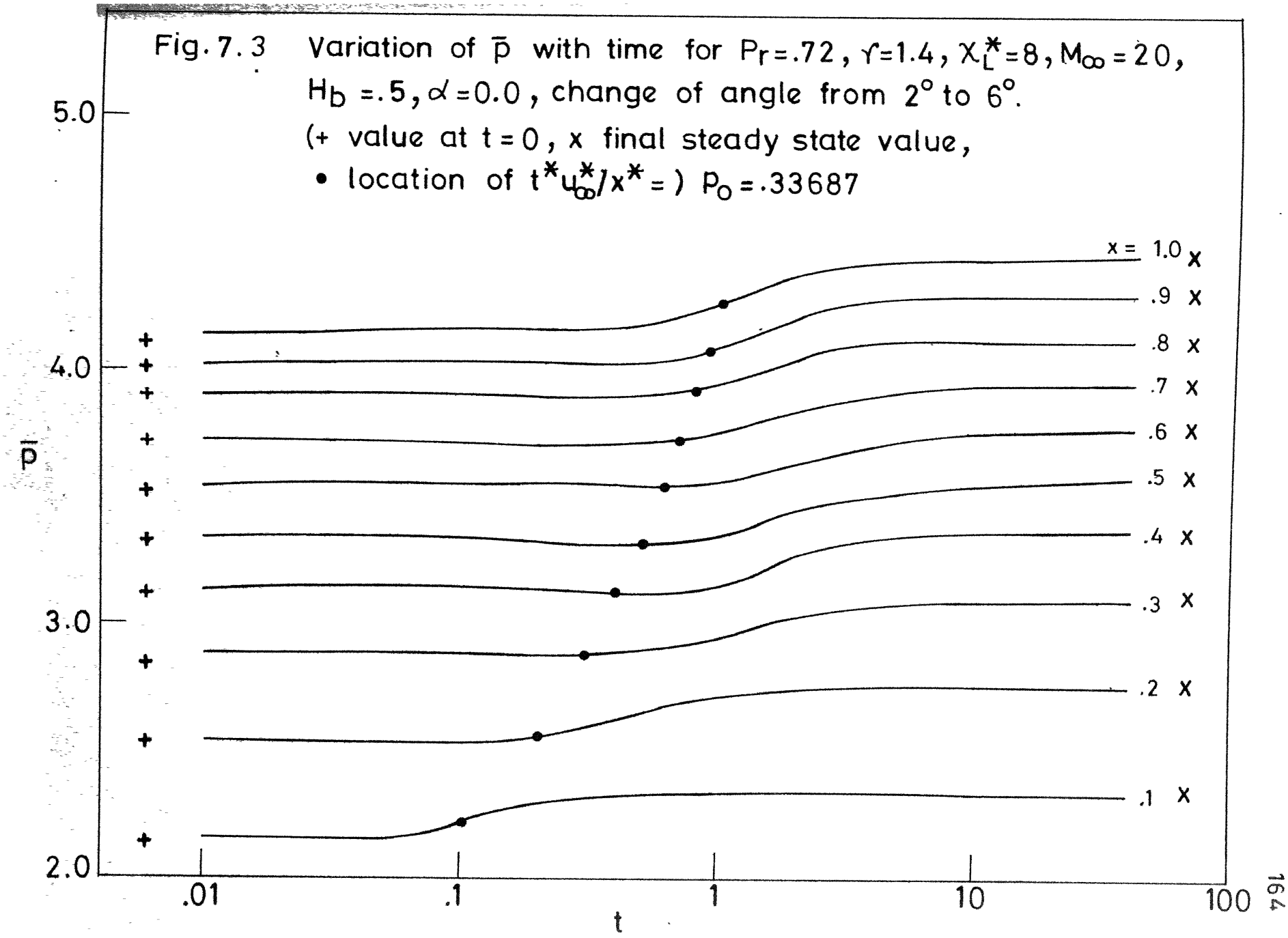
Fig. 7.3 Variation of $\bar{p}$ with time for $P_r = .72$, $\gamma = 1.4$, $X_L^* = 8$, $M_\infty = 20$, $H_b = .5$, $\alpha = 0.0$, change of angle from 2° to 6°.
(+ value at t = 0, x final steady state value,
• location of $t^* u_\infty^* / x^* =$) $P_0 = .33687$
x = 1.0 x
.9 x
.8 x
.7 x
.6 x
.5 x
.4 x
.3 x
.2 x
.1 x
5.0
4.0
3.0
2.0
$\bar{p}$
.01
.1
1
10
100
t

Fig. 7.4 Variation of $f''(o)$ with time for $P_r = .72$, $\gamma = 1.4$, $\alpha = 0$, $H_b = .5$, $M_\infty = 20$, $\bar{\chi}_L^* = 8$, change of angle from 2° to 6° (+ value at t=0, x final steady state value, • location of $t^* u_\infty^* / x^* = 1$)

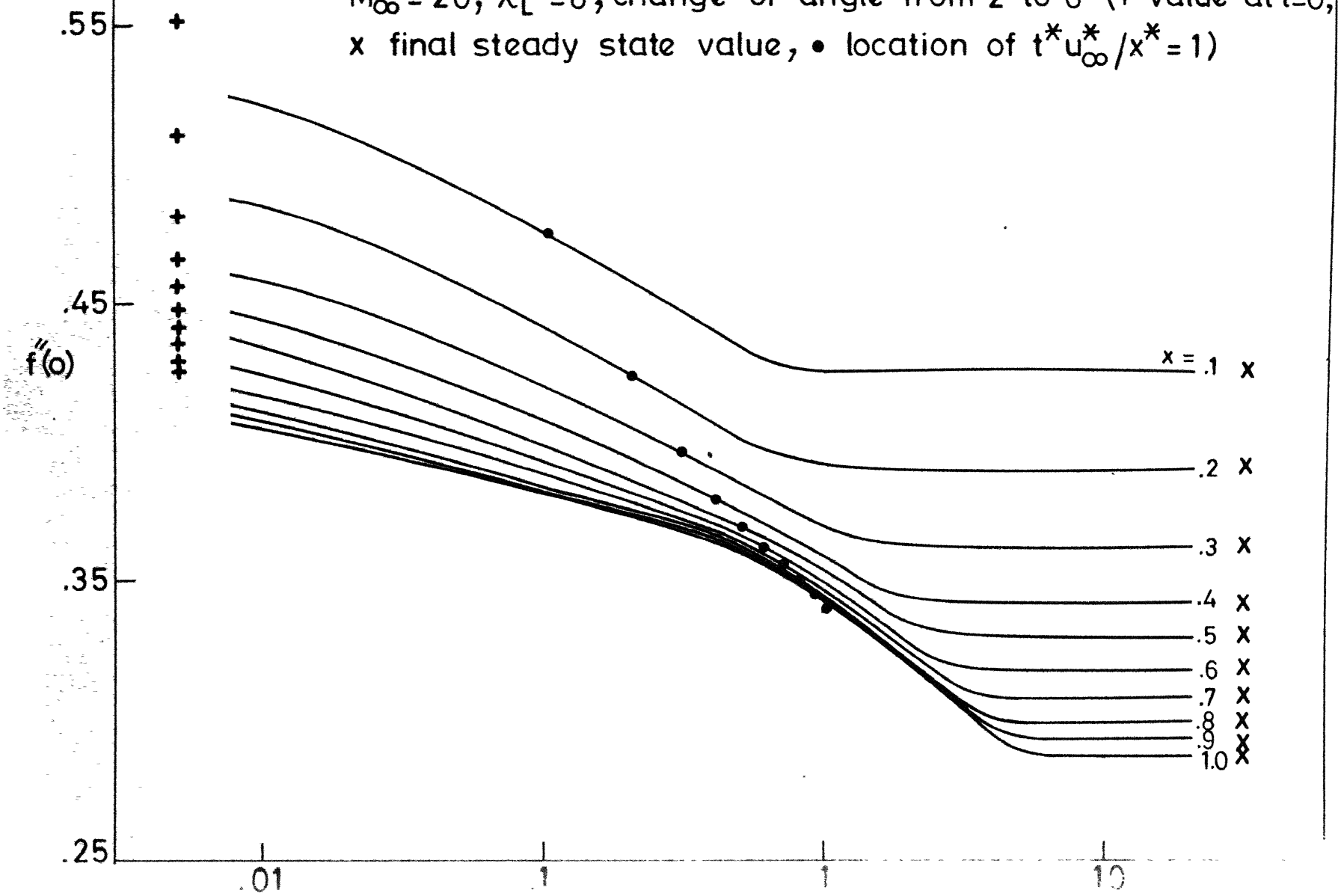

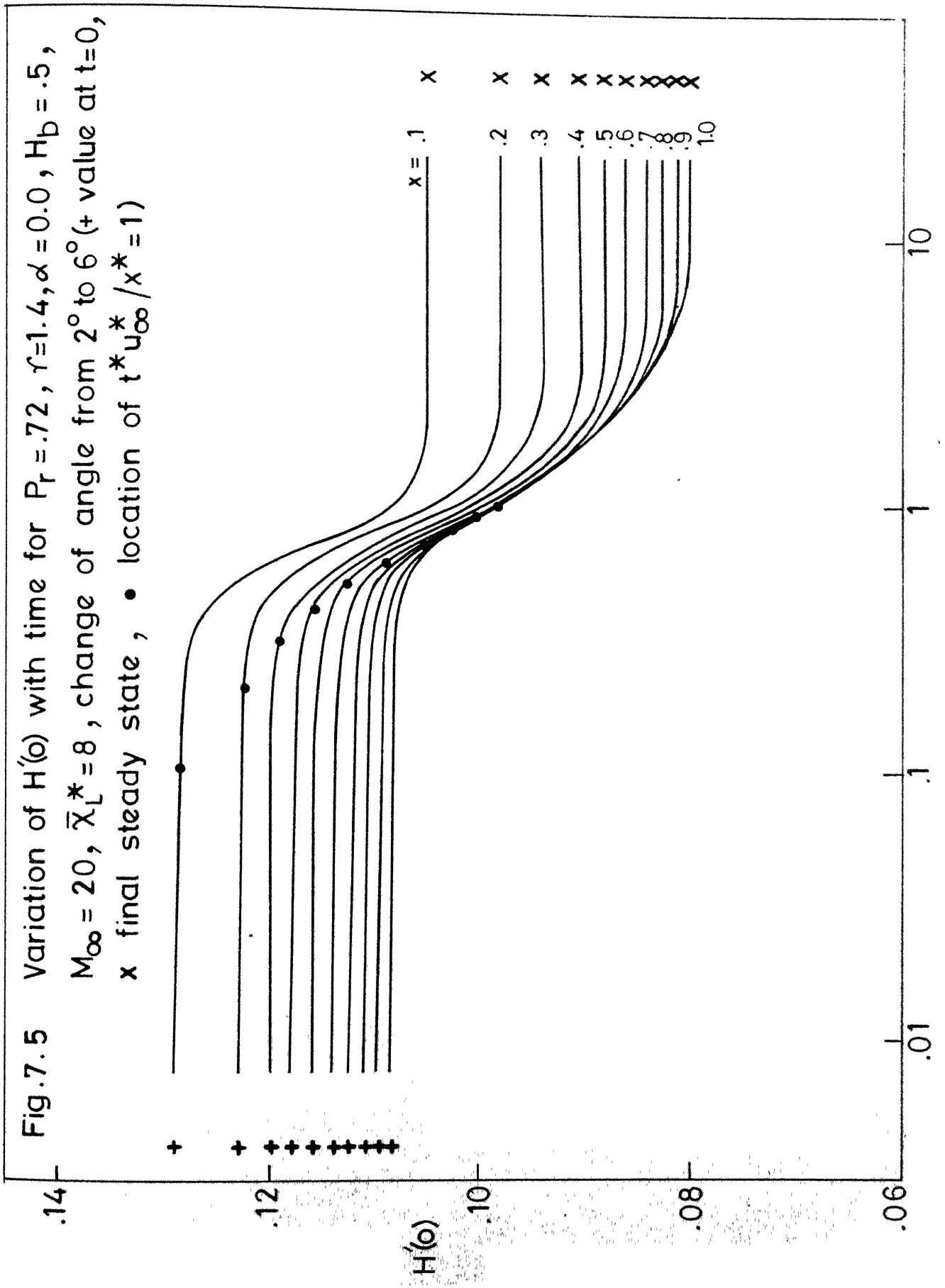

Fig. 7.5 Variation of H'(o) with time for $P_r = .72$, $\gamma = 1.4$, $\alpha = 0.0$, $H_b = .5$, $M_\infty = 20$, $\bar{\chi}_L^* = 8$, change of angle from 2° to 6°(+ value at t=0, x final steady state, • location of $t^* u_\infty^* / x^* = 1$)

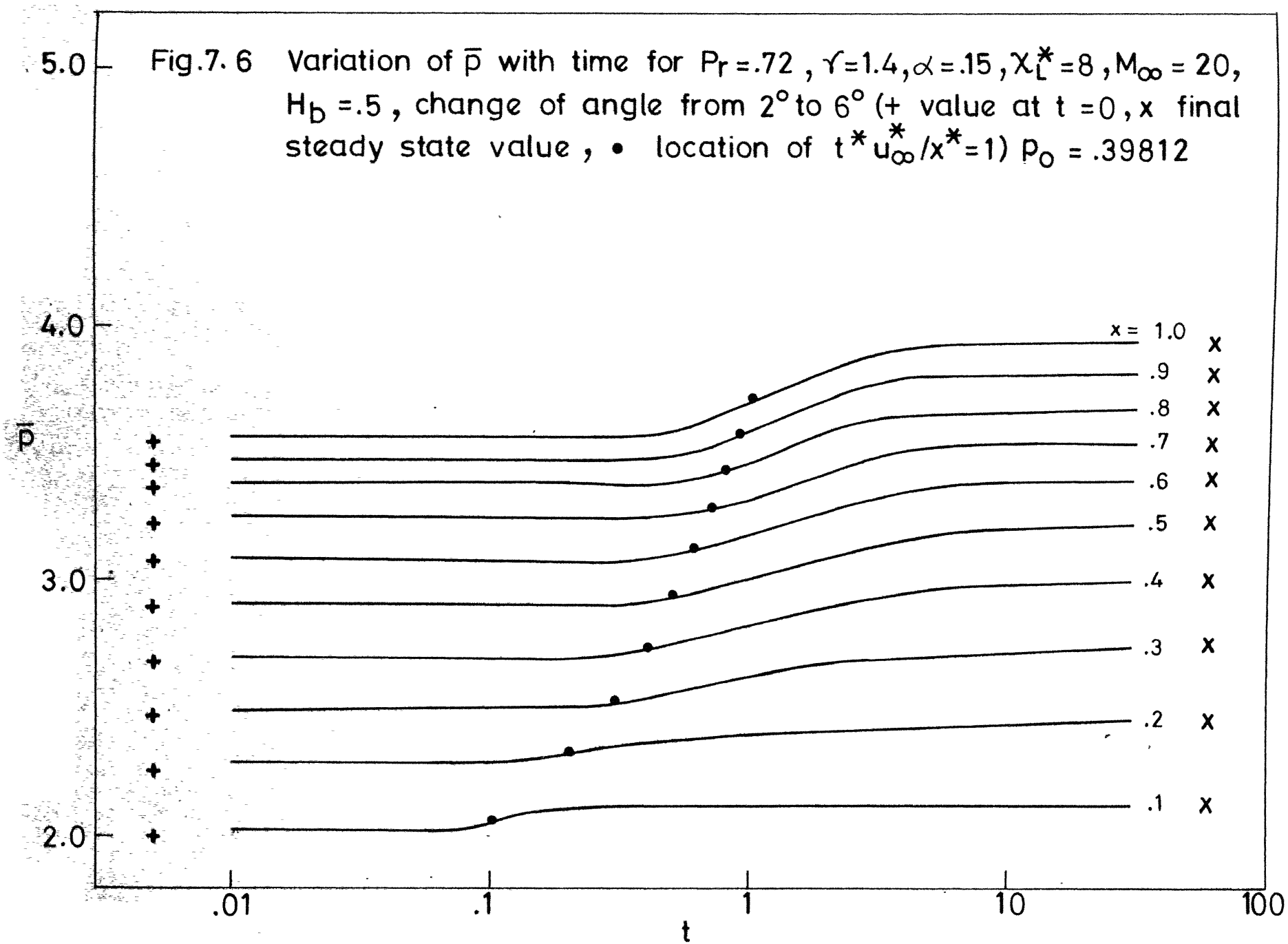

Fig.7.6 Variation of $\bar{p}$ with time for $P_r = .72$, $\gamma = 1.4$, $\alpha = .15$, $\chi_L^* = 8$, $M_\infty = 20$, $H_b = .5$, change of angle from 2° to 6° (+ value at t = 0, x final steady state value, • location of $t^* u_\infty^*/x^* = 1$) $p_0 = .39812$

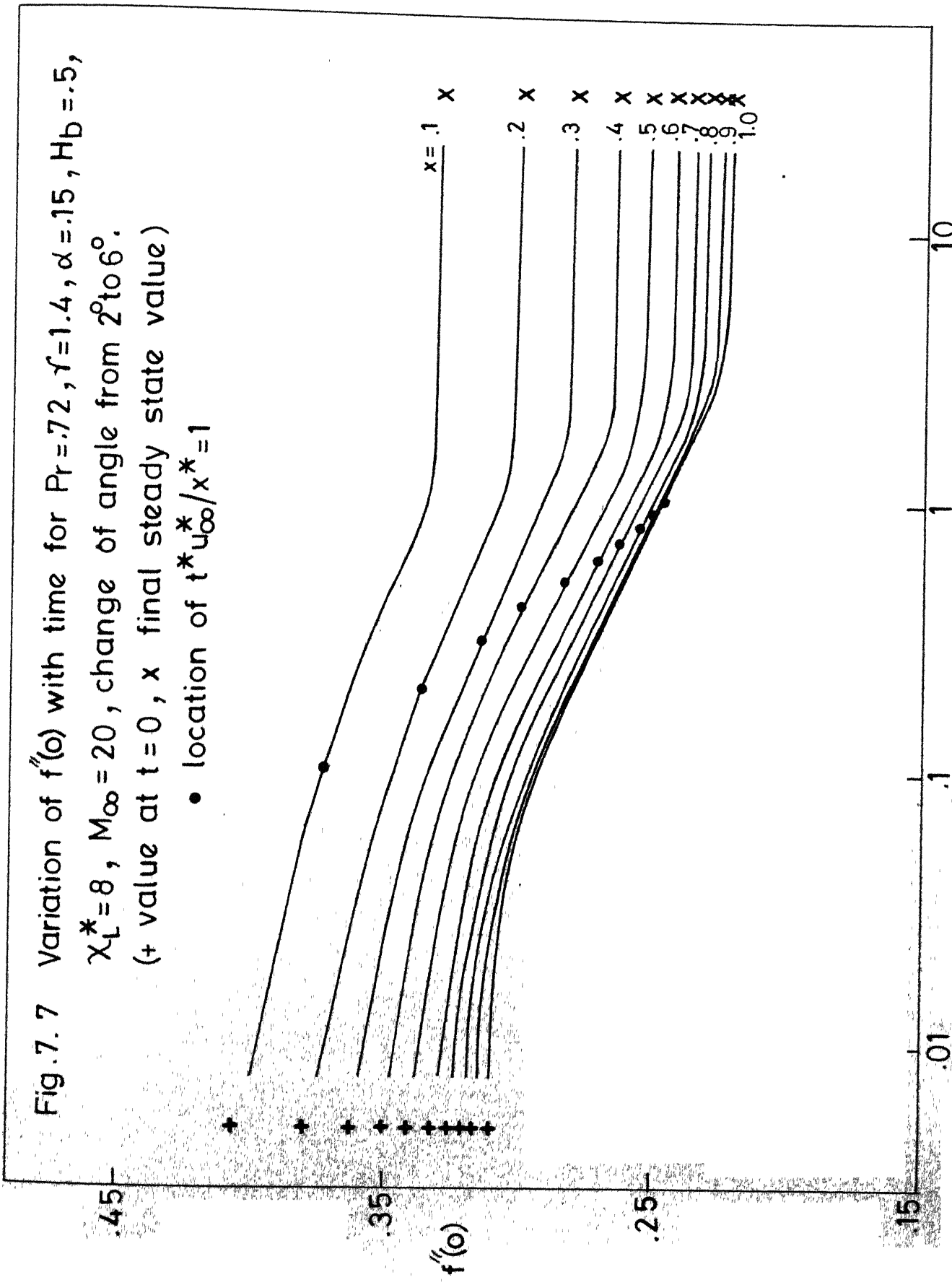

Fig. 7. 7 Variation of $f''(0)$ with time for $P_r = .72$, $\gamma = 1.4$, $\alpha = .15$, $H_b = .5$, $\chi_L^* = 8$, $M_\infty = 20$, change of angle from 2° to 6°.
(+ value at $t = 0$, x final steady state value)
• location of $t^* u_\infty^* / x^* = 1$

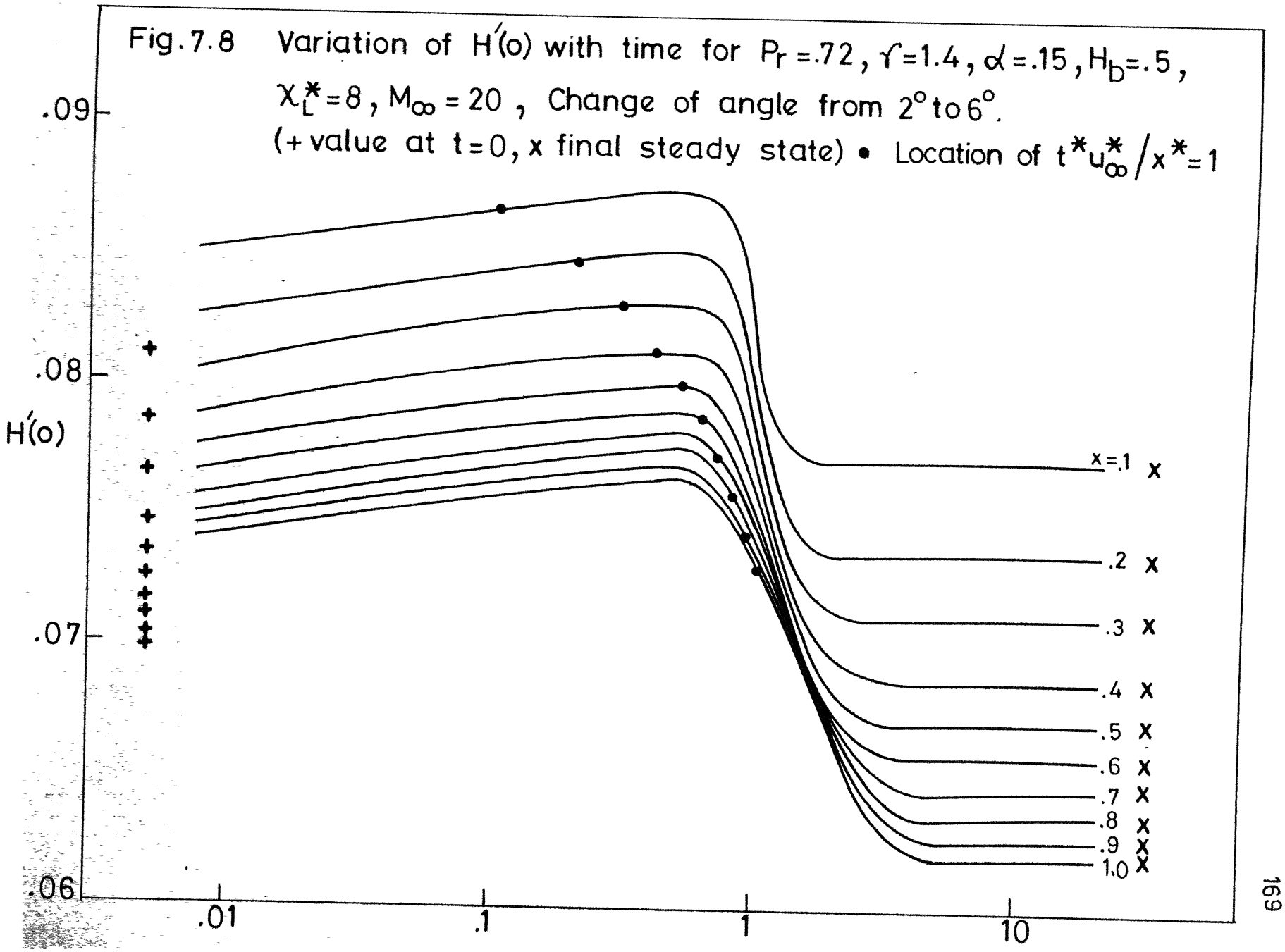
Fig. 7.8 Variation of H′(o) with time for P_r = .72, γ = 1.4, α = .15, H_b = .5, χ_L^* = 8, M_∞ = 20, Change of angle from 2° to 6°.
(+ value at t = 0, x final steady state) • Location of $t^* u_\infty^* / x^* = 1$
.09
.08
.07
.06
H′(o)
.01
.1
1
10
x = .1 x
.2 x
.3 x
.4 x
.5 x
.6 x
.7 x
.8 x
.9 x
1.0 x

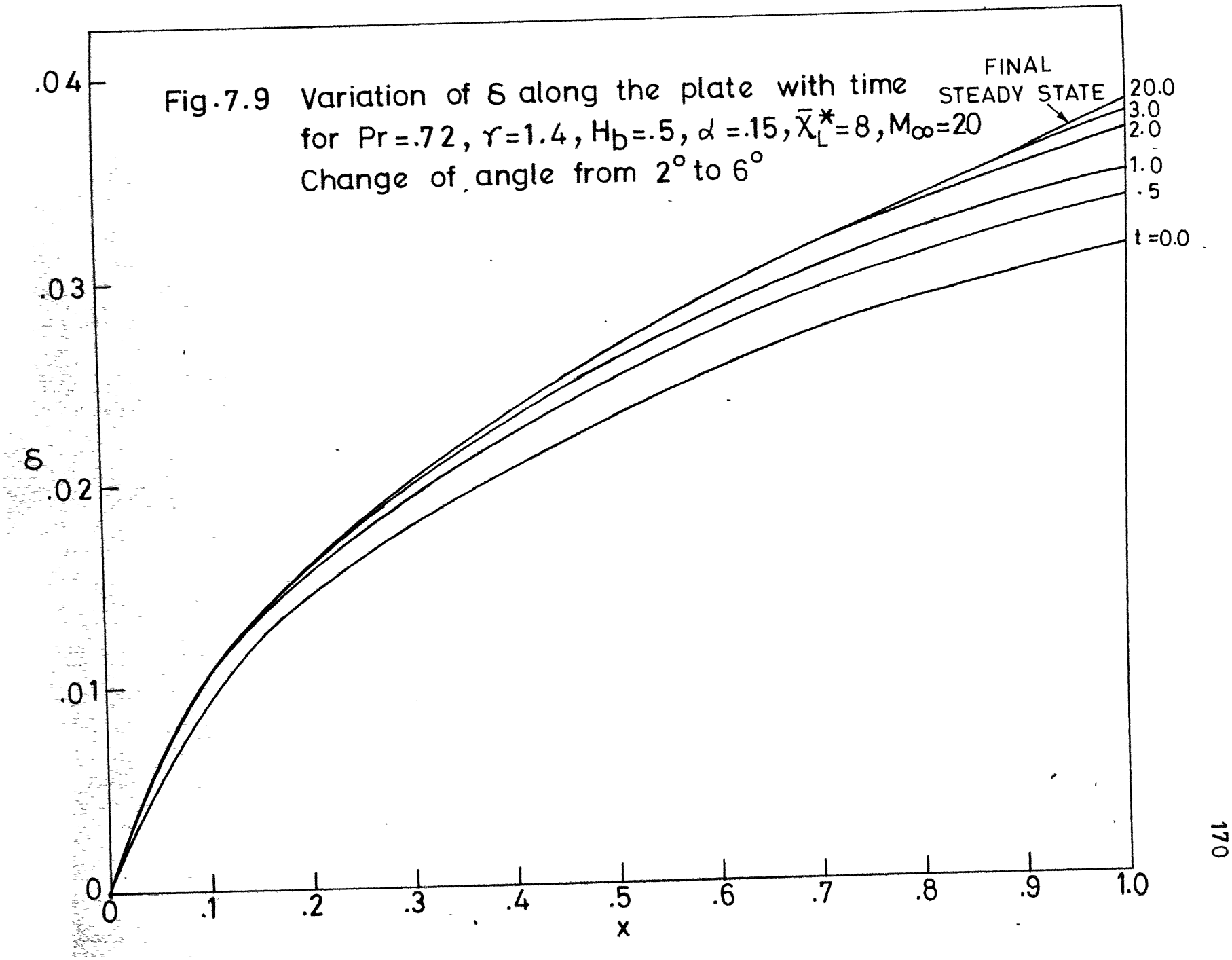
Fig.7.9 Variation of δ along the plate with time for Pr=.72, γ=1.4, H_b=.5, α=.15, $\bar{X}_L^*$=8, M_∞=20
Change of angle from 2° to 6°
FINAL STEADY STATE
20.0
3.0
2.0
1.0
.5
t =0.0
δ
.04
.03
.02
.01
0
0
.1
.2
.3
.4
.5
.6
.7
.8
.9
1.0
x

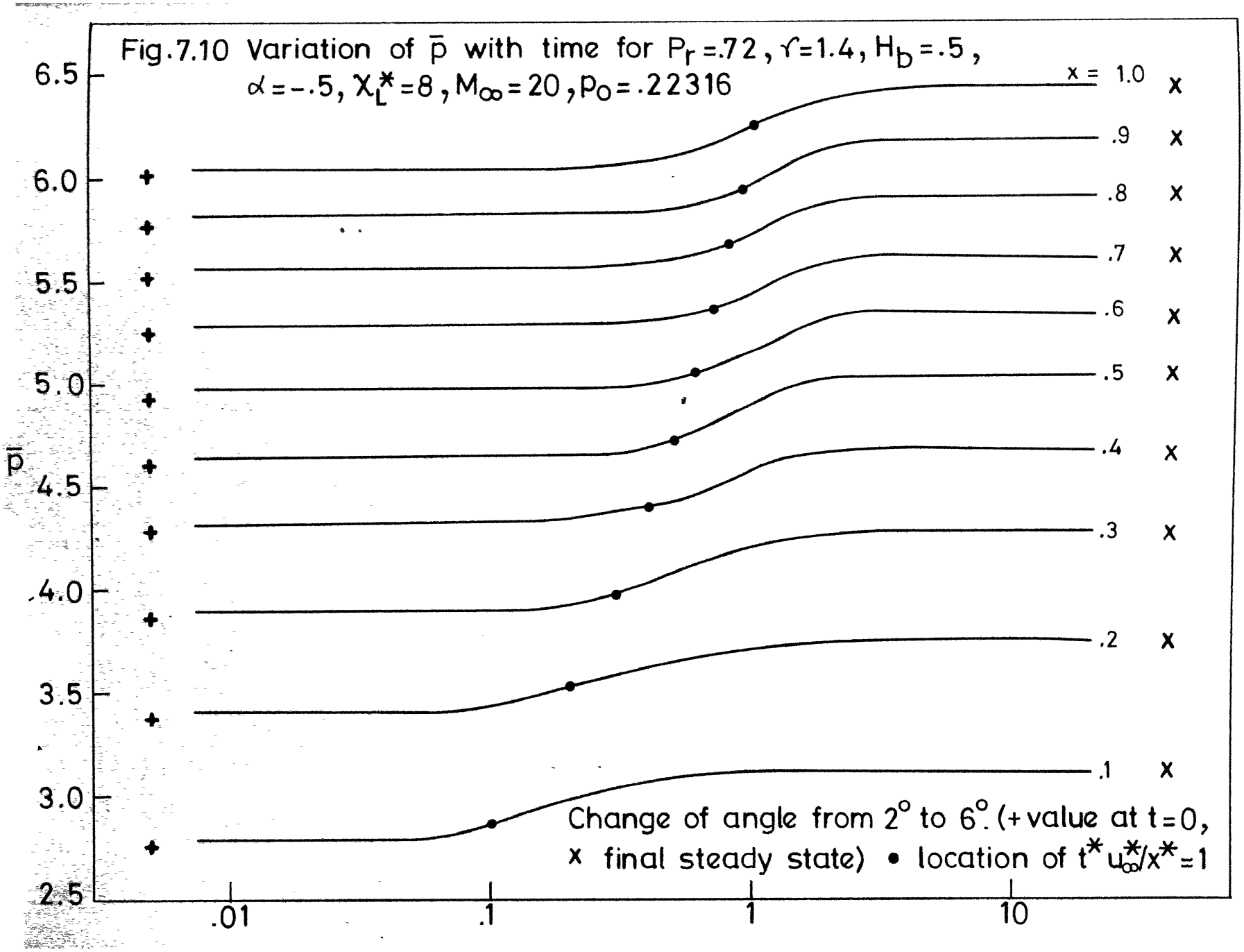
Fig.7.10 Variation of $\bar{p}$ with time for $P_r = .72$, $\gamma = 1.4$, $H_b = .5$, $\alpha = -.5$, $X_L^* = 8$, $M_\infty = 20$, $p_0 = .22316$
$\bar{p}$
6.5
6.0
5.5
5.0
4.5
4.0
3.5
3.0
2.5
.01
.1
1
10
x = 1.0
.9
.8
.7
.6
.5
.4
.3
.2
.1
Change of angle from 2° to 6°. (+ value at t = 0, x final steady state) • location of $t^* u_\infty^*/x^* = 1$

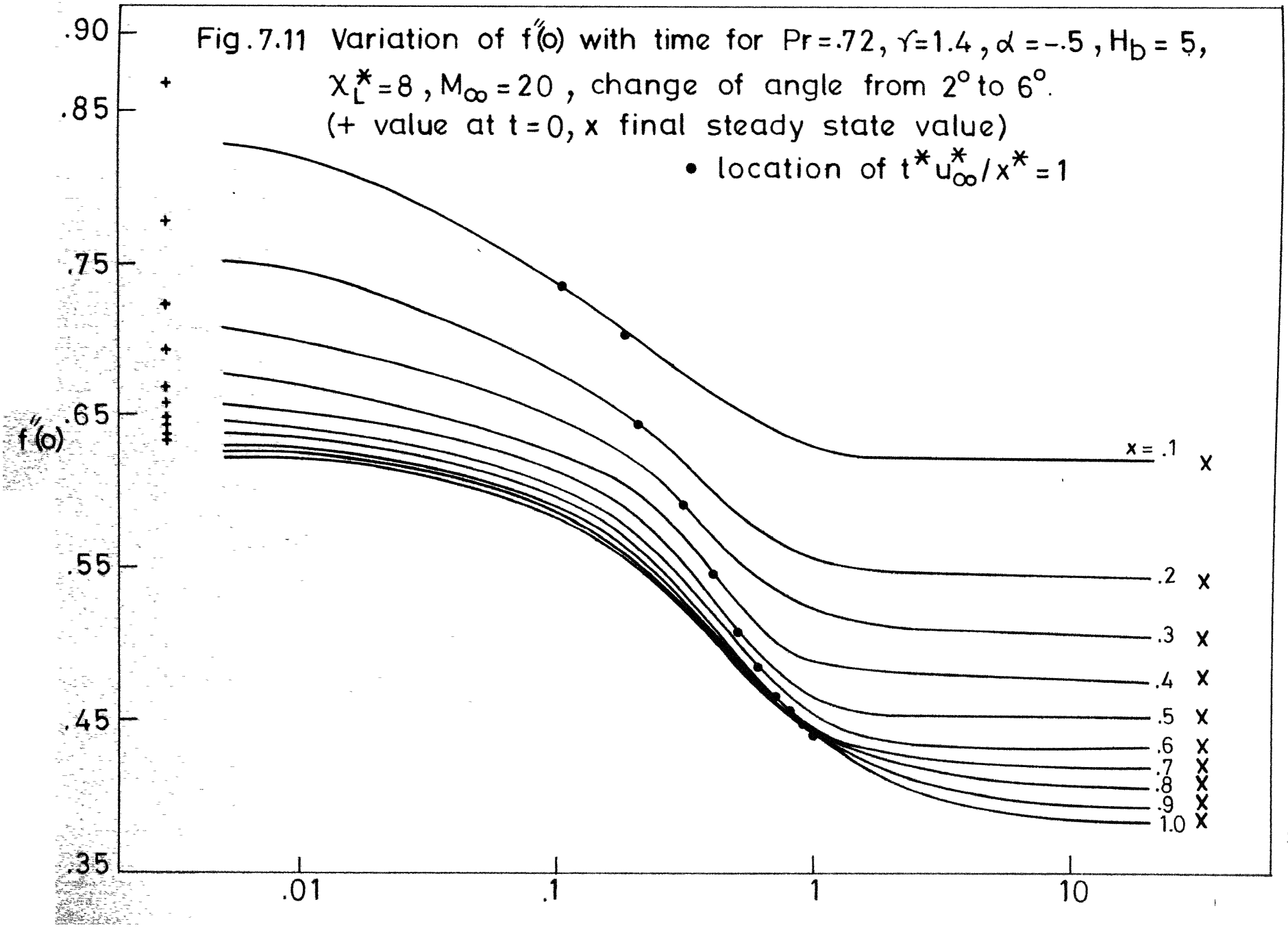
Fig. 7.11 Variation of f''(0) with time for Pr=.72, γ=1.4, α=-.5, H_b = 5,
χ_L^*=8, M_∞=20, change of angle from 2° to 6°.
(+ value at t=0, x final steady state value)
• location of $t^* u_\infty^* / x^* = 1$
f''(0)
.90
.85
.75
.65
.55
.45
.35
.01
.1
1
10
x = .1
.2
.3
.4
.5
.6
.7
.8
.9
1.0

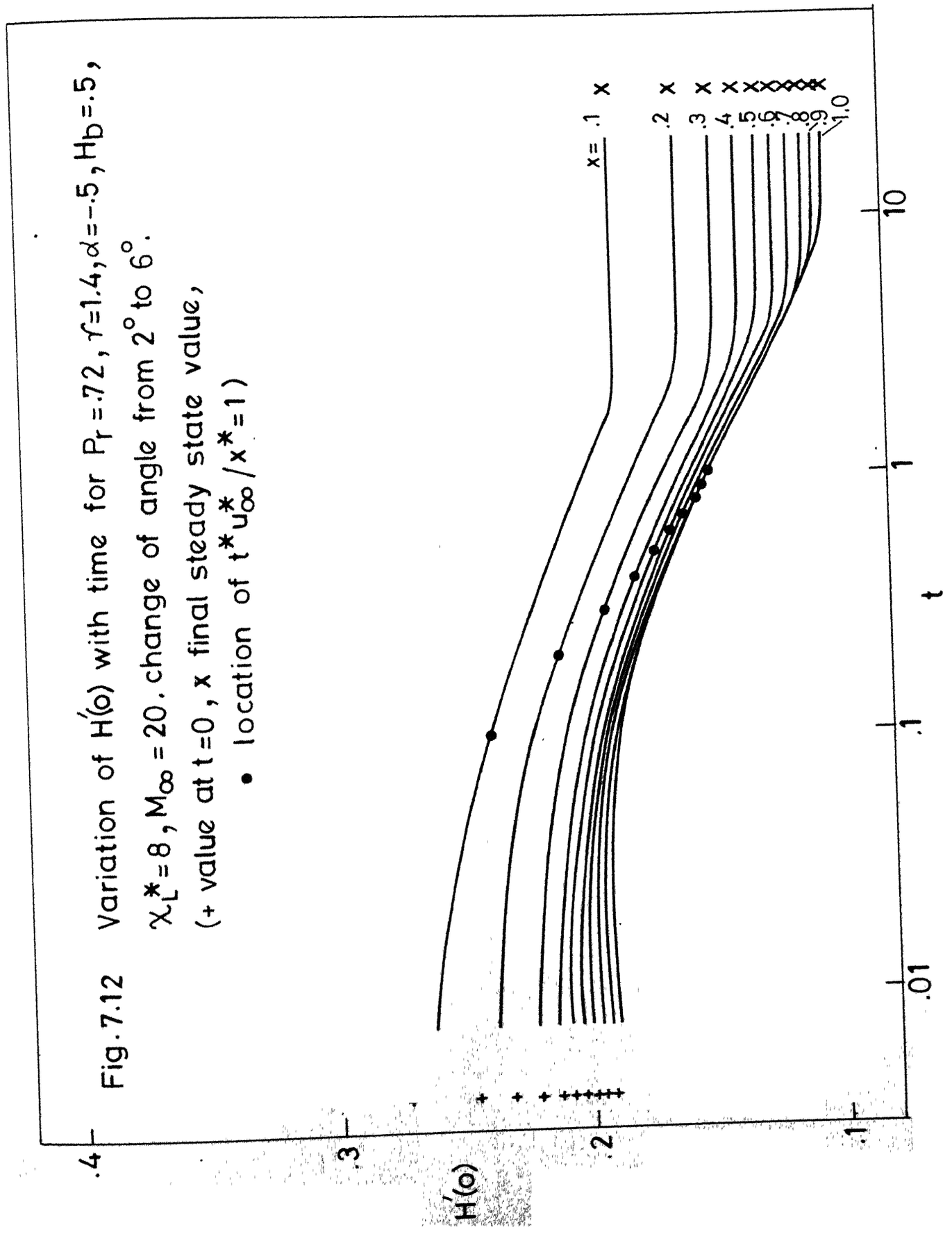

Fig. 7.12 Variation of $H'(0)$ with time for $P_r = .72$, $\gamma = 1.4$, $\alpha = -.5$, $H_b = .5$, $\chi_L^* = 8$, $M_\infty = 20$, change of angle from 2° to 6°.
(+ value at $t = 0$, x final steady state value,
• location of $t^* u_\infty^* / x^* = 1$)

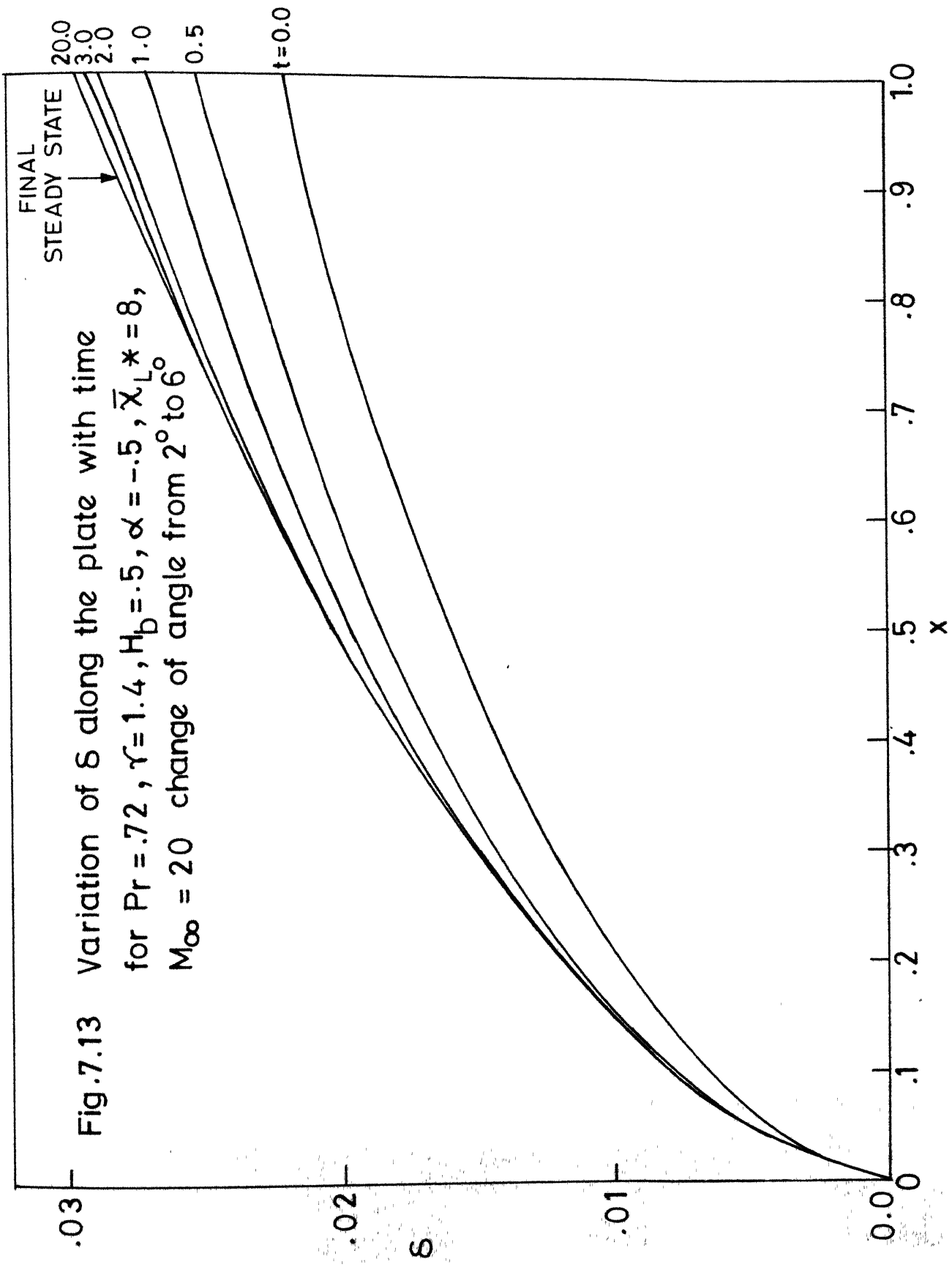

Fig.7.13 Variation of δ along the plate with time for $Pr = .72$, $\gamma = 1.4$, $H_b = .5$, $\alpha = -.5$, $\bar{\chi}_{L_o}^* = 8$, $M_\infty = 20$ change of angle from 2° to 6°

CHAPTER VIII

CONCLUDING REMARKS

The problem of high Mach number flow past a wedge has been solved. The special features of the present work are

1. The solution for the entire region $x \geq x_1$, where x_1 represents the start of the continuum regime, has been obtained
2. The starting profiles at $x=x_1$ ($x_1=O(10^{-3})$) have been obtained by series solution and thus the error of entirely neglecting the non-continuum processes in the region $0 \leq x \leq x_1$ has been avoided.
3. No use of similarity is made and hence it was not necessary to find solutions separately for the strong, transition and weak interaction sub-regions.
4. The effect of surface mass transfer-- both injection and suction -- has been considered by suitably modifying the boundary conditions at the surface. As no use of similarity is made, the rate of surface mass transfer need not be subjected to any particular law regarding x-dependence. The study includes the homogeneous case (the gas injected is the same as that in the atmosphere) and the heterogeneous case (when the injected gas is different from that in the atmosphere).
5. The study also includes considerations of the problem of the time taken for the boundary layer to adjust from the state corresponding to the plate inclination $\theta_{o,i}$ to that corresponding to $\theta_{b,f}$ when the inclination of the plate is impulsively changed from the value $\theta_{b,i}$ to $\theta_{b,f}$.

The main results obtained may be summed up as follows.

1. The surface mass transfer reduces the heat transfer appreciably. The results are shown in fig. (5.23)

2. The lift and drag coefficients, the lift to drag ratio, the position of the aerodynamic centre and the heat transfer rate per unit width of the wedge-wing have been calculated and they are presented in the form of a table on page 150.

3. The pressure distribution for various values of α — the injection/suction parameter — has been shown in fig. (3.8)

4. The change in the value of skin friction coefficient and boundary layer thickness due to injection is shown respectively in figs.(5.22) and (5.24). This data is presented for three different gases - helium, air and argon.

5. For the study of the problem of the adjustment of the boundary layer when the inclination of the plate is impulsively changed from $\theta_{b,i}$ to $\theta_{b,f}$, the variation from the initial to final values of pressure, shear stress function, wall enthalpy gradient and boundary layer thickness is shown for three cases : $\alpha = 0$, $\alpha > 0$ (injection) and $\alpha < 0$ (suction) in figures (7.3) to (7.15).

Future work may be directed towards

(i) obtaining the series solutions for a binary gas mixture.

(ii) solving the time-dependent problem with heterogeneous injection

(iii) case (ii) with gradual change in the angle of attack.

BIBLIOGRAPHY

1. Lees, L. and Probstein, R.F.,''Hypersonic Flows of a Viscous Fluid'', United States Air Force Contract No. AF 33(038)-250, Project No. 1363, Princeton Uni. Monograph, 1953.

2. Hays, W.D. and Probstein, R.F., ''Hypersonic Flow Theory'', Academic Press, New York, 1959.

3. Lees, L., ''On the Boundary-Layer Equations in Hypersonic Flow and Their Approximate Solutions'', Journal Aero. Sci., Vol. 20, No. 2, P. 143, Feb. 1953.

4. Dorrance, W.H., ''Viscous Hypersonic Flow'', McGraw-Hill Book Co. Inc., 1962.

5. Stewartson, K., ''The Theory of Laminar Boundary Layers in Compressible Fluids'', Oxford Mathematical Monographs, Oxford Univ. Press, 1964.

6. Moore, F.K., ''Hypersonic Boundary Layer Theory'', In High Speed Aerodynamics and Jet Propulsion, Vol. IV, Princeton Uni. Press, 1964.

7. Schlichting, H., ''Boundary Layer Theory'', McGraw-Hill Book Company, New York.

8. Emmons, H.W. and Leigh, D.C., Aeronautical Research Council Current Paper 157, 1954.

9. Lees, L., ''Stability of the Laminar Boundary Layer with Injection of Cool Gas at the Wall'', Project Squid, T.R. 11, Princeton Uni., May 20, 1948.

10. Eckert, E.R.G. and Livingwood, J.N.B., ''Comparison of Effectiveness of Convection-, Transpiration-, and Film-Cooling Methods with Air as Coolant'', NACA T.N. 3010, Oct. 1953.

11. Low, G.M., ''The Compressible Boundary Layer with Fluid Injection'', NACA T.N. 3404, March 1955.

12. Inger, G.R. and Swean, T.F., ''Vectored Injection into Laminar Boundary Layers with Heat Transfer'', AIAA Journal, Vol. 13, p.616, May 1975.

13. Inger, G.R. and Swean, T.F., ''Hypersonic Viscous-Inviscid Interaction with Vectored Surface Mass Transfer'', AIAA Journal, Vol. 14, No. 5, p.589, May 1976

14. Zien, T.F., ''Unsteady Compressible Boundary Layers on a Flat Plate with Mass Transfer'', AFOSR Scientific Report 69-2707 T.R., Aug. 1969.

15. Baron, J.R., ''The Binary Mixture Boundary Layer Associated with Mass Transfer Cooling at High Speeds'', M.I.T., Naval Supersonic Laboratory, Technical Report No. 16, May 1956.

16. Wuest, W., ''Laminar Boundary Layers with Injection of Another Medium (Two Fluid Boundary Layers)'', Royal Aircraft Establishment Library Translation No. 1055, Jan. 1964.

17. Moran, J.P. and Scott, P.B., ''A Mass Transfer Finite Difference Formulation Employing Crocco Variables'', M.I.T., Naval Supersonic Laboratory, Technical Report No. 443, June 1960.

18. Oulick, F.E.C., ''The Compressible Turbulent Boundary Layer with Surface Mass Transfer'', M.I.T., Naval Supersonic Laboratory Technical Report No. 454, Aug. 1960.

19. Li, T.Y. and Gross, J.F., ''Hypersonic Strong Viscous Interaction on a Flat Plate with Surface Mass Transfer'', Proceedings of the 1961 Heat Transfer and Fluid Mechanics Institute, Stanford Univ. Press, 1961.

20. Jaffe, N.A., Lind, R.C and Smith, A.M.O., ''Solution to the Binary Diffusion Laminar Boundary Layer Equations with Second-Order Transverse Curvature'', AIAA Journal, Vol. 15, No. 9, p. 1563, Sept. 1967.

21. Jain, A.C. and Li, T.Y., ''Compressible Viscous Flow Over Slinder Bodies with Pressure Gradient, Variable Fluid Properties, Arbitrary Laws of Surface Temperature, and Foreign Gas Injection Velocity Distribution'', Deptt. of Aerosp. Engg. Uni. of Cincinnati, Technical Report AE6504, Oct. 1965.

22. Blottner, F.G., ''Finite Difference Methods of Solution of the Boundary Layer Equations'', AIAA Journal, Vol. 8, No. 2, p. 193, Feb. 1970.

23. Joseph, G. Marvin and Sheaffer, Y.S., ''A Method of Solving the non-similar Laminar Boundary Layer Equations Including Foreign gas Injection'', NASA-TN-D-5516, Nov. 1969.

24 Gupta, R.N. and Chaurasia, M.K., ''Displacement Thickness Induced Pressures on a Flat Plate with Homogeneous and Heterogeneous Vectored Injection'', Int. J. Heat and Mass Transfer Vol. 23, 405-408, Pergamon Press. Ltd. 1980.

25. Gupta, R.N. and Rodkiewicz, C.M., ''Homogeneous and Heterogeneous Vectored Injection Cooling at Hypersonic Velocities'', Transactions of the CSME, Vol. 5, No. 4, 1978-79, p. 205-214.

26. Lighthill, M.J., ''Oscillating Airfoils at High Mach Number'', J. Aero. Sci., Vol. 20, No. 6, p. 402, June 1958.

27. Hayes, W.D., ''On Hypersonic Similitude'', Quart. Appl. Math., Vol. 5, p. 105, 1947.

28. Miles, J.W., ''Unsteady Flow at Hypersonic Speeds'' In ''Hypersonic Flow'', Butterworths Scientific Publications, London, p. 185, 1960.

29. Moore, F.K. and Ostrach, S., ''Displacement Thickness of the Unsteady Boundary Layer'', Journal Aero. Sci., Vol. 24, No. 1, p. 77, January 1957.

30. Resnotko, E. and Rodkiewicz, C.M., ''Pressure Induced by Weak Interaction with Unsteady Hypersonic Layers'', AIAA Journal, Vol. 7, No. 8, p. 1609, Aug., 1969.

31. Rodkiewicz, C.M. and Gupta, R.N., ''Exact Numerical Solutions for Transient Shear Stress and Boundary Layer Induced Pressure'', AIAA Journal, Vol. 9, No. 10, p. 2075, Oct. 1971.

32. Rodkiewicz, C.M. and Luft, B., ''Hypersonic Unsteady Compressible Boundary Layer Dependence on Prandtl Number'', The Physics of Fluids, Vol. 15, No. 8, p. 1391, Aug. 1972.

33. Rodkiewicz, C.M. and Gupta, R.N., ''Weak Interaction Induced Pressure due to the Stepwise-Deceleration of a Flat Plate'', Dept. Report No. 11, Mech. Engg. Deptt., Univ. of Alberta, Canada, Aug. 1977.

34. Gupta, R.N. and Rodkiewicz, C.M., ''Unsteady Boundary-Layer Induced Pressures at Hypersonic Speeds'', Physics of Fluids, Vol. 14, No. 7, p. 1332, July 1971.

35. Rodkiewicz, C.M. and Gupta, R.N., ''Time-dependent Shear Stress and Temperature Distribution over an Insulated Flat Plate Moving at Hypersonic Speed'', C.A.S.I. Transactions, Vol. 4, No. 1, p. 20, March 1971.

36. Gupta, R.N. and Rodkiewicz, C.M., ''Unified Nonlinear Approach to Both Weak and Strong Interaction Problems'' Acta Mechanica, Vol. 21, p. 53, Springer-Verlag 1975.

37. Hall, M.G., '' The Boundary Layer over an Impulsively Started Flat Plate'', Proc. of Royal Society of London, p. 401, A-310-1969.

38. Stewartson, K., ''On the Impulsive Motion of a Flat Plate in a Viscous Fluid'' Part I. Q.J. of Mechanics and Applied Maths., Vol. 4, p. 182, 1951.

39. Stewartson, K., ''On the Impulsive Motion of a Flat Plate in a Viscous Fluid'' Part II. Q.J. of Mechanics and Applied Maths. Vol. 26, p. 143, 1973.

40. Dennis, S.C.R., ''The Motion of a Viscous Fluid Past an Impulsively Started Semi-Infinite Flat Plate'', J. of Inst. of Maths. and its Applications, Vol. 10, p. 105, 1972.

41. Dennis, S.C.R. and Walker, J.D.A., ''The Boundary Layer in a Shock Tube'', J. of Fluid Mech., Vol. 56, p. 19, 1972.

42. Ban, S.D. and Kuerti, G., ''The Interaction Region in the Boundary Layer of a Shock Tube'', J. of Fluid Mech., Vol. 38, p. 109, 1969.

43. Gupta, R.N., ''The Non-Linear Problem in the Interaction Region of a Shock-Tube Boundary Layer'', AIAA J., Vol. 11, No. 4, p. 548, April 1973.

44. Vimala, C.S. and Nath, G., ''Unsteady Laminary Boundary Layers in a Compressible Stagnation Flow''., J. of Fluid Mech., (1975), Vol. 70, Part 3, p. 561.

45. Kumari, M. and Nath, G., ''Unsteady Laminar Boundary-Layer Flow at a Three-Dimensional Stagnation Point'', J. of Fluid Mech., (1978) Vol. 87, Part 4, p. 705.

46. Gupta, R.N., ''An Analysis of the Relaxation of Laminar Boundary Layer on a Flat Plate after Passage of an Interface, with Application of Expansion Tube Flow'', NASA TR R-397, Dec. 1972.

47. Gupta, R.N. and Trimpi, R.L., ''Relaxation of the Accelerating gas Boundary Layer to the Test-Gas Boundary Layer on a Glat Plate in an Expansion Tube'', in Recent Developments in Shock Tube Research, D. Bershader and W. Griffith, eds., Stanford Univ. Press, p.449,1963.

40. Dennis, S.C.R., ''The Motion of a Viscous Fluid Past an Impulsively Started Semi-Infinite Flat Plate'', J. of Inst. of Maths. and its Applications, Vol. 10, p. 105, 1972.

41. Dennis, S.C.R. and Walker, J.D.A., ''The Boundary Layer in a Shock Tube'', J. of Fluid Mech., Vol. 56, p. 19, 1972.

42. Ban, S.D. and Kuerti, G., ''The Interaction Region in the Boundary Layer of a Shock Tube'', J. of Fluid Mech., Vol. 38, p. 109, 1969.

43. Gupta, R.N., ''The Non-Linear Problem in the Interaction Region of a Shock-Tube Boundary Layer'', AIAA J., Vol. 11, No. 4, p. 548, April 1973.

44. Vimala, C.S. and Nath, G., ''Unsteady Laminary Boundary Layers in a Compressible Stagnation Flow''., J. of Fluid Mech., (1975), Vol. 70, Part 3, p. 561.

45. Kumari, M. and Nath, G., ''Unsteady Laminar Boundary-Layer Flow at a Three-Dimensional Stagnation Point'', J. of Fluid Mech., (1978) Vol. 87, Part 4, p. 705.

46. Gupta, R.N., ''An Analysis of the Relaxation of Laminar Boundary Layer on a Flat Plate after Passage of an Interface, with Application of Expansion Tube Flow'', NASA TR R-397, Dec. 1972.

47. Gupta, R.N. and Trimpi, R.L., ''Relaxation of the Accelerating gas Boundary Layer to the Test-Gas Boundary Layer on a Glat Plate in an Expansion Tube'', in Recent Developments in Shock Tube Research, D. Bershader and W. Griffith, eds., Stanford Univ. Press, p.449,1963.

48. Gupta, R.N. and Trimpi, R.L., ''An Eddy Viscosity Treatment of the Unsteady Turbulent Boundary Layer on a Flat Plate in an Expansion Tube'' in Heat Transfer 1974, Vol. II, p.339 (Proc. of the V International Heat Transfer Conf., Tokyo, Sept. 1974).

49. Gupta, R.N. and Trimpi, R.L., ''Relaxation of an Unsteady Turbulent Boundary Layer on a Flat Plate in an Expansion Tube'', NASA TN-D7499, June 1974.

50. King, W.S. ''Low Frequency, Large Amplitude Fluctuations of the Laminar Boundary Layer'', AIAA Journal, Vol. 4, No. 6, p.996, June 1966.

51. Ortlik-Rückemann, K.J., ''Stability Derivatives of Sharp Wedges in Viscous Hypersonic Flow'', National Aeronautical Establishment, Ottawa, Report LR 42, 1965 (see also AIAA Journal, Vol. 4, No. 6, June 1966 (p.1001)).

52. Demtri, P.T. and Gupta, T.R., ''Compressible Oscillating Boundary Layers'', AIAA Journal, Vol. 15, No. 7, p. 974, July 1977.

53. Rodkiewicz, C.M., ''T.K. Chattopadhyay's High Speed and Varying Direction Slender Wedge Solution'', Proc. of the V Canadian Congress of App. Mech., Fredericton, May 26-30, 1975 pp. 411-412.

54. Rodkiewicz, C.M., ''Hypersonic Flow with Viscous Interaction over a Sharp Slender Wedge'', AIAA Journal, Vol. 12, No. 1, p. 7, January 1974.

55. Moore, F.K. and Ostrach, S., ''Displacement Thickness of the Unsteady Boundary Layer'', J. Aero. Sci., Vol. 24, No. 1, p.77, Jan. 1957.

56. Goldworthy, F.A., ''Two-Dimensional Rotational Flow at High Mach Number Past Thin Aerofoils'', Quart. J. Mech. and Applied Math., Vol. V, Pt.1, p. 54, 1952.

57. Mann, W., ''Effective Displacement Thickness for Boundary Layers with Surface Mass Transfer'', AIAA Journal, Vol. 1, No. 5, p. 1181.

58. Rodkiewicz, C.M., ''Hypersonic Flow with Viscous Interaction over a Sharp Wedge'', AIAA Journal, Vol. 12, No. 1, January 1974.

59. Hartree, D.R. and Womersley, J.R., ''A Method for Certain Types of Partial Differential Equations'', Proc. Roy. Soc., Series A, Vol. 161, No. 906, p. 353, August 1937.

60. Smith, A.M.O. and Clutter, D.W., ''Solution of the Incompressible Laminar Boundary Layer Equations'', Douglas Aircraft Company, Report No. ES40446, July 1961.

61. Clutter, D.W. and Smith, A.M.O., ''Solution of the General Boundary Layer Equations for Compressible Laminar Flow, Including Transverse Curvature'', Douglas Aircraft Company, Report No. LB31088, Feb. 15, 1963, Revised October 1964 (see also AIAA J., Vol. 3, No. 4, April 1965, pp. 639-647).

62. Cebeci, T. and Smith, A.M.O., ''A Finite-Difference Method for Calculating Compressible Laminar and Turbulent Boundary Layers'', ASME Paper No. 70-FE-A, 1970.

63. Cohen, C.B. and Reshotko, E., ''Similar Solutions for the Compressible Laminar Boundary Layer with Heat Transfer and Pressure Gradient'', NACA Report No. 1293, 1956.

64. Chattopadhyay, T.K. and Rodkiewicz, C.M., ''Hypersonic Strong Interaction Flow over an Inclined Surface'', AIAA Journal, Vol. 9, No. 3, March 1971; pp.535-537.

65. Jaffe, N.A., Lind, R.C. and Smith, A.M.O.; ''Solution to the Binary Diffusion Laminar Boundary Layer Equations Including the Effects Second-Order Transverse Curvature'', Douglas Aircraft Division; Report No.LB 32613, January 9, 1966.

66. Wilke, C.R., ''A Viscosity Equation for Gas Mixtures'', J. of Chemical Phys., Vol. 18, No. 4, p. 517, April 1950.

67. Hirschfelder, J.O., Curtiss, C.F. and Bird, R., ''Molecular Theory of Gases and Liquids'', John Wiley, New York, 1964.

68. Gupta, R.N. and Rodkiewicz, C.M., ''Homogeneous and Heterogeneous Vectored Injection Cooling at Hypersonic Velocities'', Transactions of the CSME, Vol.5, No. 4, 1978-79, p. 205.

69. Conte, S.D. and Carl-de-Boor, ''Elementary Numerical Analysis'', McGraw Hill Kogakusha, 1965.

70. Varga, R.S., ''Matrix Iterative Analysis'', Prentice Hall Inc., 1962, p.194-197.

71. Rodkiewicz, C.M. and Chattopadhyay, T.K., ''Aerodynamic Characteristics of Slender Wedge-Wings in Hypersonic Strong Interaction Flows'', AIAA Journal, Vol. 9, No. 11, p.2280, Nov. 1971.

72. Mirels, H. and Lewellen, W.S., ''Hypersonic Viscous Interaction Theory for Wedge Wings'', J. of Spacecraft and Rockets, Vol. 4, No. 4, 1967, pp.492-497.

73. Gupta, R.N., Mukherjee, S. and Rodkiewicz, C.M.,''Unsteady Boundary Layer Induced Pressures at High Mach Numbers'', Accepted for publication in the Acta Mechanica, Springer-Verlag, New York, 1980-81.

APPENDIX A

DETAILS OF SIMPLIFICATIONS USED IN OBTAINING THE FLOW GOVERNING EQUATIONS

In this appendix we will describe the details of simplifications of some of the terms required in the non-dimensionalisation of the equations (2.2) and (2.4). The various terms which require these details are

$$\frac{1}{\rho^*}\frac{\partial p^*}{\partial x^*}\ ,\ \frac{1}{\rho^*}\frac{\partial p^*}{\partial t^*} \quad \text{and} \quad \sum_{i=1}^{2} h_i^* \frac{\partial c_i}{\partial y^*}\ .$$

First we simplify $\frac{1}{\rho^*}\frac{\partial p^*}{\partial x^*}$. From the equation of state :

$$p^* = \bar{R}^*\ \rho^*\ T^*$$

or,
$$p = \bar{R}^* \frac{m_A^*}{R_u^*}\ \rho T \text{ with } \frac{p_\infty^*}{\rho_\infty^*\ T_\infty^*} = R_A^* = \frac{R_u^*}{m_A^*}$$

where R_u^* is the Universal gas constant and $\bar{R}^*$ is the gas constant for the mixture.

Thus,

$$p = \bar{m}\ \rho\ T \qquad (A.1)$$

where
$$\bar{m} = \sum_i \left(c_i \frac{m_A^*}{m_i^*}\right)$$

Further,
$$H - u^2 = \frac{H^*}{\frac{1}{2}\ u_\infty^{*2}} - \frac{u^{*2}}{u_\infty^{*2}}$$

$$= \frac{2h^*}{u_\infty^{*2}} = \frac{2c_p^*\ T_\infty^*}{u_\infty^{*2}}\ T$$

or $$T = \frac{u_\infty^{*2}}{2c_p^* T_\infty^*} (H - u^2) \qquad (A.2)$$

Now, $$\frac{1}{\rho^*} \frac{\partial p^*}{\partial x^*} = \frac{p_\infty^*}{\rho_\infty^* L^*} \frac{1}{\rho} \frac{\partial p}{\partial x}$$

From (A.1) we can write :

$$\frac{1}{\rho} \frac{\partial p}{\partial x} = \frac{\bar{m} T}{p} \frac{\partial p}{\partial x}$$

Substituting for T from (A.2) we obtain

$$\frac{1}{\rho} \frac{\partial p}{\partial x} = \frac{\rho_\infty^* u_\infty^{*2}}{p_\infty^*} \frac{R_A^*}{2} \left\{ \frac{\sum_i (c_i \, m_A^*/m_i^*)}{\sum_i (c_i \, c_{pi}^*)} \right\} \frac{1}{p} \frac{\partial p}{\partial x} (H - u^2) \qquad (A.3)$$

where $c_p^* = \sum_i (c_i \, c_{pi}^*)$ has been used.

Further, for a binary mixture i = 1,2 and

$$c_1 + c_2 = 1$$

Here c_1 is for the injected gas and c_2 is for the main-stream gas, namely, air. Therefore we can write :

$$R_A^* \left\{ \frac{\sum_i (c_i \, m_A^*/m_i^*)}{\sum_i (c_i \, c_{pi}^*)} \right\} = R_A^* \left\{ \frac{c_1 s + c_2}{c_1 \, c_{p1}^* + c_2 \, c_{p2}^*} \right\} \qquad (A.4)$$

with $m_2^* \equiv m_A^*$ and $c_{p2}^* \equiv c_{p_A}^*$ and $s = m_A^*/m_1^*$.

Now, $\frac{R_A^*}{c_{p_A}^*} = \frac{\gamma - 1}{\gamma} = \beta$ and using (A.4) in (A.3) we obtain

$$\frac{1}{\rho^*}\frac{\partial p^*}{\partial x^*} = \frac{p_\infty^*}{\rho_\infty^* L^*}\frac{1}{\rho}\frac{\partial p}{\partial x} = \frac{u_\infty^{*2}}{L^*}\frac{\beta}{2}\frac{1}{p}\frac{\partial p}{\partial x}\left[H - u^2\right]\left\{\frac{1 + c_1(s-1)}{1 + c_1(r-1)}\right\} \tag{A.5}$$

Next, we will consider the simplification of $\frac{1}{\rho^*}\frac{\partial p^*}{\partial t^*}$:

$$\frac{1}{\rho^*}\frac{\partial p^*}{\partial t^*} = \frac{u_\infty^*}{\rho_\infty^*}\frac{p_\infty^*}{L^*}\frac{1}{\rho}\frac{\partial p}{\partial t}$$

If we substitute for ρ from (A.1) and eliminate T from the resulting expression with the help of (A.2) we can write, after minor simplifications,

$$\frac{1}{\rho}\frac{\partial p}{\partial t} = \frac{\rho_\infty^* u_\infty^{*2}}{2p_\infty^*}\frac{R_A^*}{c_p^*}\bar{m}\frac{1}{p}\frac{\partial p}{\partial t}\left[H - u^2\right]$$

If we use (A.4) in this expression it will further simplify to

$$\frac{1}{\rho}\frac{\partial p}{\partial t} = \left(\frac{\rho_\infty^* u_\infty^{*2}}{2p_\infty^*}\right)\beta\frac{1}{p}\frac{\partial p}{\partial t}\left[H - u^2\right]\left\{\frac{1 + c_1(s-1)}{1 + c_1(r-1)}\right\}$$

Therefore,

$$\frac{1}{\rho^*}\frac{\partial p^*}{\partial t^*} = \left(\frac{u_\infty^* p_\infty^*}{\rho_\infty^* L^*}\right)\frac{1}{\rho}\frac{\partial p}{\partial t}$$

$$= \left(\frac{u_\infty^{*3}}{2L^*}\right)\beta\frac{1}{p}\frac{\partial p}{\partial t}\left[H - u^2\right]\left\{\frac{1 + c_1(s-1)}{1 + c_1(r-1)}\right\} \tag{A.6}$$

Finally,

$$\sum_i h_i^*\frac{\partial c_i}{\partial y^*} = h_1^*\frac{\partial c_1}{\partial y^*} + h_2^*\frac{\partial c_2}{\partial y^*} = (h^* - h_2^*)\frac{\partial c_1}{\partial y^*}$$

$$= \frac{u_\infty^{*2}}{2L^*}(h_1 - h_2)\frac{\partial c_1}{\partial y}$$

Further,

$$h_1 - h_2 = \frac{h_1^*}{\frac{1}{2} u_\infty^{*2}} - \frac{h_2^*}{\frac{1}{2} u_\infty^{*2}}$$

$$= \frac{c_{p1}^* T^* - c_{p2}^* T^*}{\frac{1}{2} u_\infty^{*2}}$$

Using (A.2) and simplifying we get

$$h_1 - h_2 = \left\{ \frac{r - 1}{c_1(r-1) + 1} \right\} \left[H - u^2 \right] \qquad (A.7)$$

and

$$(h_1^* - h_2^*) \frac{\partial c_1}{\partial y^*} = \frac{u_\infty^{*2}}{2L^*} \left\{ \frac{r - 1}{c_1(r - 1) + 1} \right\} \left[H - u^2 \right] \frac{\partial c_1}{\partial y} \qquad (A.8)$$

APPENDIX B

MODIFIED SIMPSON'S RULE

The integrals S_i (i = 1,2,3,4) of Chapter VI require a special formula for evaluation if the step-size along the plate is not uniform. In the case of heterogeneous injection, where the results are obtained with the finite-difference method, there is no difficulty in the evaluation of these integrals since the x-stations employed in the computations are at equal intervals and hence Simpson's rule can be conveniently used. But in the case of Clutter-Smith method a non-uniform step-size given by $\Delta x_j = k_x \Delta x_{j-1}$ is used to reduce the computational time. Therefore, a modification is to be made in the Simpson's rule of integration to use it for the non-uniform space-intervals.

Let O_1, O_2, O_3,..., O_j ... O_J represent the value of the integrands of any of the integrals S_i (i = 1,2,3,4). Then the evaluation of the integrals can be made as follows :

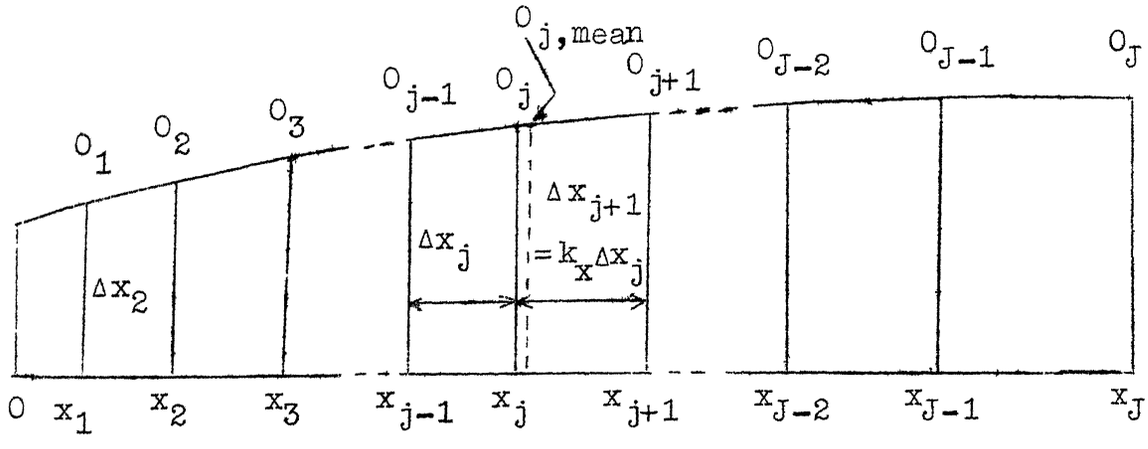

Fig. B.1 Arrangement of Ordinates at Unequal Intervals

where $\Delta x_j = k_x^{(j-2)} \Delta x_2$ has been used and J is an odd integer.

By putting $k_x = 1$ in (B.3) we can obtain Simpson's rule for equal intervals. O_j in eq. (B.3) corresponds to the value of the respective integrands appearing in the integrals S_i (i = 1,2,3,4).

The values of the integrals S_i (i = 1,2,3,4) obtained by using (B.3) was checked in three different ways :

(i) by fitting a cubic spline through the upper ends of the ordinates and applying Simpson's rule to obtain the area after computing the ordinates at equal intervals from the cubic spline.

(ii) by the trapezoidal rule applied on each segment bounded by two adjacent ordinates.

and (iii) by plotting a graph and then measuring the area.

In the first of the above three methods of checking, the results are found to agree upto fourth places after the decimal point; and with the other two methods a good agreement of the results has been noted.

As mentioned earlier, J is an odd integer as it appears in eq. (B.3). For an even value of J, expression (B.3) can be used upto (J-1)th station and the area of the last segment may be obtained by the trapezoidal rule.

APPENDIX C

UTILIZATION OF SERIES EXPANSION SOLUTIONS WITH AND WITHOUT AIR INJECTION

The expressions contained in this section for the evaluation of various aerodynamic coefficients are similar to those obtained in ref. [71]. In the evaluation of these coefficients for the case with air injection, however, appropriate solutions to the boundary layer equations obtained in Chapter III must be used.

The wall shear stress τ_b^* can be expressed in the form

$$\frac{\tau_b^*}{\frac{1}{2}\rho_\infty^* u_\infty^{*2}} = \frac{2\,\bar{x}^{-3/2}}{M_\infty^3}\,\tau_o\left[1 + \frac{\tau_1 k_b}{\bar{x}^{1/2}} + \frac{\tau_2 + \tau_3 k_b^2}{\bar{x}}\right] \qquad (C.1)$$

where the constants τ_i (i = 0,1,2,3) are given by

$$\tau_o = \left[\sqrt{p_o/2}\right] f''_{ob} \qquad (C.2a)$$

$$\tau_1 = p_1\left[1 + \bar{f}''_{1b}/f''_{ob}\right] \qquad (C.2b)$$

$$\tau_2 = p_2\left[1 + \bar{f}''_{2b}/f''_{ob}\right] \qquad (C.2c)$$

$$\tau_3 = p_3\left[1 + \bar{f}''_{2b}/f''_{ob}\right] + p_1^2\left[\bar{f}''_{1b}/f''_{ob} + \bar{f}''_{3b}/f''_{ob}\right] \qquad (C.2d)$$

Substituting for p^* and τ^* from the expressions (3.8) and (C.1) the equations (6.7) and (6.8) yield, after necessary integrations:

$$C_L = \frac{L}{\frac{1}{2}\rho_\infty^* u_\infty^{*2} L^*} = 8\bar{\alpha}\left[\frac{p_o p_3 \theta_b}{\gamma} + \frac{2A}{3}\left\{\frac{p_o p_1}{\gamma} - \frac{\tau_o \tau_2}{M_\infty^2}\right.\right.$$

$$\left.\left. - \tau_o \tau_3 (3\theta_b^2 + \bar{\alpha}^2)\right\} - 2\tau_o \tau_1 \theta_b A^2 - 2 \tau_o A^3\right] \qquad (C.3)$$

$$C_D = \frac{D}{\frac{1}{2}\rho_\infty^* u_\infty^{*2} L^*} = 4\left[\frac{p_o \theta_b}{\gamma}\left\{p_3 (\theta_b^2 + 3\bar{\alpha}^2) + \frac{p_2}{M_\infty^2}\right\}\right.$$

$$+ \frac{4A}{3}\left\{(\theta_b^2 + \bar{\alpha}^2)\left(\frac{p_o p_1}{\gamma} + \tau_o \tau_3\right) + \frac{\tau_o \tau_2}{M_\infty^2}\right\}$$

$$\left. + 2A^2 \left(\frac{p_o}{\gamma} + \tau_o \tau_1\right)\theta_b + 4 \tau_o A^3\right] \qquad (C.4)$$

where $A = \sqrt{\bar{x}_L}^*/M_\infty$

From (C.3) and (C.4) we may also write

$$\frac{L}{D} = \frac{C_L}{C_D} \qquad (C.5)$$

where $L = L_p + L_v$

and $D = D_p + D_v$

The subscripts p and v denote the contributions of the pressure and viscous forces.

Fig. C.1 compares the presently obtained L/D ratio for a flat plate ($\theta_b = 0$) with the results of Mirels and Lewellen [72] and Rodkiewicz and Chattopadhyay [71]. A good agreement is seen for small values of angle of attack. For large values of angle of attack, present computations are closer to

the results of Mirels and Lewellen [72]. It may be pointed out here that the difference between the present results and those obtained by Rodkiewicz and Chattopadhyay arises due to the variations in the values of the various constants obtained in the two calculations. As mentioned in Sec. 3.6 of Chapter III, Rodkiewicz and Chattopadhyay have evaluated their constants by integrating the governing equations near the wall with a Runge-Kutta method employing a large step-size ($\Delta\eta = 0.10$). In our calculations, however, a more precise method, namely, the Taylor's series expansion with much smaller step-size ($0.10/16$) was used to initiate the solutions at the wall.

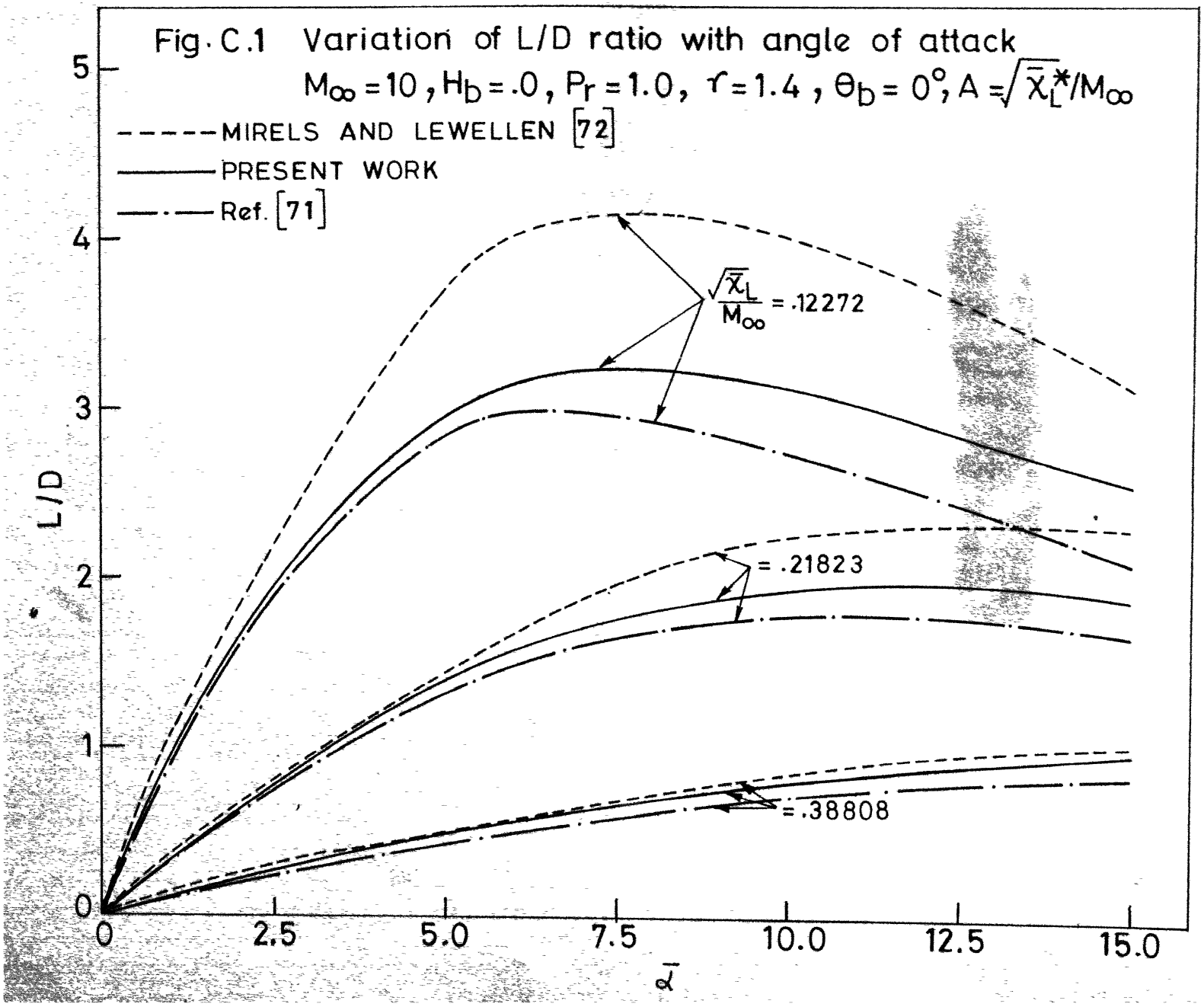
Fig. C.1 Variation of L/D ratio with angle of attack
$M_\infty = 10, H_b = .0, P_r = 1.0, \gamma = 1.4, \theta_b = 0°, A = \sqrt{\bar{\chi}_L^*}/M_\infty$
MIRELS AND LEWELLEN [72]
PRESENT WORK
Ref. [71]
$\frac{\sqrt{\bar{\chi}_L}}{M_\infty} = .12272$
$= .21823$
$= .38808$
L/D
$\bar{\alpha}$
0
1
2
3
4
5
0
2.5
5.0
7.5
10.0
12.5
15.0